Universidad de Valladolid

Escuela de Doctorado Universidad de Valladolid

PROGRAMA DE DOCTORADO EN FÍSICA

TESIS DOCTORAL:

# UNDERSTANDING THE RELATIONSHIPS BETWEEN COMPOSITION, PROCESS, CELLULAR STRUCTURE AND PROPERTIES OF CELLULAR POLYMERS BASED ON BLENDS OF POLYSTYRENE WITH INORGANIC AND ORGANIC NUCLEATING AGENTS

Presentada por Alberto Ballesteros Agudo

para optar al grado de

Doctor por la Universidad de Valladolid

Dirigida por:

Dr. Miguel Ángel Rodríguez Pérez

Dr. Ester Laguna Gutiérrez

# AGRADECIMIENTOS

Es momento de recordar a todas aquellas personas que, en mayor o menor medida, han contribuido al desarrollo de esta tesis. Temo que mi memoria no pueda recordar y agradeceros a todos, tal y como mereceríais, pero sirva este pequeño párrafo como ese mínimo agradecimiento del que os veis privados.

En primer lugar, quisiera agradecer a mi tutor, el catedrático Miguel Ángel Rodríguez Pérez, no solo por la ingente ayuda prestada durante la tesis, si no por darme la oportunidad de introducirme en un mundo tan interesante como es el de los materiales celulares, por ser un referente de exactitud y trabajo duro en cualquier investigación, y por apadrinarme en un sector tan pequeño como es el de las espumas. Estoy seguro de que cosecharás todos los éxitos y frutos por los que has trabajado tan arduamente. Seguidamente, quisiera destacar a Ester Laguna Gutiérrez, cotutora de esta tesis. Probablemente, seas la persona que más veces has leído este trabajo. Gracias por tus correcciones y comentarios, siempre acertados, y por tu sencillez en el trato y tu amabilidad. No se me ocurriría una cotutora mejor que tú.

En un momento como este, es importante recordar a José Antonio De Saja, el cual a pesar de habernos dejado antes de lo previsto, dejo una impronta en cada uno de sus "nietos científicos" y un legado que está más vigente que nunca y que ha cristalizado en lo que hoy en día es el grupo CellMatt.

Como es lógico empezar desde los comienzos, quisiera acordarme de la doctora Belén Notario. Tú fuiste la primera persona, la primera referencia, allá por 2013 que tuvo que explicar a un alumno, totalmente ignorante que venía a "colaborar", que era aquello de las espumas, los materiales celulares nano, el proceso de espumado por disolución de gas o la acústica de espumas poliméricas. Con los años, aquel alumno acabo haciendo el trabajo fin de grado (contigo), el trabajo fin de master y el doctorado en el mismo grupo. Te estaré eternamente agradecido por tu paciencia, simpatía y por enseñarme gran parte de lo que sé.

A la doctora Cristina Saiz, gracias por mostrarme que con trabajo y perseverancia se puede llegar a donde quieras. A los doctores Leandra Oliveira y Alberto López por vuestra simpatía y ayuda. A los doctores Javier Pinto y Suset Barroso, por vuestras buenas ideas durante la tesis y por mostrarme como se ha de celebrar correctamente una tradicional fiesta de cumpleaños cubano. Seréis unos padres estupendos. A la pareja inseparable de doctoras Vicky y Judith. No me dedicare a exponer aquí vuestra calidad científica, creo que con mirar brevemente todas vuestras publicaciones uno se hace una pequeña idea. Pero si me gustaría destacar toda la ayuda que me habéis prestado, no solo durante el doctorado, si no durante toda la carrera de física, habéis sido unas veteranas magnificas, os deseo la mejor de las suertes.

Quiero también agradecer a Emi, porque sin ella todo ese ingente papeleo de facturas, contratos, etc. me habría sido imposible de llevar a cabo. Espero que estés disfrutando de una más que merecida jubilación. A ti Blanca, te tengo que agradecer tu disponibilidad, tu sinceridad, toda esa cantidad de DSC, TGA, SEM que me hiciste para la tesis, y tus intentos, con el tiempo más exitosos, de "educarnos" en la limpieza y recogida del laboratorio. Fue un verdadero placer haber trabajado contigo. Laura, creo que siempre has sido una "madre" para todos los doctorandos de CellMat, una persona a la que puedes pedir consejo sobre cualquier asunto y en la que puedes confiar. A mayores de tu calidad humana, eres una gran profesional y una de las personas más metódicas que he conocido. Este mundo necesita más personas como tú. De ti Puri, siempre me sorprendió comprobar que eres una persona con una vasta cultura, que sabe y puede hablar casi

de cualquier tema. Gracias también por toda esa preparación de DSC, y esa perfección hasta el último decimal.

Muchas gracias Heura por tu humor y la forma que tenías de alegrar los días, *que tinguis molta sort.* Agradezco a los doctores Saúl y Eusebio, por todo lo que aprendí de ellos, a Haritz y Adriana, por su trabajo durante el poco tiempo que pudimos coincidir y a Dani Velasco por sus ideas y ocurrencias, en especial para las bromas. Como no, agradecer a Josías, por ser una autentica m*achina* humana. Eres un tío realmente increíble, capaz de montar y desmontar cualquier artilugio y hacerlo parecer fácil y divertido. Ha sido un privilegio trabajar contigo. A Patri, eres una persona risueña, que alegra a todos a los que tienes cerca. Además, eres una trabajadora incansable y la persona que conozco que tiene más jerséis y objetos con motivos de Disney.

A los *churros*, os podría agradecer por mil razones, todos sois maravillosos, y lo hemos pasado realmente bien durante todos estos años. Sin embargo, intentare particularizar un poco más este agradecimiento. A Sergio, le doy las gracias por su carácter y voluntad para aprender, así como por demostrarme cuantas vueltas puede dar el tubo de acústica antes de salirse de rosca. De Isma siempre recordaré su eterna sonrisa, su amor por el *Pucela*, su gran capacidad para el trabajo y su extraña habilidad de saber cuándo una bebida esta *aguada*. De Dani Cuadra, me quedo con su compromiso con el trabajo y su paciencia para ser expulsado una y otra vez de los grupos de WhatsApp. A Mikel por ser ese punto gamberro en los *churros*, pero dispuesto a echarte una mano en cualquier cosa. Estoy seguro que conseguirás, cualquier objetivo que te propongas, siempre que no haya una vaquilla de por medio. De Pablo (*señor del SEM*) eres un tío grande, enorme dirían algunos, y el gran responsable de la mayoría de las imágenes de esta tesis. Muchas gracias por tantos ratos que pasamos en el cuarto del SEM, aunque estuviese Chayanne de fondo. Nos veremos en aguas más profundas, hasta siempre …*Pirata*. Por último, a ti *Javichu*, cualquier frase que pusiese no haría justicia a lo mucho que me has ayudado durante el doctorado. Sinceramente pienso que, a nivel experimental, esta tesis es tan mía como tuya. Gracias no solo por tu ayuda en el laboratorio, también agradezco esos ratos que compartíamos todos los días en el coche o cuando venías de *palique* a nuestro cuarto. En definitiva, me llevo unos muy buenos amigos con todos vosotros.

Por último, me quedan las personas con las que más tiempo he compartido, los compañeros de cuarto. De ti, doctor Eduardo López solo se pueden hablar cosas buenas, eres un tío de lo más íntegro y honesto que he conocido. Además, eres un tipo brillante en lo científico, sé que te va a ir muy bien en la vida porque a las personas buenas, generalmente las va bien, y si no, siempre puedes dedicarte a hacer pan, "que al fin y al cabo es hacer una espuma". A la doctora Mercedes Santiago, tus infinitas enseñanzas en materia de poliuretano me salvaron la vida en más de una ocasión. Además, me demostraste lo que es ser una trabajadora implacable, un ejemplo de buena persona con todas las letras y, en resumen, una amiga, para siempre. Eres la clase de persona a la que todo el mundo quiere tener cerca, excepto si te llamas *Ronaldo* y eres un gato. A ti, querida Bea Merillas, ejemplo por antonomasia de la locura más maravillosa. Capaz de expresar pena y pesar por una nutria o un ajolote, y al segundo siguiente intentar ver como un león se come a cualquier "*bicho viviente*". Un día me tienes que dar una de esas *pastillas* para ver el mundo con tus ojos. Eres una científica excepcional, con un gran talento y una incuestionable ética de trabajo, pero a la vez una amiga fiel y sincera. El mundo sería un lugar maravilloso si hubiese más personas como tú. Nos vemos en *Nutriopolis*. A ti, mi buen amigo, y reciente doctor, Santi, si la bondad y la sabiduría decidiesen algún día tener un hijo sería una copia de ti. Eres una de las personas más talentosas y excepcionales, que he tenido el gusto de conocer. De nuevo me siento

incapaz de darte las gracias, por tantos y tantos momentos que hemos compartido. Lo único que te puedo decir es que eres uno de esos pocos amigos que se cuentan con los dedos de una mano. Sé que encontraras un trabajo que te haga feliz y lo harás más pronto de lo que crees. Tenemos pendiente un día de estos tomarnos una Coca-Cola o un café, solo uno que nos conocemos. Por último, a Paula Cimavilla, una de las personas más maravillosas y fantásticas que existen. Es demasiado, y no se puede agradecer en pocas palabras lo mucho que me has aportado durante todos estos años de doctorado. Estoy más que seguro que lograras superar todas las expectativas que tenemos puestas en ti, y eso es mucho decir, créeme. Ha sido un placer conocer a una persona tan buena, una trabajadora sin par y la mejor dobladora de voz de cajas de cartón que ha existido en la historia de CellMat.

Finalmente, y como no solo se vive de CellMat durante el doctorado, quiero agradecer de manera general a mis amigos del colegio y de futbol y mis recientes amigos de suiza, que me ayudaron y ayudan a formar mi personalidad. A mis actuales compañeros de Sulzer: Oliver, Claudio, Ulla, Nav, Christopher, Zejdan, Nereo, Francesco, Andreas, Janoi etc. *Thank you very much for all your support and time we have spent together during these two years. Danke Schöne.*

A los compañeros de la carrera, y mis amigos, en especial a Coronas, Suaña, Arturo, Néstor, Edu, Óscar y Camarero, hay gente a los que le toca la lotería, a mí me ha tocado siete veces con vosotros. Seguidamente, a mis antiguos compañeros de árabe, y en particular, a Irene, por tanto y por todo.

Finalmente, a mi familia en general, por guiarme en cada uno de mis pasos y cuidar de mi con infinita caridad y ternura, con especial gratitud a mis padres, gracias por darme la vida, en todos los sentidos. Estas líneas finales son para recordar a mis tíos José y Miguel Ángel, y a mis abuelos Mari y Fermín, que nos dejasteis demasiado pronto. Os agradezco por todas las experiencias vitales que me trasmitisteis. Por último, a la persona más especial, mi abuelo Goyo, allá donde estés. Para mí el éxito de la vida no consiste en ser rico, famoso o poderoso, consiste en parecerme cada día un poquito más a ti.

## Resumen en español.



## CHAPTER 1: Introduction.

## CHAPTER 2: Background and state of the art.



## CHAPTER 3: Materials, production processes and characterization techniques.

# Resumen en español.

“Eintritt nur für verrukte, eintritt kosten der vestand ”

Der Steppenwolf, Herman Hesse.

*“Entrada solo para locos, cuesta la razón”*

El lobo estepario, Herman Hesse.

# ÍNDICE

## 0.1 Introducción

Hoy en día basta con abrir cualquier diario digital, sintonizar una emisora radiofónica o simplemente visualizar cualquier telediario para, a los pocos minutos, poder leer o escuchar la palabra plástico. No es difícil por ello suponer el interés, a cada momento más acuciante, de la población por entender y comprender estos productos. La palabra plástico deriva del griego *plastikós (πλαστικός)* que significa moldear o amasar.[1] Si bien los plásticos sintéticos no son tan antiguos como el origen etimológico de la palabra, estos no se pueden considerar un material novedoso sacado de esta era de desarrollo tecnológico, pues cumplen su centésimo decimocuarto aniversario en 2021.[2] De hecho, la creación del primer plástico termoestable (la baquelita) se atribuye al químico belga, nacionalizado estadounidense, Hendrick Baekeland en 1907.[3]

Los plásticos sintéticos, realizados a partir de productos naturales, son aún más antiguos. En 1856 Alexander Parkes desarrolló a través del nitrato de celulosa un material, la parkesina, que era duro como el marfil y a la vez flexible como el papel, que era opaco y resistente a la humedad, y que era posible calentarlo y moldearlo.[4] Doce años después, en 1868, la empresa Phelan and Collander prometió la cuantiosa suma, para la época, de 10.000 dólares a aquel que pudiese sustituir el marfil en la producción de bolas de billar.[5] John W. Hyatt lo consiguió mejorando el material desarrollado por Alexander Parkes gracias a la sustitución del aceite de ricino, usado por Parkes en su producto, por el alcanfor.[6] El nuevo material conseguido fue llamado celuloide, denominación que sigue hasta hoy en día y las bolas de billar de celuloide se reconocen actualmente como el primer producto de la historia que fue desarrollado empleando plástico.[7] Desde entonces ha transcurrido mucho tiempo y la síntesis de múltiples macromoléculas ha dado lugar a una carrera desenfrenada y vertiginosa en la producción de nuevos plásticos. Aun así, hay que hacer una apreciación, si bien todos los plásticos son polímeros, no ocurre el mismo supuesto a la inversa. Solo se pueden considerar plásticos a aquellos polímeros que presentan propiedades plásticas, aunque por abuso de lenguaje se ha adoptado la denominación de plástico para la mayoría de los materiales poliméricos. Continuando con el resumen cronológico, en 1912, unos pocos años antes de la primera guerra mundial, la patente de los alemanes Klatte y Zacharias dio lugar a la polimerización del cloruro de vinilo, que posteriormente se convertiría en el policloruro de vinilo (PVC).[8] La década 1930 trajo consigo la generación de múltiples patentes de nuevos productos

sintetizados. Entre ellos encontramos la síntesis del polietileno de baja densidad (LDPE) por Reginald Gibson y Eric Fawcett.[9] El desarrollo de la poliamida 6 (Nailon), en 1933, por Wallace Carothers o la síntesis del poliuretano (PU) por Otto Bayer en 1937.[10,11] En esta década también observamos la primera producción de manera industrial del poliestireno (PS), en 1930, por el grupo alemán de empresas químicas Interessen-Gemeinschaft Farbenindustrie AG (IG Farben).[12] Este grupo sería disuelto al término de la segunda guerra mundial (1949) por, entre otros motivos, la producción del llamado gas Zyklon B usado durante el Holocausto.[13] Múltiples empresas de aquellas que formaban el grupo IG Farben se refundaron y han llegado hasta nuestros días con nombres tan conocidos como BASF, Bayer o Sanofi Aventis. De la escasez de la guerra y la apremiante necesidad del Reino Unido en 1941 de sustituir el algodón proveniente de Egipto por otra materia nació el tereftalato de polietileno (PET), desarrollado por los británicos Whinfield y Dickson.[14] Así pues, una cantidad ingente de los materiales plásticos más convencionales provienen de tiempos cercanos a la segunda guerra mundial. Sin embargo, algunos polímeros usados hoy en día, no fueron desarrollados hasta unos cuantos años después. Dentro de este grupo de materiales más modernos encontramos al polipropileno (PP) y al polietileno de alta densidad (HDPE) obtenidos en 1951 y 1953, respectivamente, gracias a los trabajos de Zieggler y Natta, ambos ganadores del Premio Nobel de Química por los catalizadores que llevan su nombre.[15] En 1954 la empresa americana DuPont patentó el proceso creado por Carothers en 1932 para calentar el ácido láctico y someterlo a vacío logrando una sustancia a la que llamarían ácido polilactico (PLA).[16] Algunas de las fotos de los investigadores y laboratorios citados se encuentran en la **Figura 0.1**.

Todos los polímeros anteriormente mencionados son utilizados para un sinfín de aplicaciones desde las más especializadas como, por ejemplo, los trajes de Neopreno, para resistir unas temperaturas muy bajas en los deportes acuáticos, o chalecos antibalas realizados con Kevlar hasta productos más comunes como juguetes para niños o films para embalaje de productos alimenticios, utensilios desechables o bolsas de basura.[17–21] Además de tener múltiples aplicaciones, los plásticos son utilizados en sectores muy diversos: construcción, transporte, envase y embalaje, electrónica, medicina, etc.[22,23] Este hecho hizo que la producción mundial de materiales plásticos se pronosticase en una cifra de 500 millones de toneladas para 2020, a pesar del impacto del COVID 19.[24] En la revista Science Advances, Roland Geyer et al. calcularon que el volumen total de todo el plástico producido a lo largo de la historia es de 8300 millones de toneladas de

los cuales casi 5000 millones de toneladas se encuentran en vertederos o en medios naturales formando, por ejemplo, un protocontinente en el océano Pacífico.[25] Es por ello indispensable buscar soluciones para hacer que la cantidad de plástico desechado se reduzca considerablemente. Para ello, rutas como el estudio de la biodegradabilidad de los plásticos, que permiten modificar su estructura química y descomponerles en componentes compatibles con el medio ambiente, el reciclado de plásticos para su posterior reutilización como materia prima de nuevos productos o el proceso de espumado, que permite producir materiales celulares poliméricos donde parte de la fase sólida integrada por el polímero es sustituida por aire, son de gran ayuda. [26–28]

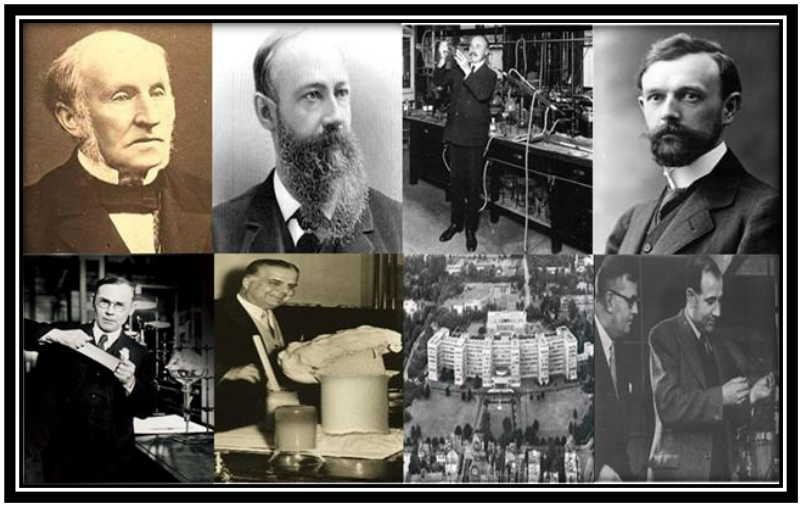

**Figura 0.1**. De izquierda a derecha y de arriba abajo: Alexander Parkes, J. W. Hyatt, Hendrick Baekeland, Fritz Klatte, Wallace Carothers, Otto Bayer, I. G. Farben, Whinfield y Dickson.

## 0.2 Materiales Celulares

Un material celular es aquel compuesto por dos fases bien diferenciadas: una fase gaseosa que se encuentra dispersa en una matriz solida continua.[29] La naturaleza presenta multitud de ejemplos de estos materiales celulares como se puede apreciar en la **Figura 0.2**.

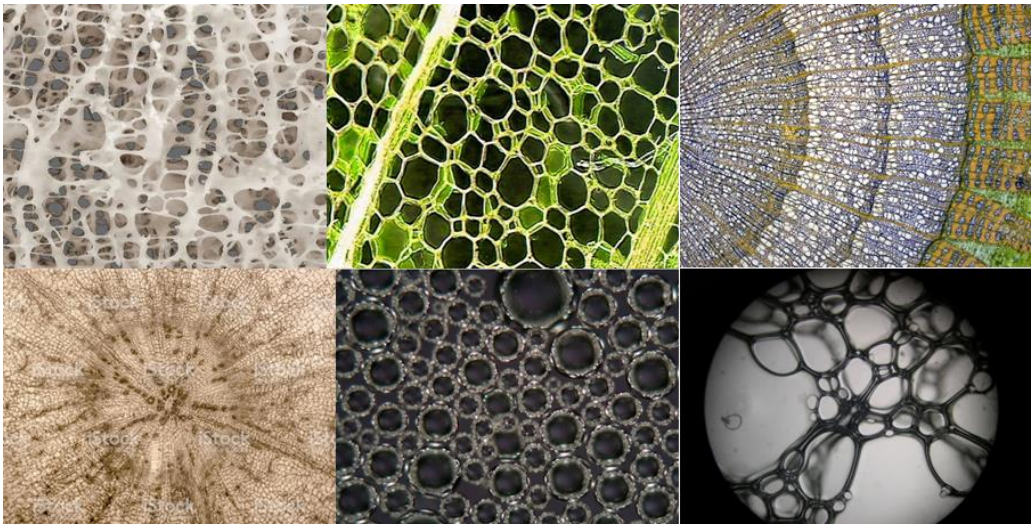

**Figura 0.2**. Ejemplos de estructuras celulares presentes en la naturaleza. De izquierda a derecha y de arriba abajo: interior de un hueso, madera de balsa, tallo de Tilo, estructura celular del interior de una zanahoria, burbujas de la cerveza, clara de huevo.

Debido a las excelentes propiedades que presentan estos materiales celulares naturales, el ser humano ha intentado recrearlos artificialmente usando como material base: metales, cerámicas, o polímeros.[29–31] Por lo tanto, los materiales celulares poliméricos son aquellos cuya estructura sólida viene dada por una matriz polimérica.

La generación de una estructura celular permite reducir el peso de los materiales y el consumo de materia prima, así como los costes de producción. Además, estos materiales presentan una serie de propiedades únicas y realmente interesantes que les han hecho ocupar un lugar privilegiado en múltiples sectores. Entre estas propiedades es importante destacar su capacidad para funcionar como aislantes térmicos, gracias a su baja conductividad térmica, sus buenas propiedades mecánicas en especial la absorción de energía al impacto, en materiales de baja densidad, o una alta relación rigidez/peso, así como una alta flotabilidad y capacidad de amortiguamiento.[32] También pueden emplearse en aplicaciones que requieren de una buena permeabilidad magnética, una alta absorción o baja transmisión acústica o en aplicaciones que demanden una elevada resistencia química.[23] Estas propiedades convierten a los materiales celulares en candidatos perfectos para satisfacer los requerimientos de un número ingente de sectores tecnológicos. Por otra parte, la posibilidad de fabricar materiales celulares empleando diferentes matrices poliméricas, así como la posibilidad de modificar la estructura celular, mediante el uso de aditivos o modificando los parámetros de procesado, nos permite diseñar y producir un material único para cada aplicación logrando así obtener los llamados materiales a la carta.

Los principales sectores industriales donde los materiales celulares encuentran una mayor aplicación son: el sector de la construcción, gracias a su capacidad de aislamiento y a su elevada rigidez y resistencia en relación a su peso, en el sector aeronáutico por su ligereza y la capacidad de cumplir requerimientos muy específicos, en el sector alimenticio en particular en aplicaciones de envase y embalaje debido a su bajo coste y a su buena resistencia al impacto, en el sector de la automoción, que demanda productos ligeros con una alta amortiguación, una buena resistencia a la fatiga y al impacto o en otros sectores lúdicos como son el de los juguetes y el sector deportivo.[33–36] En la **Figura 0.3** vienen recogidos en forma de imágenes un conjunto de ejemplos de materiales y sectores donde los materiales celulares poliméricos juegan un papel crítico y definitivo.

**Figura 0.3.** Ejemplos de materiales y sectores industriales que utilizan los materiales celulares poliméricos de manera habitual.

Entre las matrices poliméricas más utilizadas para producir materiales celulares encontramos poliuretano (PU), el poliestireno (PS), el policloruro de vinilo (PVC), y las poliolefinas (PO).[37–41] Todas estas matrices presentan unas propiedades fisicoquímicas realmente interesantes que repercuten en las aplicaciones finales de los materiales celulares. Para tener una idea de la importancia de las espumas fabricadas con estas matrices la **Figura 0.4(a)** representa el aumento del mercado de espumas (en billones de dólares) estimado entre los años 2014 y 2025, en los Estados Unidos de América, clasificado por tipo de matriz polimérica.[42] En la gráfica se puede ver como las espumas realizadas con matrices de PU y PS son las más consumidas y así se espera para los próximos años, pero sin lugar a duda tampoco hay que desestimar la importancia de otras matrices como el PVC o PO

que presentan año a año un notable aumento. Por último, con un mercado inferior quedan recogidas en esta grafica las espumas producidas con matrices de melamina y espumas realizadas con otras matrices poliméricas.

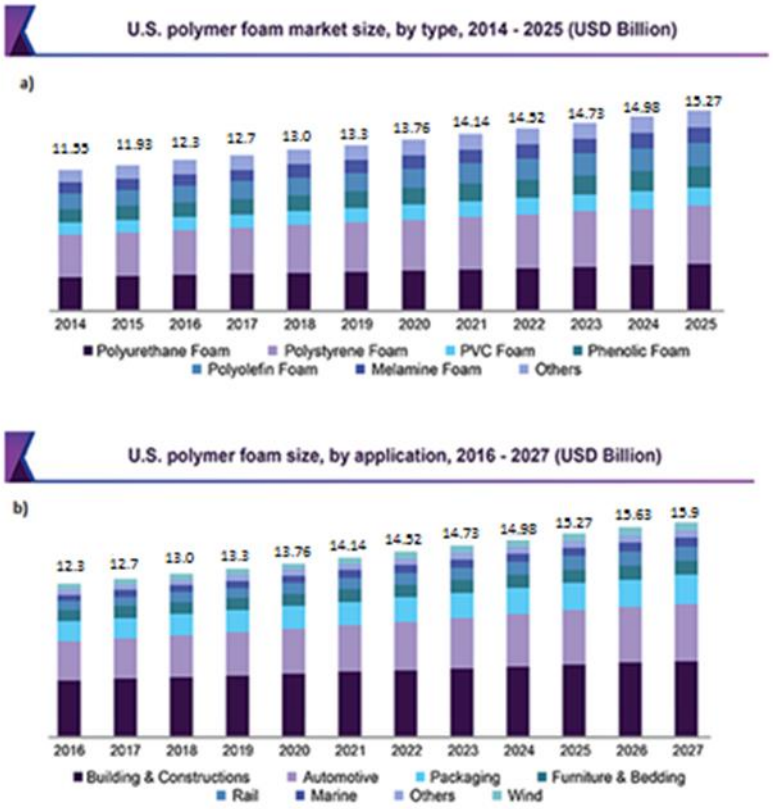


**Figura 0.4**. **a)** Mercado estadounidense de espumas poliméricas durante los años 2014-2025, clasificado por tipo de matriz polimérica. **b)** Mercado estadounidense de espumas poliméricas durante los años 2016-2027, clasificado por sector de aplicación.

Así mismo la **Figura 0.4(b)** analiza el mercado de las espumas en Estados Unidos durante el periodo de años de (2016-2027) en billones de dólares americanos, clasificado por aplicación.[42] En la citada figura se divide, para cada año, los valores totales de mercado en función de la aplicación o sectores donde se prevé que las espumas serán más utilizadas. La triada de los sectores de la construcción, automoción y embalaje representan más del 60% del volumen de mercado de las aplicaciones habituales de las espumas.

Los materiales celulares en base PVC son principalmente utilizados en la producción de perfiles, laminas o tubos que encuentran cabida en sectores tan diversos como elementos de decoración ya sea en expositores, escaparates, interiores, cartelería o rotulado, así como formando parte de paneles sándwich usados en aplicaciones de la marina o en la producción de ciertas piezas de yates o aviones.[43] Así mismo son útiles para el diseño de maquetas o de elementos de

atrezo en obras de teatro.[44] Finalmente, debido a sus buenas propiedades de resistencia a la humedad y a los agentes externos del clima, también son utilizados en el interior de tuberías o de sistemas de canalización.[45] Las espumas basadas en PO (por lo general las realizadas con base PP y PE) presentan unas buenas propiedades mecánicas y elastómeras, respectivamente. Estas propiedades hacen que estos materiales puedan ser utilizados en aplicaciones de piezas de automoción como elementos de absorción de impacto o aislantes acústicos en el sector del envase y embalaje o para aplicaciones de confort como colchones o elementos protectores de diversas piezas, así como para aislamiento de tuberías gracias a su capacidad de barrera contra el agua.[46–48] Los materiales celulares de PU rígido (PUR) se emplean principalmente como aislantes térmicos en edificios o electrodomésticos (en particular frigoríficos), debido a su buena capacidad como aislantes térmicos.[49] Por su parte las espumas de PU flexibles (PUF) se encuentran en aplicaciones donde se requiera un buena absorción acústica o una alta elasticidad.[50] Su mayor nicho de mercado son elementos como: techos de automóviles, colchones, asientos, embalaje, etc.[51] Finalmente, las espumas producidas en base PS se utilizan comúnmente en aislamiento de edificios gracias también a su buena capacidad como aislante térmico (esta espuma generalmente es el competidor por excelencia del PUR).[52] Así mismo también se emplea en aplicaciones arquitectónicas como bases o soportes de pilares ornamentales, como material de envase de yogures, o como material de protección para el embalaje de distintos productos, o en aplicaciones más específicas como rellenos ligeros en la construcción de carreteras y railes o en los cascos para las bicicletas, en las tablas de surf, etc.[53]

En esta tesis se ha seleccionado el PS como matriz polimérica**, con el objetivo de estudiar, entender y mejorar las características estructurales y las propiedades térmicas de las espumas producidas con este polímero.** La importancia de los materiales celulares poliméricos en base PS es tal que, por ejemplo, en el caso de Estados Unidos en el año 2017 el volumen de mercado del PS general y del PS expandido (EPS) se cifró en 35 billones de Dólares Americanos.[54] Así mismo se espera que para el periodo de 2018 a 2025 la tasa de crecimiento anual compuesto (CAGR) arroje valores cercanos al 4.5%.

La elección de este polímero no es casual y se debe a sus buenas propiedades. El PS es un material que presenta una buena capacidad de espumar, en un rango diverso de pesos moleculares, y una buena capacidad para dispersar en él partículas, tanto orgánicas como inorgánicas, debido a sus bajas temperaturas de

procesado y su buena compatibilidad y miscibilidad usando procesos de mezclado habituales como extrusión [55]. Respecto a las espumas de PS, estas se caracterizan por sus bajas conductividades térmicas y sus buenas propiedades mecánicas, lo que a la postre refleja una gran capacidad para funcionar como aislantes térmicos. Así mismo, las espumas de PS tienen otras grandes ventajas como su baja capacidad de absorción de agua, su incapacidad de congelarse o su resistencia a ciertos agentes naturales como los hongos.[56] Industrialmente las espumas de PS se suelen producir mediante dos métodos diferentes dando lugar a las espumas de PS extruido (XPS) y a las espumas de PS expandido (EPS).[54,57–59] Sin embargo, la conductividad térmica de las espumas de PS es todavía superior a la de otros materiales típicamente utilizados en el sector de la construcción como el PUR. Mientras que las espumas de PS tienen conductividades de 34 mW/mk (medidas a una temperatura de 10 ºC), las espumas de PUR tienen conductividades de 23 mW/mK a la misma temperatura.[60–62]

Esta tesis, tendrá como finalidad mejorar **las propiedades térmicas de estos materiales, es decir, reducir su conductividad térmica,** con la idea de que sean más aptos para la citada aplicación. La finalidad de este trabajo consiste en diseñar nuevas formulaciones que permitan fabricar espumas de PS de baja densidad y con una estructura celular óptima que permita minimizar su conductividad térmica.

Para reducir la conductividad térmica de una espuma se pueden utilizar diferentes estrategias. Desde trabajar con agentes espumantes que tengan baja conductividad térmica, pasando por la incorporación de bloqueadores de infrarrojo (IR) o la modificación de la estructura celular, entre otras.[63–65] Para el presente trabajo, se intentara reducir la conductividad térmica cambiando la estructura celular, reduciendo el tamaño de celda hacia valores micrométricos sin incrementar la densidad relativa de las espumas. Para ello se incorporarán nanopartículas inorgánicas y fases poliméricas orgánicas.

Dentro de los materiales celulares, es importante hablar de los materiales micro celulares, es decir aquellos que presentan celdas con un tamaño de decenas de micras, aproximadamente.[66] Estos materiales nacieron en la década de 1980 en el MIT (Instituto Tecnológico de Massachusetts), motivados por la problemática de encontrar materiales que permitiesen reducir la cantidad de material plástico empleado sin reducir por ello su desempeño mecánico.[21] Mediante las tesis de máster realizadas por Waldman y Martini y su patente común con el profesor Shu, se llegó a la conclusión de que dotar al material de un mayor número de

celdas (mayor de $10^9$ celdas por $cm^3$) con un tamaño inferior a los 100 micrómetros, que solían tener las espumas con menor tamaño de celda en aquella época, haría posible que ciertos productos pudiesen reducir su contenido plástico, y por ende su espesor, sin comprometer sus propiedades mecánicas.[67,68] Sin embargo, la producción de estos materiales necesitaba de nuevos métodos de espumación.[69] El proceso de espumado por disolución de gas permite la introducción del agente espumante, y su difusión en la matriz polimérica a unas ciertas condiciones de temperatura y presión.[70–73] Actualmente el método de espumado por disolución de gas es uno de los más utilizados a escala de laboratorio para producir materiales microcelulares (algunos con tamaños de celdas menores que una micra) e inclusive en la década de los 2000 los avances en las tecnologías de espumado permitieron el desarrollo de una nueva generación de materiales celulares con tamaños de celda menores que los 500 nanómetros (materiales nanocelulares) y propiedades que actualmente se encuentran en estudio.[32,71,74–76] Sin embargo, uno de los mayores impedimentos que encuentran estos materiales nanocelulares para imponerse en el mercado actual es que hasta la fecha no se han podido escalar satisfactoriamente de un ambiente de laboratorio a un proceso industrial.[77]

La generación de materiales celulares mediante procesos de espumación es un fenómeno que se ha estudiado en detalle en diversos artículos científicos.[78,79] Los mecanismos del proceso de espumado son: nucleación, crecimiento, degeneración y estabilización. Una vez que el gas está disuelto en la matriz polimérica una inestabilidad termodinámica (reducción brusca de la presión o aumento de la temperatura) produce una separación de la fase sólida y gaseosa dando lugar a pequeños agregados de gas conocidos como puntos de nucleación. Posteriormente, el gas, de la mezcla polímero/gas, difunde hacia los puntos de nucleación. Los núcleos crecen como resultado de esa entrada de gas que está ocurriendo, dando lugar a las celdas del material celular. Para que esto ocurra es necesario aportar temperatura al sistema para permitir que las cadenas poliméricas adquieran movilidad. Si la estructura celular no se estabiliza en el instante adecuado, por ejemplo enfriando rápidamente el material celular, o si el material no tiene una resistencia en fundido adecuada, tendrán lugar los mecanismos de degeneración (coalescencia, engrosamiento y drenaje) que dan como resultado estructuras celulares heterogéneas, celdas de mayor tamaño, celdas abiertas, e incluso un aumento de la densidad del material celular[23,80,81]

Todos estos mecanismos son bien conocidos por la comunidad científica. Un esquema con los mismos puede verse en la **Figura 0.5.**


**Figura 0.5.** Esquema de los mecanismos del proceso de espumado.

El control de los mecanismos de espumado, en particular de las fases de nucleación y degeneración, tendrá una influencia crítica en la posterior estructura celular. Una estrategia para controlar la nucleación consiste en introducir agentes nucleantes en la matriz polimérica. En el presente trabajo se introducirán tanto agentes nucleantes inorgánicos, sepiolitas, como agentes nucleantes orgánicos, estireno-etileno-butileno-estireno (SEBS). Tras la incorporación de estos aditivos, la nucleación dominante pasa de ser una nucleación homogénea a ser una nucleación heterogénea, que necesitará de menos energía para ocurrir. La teoría de la nucleación se analizará con detalle en el Capítulo 2 de la presente tesis. Así mismo, artículos y trabajos anteriores han situado al grado de dispersión de los agentes nucleantes en las matrices poliméricas como uno de los parámetros fundamentales para tener una nucleación eficiente.[82,83] Si la dispersión del agente nucleante en la matriz polimérica no es adecuada puede ocurrir que el material celular generado tenga una estructura celular más imperfecta (mayores tamaños de celda, mayor heterogeneidad, etc.) que la obtenida con el polímero virgen. Teniendo en cuenta estas ideas, un punto fundamental de la presente tesis se centra, por un lado, en analizar el grado de dispersión de los agentes nucleantes (sepiolitas y SEBS) en la matriz polimérica (PS) y, por otro lado, en entender como el grado de dispersión obtenido condiciona las características estructurales y las propiedades físicas de los materiales espumados generados. Como se indica en la **Figura 0.5**, tras la etapa de nucleación comienza la etapa de crecimiento de las celdas. Durante el proceso de crecimiento celular el polímero, localizado en la estructura de las paredes celulares, se ve sometido a una fuerza extensional que induce una deformación que aumenta con el crecimiento de las celdas. Aunque se haya conseguido una dispersión óptima de las partículas en la matriz polimérica y, por lo tanto, una nucleación adecuada, si la matriz polimérica no presenta una resistencia adecuada a estas fuerzas extensionales, las paredes celulares se romperán favoreciendo así los mecanismos de degeneración celular.[84,85] El comportamiento reológico extensional (entendido como la manera en la que la viscosidad extensional de los polímeros depende de la extensión a la

que éstos son sometidos), condiciona la capacidad de espumar (o espumabilidad) de un polímero y, es un aspecto fundamental para obtener materiales celulares con una baja densidad y con una estructura celular adecuada (pequeños tamaños de celda, bajos contenidos de celda abierta, estructuras homogéneas, etc.).[23] Es por ello necesario que el polímero presente un aumento de la viscosidad a medida que las fuerzas extensionales aumentan. A este fenómeno se le conoce como endurecimiento por deformación (*strain hardening*). Así pues, el control del grado de dispersión de los agentes nucleantes en la matriz polimérica, así como el estudio del endurecimiento por deformación de las formulaciones realizadas, proveerá de un conocimiento necesario para entender el comportamiento del material durante el proceso de espumado. Además, varios trabajos han demostrado que las propiedades finales de los materiales celulares (propiedades térmicas, mecánicas o acústicas) van a depender de una manera crítica de las estructuras celulares obtenidas.[33,71,86]

En la presente tesis las espumas de PS se fabricarán mediante un proceso de disolución de gas en autoclave (este proceso se explicará con detalle en el Capítulo 2 de esta tesis). El proceso de disolución de gas en autoclave ofrece una gran versatilidad y es posible producir espumas empleando diferentes matrices poliméricas, así mismo, la cantidad de material requerido para realizar las espumas no es tan elevado como con la extrusión, por ejemplo. Así mismo, este proceso permite la modificación de múltiples variables: la presión, la temperatura o los tiempos de saturación que ayudan a encontrar unas condiciones óptimas para el espumado de una determinada matriz polimérica. Por último, es posible escalar a procesos industriales que requieren un mayor coste (como puede ser el espumado por extrusión) los datos y valores obtenidos en el proceso de espumado por disolución de gas usando un autoclave.

En resumen, para generar los materiales celulares adecuados es necesario seleccionar las mejores formulaciones posibles, de acuerdo con las características propias del polímero base, así como estudiar la dispersión de los agentes nucleantes orgánicos e inorgánicos y las propiedades reológicas que afectarán al proceso de espumado. Una vez realizados estos estudios, se analizará si existe una relación entre la formulación y los parámetros de fabricación con las estructuras celulares conseguidas. Finalmente, se analizará la relación entre la estructura celular y las propiedades finales de las espumas (en este caso la conductividad térmica). Todos estos trabajos permitirán cumplir con el objetivo fundamental de la presente tesis, que es el análisis exhaustivo del círculo

composición, proceso, estructura, propiedades para materiales celulares basados en PS.

## 0.3 Marco de la Tesis

Esta tesis se ha realizado en el laboratorio de materiales celulares (Laboratorio CellMat: www.cellmat.es) del Departamento de Física de la Materia Condensada, Cristalografía y Mineralogía de la Universidad de Valladolid.[87] CellMat está dirigido por el Prof. Dr. Miguel Ángel Rodríguez Pérez, el cual es también codirector de la presente tesis doctoral.

CellMat nace en el año 1999 de la mano del Prof. Dr. José Antonio de Saja Sáez y el mencionado Prof. Dr. Miguel Ángel Rodríguez Pérez con el ánimo de desarrollar un laboratorio centrado en el estudio de los materiales celulares.

En los primeros años la principal actividad del laboratorio fue la caracterización de espumas, en especial aquellas basadas en poliolefinas.[88] No fue hasta 2005 que el laboratorio pudo adquirir los equipos necesarios para la producción de materiales celulares, dando como resultado que en el año 2012 se presentase una tesis que analizaba la relación entre la producción, la estructura celular y las propiedades de materiales celulares a cargo de la Dr. Cristina Saiz Arroyo.[33] Desde entonces y con el transcurrir del tiempo y las tesis, el grupo se ha ido especializando en temas de producción (optimización de formulaciones y parámetros de procesado), estudios de los mecanismos de espumado mediante diferentes técnicas no convencionales (radioscopía de Rayos-X, termografía IR, expandometría óptica, reología extensional, etc.), caracterización de la estructura y propiedades de los materiales celulares, y modelización (relación entre formulación, estructura y propiedades). CellMat cuenta en la actualidad con diversas líneas de investigación, como el estudio de materiales microcelulares y nanocelulares, la producción de materiales celulares basados en bioplásticos, la producción de materiales celulares reactivos, en concreto PU tanto rígido como flexible, el estudio de nanocompuestos celulares y la investigación en materiales celulares multifuncionales.[32,38,39,76]

Todas las investigaciones completadas en CellMat tienen en su propósito un afán de aplicabilidad, ya que uno de los principales objetivos de este grupo es la relación y transferencia de conocimiento entre la Universidad y la industria, dotando a esta última de unos fundamentos que la hacen progresar

susceptiblemente más rápido. Prueba de esta relación universidad-industria, nació en 2012 una empresa spin-off llamada CellMat Technologies S.L.

En el año 2014, CellMat consigue un gran hito; producir materiales nanocelulares, convirtiéndose CellMat en uno de los laboratorios pioneros en la producción de este tipo de materiales. La primera tesis que abordo este tema fue la presentada por el de Dr. J. Pinto Sanz.[89]

Parte del trabajo de investigación realizado en la presente tesis es una continuidad de aquel defendido en 2016 por la Dra. Ester Laguna Gutiérrez, codirectora de este trabajo, focalizado en explicar la espumabilidad de un conjunto de materiales a través del estudio de la reología extensional. Esta es una de las tesis que mantiene la filosofía de establecer una relación entre la estructura del material, su producción o métodos de producción, su estructura celular y las propiedades finales de la espuma.[23]

Como se ha mencionado, todas las investigaciones en CellMat tienen como base analizar y entender las relaciones entre producción, estructura, propiedades y aplicaciones a través de la determinación experimental de los diferentes parámetros involucrados en cada etapa y mediante el uso de modelos teóricos. Este concepto se resume en el tetraedro a de la **Figura 0.6** que recoge los temas que típicamente se abordan en cualquier investigación realizada en el laboratorio CellMat.

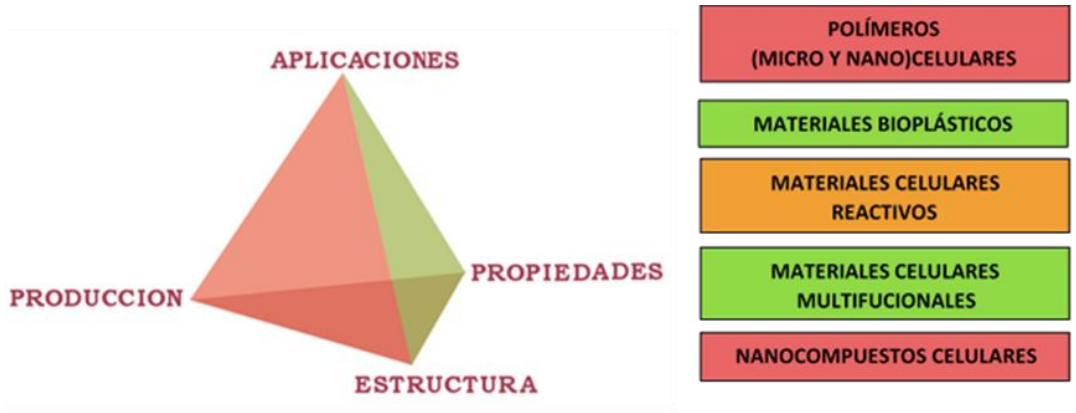


**Figura 0.6.** Tetraedro que representa los puntos básicos que persiguen las investigaciones en el grupo CellMat. A la derecha líneas básicas de las investigaciones en curso en el grupo CellMat.

Actualmente CellMat es un laboratorio de referencia mundial en el estudio, desarrollo y producción de materiales celulares. Fruto de ese trabajo se han

podido realizar más de 240 publicaciones en revistas indexadas y se han defendido 32 tesis doctorales.[87]

El trabajo de investigación que se presenta aquí es una continuidad de los primeros trabajos que estudian la relación composición-producción-estructura-propiedades y se nutre de toda la experiencia y conocimiento previo. Así pues, se podría encuadrar esta tesis en las líneas de investigación del estudio de materiales microcelulares, investigación en materiales multifuncionales y el estudio de nanocompuestos celulares. Así mismo también se intenta dotar al material de un posible marco para posteriores aplicaciones. Con este propósito se eligió el PS como matriz polimérica ya que es un material versátil que, como se ha mencionado anteriormente, cubre un gran espectro del mercado actual en espumas. El proceso de producción se ha modificado de múltiples formas, estudiando la influencia de diversos parámetros, tanto intrínsecos del material, como de producción en la posterior estructura celular obtenida. Además, se han estudiado algunas de sus propiedades físicas, en particular las propiedades térmicas.

Es importante mencionar que parte de esta tesis se enmarca en el proyecto NEOADFOAM (Aditivos Innovadores para Espumas con mejores Prestaciones de Aislamiento Térmico y Comportamiento frente al Fuego) relativo al programa Retos Colaboración 2015 del Ministerio de Economía y Competitividad del Gobierno de España. El proyecto tenía como objetivo fundamental el desarrollo de una familia de aditivos multifuncionales para espumas poliméricas. Dichos aditivos estarían basados en partículas inorgánicas, en concreto sepiolitas con la posibilidad de su combinación con otros elementos activos que permitiesen mejorar el aislamiento térmico y comportamiento mecánico de las espumas incrementando, a su vez, las prestaciones ante el fuego. El proyecto se centró en dos materiales de gran importancia en el campo del aislamiento térmico como son las espumas de poliestireno extruidas (XPS) y las de poliuretano rígido (PUR).

## 0.4 Objetivos

En esta sección se van a detallar el objetivo principal y los objetivos específicos de este trabajo.

**El objetivo principal consiste en estudiar y entender la relación entre composición, proceso, estructura y propiedades de polímeros celulares en base**

**PS que incorporan nanopartículas inorgánicas (sepiolitas) o partículas orgánicas (SEBS) con la finalidad de reducir la conductividad térmica de los mismos.**

La **Figura 0.7** es una fiel representación de los pasos que se han seguido para conseguir este objetivo. En **primer lugar**, se ha **seleccionado el PS más adecuado en función de su fluidez,** investigando para ello las relaciones entre el peso molecular y algunas características propias del polímero, así como el efecto que causa el peso molecular en el proceso de espumado y en la posterior estructura celular. **Seguidamente,** se han **incorporado agentes nucleantes orgánicos (SEBS) e inorgánicos (sepiolitas) a la matriz polimérica de PS**. En particular se han fabricado formulaciones de PS con tres tipos diferentes de sepiolitas (con diferente tratamiento superficial), donde se ha variado el contenido de sepiolitas, y con un grado de SEBS, donde se ha variado el contenido de este polímero. Estas formulaciones se han diseñado de tal manera que den lugar a unas espumas con propiedades óptimas y que sean factibles de ser escaladas industrialmente. El proceso de mezclado del polímero y los agentes nucleantes se ha realizado utilizando una extrusora de doble husillo (más información sobre este proceso se puede encontrar en el Capítulo 3) empleando distintas condiciones de mezclado, para ver cómo influye este parámetro en los posteriores pasos del ciclo composición-proceso-estructura-propiedades. **Una vez fabricados, estos compuestos se han caracterizado detalladamente para poder determinar propiedades como su comportamiento reológico, grado de dispersión del agente nucleante en el polímero, etc.** Los agentes nucleantes añadidos afectan de una manera crítica a la estructura del polímero. La alteración de las propiedades reológicas del producto (en especial de las propiedades reológicas extensionales que se estudiaran en detalle durante esta tesis), tiene mucho que ver con la posterior espumabilidad y el grado de expansión de las espumas. Todos estos efectos dependerán del tipo de partícula utilizado (composición química, morfología, condiciones de procesado de las partículas etc.), de la concentración empleada y del método de mezclado que permite dispersar las partículas en la matriz polimérica.

A continuación, las **formulaciones** producidas se han introducido en una autoclave para ser **sometidas a un proceso de espumado por disolución de gas** (más información en los Capítulos 2 y 3). Es importarte mencionar que se han modificado los parámetros de procesado y las propiedades de las formulaciones para poder **determinar el efecto que estas modificaciones tienen sobre el**

**propio proceso de espumado (solubilidad, difusividad) y sobre las características de los materiales espumados (densidad, estructura celular).** Por ejemplo, la incorporación de agentes nucleantes inorgánicos puede afectar a los parámetros característicos del proceso de disolución de gas, pudiendo ser que el material compuesto (polímero más agente nucleante) absorba una mayor cantidad de gas que el polímero virgen por sí solo. La afinidad química de los agentes nucleantes añadidos con el gas o bien la morfología de los mismos pueden provocar, como se ha mencionado, que el material compuesto absorba un mayor porcentaje de agente espumante que el polímero puro.[90] Así mismo, cuando un polímero absorbe gas, la reología de este se ve alterada y la viscosidad se ve reducida en lo que se conoce como efecto plastificante. Durante el efecto plastificante lo que ocurre es que el gas dispersado en el polímero hace que las cadenas poliméricas tengan más facilidad para desenrollarse y quedar estiradas, frente a su posición enmarañada habitual en condiciones estándar. Esta mayor movilidad que presentan las cadenas tiene un efecto notorio en la reducción de variables como la temperatura de transición vítrea (temperatura donde el material pasa de encontrarse en un estado sólido a uno gomoso).[41] La mencionada reducción determina las condiciones de espumado (temperaturas, y los tiempos óptimos de este proceso) que pueden ser muy diferentes a los utilizados cuando se trabaja con el polímero virgen. Por lo tanto, es muy importante conocer el efecto en la absorción de gas que tienen los agntes nucleantes que se han incorporado al polímero.

Por otro lado al añadir una segunda fase solida a una matriz polimérica, se promociona la nucleación heterogénea frente a la nucleación homogénea (una explicación más completa sobre el proceso de espumado y los tipos de nucleación se puede encontrar en el Capítulo 2 de esta tesis).[91] La modificación de la nucleación viene principalmente debida a que al añadir una segunda fase se produce un decrecimiento en la barrera energética necesaria para que aparezcan los núcleos (especialmente en la interfase entre polímero y agente nucleante). Así mismo, también modifica la tensión superficial que es responsable de la nucleación.[92] En este caso es fundamental entender como la incorporación de los agentes nucleantes afecta a los mecanismos de nucleación, analizando los efectos asociados a modificar el tipo de agente nucleantes, su contenido y su dispersión en la matriz polimérica.

**La estructura celular se analizará en detalle,** poniendo especial énfasis en como el tamaño de celda, el número de celdas por centímetro cubico también llamado

densidad de celdas, la homogeneidad y regularidad del conjunto de celdas o su naturaleza de celda cerrada o abierta influye en las propiedades finales (en este caso térmicas) de las espumas. Así mismo en el caso de haber una segunda fase presente en las materias primas se podrán obtener estructuras celulares de carácter bimodal (es decir, dos tipos bien diferenciados, en cuanto a tamaño, de celdas). Las citadas estructuras bimodales, serán así mismo caracterizadas con un parámetro llamado fracción volumétrica de celdas, que pondrá de manifiesto el porcentaje presente de cada tipo de celdas en la estructura celular.

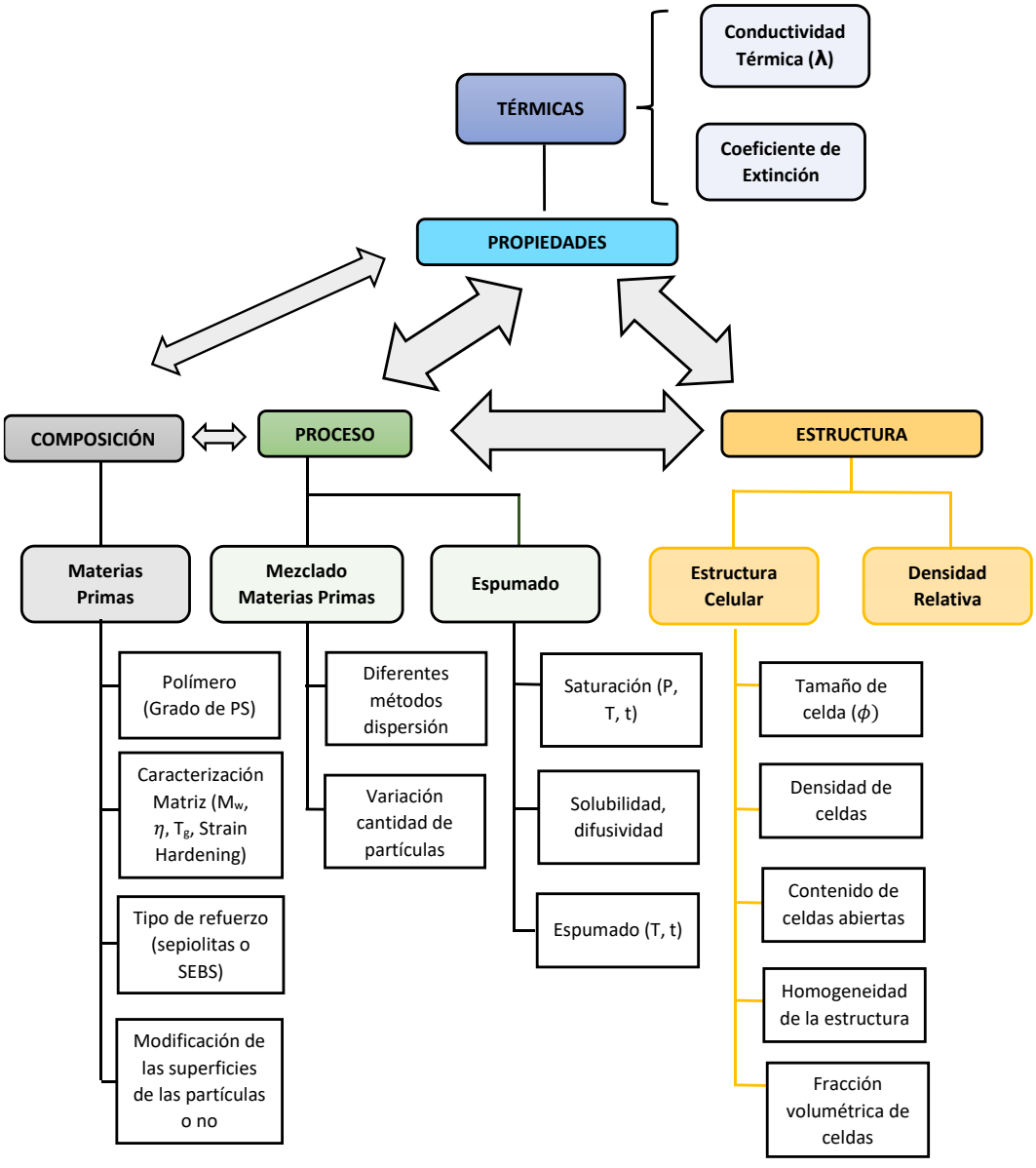


**Figura 0.7.** Esquema de la metodología de trabajo que se ha seguido en la presente tesis.

Por último, se verá cómo tanto la anteriormente citada **estructura celular, como todos los distintos parámetros de proceso y composición, ya mencionados, tienen una importancia capital en las propiedades térmicas de las espumas obtenidas**. Por lo tanto, es un objetivo de esta tesis explicar las diferencias obtenidas en las propiedades de las espumas a través de los distintos pasos dados en las etapas de composición, producción y de la estructura celular obtenida, **cerrando por lo tanto el circulo composición-proceso-estructura-propiedades.**

Para cumplir este objetivo principal, se plantean los siguientes objetivos secundarios:

**Análisis de la influencia del peso molecular del PS en la espumabilidad.**

Esta tarea se ha realizado con la finalidad de seleccionar el PS o PS más adecuados para aplicaciones de espumado que será aquel que permita lograr las mayores reducciones de tamaño de celda y las estructuras celulares más homogéneas y regulares, sin provocar un aumento de la densidad de los materiales celulares. Con el grado de polímero (o grados) más adecuados se realizarán los posteriores trabajos. Para cumplir este objetivo se plantean las siguientes actividades:

- **Determinación del peso molecular de diferentes grados de PS, con diferente índice de fluidez (MFI), empleando diferentes técnicas de medida: reología de cizalla y cromatografía por permeación de gel (GPC).**
- **Análisis de las relaciones entre el peso molecular y otros parámetros como la temperatura de transición vítrea, la viscosidad extensional (y en concreto, el coeficiente de endurecimiento por deformación), la longitud de las cadenas moleculares y el radio de giro.**
- **Influencia del peso molecular del polímero en el proceso de disolución de gas. Para ello se determinará como el peso molecular afecta a parámetros tales como la solubilidad y la difusividad durante el proceso de sorción y durante el proceso de desorción.**
- **Producción de espumas mediante la técnica de espumado por disolución de gas, utilizando $CO_2$ como agente espumante.**
- **Análisis de densidad y de las características estructurales de los materiales celulares generados: tamaño de celda, anisotropía, densidad de celdas, etc.**
- **Análisis de las relaciones entre composición, proceso y estructura celular.**

Después de este estudio será posible conocer que grados de PS son los más adecuado para los procesos de espumado. Estos grados de PS se utilizarán como matrices poliméricas en los estudios centrados en analizar el efecto sobre el proceso de espumado asociado a incorporar partículas orgánicas o inorgánicas. Del presente estudio ha resultado una publicación con título: "***Influence of the Molecular Weight, on the solubility, diffusivity and subsequent cellular structure of PS foams***". El artículo se encuentra actualmente pendiente de enviar a una revista científica para su publicación.

**Inclusión de un agente nucleante inorgánico (sepiolitas) en la matriz de PS. Análisis de la influencia de la dispersión y de las propiedades reológicas extensionales del compuesto PS/sepiolitas sobre la estructura celular de las espumas generadas a partir de estos nanocompuestos.**

El objetivo principal de esta actividad es entender cuál de estos dos parámetros (dispersión o propiedades reológicas extensionales) tiene una mayor influencia en las características de la estructura celular de las espumas. Para ello, durante esta actividad, por un lado, se ha analizado la dispersión de diferentes compuestos poliméricos en base PS que contienen diferentes tipos de sepiolitas, diferentes contenidos de sepiolitas y que además han sido fabricados utilizando diferentes parámetros de procesado (extrusión). Por otro lado, se ha analizado el comportamiento reológico extensional de estos compuestos. Estos análisis se han realizado para, posteriormente, evaluar y entender como la estructura celular de las espumas generadas a partir de estos compuestos se ve afectada por el grado de dispersión alcanzado y por el comportamiento reológico extensional de los mismos, que a su vez están condicionados por su composición y por las condiciones de fabricación empleadas.

Para lograr el objetivo se han propuesto las siguientes actividades:

- **Producción de formulaciones de PS con diferentes tipos de sepiolitas: sepiolitas organomodificadas con sales cuaternarias de amonio, sepiolitas organomodificadas con grupos silano y sepiolitas naturales (sin tratamiento superficial).**
- **Producción de formulaciones de PS con diferentes contenidos de sepiolitas que varían entre un 2 wt.% y un 10 wt.%.**

- **Fabricación de formulaciones (compuestos de PS y sepiolitas) modificando las condiciones de procesado (someter a las formulaciones a un único ciclo de extrusión o a dos).**
- **Análisis de la dispersión de las partículas mediante técnicas de tomografía de Rayos X y reología dinámica de cizalla.**
- **Medición de la reología extensional de las distintas formulaciones.**
- **Producción de espumas, con las formulaciones anteriormente analizadas, mediante el método de disolución de gas, utilizando $CO_2$ como agente espumante y manteniendo constantes los parámetros de espumado.**
- **Análisis de la influencia del grado de dispersión y del comportamiento reológico extensional sobre las características de las estructuras celulares obtenidas.**

Después de este estudio sistemático, podríamos conocer de manera precisa como la dispersión afecta a la nucleación y como el comportamiento reológico extensional afecta a los mecanismos de degeneración celular. De esta manera será posible descubrir cuál de ellas tiene una mayor importancia a la hora de conseguir una estructura celular más homogénea y con mayores reducciones del tamaño de celda cuando se trabaja con formulaciones en base PS. Gracias al análisis de este objetivo han surgido dos publicaciones con títulos: "***Influence of the dispersion of nanoclays on the cellular structure of foams based on polystyrene***" y "***Polystyrene/sepiolites nanocomposite foams:Relationship between composition, particle dispersion, extensional rheology and cellular structure***". Ambos artículos están publicados en las revistas Journal of Applied Polymer Science y Materialstoday Communications, respectivamente.

El conocimiento adquirido, en el objetivo previo, será utilizado para profundizar en el siguiente objetivo secundario de esta tesis:

**Análisis de la relación entre composición, estructura y propiedades térmicas de los materiales en base PS/sepiolitas.**

Este análisis tiene como objetivo el estudio de la relación entre las propiedades térmicas (conductividad térmica y coeficiente de extinción) y la estructura celular obtenida en espumas de PS/sepiolitas. A largo plazo se puede obtener un aprendizaje para el desarrollo de unas directrices que den lugar a un conocimiento exhaustivo de los parámetros que hay que modificar en pos de mejorar las propiedades térmicas de los materiales celulares y de la influencia

que tiene la estructura celular en la conductividad térmica de materiales en base PS. Para la consecución de este objetivo se han llevado a cabo una serie de tareas:

- **Producción de formulaciones de PS con diferentes tipos de sepiolitas: sepiolitas organomodificadas con sales cuaternarias de amonio, sepiolitas organomodificadas con grupos silano y sepiolitas naturales (sin tratamiento superficial).**
- **Producción de formulaciones de PS con diferentes contenidos de sepiolitas que varían entre un 2 wt. % y un 10 wt.%.**
- **Fabricación de formulaciones (compuestos de PS y sepiolitas) mediante proceso de extrusión con un único ciclo de procesado.**
- **Producción de espumas, con las anteriores formulaciones, mediante el método de espumado por disolución de gas, utilizando $CO_2$ como agente espumante y manteniendo constantes los parámetros de espumado.**
- **Medición de la conductividad térmica de las espumas mediante el método TPS (T*ransient Plane Source*).**
- **Medición del coeficiente de extinción de las espumas producidas mediante espectroscopía IR por Transformada de Fourier (FTIR).**
- **Correlación entre los valores experimentales obtenidos de la conductividad térmica y los valores calculados teóricamente aplicando modelos analíticos.**
- **Análisis de la relación entre la estructura celular y la conductividad térmica obtenida.**

Gracias a este estudio ha surgido una publicación con título: "***Optimum cell size to reduce the termal conductivity of foams based on polystyrene/sepiolites nanocomposites***". El artículo se encuentra actualmente pendiente de enviar a una revista científica para su publicación.

**Inclusión de un agente nucleante orgánico (SEBS) en la matriz de PS. Análisis de la dispersión del mismo y de la estructura celular de las espumas generadas con el compuesto PS/SEBS.**

El último objetivo de esta tesis consiste en evaluar cómo se modifica la estructura celular cuando se introduce en el PS un agente nucleante orgánico, en concreto estireno-butileno-estireno (SEBS). Además, se ha realizado una comparativa entre los efectos obtenidos cuando se incorporan agentes nucleantes inorgánicos

(sepiolitas) y cuando se incorporan agentes nucleantes orgánicos (SEBS). Para alcanzar este objetivo se han realizado las siguientes tareas:

- **Producción de formulaciones de PS /SEBS con diferentes porcentajes de fase orgánica (desde 0.25 wt. % hasta 10 wt. %) usando la extrusora de doble husillo.**
- **Análisis de la dispersión del SEBS en la matriz de PS mediante microscopia electrónica de barrido (SEM).**
- **Fabricación de espumas empleando los compuestos de PS/SEBS mediante espumado por disolución de gas usando $CO_2$ como agente espumante.**
- **Análisis de la estructura celular de las espumas generadas.**
- **Análisis de la relación entre composición, dispersión y estructura celular.**
- **Comparación entre los efectos obtenidos cuando se incorporan agentes nucleantes inorgánicos (sepiolitas o talco) y cuando se incorporan agentes nucleantes orgánicos (SEBS) en una misma matriz polimérica (PS).**

Este análisis ha dado lugar a una publicación con título: "***SEBS an effective nucleating agent for PS foams***". El artículo se encuentra publicado en la revista Polymers.

Los resultados de todas las actividades requeridas para alcanzar los objetivos específicos de esta tesis y por lo tanto para cumplir el objetivo principal se recogen en los Capítulos 4, 5, 6 y 7 de este manuscrito. Además, en la **Tabla 0.1** se indica, de manera resumida, los estudios que se han realizado y los capítulos en los que se incluyen los diferentes resultados obtenidos.

La información y metodología de esta tesis podrá ser utilizada para predecir y seleccionar matrices poliméricas apropiadas para procesos de espumación, teniendo en cuenta diferentes parámetros: su viscosidad, su peso molecular, su temperatura de transición vítrea, su resistencia en fundido, etc. Por otro lado, también permitirá seleccionar el tipo y contenido adecuado de los agentes nucleantes (tanto orgánicos como inorgánicos) que cuando se incorporan a la matriz polimérica permiten optimizar la estructura celular de las espumas generadas y mejorar sus propiedades térmicas (reducción de la conductividad térmica). Esta metodología proporciona una gran ventaja a la hora de seleccionar las formulaciones más adecuadas para producir espumas a escala industrial ya que permitiría seleccionar las matrices poliméricas y agentes nucleantes que den lugar a las espumas con las mejores propiedades térmicas, únicamente

caracterizando las propiedades de los compuestos sólidos generados, sin necesidad de fabricar las espumas. Esto supone una importante reducción de costes derivados de la selección de una formulación óptima y también una importante reducción de tiempo.

| *INFLUENCIA PESO MOLECULAR EN EL PS (CAPÍTULO 4)* |
|---|
| • **Determinación del peso molecular** de diferentes grados de PS.<br>• Análisis de las **relaciones entre el peso molecular** y **otras propiedades** de los PS.<br>• **Influencia** del **peso molecular** del polímero en la **solubilidad y difusividad** del $CO_2$.<br>• **Producción de espumas mediante la técnica de espumado por disolución de gas, utilizando $CO_2$ como agente espumante.**<br>• **Análisis de la estructura celular** de las espumas generadas.<br>• **Análisis de las relaciones entre el peso molecular, el proceso de espumado y la estructura celular.** |
| *PS/SEPIOLITAS (CAPÍTULOS 5 Y 6)* |
| • **Análisis de la dispersión de las sepiolitas en una matriz de PS, en función de su modificación superficial, del su contenido y de las condiciones de proceso.**<br>• **Análisis de las propiedades reológicas extensionales de las diferentes formulaciones de PS/Sepiolitas.**<br>• **Fabricación de espumas, utilizando las formulaciones previamente fabricadas y analizadas, mediante espumado por disolución de gas, utilizando $CO_2$ como agente espumante.**<br>• **Caracterización de la densidad y de la estructura celular de las espumas generadas.**<br>• **Caracterización de la conductividad térmica de las espumas generadas.**<br>• **Análisis de las relaciones entre composición, procesado, estructura celular y propiedades térmicas.** |
| *PS/SEBS (CAPÍTULO 7)* |
| • Fabricación de compuestos de **PS/SEBS con diferentes contenidos de SEBS.**<br>• **Análisis del comportamiento reológico (cizalla y extensional) de los compuestos generados.**<br>• **Análisis de la dispersión SEBS en la matriz de PS mediante micrografías.**<br>• **Fabricación de espumas empleando los compuestos de PS/SEBS mediante espumado por disolución de gas usando $CO_2$ como agente espumante.**<br>• **Análisis de la estructura celular de las espumas generadas.**<br>• **Análisis de las relaciones entre composición, comportamiento reológico, dispersión y estructura celular.** |

**Tabla 0.1.** Breve resumen del contenido de los Capítulos 4, 5, 6 y 7 de este manuscrito.

A continuación, se ilustra este ahorro de costes en materia prima mediante un ejemplo y un sencillo calculo numérico. Una pequeña planta común de extrusión puede producir unos 300 kg/h de espuma de PS extruido (XPS). En una típica formulación habitual, el PS, con un precio comprendido entre 1.1 y 1.6 €/kg, representa el 86.5% de la formulación, el masterbatch de grafito, con un precio de 15 €/kg y que funciona como agente nucleante y bloqueador de infrarrojo representa un 7.5 % de la formulación, el masterbatch de agente retardante a la llama, con un precio de 20 €/kg, representa un 6% del total y por último el gas, agente espumante necesario para producir la espuma (entre los que podemos encontrar dióxido de carbono (CO2), o una mezcla de pentano con isopentano suele tener unos valores que oscilan entre los 2 €/kg y los 4 €/kg y van introducidos en unos porcentajes que van desde el 4 al 6%, dependiendo del gas. Es probable que cada prueba de extrusión para desarrollar una formulación óptima lleve asociado un tiempo mínimo de unas 4 horas entre puesta a punto de la extrusora, estabilización de ésta, producción del material, y limpieza de la máquina. De estas 4 horas, al menos durante 2 horas se introducen todos los componentes en los porcentajes anteriormente citados. Durante las otras 2 horas restantes se introduce únicamente polímero puro. Esto significa que se utilizan al menos 1038 kg de polímero en cada prueba de espumado. Considerando un precio de la matriz polimérica de 1.3 €/kg y para el resto de la formulación los costes previamente indicados, el montante final de la materia prima ascienden a 4439 €. Este valor debería incrementarse aproximadamente un 25 % para poder considerar los costes asociados a la producción (consumo de la máquina, costes de personal, luz, agua, etc.). En conclusión, el coste de cada prueba de espumado es de al menos 5548 €. Este valor no incluye ni los costes asociados a la caracterización de los materiales celulares ni los costes asociados a la gestión de residuos.

Si en vez de producir el material, la compañía aplica la metodología desarrollada en esta tesis (con un coste de aproximadamente 500 €) los costes se reducirían más de 10 veces.

## 0.5 Estructura de la Tesis

La presente tesis se ha escrito en el modo compendio de publicaciones. La estructura de la tesis se resume en la **Figura 0.8.** Los Capítulos 4 a 7 recogen 5 artículos científicos de los cuales tres de ellos ya han sido publicados en revistas indexadas internacionales.

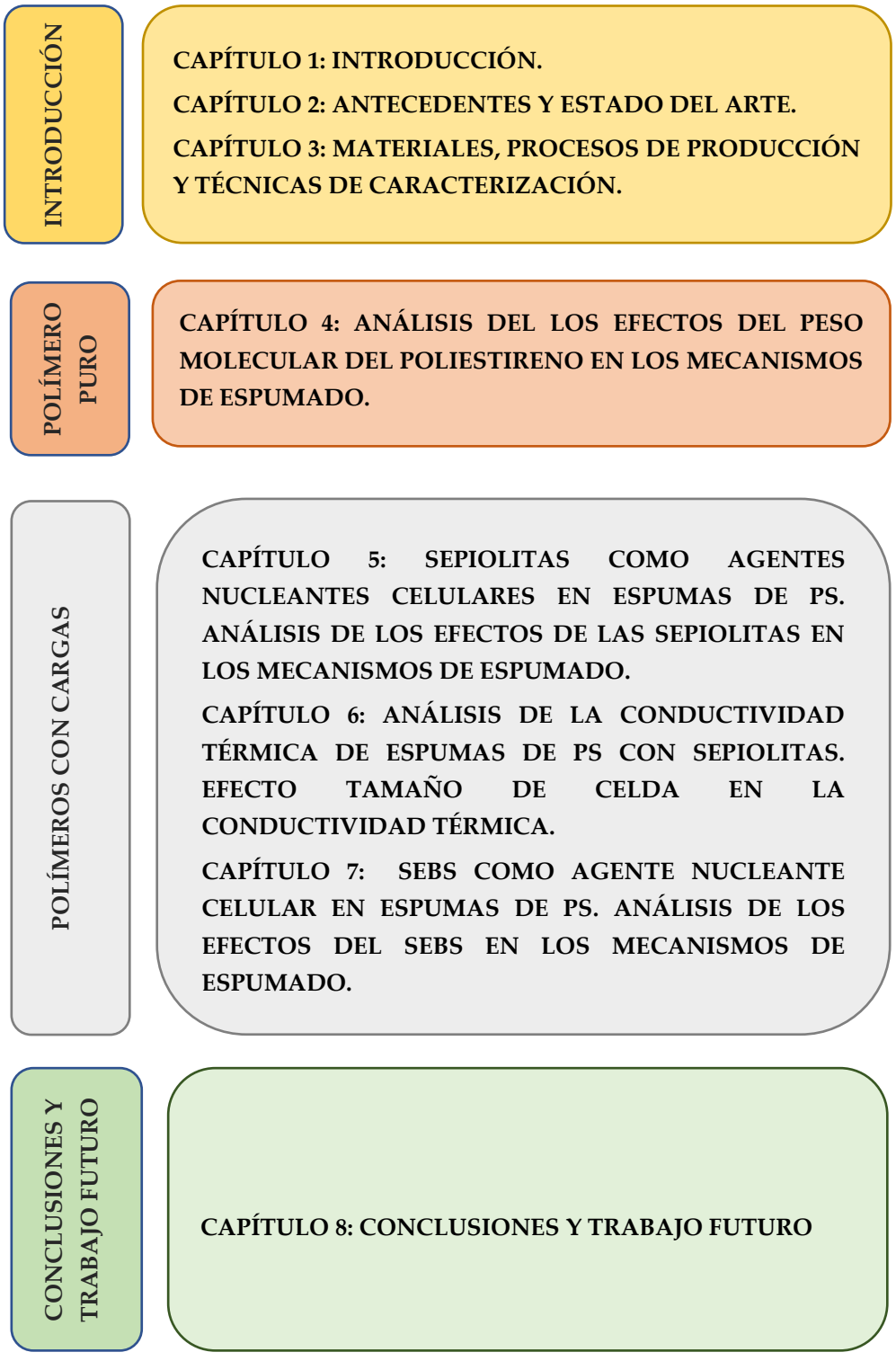


**Figura 0.8.** Distribución de los capítulos que conforman esta tesis.

El trabajo presentado se distribuye en nueve capítulos, cada uno con la información que a continuación se detalla:

**Capítulo 1. Introducción:** Este capítulo empieza con una breve exposición de que son los materiales celulares y su estatus actual en el mercado. De la misma

manera, se presenta el marco de la tesis. Posteriormente se definen los contenidos, objetivos, principales resultados y estructura de la tesis.

**Capítulo 2. Antecedentes y estado del arte:** En este apartado podemos encontrar un resumen de todo el marco teórico en el que se encuadra la tesis, además de un detallado estudio de los avances que se han realizado en el campo de los materiales celulares basados en PS. Así mismo, se reportarán en este capítulo los resultados, encontrados en literatura, relativos al uso de los dos agentes nucleantes que se utilizarán en la presente tesis: sepiolitas y SEBS.

**Capítulo 3. Materiales, procesos de producción y técnicas de caracterización:** En este capítulo se describen los materiales utilizados durante la presente tesis, así como las técnicas de producción utilizadas para generar los compuestos sólidos y los materiales celulares. Así mismo se describen las técnicas de caracterización empleadas con los sólidos y con los materiales celulares.

**Capítulo 4. Análisis de los efectos del peso molecular del poliestireno en los mecanismos de espumado:** En este capítulo se presentan los resultados obtenidos tras el análisis de tres PS con diferente fluidez y, por lo tanto, con diferente peso molecular. Este estudio ha dado lugar a una publicación científica. En el artículo se describe como el peso molecular está muy relacionado con otras características estructurales de los polímeros como la temperatura de transición vítrea o la longitud promedio de las cadenas. Finalmente se ha analizado la relación entre el peso molecular del polímero y parámetros característicos del proceso de espumado por disolución de gas como la solubilidad y los coeficientes de difusión durante los procesos de sorción y desorción, así como con la estructura celular de las espumas generadas con estos polímeros.

**Capítulo 5. Sepiolitas como agentes nucleantes celulares en espumas de PS. Análisis de los efectos de las sepiolitas en los mecanismos de espumado:** Este capítulo contiene los resultados relativos a dos artículos. En el primero de ellos se analiza cómo influye la dispersión de las nanopartículas en la posterior estructura celular. Para hacer un trabajo más detallado se tienen en cuenta diferentes efectos como el tipo de tratamiento superficial de las nanopartículas, el contenido de estas o las condiciones de proceso con las que se realizaron las mezclas del polímero con las partículas. Finalmente se han producido las espumas por la técnica de espumado por disolución de gas y se han analizado las relaciones entre la composición (dispersión), las condiciones de proceso y la estructura celular obtenida. Por otra parte, en el otro artículo, se busca hallar las relaciones entre las propiedades reológicas extensionales de las diferentes

formulaciones generadas y las posteriores estructuras celulares obtenidas en las espumas producidas a partir de dichas formulaciones. De igual forma que en el primer artículo se comprueba el efecto que los diferentes tratamientos superficiales, los porcentajes de partículas en la formulación y las condiciones de extrusión tienen en las propiedades reológicas extensionales. Finalmente se dilucida cuál de las dos condiciones si una mejor dispersión o unas mejores propiedades reológicas extensionales tiene más influencia en la estructura celular de las espumas de PS /SEP.

**Capítulo 6. Análisis de la conductividad térmica de espumas de PS con sepiolitas. Efecto del tamaño de celda en la conductividad térmica.**

Para este capítulo con las formulaciones producidas y analizadas en el anterior capitulo (Capítulo 5) se producen espumas de PS/SEP. Así mismo se mide la conductividad térmica de estas espumas mediante la técnica de TPS y se analiza su coeficiente de extinción a través espectroscopía infrarroja por transformada de Fourier (FTIR). Los resultados arrojados se han relacionado, a través de modelos teóricos, con la estructura celular para completar el circulo que une composición-procesado-estructura celular y propiedades finales de las espumas. Este capítulo tiene asociado un artículo.

**Capítulo 7. SEBS como agente nucleante celular en espumas de PS. Análisis de los efectos del SEBS en los mecanismos de espumado.**

En este trabajo y buscando de nuevo una reducción del tamaño de celda de las espumas poliméricas, se ha trabajado con un agente nucleante orgánico (SEBS). Se ha analizado la dispersión de las partículas de SEBS en la matriz de PS mediante micrografía TEM con la finalidad de relacionar este parámetro con las estructuras celulares obtenidas. De la misma forma una publicación está relacionada con el presente capitulo.

**Capítulo 8. Conclusiones y trabajo futuro:** El Capítulo 8 presenta las principales conclusiones de esta tesis. Además, se presentan ciertos puntos que podrían servir como trabajo futuro, así como una discusión global de los resultados obtenidos cuando se utilizan agentes nucleantes orgánicos e inorgánicos.

## 0.6 Publicaciones, Conferencias, Cursos y Proyectos

### *0.6.1 Publicaciones*

Durante el trabajo realizado en esta tesis se han generado una serie de publicaciones científicas. Los mencionados artículos se encuentran recogidos en la siguiente **Tabla 0.2**, la cual también indica el número de capitulo donde se encuentra cada artículo.

| Referencia de los artículos | Capítulo |
|---|---|
| A. Ballesteros, E. Laguna-Gutiérrez, M. A. Rodríguez Pérez. **Influence of the Molecular Weight, on the solubility, diffusivity and subsequent cellular structure of PS foams.** Publicación pendiente de envío | 4 |
| A. Ballesteros, E. Laguna-Gutiérrez, P. Cimavilla Román, M. L. Puertas, A. Esteban- Cubillo, J. Santaren, M. A. Rodríguez Pérez. **Influence of the dispersion of nanoclays on the cellular structure of foams based on polystyrene.** Journal of Applied Polymer Science. 2021,138, 46. | 5 |
| A. Ballesteros, E. Laguna-Gutiérrez, M. L. Puertas, A. Esteban- Cubillo, J. Santaren, M. A. Rodríguez Pérez. **Polystyrene/sepiolites nanocomposite foams: Relationship between composition, particle dispersion, extensional rheology and cellular structure** Materials Today Communications. 2021,102850. | 5 |
| A. Ballesteros, E. Laguna-Gutiérrez, M. A. Rodríguez Pérez. **Optimum cell size to reduce the termal conductivity of foams based on polystyrene/sepiolites nanocomposites.** Publicación pendiente de envío | 6 |
| A. Ballesteros, E. Laguna-Gutiérrez, M. A. Rodríguez Pérez. **SEBS an effective nucleating agent for PS foams.** Polymers. 2021, 13 (21), 3836. | 7 |

**Tabla 0.2.** Referencias de los artículos que aparecen en los capítulos de la tesis.

Así mismo, la **Tabla 0.3** presenta publicaciones realizadas durante la tesis doctoral que no han sido objeto de formar parte de uno de los capítulos del presente trabajo. Esta publicación está relacionada con la producción de polímeros nanocelulares en base polimetil-metacrilato (PMMA) y sus propiedades acústicas en contraposición a los materiales celulares microcelulares realizados con el mismo polímero.

| Referencia de los artículos |
|---|
| B. Notario, A. Ballesteros, J. Pinto, M. A. Rodríguez Pérez<br>**Nanoporous PMMA: A novel system with different acoustic properties.**<br>Material Letters. 2018,76-79. |

**Tabla 0.3.** Referencias de artículos realizados que no aparecen en los capítulos de la tesis.

### *0.6.2 Conferencias*

Los resultados obtenidos en la tesis se han presentado en varias conferencias nacionales e internacionales, como se puede ver en la **Tabla 0.4.**

| Contribución a Conferencias | |
|---|---|
| **1** | A. Ballesteros, E. Laguna-Gutierrez, M. A. Rodriguez-Perez, M. L. Puertas, A. Esteban-Cubillo, J. Santaren.<br>**Influence of the extrusion process, amount, and type of particles on the rheological properties of PS/nanoclay nanocomposites.**<br>9th European School on Molecular Nanoscience, ESMOLNA 2016, Tordesillas, Valladolid, España, Mayo 2016. **Presentación Oral** |
| **2** | A. Ballesteros, E. Laguna-Gutierrez, M. A. Rodriguez-Perez, M. L. Puertas, A. Esteban-Cubillo, J. Santaren.<br>**Influence of the extrusion process, amount, and type of particles on the rheological properties of PS/nanoclay nanocomposites.**<br>XIV Meeting of the Group of Polymers, GEP 2016, Burgos, España, Septiembre 2016. **Poster.** |
| **3** | A. Ballesteros, P. Cimavilla-Román, E. Laguna-Gutierrez, M. A. Rodríguez Pérez, M. L. Puertas, A. Esteban-Cubillo, J. Santaren.<br>**Cellular materials based on blends of polystyrene and nanometric inorganic fillers. Relation between dispersion, structure, and properties.**<br>5th CellMat 2018-Cellular Materials, Bad Staffelstein, Baviera, Alemania, Octubre 2018. **Presentación Oral.** |
| **4** | A. Ballesteros, E. Laguna-Gutierrez, M. A. Rodriguez-Perez.<br>**Influence of molecular weight in the solubility, diffusivity, and the subsequent cellular structure of polystyrene foams.**<br>5th CellMat 2018-Cellular Materials, Bad Staffelstein, Baviera, Alemania, Octubre 2018. **Poster.** |
| **5** | A. Ballesteros, E. Laguna-Gutierrez, M. A. Rodriguez-Perez, M. L. Puertas, A. Esteban-Cubillo, J. Santaren.<br>**Cellular materials based on nanocomposites of polystyrene and nanometric inorganic fillers with a needle-like morphology. Relation between dispersion, structure, and properties.**<br>Foams 2019, Valladolid, España, Octubre 2019**. Poster** |

**Tabla 0.4.** Listado de contribuciones a conferencias nacionales e internacionales.

### *0.6.3 Cursos y Proyectos*

En la **Tabla 0.5** se resumen todos los cursos realizados con motivo de esta tesis. Los cursos versaban de temas muy diversos, desde embalaje a aislamiento térmico o acústico, pasando por reología.

| **Cursos realizados durante la tesis** | |
|---|---|
| **1** | **Acoustic insulation in building. 2015,** Valladolid, Castilla y León, España**.** |
| **2** | **Seminar on characterization of materials by thermal analysis techniques: DSC, TGA.** Octubre 2015, Valladolid, Castilla y León, España. |
| **3** | **Thermal insulation in buildings.** Octubre 2015, Valladolid, Castilla y León, España. |
| **4** | **Characterization of polymeric materials.** Octubre 2016, Valladolid, Castilla y León, España. |
| **5** | **Plastic packaging, fundamentals, regulations and trends.** Febrero 2018, Valladolid, Castilla y León, España. |
| **6** | **Curso teórico-práctico de reología.** 12 y 13 de Junio de 2018, Madrid, España. |

**Tabla 0.5.** Listado de contribuciones a conferencias nacionales e internacionales.

Así mismo a lo largo de esta tesis se han realizado diferentes actividades de investigación en proyectos de carácter público y privado. La próxima tabla, **Tabla 0.6**, recoge los proyectos, la entidad financiadora, su duración, el investigador principal y el presupuesto del proyecto en cada caso.

| | |
|---|---|
| **Título del proyecto** | **NEOADFOAM:** Innovative additives to produce foams with enhanced thermal insulation properties and better fire behavior |
| **Entidad financiadora** | Ministerio de Economía y Competitividad, Gobierno de España |
| **Duración** | 2015-2018 |
| **Investigador Principal** | M. A. Rodríguez Pérez |
| **Presupuesto del Proyecto** | 234782,39 € |

| | |
|---|---|
| **Título del proyecto** | **NUMASTA:** New advanced materials for the development of equipment inside the water treatment sector. |
| **Entidad financiadora** | Ministerio de Economía y Competitividad, Gobierno de España |
| **Duración** | 2016-2018 |
| **Investigador Principal** | M. A. Rodríguez Pérez |
| **Presupuesto del Proyecto** | 78213 € |

| | |
|---|---|
| **Título del proyecto** | **INUPIPE:** Development of piping and union systems with advanced properties |
| **Entidad financiadora** | Ministerio de Economía y Competitividad, Gobierno de España |
| **Duración** | 2018-2021 |
| **Investigador principal** | M. A. Rodríguez Pérez |
| **Presupuesto del proyecto** | 310008,30 € |

| | |
|---|---|
| **Título del proyecto** | **LINPACK:** Towards a more sustainable packaging technology: development of foamed trays |
| **Entidad financiadora** | Linpack Packaging |
| **Duración** | 2018-2020 |
| **Investigador principal** | M.A. Rodríguez Pérez |
| **Presupuesto del proyecto** | 68091,02 € |

**Tabla 0.6.** Proyectos de carácter público y privado en los que se ha colaborado durante la consecución de la tesis.

## 0.7 Metodología de Trabajo

En esta sección se describe la metodología de trabajo seguida a lo largo de la tesis para desarrollar todo el trabajo experimental propuesto y cumplir con los objetivos acordados.

**1. Selección materias primas:** En primer lugar, se han seleccionado los materiales que se van a emplear durante el desarrollo de la tesis PS como matriz polimérica, sepiolitas y SEBS como agentes nucleantes, agentes espumantes físicos (dióxido de carbono) y antioxidantes. Los materiales se analizarán más en detalle durante el Capítulo 3 de la presente tesis.

**2. Producción de materiales solidos:** Una vez seleccionadas las materias primas se producirán las formulaciones solidas mediante un proceso de extrusión. Posteriormente, los compuestos de PS se han sometido a un proceso de termoconformado para generar probetas con una geometría adecuada que puedan ser utilizadas tanto para los procesos de caracterización como para la fabricación de las espumas. La **Tabla 0.7** recoge los procesos realizados para producir las formulaciones sólidas. Estos procesos se explican en detalle en el apartado 3.3.1 relativo al Capítulo 3 de la tesis.

| Producción de las formulaciones sólidas | |
|---|---|
| **Proceso de producción** | **Capítulos en los que está presente** |
| **Extrusión** | 3, 5, 6 y 7 |
| **Moldeo por compresión** | 3, 4 ,5, 6 y 7 |

**Tabla 0.7.** Procesos de producción empleados para fabricar las formulaciones sólidas de PS y para producir las dispersiones de partículas en los polioles.

**3. Caracterización de las materias primas y de las formulaciones sólidas:** Diferentes técnicas de caracterización se han empleado a lo largo de esta tesis para caracterizar tanto las materias primas como las formulaciones sólidas producidas a partir de ellas. Entre ellas cabe destacar: la medición de la densidad del solido a temperatura ambiente o temperaturas cercanas al proceso de espumado, el análisis de la morfología de los materiales mediante microscopía electrónica de barrido (SEM) y tomografía computarizada de rayos X, la reología dinámica de cizalla y reología extensional, análisis de calorimetría diferencial de barrido (DSC), determinación del peso molecular por cromatografía por permeación de gel, determinación del contenido de agentes nucleantes mediante el uso de las técnicas de termogravimetría (TGA) y de contenido de cenizas. Todas estas técnicas se ven recogidas en la **Tabla 0.8**. Así mismo, estás técnicas se describen en el capítulo 3, sección 3.4.1 o en los artículos realizados a lo largo de la tesis.

| Caracterización de los materiales sólidos | |
|---|---|
| **Técnica de caracterización** | **Capítulos en los que está presente** |
| **Determinación de la densidad (picnometría de gases)** | 3, 4, 5, 6 y 7 |
| **Microscopía Electrónica de Barrido (SEM)** | 3, 4 ,5 ,6 y 7 |
| **Tomografía computarizada de rayos X** | 3 y 5 |
| **Reología de Cizalla** | 3 ,4, 5 y 7 |
| **Reología Extensional** | 3, 4, 5 y 7 |
| **Calorimetría Diferencial de Barrido (DSC)** | 3, 4 y 7 |
| **Análisis Termogravimétrico (TGA)** | 3 y 5 |
| **Cromatografía por permeación de gel (GPC)** | 3 y 4 |
| **Determinación del contenido de partículas por cenizas** | 3 y 5 |

**Tabla 0.8.** Técnicas empleadas para la caracterización de los materiales sólidos y líquidos.

**4. Producción de los materiales celulares:** Una vez seleccionadas las materias primas, producidos los materiales sólidos y tras haber caracterizado su comportamiento se puede proceder a la fabricación de las espumas mediante el

proceso de espumado por disolución de gas, que viene recogido en la **Tabla 0.9** y del que se habla en detalle en el apartado 3.3 del Capítulo 3, así como en todos los artículos al efecto.

| Producción de los materiales celulares | |
|---|---|
| **Proceso de producción** | **Capítulos en los que está presente** |
| **Proceso de espumado por disolución de gas** | 2, 3 ,4, 5 ,6 y 7 |

**Tabla 0.9.** Procesos realizados para producir los materiales celulares.

**5. Caracterización de los materiales celulares:** Se han aplicado numerosas técnicas de caracterización en los materiales celulares generados, que han permitido entre otras cosas: analizar cualitativa y cuantitativamente parámetros de la estructura celular como el tamaño de celda, la anisotropía de las mismas, la densidad de celdas o la fracción volumétrica de celdas en el caso de estructuras bimodales, analizar la fracción de celdas abiertas presentes en la estructura. Además de estos parámetros se ha podido estudiar la densidad a través del método de Arquímedes, así como la conductividad térmica. La **Tabla 0.10** recoge las principales técnicas de caracterización utilizadas en los materiales celulares. Una explicación más detallada de la caracterización de los materiales celulares se encuentra en detalle en el Capítulo 3 de la presente tesis, o en los artículos de los Capítulos 4 a 7.

| Caracterización de los materiales celulares | |
|---|---|
| **Técnica de caracterización** | **Capítulos en los que está presente** |
| **Determinación de la densidad (método de Arquímedes)** | 3, 4, 5, 6 y 7 |
| **Determinación contenida de celda abierta (picnometría de gases)** | 3, 4, 5, 6 y 7 |
| **Microscopía electrónica de barrido (SEM)** | 3, 4, 5, 6 y 7 |
| **Medición coeficiente de extinción por FTIR** | 3 y 6 |
| **Medición de la conductividad térmica por el método de TPS** | 3 y 6 |

**Tabla 0.10**. Técnicas de caracterización empleadas en los materiales celulares.

**6. Análisis e interpretación de los resultados obtenidos:** Los resultados obtenidos a lo largo de la tesis han sido profusamente interpretados, analizados y relacionados entre sí, con el objetivo de hallar un hilo conductor que explique la relación composición-proceso-estructura-propiedades en materiales celulares

basados en PS. La discusión e interpretación de estos resultados se puede encontrar en los Capítulos 4 a 8 de esta tesis.

**7. Desarrollo de una metodología de trabajo:** Una vez interpretados y analizados los resultados de los Capítulos 4 a 8, se ha implementado una metodología de trabajo que permite elegir la fracción correcta de agente nucleante y el tipo correcto a introducir y el método de dispersión en las distintas matrices poliméricas. Por otra parte, con esta metodología de trabajo es posible determinar que parámetro influye más a posteriori en las propiedades térmicas y mecánicas de las espumas, y, por lo tanto, modificar esos parámetros en pos de una mejora sustancial de las citadas propiedades.

En la **Figura 0.9** se puede apreciar un esquema que representa los anteriores puntos.

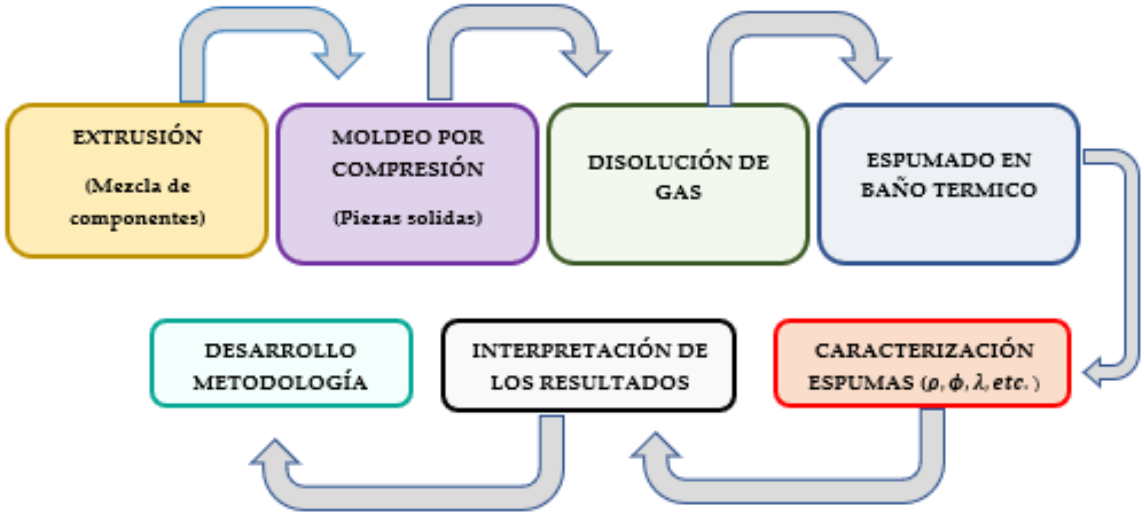


**Figura 0.9.** Esquema de la metodología seguida en la presente tesis.

## 0.8 Principales Resultados y Conclusiones

En los siguientes párrafos de este apartado se resumen las principales conclusiones obtenidas con cada sistema estudiado.

**1. Poliestirenos puros e influencia del peso molecular:**

- Las propiedades características de los PS puros están íntimamente ligadas con su peso molecular (o su índice de fluidez) presentando así el polímero con mayor peso molecular la mayor temperatura de transición vítrea ($T_g$), la mayor viscosidad de cizalla en la región terminal ($|\eta^*|$) y el mayor coeficiente de endurecimiento por deformación (*Strain Hardening Coefficient*). El polímero

con mayor peso molecular presenta un 76% más del coeficiente de endurecimiento por deformación que el PS con menor peso molecular. De la misma manera el polímero con menor peso molecular posee los menores valores de las propiedades anteriormente citadas.

- El PS con menor peso molecular es capaz de absorber una mayor cantidad de $CO_2$ en estado supercrítico (a unas mismas condiciones de presión, tiempo y temperatura) que los otros grados de PS. Así mismo la saturación del polímero con menor peso molecular se produce antes que las de los PS con mayor peso molecular. Los anteriores efectos se explican a través del mayor volumen libre que presenta el polímero con menor peso molecular.
- De igual manera, el PS con menor peso molecular presenta una difusividad del gas ligeramente mayor que sus semejantes con mayor peso molecular.
- El efecto plastificante es similar para los tres grados de PS estudiados sin importar el valor del peso molecular. Cabe destacar que, en el caso del polímero de menor valor del peso molecular, debido a su baja Tg de partida, se llega a valores de la Tg efectiva ligeramente superiores a los de la temperatura de saturación. Por lo tanto, cuando el material se extrae del autoclave, presenta una opacidad propia de un material semi-espumado.
- Una vez producidas las espumas utilizando los mismos parámetros en los procesos de saturación y espumado, es posible ver como el material con menor densidad (que expande más) es aquel con el menor peso molecular. Sin embargo, el porcentaje de celda abierta obtenido para el material con menor peso molecular es más del doble en comparación con el polímero con mayor peso molecular. Este hecho puede ser debido a la menor capacidad del material para resistir la expansión de los gases, de acuerdo con su menor coeficiente de endurecimiento por deformación.
- Así mismo, el material que presenta el menor tamaño de celda, con una densidad celular mayor, y una estructura más regular y homogénea, es el PS con mayor peso molecular. El polímero con mayor peso molecular presenta un tamaño de celda de 43 micras en comparación con las 264 micras que posee el polímero con menor peso molecular. A pesar de que el PS con mayor peso molecular es el que menos gas absorbe, también es el que mayor capacidad tiene de aguantar la expansión de los gases, esto hace que no se produzcan, de una manera tan crítica, fenómenos de degeneración de la estructura celular

como coalescencia, que repercuten en el tamaño de celda y la homogeneidad de la estructura celular.

- Por último, queda seleccionado para los posteriores estudios un PS de carácter intermedio, que permita alcanzar altas expansiones (bajas densidades) sin comprometer el tamaño de celda ni el contenido de celda abierta.

## 2. Formulaciones de PS y sepiolitas

- Los resultados de reología de cizalla, así como de tomografía de Rayos X, demuestran que son las sepiolitas órgano-modificadas con sales cuaternarias de amonio, aquellas que consiguen dispersarse mejor en la matriz de PS.
- Las propiedades reológicas extensionales se ven reducidas con la inclusión de sepiolitas. Sin embargo, son mejores para las formulaciones que contienen sepiolitas no modificadas en su superficie (sepiolitas naturales) que para el resto de los materiales compuestos. Presentando estas (por ejemplo, a un 2 wt.% de sepiolitas) un 7% mayor coeficiente de endurecimiento por deformación que la formulación con sales cuaternarias de amonio y un 15% mayor que las formulaciones con grupo silano.
- Someter a las formulaciones a un mayor número de ciclos de extrusión, reduce ligeramente las viscosidades de cizalla de los polímeros puros, y tampoco ayuda a mejorar la dispersión de las sepiolitas en los polímeros puros. Las propiedades reológicas extensionales también se ven reducidas por el aumento del número de ciclos de extrusión.
- Para lograr la percolación de la estructura, es necesario un 6 wt. % de partículas organomodificadas con sales cuaternarias de amonio, mientras que se necesita un 8 wt. % de las sepiolitas naturales (no modificadas superficialmente) y hasta un 10 wt. % para las sepiolitas tratadas con grupos silano.
- El uso de sepiolitas consigue incrementar ligeramente (c.a. 5%) el gas absorbido por la matriz polimérica de PS, hasta que el porcentaje de sepiolitas introducido es mayor de un 8 wt.%. De acuerdo con la bibliografía estudiada y referenciada, las sepiolitas pueden funcionar como absorbedores de gas gracias a sus canales internos. Con altos contenidos de sepiolitas (c.a. 10 wt. %) sin embargo, la densidad relativa de las espumas producidas incrementa, debido a la mayor densidad de las sepiolitas frente a la densidad del PS puro.
- El contenido de celda abierta es mayor cuanto más alto es el contenido de sepiolitas introducidas. Este hecho no es tan notorio para las formulaciones

que contienen sepiolitas naturales. Sin embargo, el máximo valor obtenido para este contenido es de un 15% (para la formulación con 10 wt. % de sepiolitas modificadas con grupos silano) lo cual es un dato relativamente bajo y no debería causar excesivos problemas en las posteriores estructuras celulares.

- Los tamaños de celda se ven notablemente reducidos por el uso de sepiolitas. Con apenas un 2wt. % de sepiolitas modificadas con sales cuaternarias de amonio, el tamaño de celda se ve reducido en un 82% en comparación con el del PS puro. Lo cual indica un buen comportamiento de esta nanopartícula como agente nucleante en el PS. El mínimo tamaño de celda alcanzado fue de 9 micras para un 8wt. % de sepiolitas modificadas con sales cuaternarias de amonio.
- La adición de sepiolitas provoca una estructura celular bimodal con celdas de diferente tamaño. El número de celdas más grandes representa desde un 10% hasta un 20% del volumen de la muestra.
- Como conclusión, para lograr tamaños de celda más pequeños y estructuras celulares más homogéneas, hay que optimizar la dispersión de las partículas. Es por ello que las formulaciones que presentan un menor tamaño de celda son aquellas que tienen sepiolitas modificadas con sales cuaternarias de amonio (las partículas que mejor grado de dispersión presentaban).
- Se estudia la conductividad térmica de espumas con densidades relativas similares. La conductividad térmica se ve reducida a medida que se reduce el tamaño de celda. Este fenómeno es cierto hasta alcanzar unos valores entre 35-40 micras. Para valores más bajos del tamaño de celda la conductividad térmica vuelve a crecer. Esto se debe al cambio de método de dispersión de la radiación infrarroja. Para valores muy bajos del tamaño de celda, la espuma se convierte en un material cuasi "transparente" a la radiación infrarroja, subiendo por lo tanto la conductividad térmica global de la espuma.
- El coeficiente de extinción medido presenta un comportamiento muy similar a la conductividad térmica. Este fenómeno explica que es el termino radiativo de la conductividad térmica (la radiación infrarroja) la que está variando de manera más notoria debido a la reducción del tamaño de celda.

## 3. Formulaciones de PS y SEBS

- Los resultados de reología de cizalla demuestran que al añadir SEBS la viscosidad de cizalla se ve reducida, dado el bajo índice de fluidez y la menor densidad de la matriz de SEBS. Por otra parte, no hay una percolación de la estructura PS/SEBS ni a altos contenidos de SEBS (5wt. % o 10 wt. %). Esto se debe a que el SEBS no es una fase inorgánica como las sepiolitas si no que se trata de una fase polimérica orgánica.
- La adición de cantidades de SEBS superiores a 3 wt. %, hace que la temperatura de transición vítrea de la muestra conjunta se vea aumentada en comparación con la Tg del PS puro.
- Añadir SEBS reduce el coeficiente de endurecimiento por deformación. Este fenómeno es muy notorio para valores de SEBS superiores al 5 wt.%. En particular, para la formulación con un 10 wt. % de SEBS el valor del coeficiente de endurecimiento por deformación es un 61% menor que el del polímero puro de PS.
- La densidad de las espumas se ve incrementada con la introducción de SEBS en la matriz polimérica. Este fenómeno se debe a que el SEBS limita la expansión y el crecimiento de la espuma. Por otra parte, el contenido de celda abierta se mantiene constante para bajos contenidos de SEBS. Sin embargo, para un 10 wt. % de SEBS el contenido de celda abierta se dispara hasta alcanzar un valor del 45%.
- Es importante destacar la gran capacidad de nucleación del SEBS en PS. Con tan solo un 0.25 wt. % de SEBS en el PS se logra reducir el tamaño de celda en un 78%, en comparación con el polímero puro, o con un 3 wt. % de SEBS se logra una reducción del 90% del tamaño de celda. Estas reducciones son mucho más notorias que las alcanzadas con otras partículas inorgánicas como pueden ser sepiolitas o agentes nucleantes más convencionales como talco. Por otra parte, los mejores resultados en el tamaño de celda alcanzado, así como la homogeneidad de la estructura celular se alcanzan precisamente con un 3 wt. % de SEBS en el polímero. Para valores mayores de esta fase orgánica, se tiene o un aumento notorio del tamaño de celda o un aumento remarcable de la densidad o ambos. Este fenómeno viene en gran parte debido a la reducción observada en las propiedades reológicas extensionales para altos contenidos de SEBS.

**A partir de todos estos objetivos ha sido posible establecer una metodología de trabajo y una guía de pasos que permiten entender las relaciones entre composición, proceso, estructura celular y propiedades** en diferentes

formulaciones en base PS. Consiguiendo por lo tanto una herramienta que es capaz de predecir la importancia de los distintos pasos en las propiedades finales de la espuma y que permite **poder seleccionar,** sin necesidad de fabricar las espumas, **las formulaciones más interesantes que den lugar a las espumas con las mejores propiedades finales de acuerdo con su dispersión o sus propiedades reológicas, entre otras**. Este sistema permitirá el ahorro de una ingente cantidad de costes asociados al sistema ensayo-error tan típico en la puesta a punto de procesos de producción industrial.

## 0.9 Bibliografía


[1] H.G. Liddell, R. Scott, H.S. Jones,R. McKenzie. *A Greek-English Lexicon*. **1940,** Ninth Edition. Oxford University Press, United Kingdom.

[2] Imperial Chemical Industries LPD. *Landmarks of the Plastics Industry 1862-1962*. **1962**, Welwyn Garden City, United Kingdom.

[3] M.E. Bowden. *Chemical achievers: the human face of the chemical sciences*. **2015**, first Edition. Chemical Heritage Foundation, United States.

[4] Anonymous. *A Short Memoir of Alexander Parkes (1813–1890), Chemist and Inventor*. **1890**, printed for private circulation.

[5] C. Everton. *The History of Snooker and Billiards*. **1986**, first edition. Partridge Press, India.

[6] J.W. Hyatt. *J Ind Eng Chem*. **1914**,6(2),158-161.

[7] J.L. Nicholson G.R. Leighton. *Plastics Come of Age*. **08-01-1942**, Harper's Magazine, United States.

[8] K. Mulder, M. Knot. *Technol Soc*. **2001**;23(2),265-286.

[9] M. Demirors. *The History of Polyethylene, chapter 9 In: 100+ years of plastics, Leo Baekeland and beyond. **2011**, ACS Symposium Series, Vol. 1080*

[10] M.E. Hermes. *Enough for One Lifetime: Wallace Carothers, Inventor of Nylon*. **2005**, Chemical Heritage Foundation; United States.

[11] O. Bayer. *Angew Chemie*. **1947**;59(9),257-272.

[12] J. Scheirs, D. Priddy. *Historical Overview of Styrenic Polymers. In: Modern Styrenic Polymers: Polystyrenes and Styrenic Copolymers*. **2003**, first edition, John Wiley & Sons, United States.

[13] J. Borkin. *The Crime and Punishment of I. G. Farben*. **1978**, first edition, Free Press, United States.

[14] S. Vecchiato, J. Ahrens, A. Pellis, D. Scaini, B. Mueller, E. Herrero-Acero, G.M.Guebity.*ACS Sustain Chem Eng*. **2017**;5(8):6456-6465.

[15] G. Cecchin, G. Morini, F. Piemontesi. *Kirk-Othmer Encyclopedia of Chemical Technology*. **2003,**351-362.

[16] R.A. Auras, L.T. Lim, S.E.M. Selke, H. Tsuji. *Poly (Lactic Acid): Synthesis, Structures, Properties, Processing, and Applications*. **2010**, first edition, Wiley, New Jersey United states.

[17] F. Ullman. *Ullmann's Encyclopedia of Industrial Chemistry*. **2016**. Seventh edition. Wiley, New Jersey United states.

[18] H. Mera, T. Takata. *High-Performance Fibers. In: Ullmann's Encyclopedia of Industrial Chemistry*. **2000**. Seventh edition. Wiley, New Jersey United states.

[19] E. Frank, V. Bauch, F. Schultze-Gebhardt, K.H. Herlinger. *Fibers, 1. Survey. In: Ullmann's Encyclopedia of Industrial Chemistry*. **2000**. Seventh edition. Wiley, New Jersey, United states.

[20] E. Kishi, A. Ozaki, T. Ooshima, Y. Abe, M. Mutsuga, Y. Yamaguchi, T. Yamano. *Packag Technol Sci*. **2020**,33 (4-5),183-193.

[21] D. Eaves. *Handbook of Polymer Foams.**2004**,* first edition, Rapra Technology, Shropshire, United Kingdom.

[22] https://www.gellnerindustrial.com/applications-polymers. *Accessed November*

***2021***.

[23] E. Laguna-Gutierrez. *Understanding the Foamability of Complex Polymeric systems by Using Extensional Rheology*. **2016**, PhD Thesis, University of Valladolid, Spain.

[24] https://www.euractiv.com/section/energy-environment/news/while-global-plastic-production-is-increasing-worldwide-it-is-slowin-down-in-europe/. *Acessed November* ***2021***.

[25] R. Geyer, J.R. Jambeck, K.L. Law KL. *Sci Adv*. **2017**,3(7).

[26] G. Swift. *FEMS Microbiol Lett*. **1992**; 9(2-4):339-345.

[27] C.C. Ibeh, *Thermoplastic Materials: Properties, Manufacturing Methods, and Applications*. **2011,** first Edition. CRC press Taylor and Francis Group, Bocaraton, United States.

[28] J.Hopewell, R. Dvorak, E. Kosior. *Philos Trans R Soc B Biol Sci*. **2009**;364(1526),2115-2126.

[29] L.J. Gibson, M.F. Ashby. *Cellular solids. Structure and properties*. **2014**, second edition, Cambridge University Press, Cambridge, United Kingdom.

[30] P.S. Liu, G.F. Chen. *Porous Materials: Processing and Applications*. **2014**, first edition, Elsevier, Amsterdam, The Netherlands.

[31] M.Scheffler, P.Colombo. *Cellular Ceramics*: Structure, Manufacturing, Properties and Applications. **2005**, Wiley, New Jersey, United states.

[32] J. Martin-de Leon. *Understanding the Production Process of Nanocellular Polymers Based on PMMA Driven by Homogeneous Nucleation*. **2019**, PhD Thesis, University of Valladolid, Spain.

[33] C. Saiz-Arroyo. *Fabricación de Materiales Celulares Mejorados Basados en Poliolefinas. Procesado-Composicion-Estructura-Propiedades*. **2012**, PhD Thesis, University of Valladolid, Spain.

[34] *www.Foam-Expo.Eu. Accessed November* ***2021***.

[35] N. Mills. *Polymer Foams Handbook: Engineering and Biomechanicals Applications and Design Guide*.**2007**, first edition, Butterworth-Heinemann, Oxford, United Kingdom.

[36] S.T.Lee, C.B. Park, N.S.Ramesh. *Polymeric Foams*. **2016**, first edition, CRC press Taylor and Francis Group, Bocaraton, United States.

[37] N.L. Thomas. *J Cell Plast*. **2007**, 43(3), 237-255.

[38] M. Santiago-Calvo. *Synthesis, Foaming Kinetics and Physical Properties of Cellular Nanocomposites Based on Rigid Polyurethane*.**2019**, PhD Thesis, University of Valladolid, Spain.

[39] E. Lopez-Gonzalez. *Analysis of the Composition -Structure Properties Relationship of Open-Cell Polyolefin-Based Foams with Tailored Levels of Gas Phase Tortuosity*. **2019**, PhD Thesis, University of Valladolid, Spain.

[40] C.C. Kuo, L.C. Liu, W.C. Liang, H.C. Liu, C.M. Chen. *Compos Part B Eng*. **2015**,79,1-5.

[41] M. Sabzi, L. Jiang, M. Atai, I. Ghasemi. *J Appl Polym Sci*. **2013**, 129(4), 1734-1744.

[42] https://www.grandviewresearch.com/industry-analysis/polymer-foam-market. *Accessed November* ***2021***.

[43] https://stratongroup.com/blog/everything-you-need-to-know-about-pvc-foam-boards/. *Accessed November* ***2021***.

[44] https://www.zouchconverters.co.uk/news/2018/what-is-pvc-foam-and-what-is-it-used-for. *Accessed November* ***2021***.

[45] https://www.acmeplastics.com/Expanded-PVC-Foam.*Accessed November* ***2021***.

[46] https://www.arpro.com. *Accessed November* ***2021.***

[47] https://www.marketstudyreport.com/global-polypropylene-foams-market-size-research. *Accessed November* ***2021.***

[48] https://www.marketsandmarkets.com/Market-Reports/polyethylene-foam-market-129894004.html. *Accessed November* ***2021.***

[49] https://polyurethane.americanchemistry.com/polyurethane/Introduction-to-Polyurethanes/Applications/Rigid-Polyurethane-Foam/.*Accessed November* ***2021.***

[50] http://www.recticel.com/index.php/company/what-is-polyurethane.*Accessed November* ***2021.***

[51] https://polyurethane.americanchemistry.com/Flexible-Polyurethane-Foam/. *Accessed November* ***2021.***

[52] Y. Li, S. Ren. *Acoustic and Thermal Insulating Materials. In: Building Decorative Materials*. **2011**, first edition, Elsevier, Amsterdam, The Netherlands.

[53] M. Biron. *Composites, in: Thermosets and Composites*. **2013**, first edition, Elsevier, Amsterdam, The Netherlands.

[54] K. Pulidini, S. Mukherjee. *Report ID: GMI2063*. **2017**.

[55] J. Shen, C. Zeng, L.J. Lee. *Polymer (Guildf)*. **2005**;46(14), 5218-5224.

[56] https://engineer.decorexpro.com/en/otoplenie/uteplenie/ekstrudirovannyj-penopolistirol-kak-uteplitel.html. *Accessed November* ***2021.***

[57] N.H.R. Sulong, S.A.S. Mustapa, M.K.A. Rashid MK. *J Appl Polym Sci*. **2019**, 136 (20), 47529.

[58] S. Doroudiani, M.T. Kortschot, *J. Appl. Polym. Sci.* ***2003,*** 90, 1421–1426.

[59] M. Aksit, C. Zhao, B. Klose, K. Kreger, H.W. Schmidt, V. Altstädt. *Polymers(Basel)*. **2019**,11(2),268.

[60] G. Wypych. *Handbok of Polymers*.**2016**, second edition, Elsevier, Amsterdam, The Netherlands.

[61] H. Gausepohl, N. Nießner. Polystyrene and Styrene Copolymers. In: *Encyclopedia of Materials: Science and Technology*. **2001**, first edition, Elsevier Amsterdam, The Netherlands.

[62] H. Zhang, W.Z. Fang, Y.M. Li, W.Q.Tao. *Appl Therm Eng*. **2017**,115,528-538.

[63] M. L. Huber, A.H. Harvey. *Thermal Conductivity of Gases*. **2011**, ninety second Edition. CRC press Taylor and Francis Group, Bocaraton, United States.

[64] P. Acuña, Z. Li, M. Santiago-Calvo, F. Villafañe, M.A. Rodriguez-Perez, D.Y.Wang. *Polymers (Basel)*. **2019**;11(1):168.

[65] O.A. Almanza, M.A. Rodriguez-Perez, J.A.De Saja. *J Polym Sci Part B Polym Phys*. **2000**,38(7),993-1004.

[66] N.P. Suh. *Impact of microcellular plastics on industrial practice and academic research*. In Proceedings of the IUPAC Polymer Conference on Mission and Challenges of Polymer Science and Technology, Kyoto, Japan, 2–5 December

**2002**.

[67] F.A. Waldman.The *processing of microcellular foam*. **1982**, PhD Thesis, Massachusetts Institute of Technology (MIT), United States.

[68] J.E. Martini-Vvedensky, N.P.Shu, F.A. Waldman. *Microcellular closed cell foams and their method of manufacture*.**1982**, US 4473365A, patent.

[69] V. Kumar. N.P. Shu. *Polym Eng Sci*. **1990**;30(20), 1323-1329.

[70] K. Nadella, V. Kumar, W. Li. *Cell Polym*. **2005**, 24(2), 71-90.

[71] B. Notario, A. Ballesteros, J. Pinto, M.A. Rodríguez-Pérez. *Mater Lett*. **2016,** 168,76-79.

[72] V. Bernardo, J. Martín-de León, E. Laguna-Gutiérrez, M.A. Rodríguez-Pérez. *Eur Polym J*. **2017**,96,10-26.

[73] C.Forest, P. Chaumont,P. Cassagnau, B. Swoboda, P. Sonntag. *Prog Polym Sci*. **2015**, 41(6),122-145.

[74] B. Notario, J. Pinto, E. Solorzano, J.A. De Saja, M. Dumon, M.A. Rodriguez-Perez. *Polym (United Kingdom)*. **2015**,56,57-67.

[75] B. Notario, J. Pinto, E. Solorzano, A. Martin-Cid, M.A. Rodriguez-Perez. *Physical properties of nanocellular foams: the transition from the micro to the nano scale*. Polymer Conference international conference on Foams and Foams Technology, FOAMS 2014, New Jersey, United States, **2014**.

[76] V. Bernardo. *Production and Characterization of Nanocellular Polymers Based on Nanostructured PMMA Blends and PMMA Nanocomposites*. **2019**, PhD Thesis, University of Valladolid, Spain.

[77] S. Liu, J. Duvigneau, G.J. Vancso. *Eur Polym J*. **2015**,65,33-45.

[78] J.A. Reglero, P. Viot, M. Dumon. *J Cell Plast*. **2011**, 47(6), 535-548.

[79] E. Laguna-Gutierrez, A. Lopez-Gil, C. Saiz-Arroyo, R. Van Hooghten, P. Moldenaers, M.A. Rodriguez-Perez. *E.J Polym Res*. **2016**,23(12),251.

[80] H.E.Naguib, C.B.Park, N. Reichelt. *J Appl Polym Sci*. **2004**, 91(4), 2661-2668.

[81] R. Liao, W. Yu, C. Zhou. *Polymer (Guildf)*. **2010**;51(2),568-580.

[82] A. Ballesteros, E. Laguna-Gutierrez, P. Cimavilla-Roman, M.L. Puertas, A. Esteban-Cubillo, J. Santaren, M.A. Rodriguez-Perez. *J. Appl. Polym. Sci*. **2021,** 10, 51373.

[83] E. Laguna-Gutierrez, R. Van Hooghten, P. Moldenaers, M.A. Rodriguez-Perez. *J Appl Polym Sci*. **2015**, 132(47),1-12.

[84] R.K. Gupta RK, V. Pasanovic-Zujo, S.N. Bhattacharya. *J Nonnewton Fluid Mech*. **2005**,128(2-3), 116-125.

[85] E. Laguna-Gutierrez, R. Van Hooghten, P. Moldenaers, M.A. Rodriguez-Perez. *J Appl Polym Sci*. **2015** ,132(33).

[86] M.A. Rodriguez-Perez, J. Lobos, C.A Perez-Muñoz, J.A. De Saja, L. Gonzalez, B.M.A. Del Carpio. *Cell Polym*. **2008**;27(6):347-362.

[87] www.cellmat.es. *Accessed November **2021.***

[88] M.A. Rodriguez-Perez. *Propiedades Térmicas y Mecánicas de Espumas de Poliolefinas*. **1998**, PhD Thesis, University of Valladolid, Spain.

[89] J. Pinto. *Fabrication and Characterization of Nanocellular Polymeric Materials from Nanostructured Polymers*. **2014**, PhD Thesis, University of Valladolid, Spain.

[90] C.Yang, M. Wang, Z. Xing, Q. Zhao, M. Wang, G. Wu G. *RSC Adv*. **2018**,8(36),20061-20067.

[91] X. Han, K.W. Koelling, D.L. Tomasko, L.J. Lee. *Polym Eng Sci*. **2003**, 43(6),1206-1220.

[92] V.Kalimaknov. *Nucleation Theory*. **2013,** first edition**,** Springer,Berlin, Germany.

# Chapter 1

# Introduction

"Eintritt nur für verrukte, eintritt kosten der vestand "

Der Steppenwolf, Herman Hesse.

*"Entrada solo para locos, cuesta la razón"*

El lobo estepario, Herman Hesse.

# INDEX

## 1.1 Introduction

Nowadays, it is enough to open a digital newspaper, tune in to a radio station or simply view any newscast to after a few minutes read or listen the word "plastic". Therefore, it is not difficult to assume the interest of the population to understand these materials. The word plastic comes from the Greek form *plastikós* (πλαστικός), which means to mold or mash.[1] Although synthetic plastics are not as old as the etymological origin of the word, they cannot be considered a novel material from this era of technological development, as they have celebrated their one hundred fourteenth anniversary in 2021.[2] In fact, the creation of the first thermoset plastic (Bakelite) is attributed to the Belgian chemistry, nationalized from the United States, Hendrick Baekeland in 1907.[3]

Synthetic plastics made from natural products are even older. In 1856 Alexander Parkes developed, using cellulose nitrate, a material, Parkesine, that was as hard as ivory and as flexible as paper. It was also opaque and resistant to humidity, and it could be heated and molded.[4] Twelve years later, in 1868, the company Phelan and Collander promise the large sum, in those years, of 10.000 US$ to anyone who could substitute ivory in the production of billiard balls.[5] John W. Hyatt achieved this goal by modifying the material of Alexander Parkes, thanks to the substitution of the castor oil, used in the product of Alexander Parkes, by camphor.[6] The new material obtained was called celluloid, a name that continues being used nowadays, and the celluloid billiard balls are recognized as the first plastic product in the history.[7] Since then, a long time has passed, and the synthesis of multiple macromolecules has led to a frenzied and dizzying race in the production and creation of new plastics. Even so, an appreciation must be done, although all plastics are polymers, the reverse assumption is not true. A polymer can be only named as plastic if it presents a plastic behavior. Continuing with the chronological summary, in 1912, few years before the First World War, a patent reported by the Germans Klatte and Zacharias presented the polymerization of the vinyl chloride, which lately will conform the polyvinyl chloride (PVC).[8] The 30s decade brought with it the generation of multiple patents for the synthesis of new products. Among them, we find the synthesis of low-density polyethylene (LDPE) by Reginald Gibson and Eric Fawcett, the development of polyamide 6 (Nylon), in 1933, by Wallace Carothers or the synthesis of polyurethane (PU) by Otto Bayer in 1937.[9,10,11] In this decade we also observe the first industrial production of polystyrene (PS), in 1930, by the German group of chemical companies Interessen-Gemeinschaft Farbenindustrie

AG (IG Farben).[12] This group was dissolved at the end of the Second War World (1949) for, among other reasons, being the responsible of the production of the Zyklon B gas used during the Holocaust.[13] Several companies that formed the IG Farben group were re-founded and have continue working until today with well-known names such as BASF, Bayer or Sanofi Aventis. Polyethylene terephthalate (PET), developed by the British Whinfield and Dickson, was born from the shortage of the war and the pressing need of the United Kingdom in 1941 to replace cotton from Egypt with another material. Therefore, a huge amount of the most conventional plastic materials come from the times close to the Second World War. However, some polymers, which are commonly used today, were not developed until a few years later. Within this group we can find polypropylene (PP) and high-density polyethylene (HDPE) obtained in 1951 and 1953, respectively, thanks to the work of Zieggler and Natta, both winners of the Nobel Prize in Chemistry.[15] In 1954, the American company DuPont patented the process created by Carothers in 1932 to heat lactic acid and put it under vacuum, obtaining a substance that they would call polylactic acid (PLA).[16] Some of the photos of the researchers and cited laboratories are found in **Figure 1.1.**

**Figure 1.1.** From left to right and top to bottom: Alexander Parkes, J.W. Hyatt, Hendrick Baekeland, Fritz Klatte, Wallace Carothers, Otto Bayer, I.G. Farben, Whinfield and Dickson.

All the aforementioned polymers are used for a myriad of applications from the most specialized such as, for example, Neoprene suits, to resist very low temperatures in water sports, or bulletproof vests made with Kevlar, to more common products such as toys for children or films for packaging.[17-21] Plastics are used in very diverse sectors such as construction, transport, packaging, electronics, medicine, etc.[22,23] Consequently, the global production of plastic

materials in 2020 was 500 million tons, despite the impact of COVID 19.[24] In the Journal of Science Advances, Roland Geyer et al. reported that the total volume of plastic produced throughout history is 8,300 million tons. Of this amount, almost 5,000 million tons are in landfills or in natural environments, forming, for example, a proto continent in the Pacific Ocean.[25] Therefore, it is essential to find solutions to reduce the amount of plastic wastes. Some strategies that can be used are based on studying the biodegradability of plastics, to modify their chemical structure and decompose the plastics into components compatible with the environment, or the development of advance recycling technologies. The foaming process is also a very interesting strategy because this technology allows producing polymeric products where part of the solid phase, integrated by the polymer, is replaced by air.[26–28]

## 1.2 Cellular Materials

A cellular material is composed of two well differentiated phases: a gaseous phase that is dispersed in a continuous solid matrix.[29] Nature presents many examples of these cellular materials, as it can be seen in **Figure 1.2.**

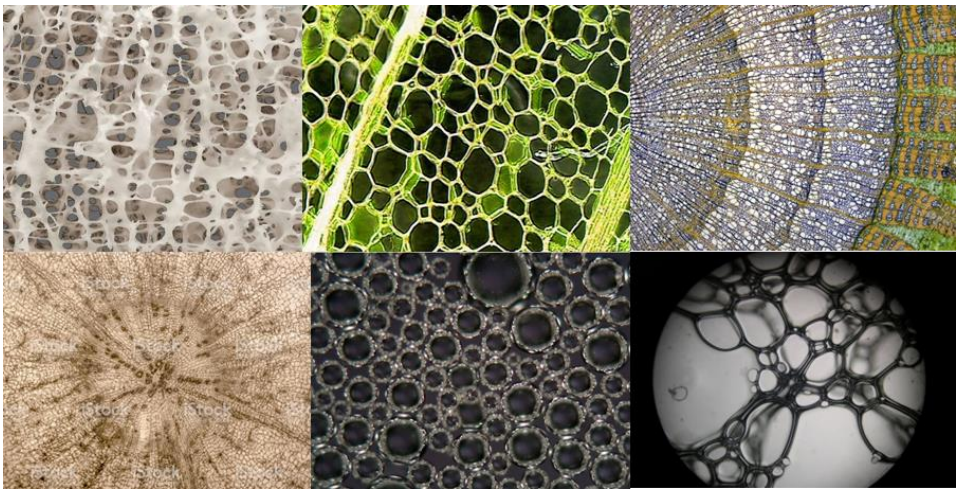

**Figure 1.2.** Examples of cell structures present in nature. From left to right and top to bottom: interior of a bone, balsa wood, linden stem, cellular structure of the interior of a carrot, beer bubbles, egg white.

Due to the excellent properties that these natural cellular materials present, humans have tried to artificially recreate them using as base material: metals, ceramics, or polymers.[29-31] Therefore, polymeric cellular materials are those whose solid structure is given by a polymeric matrix.

By means of the generation of the cellular structure, it is possible to reduce the weight of the materials and the consumption of raw materials, as well as the production costs. In addition, these materials present a series of interesting properties and therefore, they occupy a privileged place in multiple sectors. One of their most interesting properties is their ability to function as thermal insulators, thanks to their low thermal conductivity. It is also important to remark their good mechanical properties, especially the impact energy absorption, in low-density materials, their high stiffness/weight ratio and their high buoyancy and damping capacity.[32] They can also be used in applications that require a good magnetic permeability, a high absorption or a low acoustic transmission and in applications that demand high chemical resistance.[23] These properties make cellular materials perfect candidates to satisfy the requirements of a huge number of technological sectors. On the other hand, the possibility of manufacturing cellular materials using different polymeric matrices, as well as the possibility of modifying the cellular structure, for instance by the incorporation of additives or by modifying the processing parameters, allows us to design and produce a unique material for each application (on-demand materials).

**Figure 1.3.** Examples of materials and industrial sectors that use polymeric cellular materials on a regular basis.

The main industrial sectors where cellular materials find a greater application are: the construction sector, thanks to the high insulation capacity, the high rigidity and the high ratio resistance (with respect to their weight) of these materials , in the aeronautical sector due to their lightness and the their ability to

comply very specific requirements, in the food sector, in particular in packaging applications, due to their low cost and good resistance to impact, in the automotive sector, which demands light products with high damping, good resistance to fatigue and to impact and in other recreational sectors such as toys and sports.[33–36] **Figure 1.3** shows a set of examples of materials and sectors where polymeric cellular materials play a critical role.

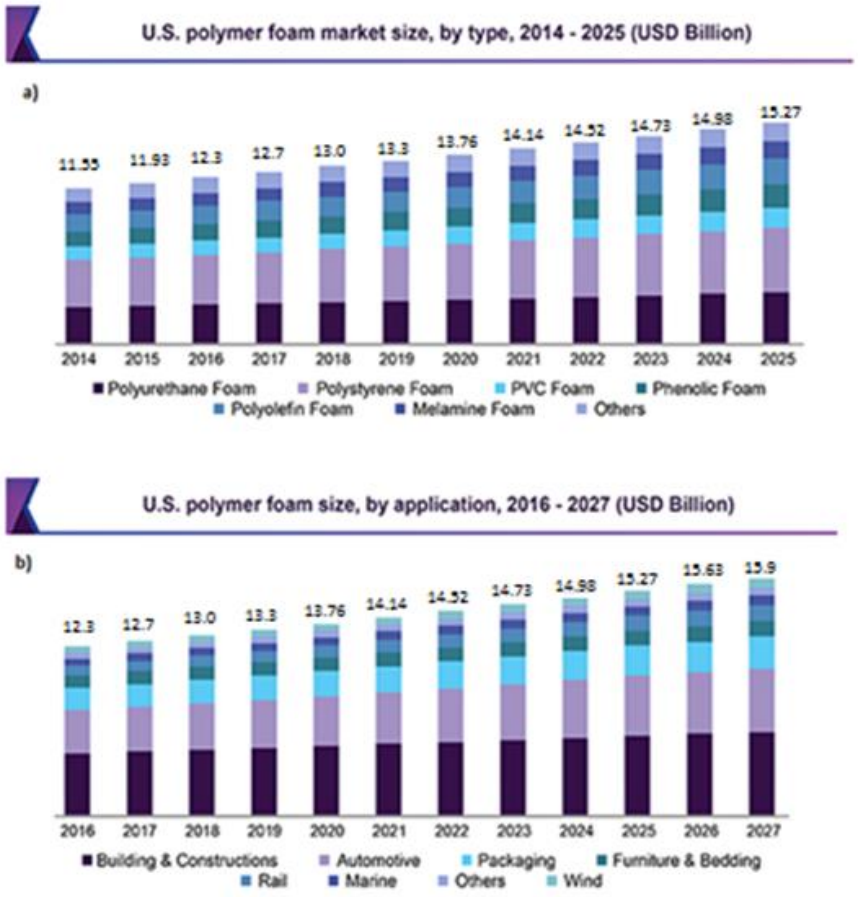


**Figure 1.4**. US market for polymeric foams during the years 2014-2025, classified by type of polymeric matrix. b) US market for polymeric foams during the years 2016-2027, classified by application sector.

Among the different polymeric matrices, the most used to produce cellular materials are polyurethane (PU), polystyrene (PS), polyvinyl chloride (PVC), and polyolefins (PO).[37–41] All these matrices have some interesting physicochemical properties, which have a significative impact on the final properties and applications of the cellular materials. **Figure 1.4(a)** represents the increase in the foam market (in billions of dollars) between 2014 and 2025, in the United States of America, classified by type of polymeric matrix.[42] The graph indicates that the foams based on PU and PS are the most consumed and this trend is expected to be remaining for the next few years. The importance of other polymer matrices

such as PVC or PO, which show a notable increase year after year, does not should be underestimated. Finally, a lower market is found with the foams produced with melamine matrices and with other polymeric matrices. **Figure 1.4(b)** analyzes the foam market in the United States during the period of years (2016-2027) in billions of US dollars, classified by application.[42] The triad of the construction, automotive and packaging sectors account for more than 60% of the foam market.

PVC-based cellular materials are mainly used in the production of profiles, sheets or tubes, which are find in sectors as diverse as decoration elements, whether in exhibitors, shop windows, interiors, signage or labeling, as well as part of sandwich panels in marine applications or in the production of certain pieces of yachts or airplanes.[43] They are also useful for the design of models or props in theater plays.[44] Finally, due to their good properties of resistance to humidity and external weather agents, PVC foams are also used in pipes or canalization systems.[45] Foams based on PO (generally those made with polypropylene (PP) and polyethylene (PE)) have good mechanical properties and elastomeric properties, respectively. Due to these properties, these materials can be used in automotive applications, as impact absorption elements or acoustic insulators, in the container and packaging sector or for comfort applications such as mattresses or protective elements of various pieces, as well as for insulation of pipes thanks to their ability to acting as barrier against water.[46-48] Rigid polyurethane (PUR) cellular materials are mainly used as thermal insulators in buildings or household appliances (particularly refrigerators), due to their good capacity as thermal insulators.[49] On the other hand, flexible polyurethane foams (PUF) are found in applications where good acoustic absorption or high elasticity is required.[50] These foams are used in elements such as: car roofs, mattresses, seats, packaging, etc.[51] Finally, foams based on polystyrene (PS) are commonly used in building insulation thanks due to their good capacity as thermal insulators. These foams are generally the competitors of PUR foams.[52] Likewise, PS foams are also used in architectural applications such as bases or supports for ornamental pillars, as packaging materials for yoghurts, or as protective materials for the packaging of different products. they are also used in more specific applications such as light fillers in road and rail constructions or in bicycle helmets, surfboards, etc.[53]

In this thesis, PS has been selected as polymeric matrix, **with the aim of studying, understanding, and improving the thermal properties (thermal insulation) of**

**the foams produced with this polymer**. In the case of the United States in 2017, the market volume of general PS and expanded PS (EPS) was estimated at 35 billion US dollars.[54] Likewise, it is expected that for the period from 2018 to 2025 the compound annual growth rate (CAGR) will yield values close to 4.5%.

The choice of this polymer is not by chance, and it is due to the good properties of PS. PS is a material that has a good foaming capacity, in a diverse range of molecular weights. This polymer presents a good ability to disperse particles in it , both organic and inorganic, due to its low processing temperatures and its good compatibility and miscibility using common mixing processes such as extrusion.[55] Regarding PS foams, these are characterized by their low thermal conductivities and good mechanical properties, which ultimately reflects a great capacity to work as thermal insulators. Likewise, PS foams have other great advantages such as their low water absorption capacity, their inability to freeze or their resistance to certain natural agents such as fungi.[56] Industrially, PS foams are usually produced by two different methods, resulting in extruded PS foams (XPS) and expanded PS foams (EPS).[54,57-59] However, the thermal conductivity of PS foams is still higher than that of other materials typically used in the sector of the construction like PUR. While PS foams have conductivities of 34 mW/mk (determined at a temperature of 10 °C), PUR foams have conductivities of 23 mW/mK at the same temperature.[60–62]

This thesis will aim to reduce the thermal conductivity **of these PS based materials** so they can be more suitable for the previously mentioned application (thermal insulators for the construction sector). The purpose of this work is to design new formulations that allow manufacturing low-density PS foams with an optimal cellular structure, which is a key factor to reduce their thermal conductivity.

To reduce the thermal conductivity of a foam different strategies can be used. For example, to produce the foam with blowing agents with a low thermal conductivity and a low diffusivity, to incorporate to the formulation IR blockers to reduce the radiation term of the thermal conductivity or to modify the cellular structure looking for a material with a low cell size.[63–65] For the present work, an attempt will be made to reduce the thermal conductivity by acting on the cellular structure, reducing the cell size towards micrometer values without increasing the relative density of the foams. To meet this goal, both inorganic nanoparticles and organic polymeric phases will be incorporated to the PS matrix.

Within cellular materials, it is important to highlight the microcellular materials, which are those whose cells have a size in the micrometric range.[66] These materials were born in the 1980s at the MIT (Massachusetts Institute of Technology), motivated by the problem of finding materials which allow reducing the amount of plastic material required to produce them without reducing their mechanical performance.[21] Through the Master's project carried out by Waldman and Martini and their patent with Professor Shu, it was concluded that the cellular materials with a cell density higher than $10^9$ cells/$cm^3$ and a cell size lower than 10 micrometers were suitable to reduce the plastic content while maintain the mechanical properties of their solid counterparts.[67,68] However, to produce these materials new foaming methods were required.[69] The gas dissolution foaming process allows the introduction of the blowing agent and its diffusion into the polymer matrix at certain conditions of temperature and pressure.[70-73] Currently the gas dissolution foaming method is one of the most widely used to produce microcellular materials. I In the 2000s the advances in the foaming technologies allowed the development of a new generation of cellular materials with cell sizes smaller than 500 nanometers (nanocellular materials) and properties that are currently under study.[32,71,74-76] However, one of the biggest impediments that these nanocellular materials find to prevail in the current market is that nowadays it has not been possible to scale their production satisfactorily from an environment of laboratory to an industrial process.

The generation of cellular materials by foaming is a phenomenon that has been extensively studied. Once the gas is dissolved in the polymeric matrix, a thermodynamic instability (for instance, a sudden reduction of the pressure or an increase in the temperature) produces a separation of the solid and gaseous phase, giving rise to small gas aggregates known as nucleation points. Subsequently, the gas, which is dissolved in the polymer matrix, diffuses towards the nucleation points. Nuclei grow due to this gas diffusion forming the cells of the cellular material. For this to happen, it is necessary to provide temperature to the system so the polymeric chains can acquire mobility. If the cellular structure is not stabilized at the right time, for example by rapidly cooling the cellular material, or if the material does not have an adequate melt strength, degeneration mechanisms will take place (coalescence, thickening and drainage), which result in foams with heterogeneous structures, large cells, high open cell contents and high densities.[23,80,81] All these mechanisms are well known by the scientific community. A diagram with them can be seen in **Figure 1.5**.


**Figure 1.5.** Diagram of the foaming steps for a cellular material

The control of the foaming mechanisms, in particular the nucleation and degeneration mechanisms, will have a critical influence on the subsequent cellular structure. One strategy to control nucleation is to introduce nucleating agents into the polymer matrix. In the present work, both inorganic nucleating agents, sepiolites, and organic nucleating agents, styrene-ethylene-butylene-styrene (SEBS) will be introduced. After the incorporation of these additives, the dominant nucleation changes from a homogeneous nucleation to heterogeneous nucleation, which requires less energy to occur. The nucleation theory will be analyzed in detail in the Chapter 2 of this manuscript. Likewise, previous research works have demonstrated that the degree of dispersion of the nucleating agents in the polymeric matrices is one of the fundamental parameters for an efficient nucleation.[82,83] If the dispersion of the nucleating agent in the polymeric matrix is not adequate, the cellular material generated could have a cellular structure (larger cell sizes, greater heterogeneity, etc.) worse than that obtained with the virgin polymer. Taking these ideas into account, a fundamental point of this thesis focuses on the one hand, on analyzing the dispersion degree of the nucleating agents (sepiolites and SEBS) in the polymer matrix (PS) and, on the other, on understanding how the dispersion degree conditions the structural characteristics and physical properties of the generated foamed materials. As it is indicated in **Figure 0.5**, after the nucleation stage, the cell growth stage begins. During the cell growth process the polymer, located in the structure of the cell walls, is subjected to an extensional force that induces a deformation that increases with the cell growth. Although an optimal dispersion of the particles in the polymeric matrix and, therefore, an adequate nucleation was achieved, if the polymeric matrix does not show resistance to these extensional forces, the cell walls will break favoring the mechanisms of cell degeneration.[84,85] The extensional rheological behavior (understood as the way in which the extensional viscosity of polymers depends on the extension to which they are subjected) determines the foamability of a polymer and, which is a key aspect to obtain cellular materials with a low density and with an adequate cellular structure (small cell sizes, low open cell contents, homogeneous structures, etc.).[23] It is therefore necessary for the polymer to present an increase in viscosity as that

extensional deformation increases. This phenomenon (increase in the viscosity as time or strain increases) is known as strain hardening. Thus, the analysis of both the dispersion degree of the nucleating agents in the polymeric matrix and their extensional rheological behavior will provide the necessary knowledge to understand the behavior of the material during the foaming process. Furthermore, several studies have shown that the final properties of cellular materials (thermal, mechanical, or acoustic properties) will depend critically on the cellular structures obtained.[71,86,87]

In this thesis, PS foams will be manufactured by means of a gas dissolution foaming process in an autoclave (this process will be explained in detail in the Chapter 2 of this thesis). The gas dissolution foaming process in very versatile and with this process it is possible to produce foams with different polymeric matrices. This process allows the modification of multiple variables, like pressure, temperature, or saturation times, which help to find optimal foaming conditions for each system. Moreover, the amount of material necessary to produce the foam is low in comparison with that required with other foaming process, like for instance extrusion foaming. Finally, it is possible to scale up the data and resultsobtained in the gas solution foaming process to other industrial processes that require a higher cost (such as extrusion foaming).

In summary, to generate the appropriate cellular materials it is necessary to select the optimum formulations, according to the characteristics of the base polymer. For this purpose, both the dispersion degree of the nucleating agent in the polymer matrix and the extensional rheological behavior of the polymeric formulation should be analyzed in detail. Once the formulation is defined, it would be also necessary to select the optimum processing parameters. Finally, an attempt will be made to verify the relationships between the cellular structure and the final properties of the foams (in this case the thermal conductivity). These steps will help to fulfill the great objective of this thesis, which is the exhaustive analysis of the composition, process, structure, properties circle for cellular materials based on PS.

## 1.3 Thesis Framework

This thesis has been carried out in the cellular materials laboratory (CellMat Laboratory: www.cellmat.es) of the Department Condensed Matter Physics, Crystallography and Mineralogy of the University of Valladolid.[88] CellMat is

directed by Prof. Dr. Miguel Ángel Rodríguez Pérez, who is also co-director of this doctoral thesis.

CellMat was founded in 1999 by Prof. Dr. José Antonio de Saja Sáez and by Prof. Dr. Miguel Ángel Rodríguez Pérez with the aim of developing a laboratory focused on the study of cellular materials.

In the early years, the main activity of the laboratory was the characterization of foams, especially those based on polyolefins.[89] It was not until 2005 that the laboratory was able to acquire the necessary equipment to produce cellular materials. As a result in 2012 a PhD thesis was defended by Dr. Cristina Saiz Arroyo in which the relationships between production process, cellular structure and physical properties of cellular materials were analyzed.[33] Since then, the group has acquired a wide experience in production issues (optimization of formulations and processing parameters), in the analysis of the foaming mechanisms using conventional and non-conventional techniques (X-ray radioscopy, IR thermography, optical expandometry, extensional rheology, etc.), and in the characterization of the structure and properties of cellular materials,. Th group is also specialized in analytical modeling to understand the relationships between formulation, structure and properties.

Currently CellMat has several research lines such as: the study of microcellular and nanocellular materials, the production of cellular materials based on bioplastics, the production of reactive cellular materials, specifically rigid and flexible polyurethane (PU) foams, the study of cellular nanocomposites. and on the development of multifunctional cellular materials.[32,38,39,76]

All the research works completed in CellMat have in their purpose a desire for applicability, since one of the main objectives of this group is the transfer of knowledge between the University and the industry. this transfer of knowledge will help to progress susceptibly faster. The proof of this university-industry relationship, is a spin-off company, called CellMat Technologies S.L., which was born in 2012.

In 2014, CellMat achieves a great milestone; the production of nanocellular materials, making CellMat one of the pioneering laboratories in the production of this type of materials. The first thesis that addressed this topic was the one presented by Dr. Javier Pinto Sanz.[90]

Part of the research work carried out in the present thesis is a continuity of that defended in 2016 by Dr. Ester Laguna Gutiérrez, co-director of this work, focused

on explaining the foamability of a set of materials, all of them based on polypropylene, through the study of extensional rheology. This is one of the theses that maintains the philosophy of establishing a relationship between the characteristics of the polymeric formulation, the production parameters and the characteristics of the cellular structure and final properties of the generated foams.[23]

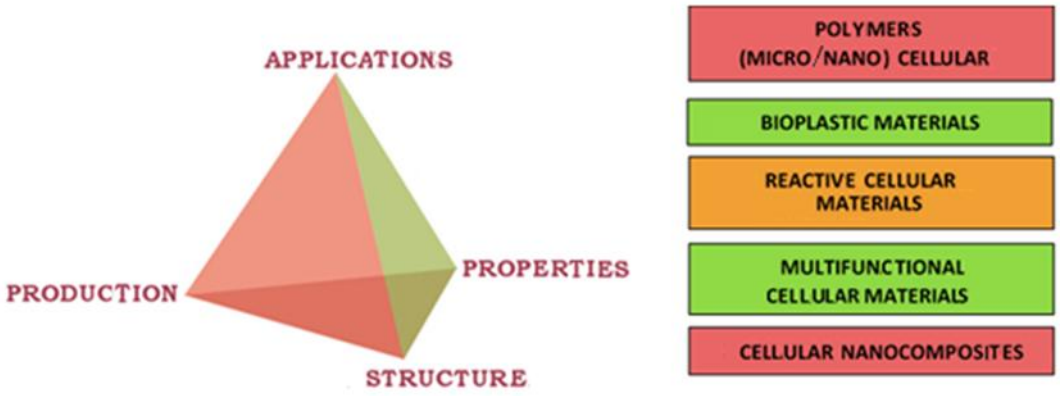


**Figure 1.6.** Tetrahedron representing the basic points pursued by the investigations in the CellMat group. On the right, basic lines of ongoing research in the CellMat group.

As it was previously mentioned, all the investigations in CellMat are based on analyzing and understanding the relationships between production, structure, properties, and applications through the experimental determination of the different parameters involved in the foaming process and by the use of analytical models. This concept is summarized in the tetrahedron in **Figure 1.6**, which collects the topics that are typically addressed in any investigation carried out in the CellMat laboratory.

CellMat is currently a world reference laboratory in the study, development, and production of cellular materials. As a result of this work, more than 240 publications have been made in indexed journals and 32 doctoral theses have been defended.[88]

The research work presented here is a continuity of the first works that study the relationships between formulation-production-structure-properties and has its basis on the previous experience and knowledge acquired by the laboratory. Thus, this thesis could be framed within the research lines of the study of microcellular materials, research in multifunctional materials and the study of

cellular nanocomposites. Likewise, an attempt is also made to provide the material with a possible framework for subsequent applications. For this purpose, PS was chosen as polymer matrix since it is a versatile material that covers a wide spectrum of the current foam market. The production process has been modified in multiple ways, studying the influence of various parameters, on the subsequent cellular structure obtained. In addition, some of the physical properties of these materials have been analyzed, in particular their thermal conductivity.

It is important to mention that some works of this thesis are part of the NEOADFOAM project (Innovative Additives for Foams with better Thermal Insulation and Fire Behavior) relative to the 2015 Collaboration Challenges program of the Ministry of Economy and Competitiveness of the Government of Spain. The project's main objective was the development of a family of multifunctional additives for polymeric foams. Those additives would be based on inorganic particles, sepiolites and sepiolites combined with other active elements, which would improve the thermal insulation and mechanical behavior of the foams, increasing, in turn, the performance against fire. The project considered two materials of great importance in the field of thermal insulation such as extruded polystyrene foams (XPS) and rigid polyurethane foams (PUR).

In the following section the objectives of this thesis are presented.

## 1.4 Objectives

In this section the main objective and the specific objectives of this work will be detailed.

**The main objective of this thesis is to study and understand the relationships between composition, process, structure, and properties of cellular polymers based on PS incorporating both inorganic nanoparticles (sepiolites) and organic particles (SEBS) to improve their thermal properties.**

**Figure 1.7** is a faithful representation of the steps that have been followed to achieve this objective. **First**, the most suitable **PS grades have been selected** considering their melt flow index. For this purpose, the relationships between the polymer molecular weight and some intrinsic characteristics of the polymer, as well as the effects caused by the molecular weight in the foaming process and in the subsequent cellular structure were analyzed in detail. **Subsequently, organic (SEBS) and inorganic (sepiolites) nucleating agents were incorporated into the**

**PS** polymers. In particular, PS formulations have been manufactured using different contents of three different types of sepiolites (with different surface treatment) and with different contents of a specific grade of SEBS. These formulations have been designed thinking in the production of foams with optimal properties and in the feasible to be industrially scaled. The mixing process of the polymer and the blowing agents has been carried out using a twin-screw extruder (more information about this process can be found in Chapter 3) and with different processing conditions. **Once these compounds have been manufactured, they have been characterized in detail to determine their rheological behavior and the dispersion degree of the nucleating agents in the polymer matrix.** The modification of the rheological properties of the product (especially the extensional rheological properties that will be studied in detail during this thesis), has a significative effect in the material foamability and in the final density and cellular structure of the generated foams. All these effects will depend on the type of nucleating agent employed (chemical composition, morphology, etc.), on the concentration of nucleating agent used and on the mixing method that allows dispersing the nucleating agent in the polymer matrix.

The **formulations** produced have been **introduced in an autoclave** for their foaming by using the gas dissolution foaming process (more information in Chapters 2 and 3). It is important to mention that the process parameters and the properties of the formulations have been modified to determine their effect in the foaming process (solubility and diffusivity) and in the characteristics in the foamed samples (density and cellular structure). For instance, the nucleating agents could affect the gas saturation process parameters making that the formulations absorb a higher quantity of gas than the pure polymer. The chemical affinity between the and the nucleating agent or the morphology of the particles, with internal channels, can make that the composites absorb a higher percentage of blowing agent than the pure polymer.[91] Likewise, when a polymer absorbs gas, its rheology is altered, and the viscosity is reduced due to the plasticizing effect. During the plasticizing effect, the gas dispersed in the polymer makes the polymeric chains easier to unwind and remain stretched, compared to their usual entangled position under standard conditions. This greater mobility of the chains has a notorious effect on reducing parameters like the glass transition temperature.[41] The reduction determines the foaming conditions (foaming temperatures and foaming times). Therefore, it is very important to

know the effect that the particles have on the solubility when they are added to the polymer matrix.

On the other hand, when a second phase is added to a polymeric matrix, heterogeneous nucleation is promoted (a more complete explanation of the foaming process and the types of nucleation can be found in the Chapter 2 of this thesis..[92] The modification of nucleation is mainly due to the fact that when a second phase is added there is a decrease in the energy barrier necessary for nuclei to appear (especially at the interface between polymer and the particle). Likewise, it also modifies the surface tension that is responsible for nucleation.[93] It is necessary to understand how the incorporation of the nucleating agents affects the foaming mechanisms by analyzing the effects associated to modify the type of nucleating agent, its concentration, and its dispersion in the polymer matrix.

**The cellular structure will be analyzed in detail**, by determining the cell size, the number of cells per cubic centimeter, also called cell density, its homogeneity, and the open cell content. All these parameters affect the final properties of the cellular materials. Likewise, in the case of having a second phase present in the raw materials, it will be possible to obtain bimodal cellular structures (that is, two well differentiated types of cells with different sizes). The bimodal structures will be also characterized with a parameter called volumetric fraction of cells, which will reveal the percentage of each type of cells in the structure.

Finally, the effects of the **cellular structure, as well as all the different process and composition parameters, already mentioned, on the thermal properties (thermal conductivity) of the different foamed samples will be characterize din detail.** Therefore, it is an objective of this thesis to explain the differences obtained in the properties of the foams through the different steps taken in the stages of composition, production and the cellular structure obtained, thus closing the **composition-process-cellular structure-properties circle**.

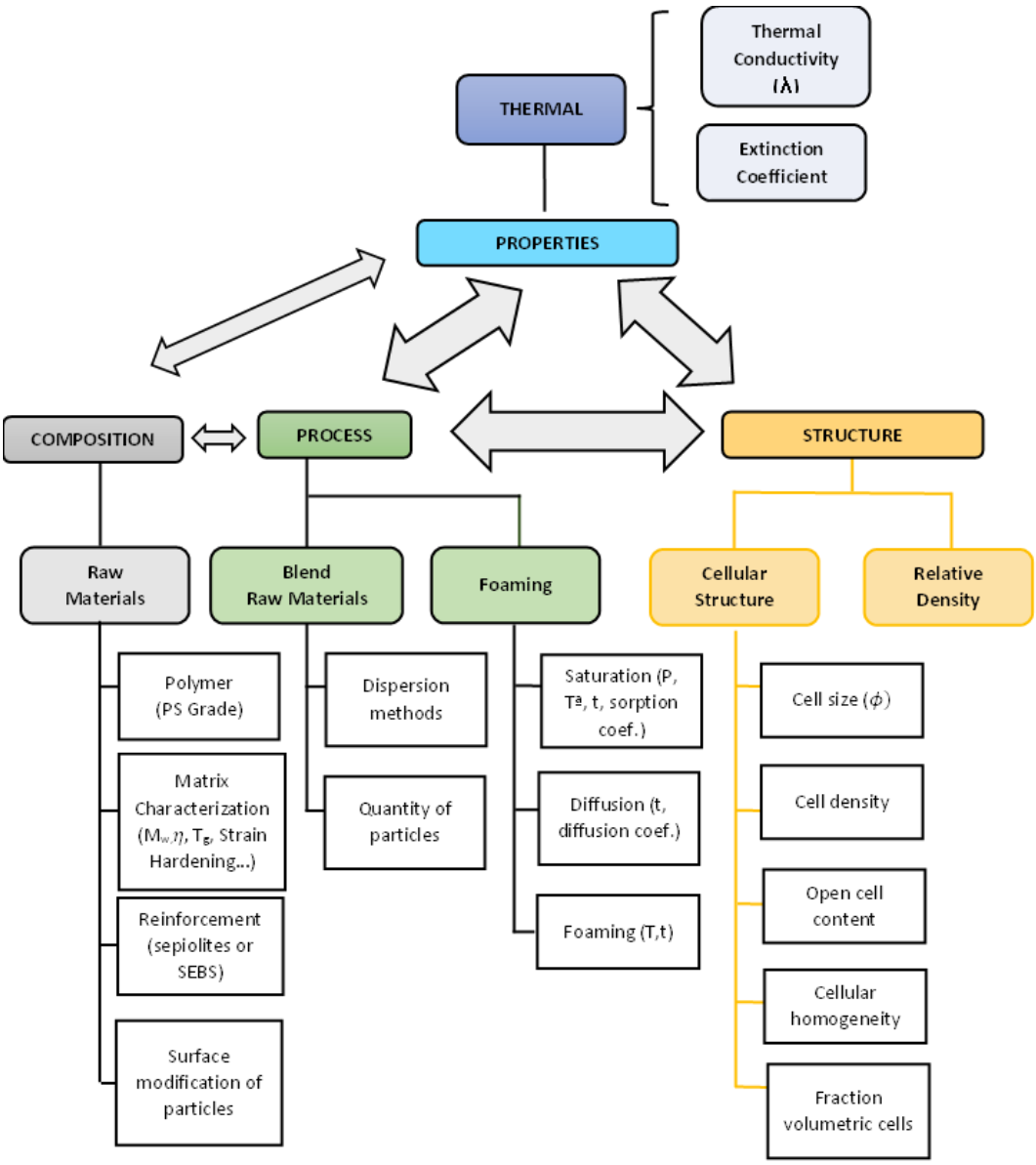


**Figure 1.7**. Scheme of the methodology that has been used in this thesis.

To fulfill this objective, the following secondary objectives are proposed:

**Analysis of the influence of molecular weight of PS on its foamability.**

This task has been carried out to select the most suitable grades of PS for foaming applications, which are those that allow achieving the greatest reductions in cell size and the most homogeneous and regular cellular structures, without causing an increase in the density of the foamed materials. To meet this objective, the following activities are proposed:

- **Determination of the molecular weight of different grades of PS, with different molecular weight, using different techniques: shear rheology and gel permeation chromatography (GPC).**
- **Analysis of the relationships between molecular weight and other parameters such as the glass transition temperature, the extensional viscosity (and more specifically, the strain hardening coefficient), the length of the molecular chains and the radius of gyration.**
- **Influence of the polymer molecular weight in the gas dissolution process. We will analyze how the molecular weight affects parameters such as solubility and diffusivity during the sorption process and during the desorption process.**
- **Production of foams using the gas dissolution foaming technique, using CO2 as blowing agent.**
- **Analysis of the density and structural characteristics of the cellular materials generated: cell size, anisotropy, cell density, etc.**
- **Analysis of the relationships between composition, process, and cellular structure.**

After this study, it will be possible to know what PS grades, according to their melt flow index or molecular weight, are the most suitable for foaming applications. The present study has resulted in a publication with the title: "***Influence of the molecular weight on the solubility, diffusivity and subsequent cellular structure of PS foams***". The article is currently pending submission to a scientific journal for publication.

**Analysis of the influence of the dispersion degree and the extensional rheological properties of nanocomposites based on PS and sepiolites on the cellular structure of foams generated from these nanocomposites.**

The main objective of this activity is to understand which of these two parameters (dispersion or extensional rheological properties) has a greater influence on the characteristics of the cellular structure of the foams. For this purpose, during this activity, on the one hand, the dispersion degree of different types and contents of sepiolites, which have been dispersed in a PS matrix using different extrusion conditions, will be characterized. On the other hand, the extensional rheological behavior of these compounds has been also analyzed. this way it will be possible to evaluate and understand how the cellular structure of foams generated from

these composites is affected by the degree of dispersion achieved and by their extensional rheological behavior, which in turn are conditioned by the composition of the compounds and by the manufacturing conditions used.

To achieve this objective, the following activities have been proposed:

- **Production of PS formulations with different types of sepiolites: organomodified sepiolites with quaternary ammonium salts, organomodified sepiolites with silane groups and natural sepiolites (without surface treatment).**
- **Production of PS formulations with different sepiolite contents that vary between 2% and 10%.**
- **Manufacture of formulations (compounds of PS and sepiolites) altering the processing conditions (subjecting the formulations to a single extrusion cycle or two).**
- **Analysis of the dispersion of the particles by means of X-ray tomography and dynamic shear rheology.**
- **Measurement of the extensional viscosity of the different formulations and determination of the strain hardening coefficient.**
- **Production of foams, with the formulations previously analyzed, by the gas dissolution method, using CO2 as a foaming agent and keeping the foaming parameters constant.**
- **Analysis of the influence of the degree of dispersion and the extensional rheological behavior on the characteristics of the cellular structures obtained.**

After this systematic study, we could know precisely how dispersion affects nucleation and how the extensional rheological behavior affects the degeneration mechanisms. This way, it will be possible to determine which of them has a higher effect when it deals on producing foams with low density, low cell size and homogeneous structures. From this work two publications have emerged with titles: "***Influence of the dispersion of nanoclays on the cellular structure of foams based on polystyrene***" and "***Polystyrene/sepiolites nanocomposite foams: Relationship between composition, particle dispersion, extensional rheology and cellular structure***". Both articles are published in the Journal of Applied Polymer Science and Materials Today Communications, respectively.

The knowledge acquired, in the previous objective, will be used to deepen the following secondary objective of this thesis:

**Analysis of the relationship between composition, structure and thermal properties in foamed materials based on PS/Sepiolites.**

This analysis aims to study the relationship between thermal properties (thermal conductivity and extinction coefficient) and the cellular structure obtained in PS/sepiolites foams. In the long term, learning can be obtained for the development of a guidelines that give rise to an exhaustive knowledge of the parameters that must be modified in order to improve the thermal properties of cellular materials and the influence that the cellular structure has on the thermal conductivity of PS-based materials. To achieve this objective the following tasks have been performed:

- **Production of PS formulations with different types of sepiolites: organomodified sepiolites with quaternary ammonium salts, organomodified sepiolites with silane groups and natural sepiolites (without surface treatment).**
- **Production of PS formulations with different sepiolite contents that vary between 2% and 10%.**
- **Manufacture of formulations (compounds of PS and sepiolites) by extrusion process with a single processing cycle.**
- **Production of foams, with the previous formulations, by means of the gas dissolution foaming method, using CO2 as the foaming agent and keeping the foaming parameters constant.**
- **Measurement of thermal conductivity of foams using the TPS method.**
- **Measurement of the extinction coefficient of the foams by means of FTIR.**
- **Correlation between the experimental values obtained from the thermal conductivity and the theoretically values determined by using analytical models available in the literature.**
- **Analysis of the relationship between the cellular structure and the thermal conductivity obtained.**

Thanks to this study, a publication has emerged with the title: "***Optimum cell size to reduce the thermal conductivity of foams based nanocomposites of polystyrene and sepiolites***". The article is currently pending submission to a scientific journal for publication.

**Inclusion of an organic reinforcement (SEBS) in the PS matrix. Analysis of its dispersion and of the cellular structure of the foams generated with the compound PS/SEBS.**

The last objective of this thesis is to evaluate how the cellular structure is modified when an organic reinforcement, specifically styrene-butylene-styrene (SEBS), is introduced into the PS matrix. Furthermore, a comparison has been made between the effects obtained when inorganic fillers (sepiolites) are incorporated and when organic fillers (SEBS) are incorporated. To achieve this objective, the following tasks have been carried out:

- **Production of PS/SEBS formulations with different percentages of SEBS (from 0.25 wt.% to 10 wt.%) using a twin-screw extruder.**
- **Analysis of the dispersion of SEBS in the PS matrix by means of scanning electron microscopy (SEM).**
- **Production of foams using the PS/SEBS compounds by gas dissolution foaming using CO2 as a foaming agent.**
- **Analysis of the cellular structure of the foams generated.**
- **Analysis of the relationship between composition, dispersion, and cellular structure.**
- **Comparison between the effects obtained when using inorganic fillers (sepiolites or talc) and those obtained when using organic fillers (SEBS).**

This analysis has led to a publication entitled: "***SEBS an effective nucleating agent for PS foams***". The article has been published in the journal Polymers.

he results of all the activities required to achieve the specific objectives of this thesis and therefore, to fulfill the main objective are collected in the Chapters 4, 5, 6 and 7 of this manuscript.

**Table 1.1** summarizes the studies that have been carried out and the chapters that include the different results obtained.

| *INFLUENCE OF MOLECULAR WEIGHT ON PS (CHAPTER 4)* |
|---|
| • **Determination of the molecular weight of different grades of PS.**<br>• **Analysis of the relationships between molecular weight and other properties of PS.**<br>• **Influence of the molecular weight of the polymer on the $CO_2$ solubility and diffusivity.**<br>• **Production of foams using the gas dissolution foaming process, using $CO_2$ as a foaming agent.**<br>• **Analysis of the cellular structure of the foams generated.**<br>• **Analysis of the relationships between molecular weight, foaming process and cellular structure.** |
| **PS/SEPIOLITES (CHAPTERS 5 & 6)** |
| • **Analysis of the dispersion of sepiolites in a PS matrix, depending on their modification, the percentage of particles and the process conditions.**<br>• **Analysis of the extensional rheological properties of the different PS/Sepiolites formulations.**<br>• **Manufacture of foams, using the formulations previously manufactured and analyzed, by gas dissolution foaming, using $CO_2$ as a foaming agent.**<br>• **Characterization of the density and cellular structure of the foams generated.**<br>• **Characterization of the thermal conductivity of the foams generated.**<br>• **Analysis of the relationships between composition, processing, cell**ular **structure, and thermal properties.** |
| **PS/SEBS (CHAPTER 7)** |
| • **Production of PS/SEBS compounds with different SEBS contents.**<br>• **Analysis of the rheological behavior (shear and extensional) of the generated compounds.**<br>• **Analysis of the SEBS dispersion in the PS matrix by means of SEM.**<br>• **Production of foams, using the PS/SEBS compounds, by gas dissolution foaming using $CO_2$ as a foaming agent.**<br>• **Analysis of the cellular structure of the foams generated.**<br>• **Analysis of the relationships between composition, rheological behavior, dispersion, and cellular structure.** |

**Table 1.1.** Summary of the content of Chapters 4,5,6, and 7.

The information and methodology of this thesis can be used to predict and select the most suitable polymeric matrices for foaming processes, considering different parameters: their viscosity, their molecular weight, their glass transition

temperature, their melt strength, etc. On the other hand, it will also allow the selection of the appropriate type and content of nucleating agents (both organic and inorganic) that when incorporated into the polymeric matrix allow optimizing the cellular structure of the foams generated and improving their thermal properties (reduction in the thermal conductivity). This methodology provides a great advantage when selecting the most suitable formulations to produce foams at industrial scale since it would allow to select the polymeric matrices and nucleating agents that give rise to the foams with the best thermal properties, only by characterizing the properties of the compounds, without the need to manufacture the foams. This means a significant reduction in costs derived from the selection of an optimal formulation and a significant reduction in time.

This raw material cost saving is illustrated below using an example and a simple numerical calculation. A small common extrusion plant can produce about 300 kg/hour of extruded PS foam (XPS). In a typical formulation, the PS, with a price between 1.1 and 1.6 €/kg, represents 86.5% of the formulation, the graphite masterbatch, with a price of 15 €/kg, which is employed as nucleating agent and infrared blocker represents 7.5% of the formulation, the flame retardant agent masterbatch, with a price of 20 €/kg, represents 6% of the total and finally the foaming agents necessary to produce the foam ($CO_2$ or a mixture of pentane with isopentane) usually have values that range between 2 €/kg and 4 €/kg and are introduced in percentages ranging from 4 to 6%, depending on the gas. Each extrusion test required to develop an optimal formulation is likely to be associated with a minimum time of about 4 hours between the set-up of the extruder, its stabilization, the production of the material, and the cleaning of the machine. From these 4 hours, at least for 2 hours all the components are introduced in the percentages mentioned above. During the remaining 2 hours only, pure polymer is introduced. This means that at least 1038 kg of polymer is used in each foaming test. Considering a price of the polymeric matrix of 1.3 €/kg and for the rest of the formulation the previously indicated costs, the final amount of the raw material would be 4,439 €. This value should be increased by approximately 25% to be able to consider the costs associated with production (machine consumption, personnel costs, electricity, water, etc.). In conclusion, the cost of each foaming test is at least 5,548 €. This value does not include the costs associated with the characterization of cellular materials nor the costs associated with waste management.

If instead of producing the material, the company applies the methodology developed in this thesis (with a cost of approximately 500 €), the costs would be reduced more than 10 times.

## 1.5 Structure of the Thesis

This thesis has been written in the compendium of publications mode. The structure of the thesis is summarized in **Figure 1.8**.

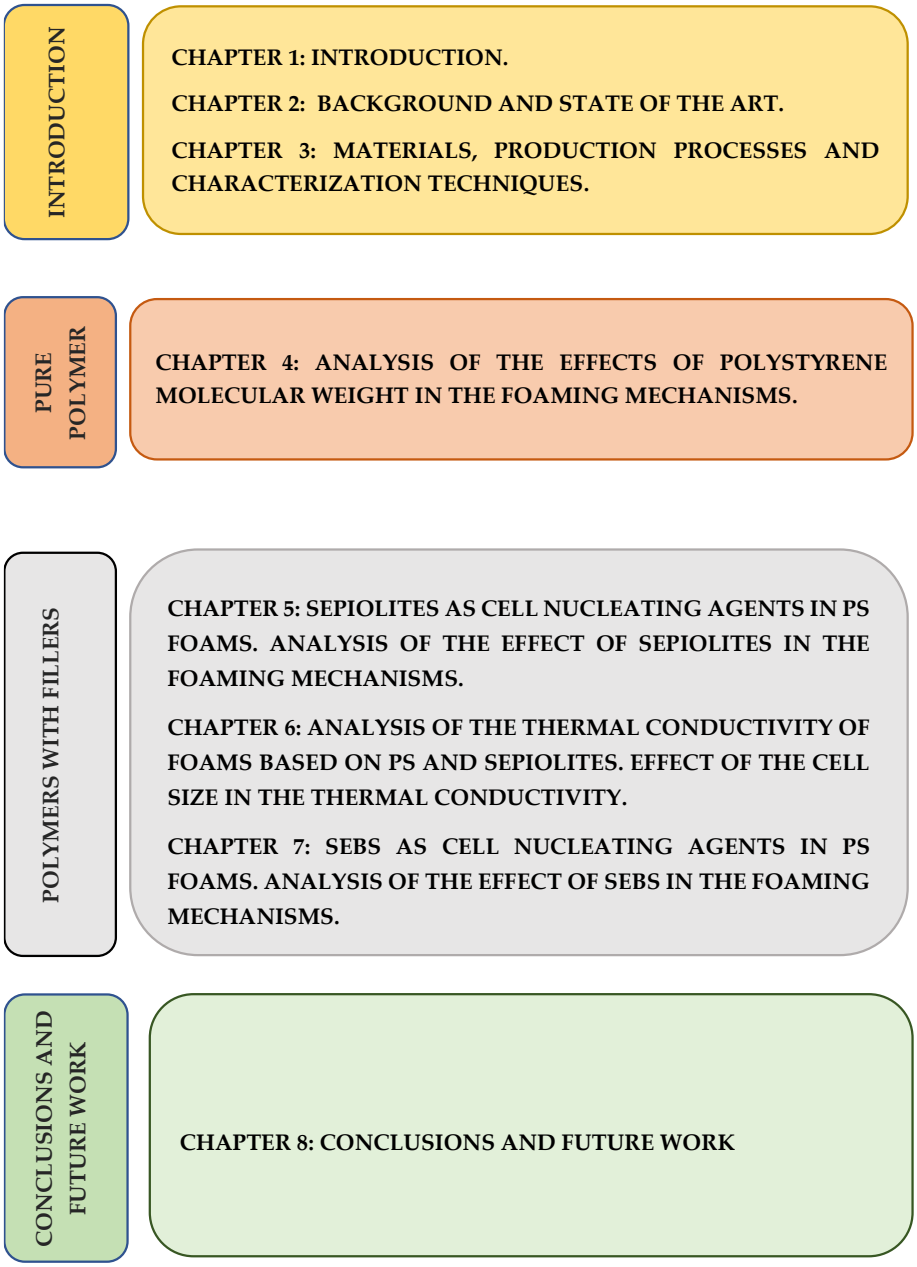


**Figure 1.8.** Distribution of the chapters that make up this thesis

Chapters 4 to 7 collect 5 scientific articles sent to international journals. Three of them have been already published and the other two are still pending acceptance. Figure 0.9 details the structure of the thesis.

The work presented is divided into nine chapters:

**Chapter 1. Introduction:** This chapter begins with a brief discussion of what cellular materials are and their status in the market. In the same way, the thesis framework is presented. Subsequently, the contents, objectives, and structure of the thesis are defined.

**Chapter 2. Background and state of the art:** In this section we can find a summary of the theoretical framework in which the thesis is framed, as well as a detailed study of the advances that have been made in the field of cellular materials based on PS. Likewise, this chapter will report the results, found in literature, regarding the use of the two nucleating agents employed in this thesis: sepiolites and SEBS.

**Chapter 3. Materials, production processes and characterization techniques:** This chapter describes the characteristics of the materials used during this thesis, as well as the production techniques used to generate solid compounds and cellular materials. Likewise, the characterization techniques used with solids and cellular materials are described.

**Chapter 4. Analysis of the effects of polystyrene molecular weight in the foaming mechanisms:** This chapter presents the results obtained after the analysis of three PS with different fluidity and therefore, with different molecular weight. This study has resulted in a scientific publication. The article describes how molecular weight is closely related to other structural characteristics of polymers such as glass transition temperature or average chain length. Finally, the relationship between the molecular weight of the polymer and characteristic parameters of the gas dissolution foaming process such as solubility and diffusivity, as well as the relationships between the polymer molecular weight and the cellular structure of the foams generated with these polymers Are analyzed in detail.

**Chapter 5. Sepiolites as cell nucleating agents in PS foams. Analysis of the effect of sepiolites in the foaming mechanisms:** This chapter contains the results related to two articles. The first one analyzes how the dispersion of the nanoparticles influences the subsequent cellular structure. To carry out a more detailed work, different effects are taken into account, such as the type of surface

treatment of the nanoparticles, their content or the process conditions used to produce the blends of the polymer with the sepiolites Finally, the foams have been produced by the gas dissolution foaming technique and the relationships between the composition (dispersion), the process conditions and the cellular structure obtained have been analyzed. On the other hand, the other article analyzes the relationships between the extensional rheological properties of the different formulations generated and the subsequent cellular structures of the foams produced with these formulations. n the same way as in the first article, the effects associated to the surface treatment of the sepiolites, their concentration in the polymer matrix and the process conditions employed to produce the blends are analyzed. With this two works it has been possible to determine which of the two conditions, a better dispersion of the particles in the PS matrix or a better extensional rheological behavior, has more influence on the cellular structure of PS based foams.

**Chapter 6. Analysis of the thermal conductivity of foams based on PS and sepiolites. Effect of the cell size in the thermal conductivity.** The formulations produced and analyzed in the previous chapter (Chapter 5) has been foamed and the thermal conductivity of the different cellular materials have been determined. The thermal conductivity of these foams has been measured using the TPS (transition plane source) technique and their extinction coefficient has been analyzed by means of FTIR (Fourier transform infrared spectroscopy. The results obtained have been related, through theoretical models, with the cellular structure to complete the circle that relates composition-processing-cellular structure and final properties of the foams. This chapter has an associated article.

**Chapter 7. SEBS as cell nucleating agent in PS foams. Analysis of the effect of SEBS in the foaming mechanisms:** In this work and once again looking a reduction in the cell size of PS foams, while maintaining their density, we have worked with an organic nucleating agent (SEBS). The dispersion of the SEBS particles in the PS matrix was analyzed by SEM to relate this parameter to the cellular structures obtained. In the same way, a publication is related to this chapter.

**Chapter 8. Conclusions and future work:** Chapter 8 presents the main conclusions of this thesis. In addition, certain points are presented that could serve as future work, as well as a global discussion of the results obtained when using organic and inorganic nucleating agents.

## 1.6 Publications, Conferences, Courses and Projects

### *1.6.1 Publications*

During the work carried out on this thesis, a series of scientific publications have been generated. The articles are listed in **Table 1.2**, which also indicates the number of the chapter where each article is found.

| Articles | Chapter |
|---|---|
| A. Ballesteros, E. Laguna-Gutiérrez, M. A. Rodríguez Pérez. **Influence of the Molecular Weight, on the solubility, diffusivity and subsequent cellular structure of PS foams.** Pending of submission | 4 |
| A. Ballesteros, E. Laguna-Gutiérrez, P. Cimavilla Román, M. L. Puertas, A. Esteban- Cubillo, J. Santaren, M. A. Rodríguez Pérez. **Influence of the dispersion of nanoclays on the cellular structure of foams based on polystyrene.** Journal of Applied Polymer Science. 2021,138, 46. | 5 |
| A. Ballesteros, E. Laguna-Gutiérrez, M. L. Puertas, A. Esteban- Cubillo, J. Santaren, M. A. Rodríguez Pérez. **Polystyrene/sepiolites nanocomposite foams: Relationship between composition, particle dispersion, extensional rheology and cellular structure** Materials Today Communications. 2021,102850. | 5 |
| A. Ballesteros, E. Laguna-Gutiérrez, M. A. Rodríguez Pérez. **Optimum cell size to reduce the termal conductivity of foams based on polystyrene/sepiolites nanocomposites.** Pending of submission | 6 |
| A. Ballesteros, E. Laguna-Gutiérrez, M. A. Rodríguez Pérez. **SEBS an effective nucleating agent for PS foams.** Polymers. 2021, 13 (21), 3836. | 7 |

**Table 1.2.** References of the articles that appear in the chapters of the thesis.

**Table 1.3** presents the publications performed during the doctoral thesis, which have not been included in this manuscript. This publication is related to the production of nanocellular polymers based on polymethyl-methacrylate (PMMA) and the analysis of their acoustic properties in contrast to microcellular cellular materials made with the same polymer.

| Articles |
|---|
| B. Notario, A. Ballesteros, J. Pinto, M. A. Rodríguez Pérez<br>**Nanoporous PMMA: A novel system with different acoustic properties.**<br>Material Letters. 2018,76-79. |

**Table 1.3.** References of articles made that do not appear in the chapters of the thesis.

### *1.6.2 Conferences*

The results obtained in the thesis have been presented in various national and international conferences, as it can be seen in **Table 1.4**.

| Conferences | |
|---|---|
| **1** | A. Ballesteros, E. Laguna-Gutierrez, M. A. Rodriguez-Perez, M. L. Puertas, A. Esteban-Cubillo, J. Santaren.<br>**Influence of the extrusion process, amount, and type of particles on the rheological properties of PS/nanoclay nanocomposites.**<br>9th European School on Molecular Nanoscience, ESMOLNA 2016, Tordesillas, Valladolid, Spain, May 2016. **Oral Presentation** |
| **2** | A. Ballesteros, E. Laguna-Gutierrez, M. A. Rodriguez-Perez, M. L. Puertas, A. Esteban-Cubillo, J. Santaren.<br>**Influence of the extrusion process, amount, and type of particles on the rheological properties of PS/nanoclay nanocomposites.**<br>XIV Meeting of the Group of Polymers, GEP 2016, Burgos, Spain, September 2016. **Poster.** |
| **3** | A. Ballesteros, P. Cimavilla-Román, E. Laguna-Gutierrez, M. A. Rodríguez Pérez, M. L. Puertas, A. Esteban-Cubillo, J. Santaren.<br>**Cellular materials based on blends of polystyrene and nanometric inorganic fillers. Relation between dispersion, structure, and properties.**<br>5th CellMat 2018-Cellular Materials, Bad Staffelstein, Baviera, Germany, October 2018. **Oral Presentation.** |
| **4** | A. Ballesteros, E. Laguna-Gutierrez, M. A. Rodriguez-Perez.<br>**Influence of molecular weight in the solubility, diffusivity, and the subsequent cellular structure of polystyrene foams.**<br>5th CellMat 2018-Cellular Materials, Bad Staffelstein, Baviera, Germany, October 2018. **Poster.** |
| **5** | A. Ballesteros, E. Laguna-Gutierrez, M. A. Rodriguez-Perez, M. L. Puertas, A. Esteban-Cubillo, J. Santaren.<br>**Cellular materials based on nanocomposites of polystyrene and nanometric inorganic fillers with a needle-like morphology. Relation between dispersion, structure, and properties.**<br>Foams 2019, Valladolid, Spain, October 2019**. Poster** |

**Table 14.** List of contributions to national and international conferences.

### *1.6.3 Courses and Projects*

**Table 1.5** summarizes all the courses performed in the frame of this thesis. The courses covered very diverse topics, from packaging to thermal or acoustic insulation, passing through rheology.

| Courses | |
|---|---|
| 1 | **Acoustic insulation in building. 2015,** Valladolid, Castilla y León, Spain**.** |
| 2 | **Seminar on characterization of materials by thermal analysis techniques: DSC, TGA.** October 2015, Valladolid, Castilla y León, Spain. |
| 3 | **Thermal insulation in buildings.** October 2015, Valladolid, Castilla y León, Spain. |
| 4 | **Characterization of polymeric materials.** October 2016, Valladolid, Castilla y León, Spain. |
| 5 | **Plastic packaging, fundamentals, regulations, and trends.** February 2018, Valladolid, Castilla y León, Spain. |
| 6 | **Curso teórico-práctico de reología.** 12, 13 of June 2018, Madrid, Spain. |

**Table 1.5.** List of courses taken during the thesis.

Likewise, throughout this thesis, different research activities have been carried out in public and private projects. The next table, **Table 1.6**, lists the projects, the financing entity, their duration, the main researcher, and the project budget in each case.

| | |
|---|---|
| **Project Title** | **NEOADFOAM:** Innovative additives to produce foams with enhanced thermal insulation properties and better fire behavior |
| **Financing Entity** | Ministerio de Economía y Competitividad, Spain Goverment. |
| **Time** | 2015-2018 |
| **Main Researcher** | M. A. Rodríguez Pérez |
| **Project Budget** | 234782,39 € |

| | |
|---|---|
| **Project Title** | **NUMASTA**: New advanced materials for the development of equipment inside water treatment sector. |
| **Financing Entity** | Ministerio de Economía y Competitividad, Spain Goverment. |
| **Time** | 2016-2018 |
| **Main Researcher** | M.A. Rodríguez Pérez |
| **Project Budget** | 78213 € |

| | |
|---|---|
| **Project Title** | **INUPIPE:** Development of Piping and Union Systems with Advanced Properties |
| **Financing Entity** | Ministerio de Economía y Competitividad, Gobierno de España |
| **Time** | 2018-2021 |
| **Main Researcher** | M.A. Rodríguez Pérez |
| **Project Budget** | 310008,30 € |

| | |
|---|---|
| **Project Title** | **LINPACK:** Towards a more sustainable packaging technology: development of foamed trays |
| **Financing Entity** | Linpack Packaging |
| **Time** | 2018-2020 |
| **Main Researcher** | M.A. Rodríguez Pérez |
| **Project Budget** | 68091,02 € |

**Table 1.6.** Projects of public and private nature in which collaboration has been carried out during the achievement of the thesis.

## 1.7 Work Methodology

This section describes the work methodology followed throughout the thesis to develop all the proposed experimental work and meet the defined objectives.

**1. Selection of raw materials:** First, the materials that will be used during the development of the thesis has been selected: PS as polymeric matrix, sepiolites and SEBS as nucleating agents, physical foaming agents (carbon dioxide) and antioxidants. The materials will be analyzed in more detail in the Chapter 3 of this thesis.

**2. Production of solid materials:** Once the raw materials have been selected, the solid formulations will be produced through an extrusion process. Subsequently, the PS compounds have been subjected to a thermoforming process to generate specimens with a suitable geometry, which can be used both for the characterization processes and for the manufacture of foams. **Table 1.7**lists the processes carried out to produce the solid formulations. These processes are explained in detail in the Chapter 3 of this thesis.

| Process of Production | Chapters |
|---|---|
| **Extrusion** | 3, 5, 6 y 7 |
| **Compression Molding** | 3, 4 ,5, 6 y 7 |

**Table 1.7.** Production processes used to manufacture the solid formulations of PS.

**3. Characterization of raw materials and solid formulations:** Different characterization techniques have been used throughout this thesis to characterize both the raw materials and the solid formulations produced from them. Among them, it is worth highlighting: the measurement of the density of the non-foamed composites at room temperature or at temperatures close to the foaming process, the analysis of the morphology of the materials by means of scanning electron microscopy (SEM) and X-ray computerized tomography, their characterization by shear dynamic rheology and extensional rheology, the analysis of the their thermal properties by means of differential scanning calorimetry (DSC) , the determination of the polymer molecular weight by gel permeation chromatography, and the determination of the nucleating agent content using thermogravimetry (TGA) and ash content techniques. All these techniques are listed in **Table 1.8**. Likewise, these techniques are described in the Chapter 3.

| Solid materials characterization | |
|---|---|
| **Characterization Technique** | Chapters |
| **Denisty determination (pycnometry)** | 3, 4, 5, 6 and 7 |
| **Scanning Electron Microscopy (SEM)** | 3, 4 ,5 ,6 and 7 |
| **X-Ray Micro-Tomography** | 3 and 5 |
| **Shear Rheology** | 3 ,4, 5 and 7 |
| **Extensional Rheology** | 3, 4, 5 and 7 |
| **Differential Scanning Calorimetry** | 3, 4 and 7 |
| **Thermogravimetric Analysis (TGA)** | 3 and 5 |
| **Gel Permeation Cromatography (GPC)** | 3 and 4 |
| **Ash Determination** | 3 and 5 |

**Table 1.8.** Techniques used for the characterization of solid and liquid materials.

**4. Production of cellular materials:** Once the raw materials have been selected, the solid materials produced and after having characterized their behavior, the foams were manufactured using the gas dissolution foaming process, which is listed in **Table 1.9** and which is discussed in detail in the Chapter 3 of this manuscript.

| Cellular materials production | |
|---|---|
| **Production Process** | **Chapters** |
| **Gas Dissolution Foaming Process** | 2, 3 ,4, 5 ,6 and 7 |

**Table 1.9.** Processes carried out to produce cellular materials.

**5. Characterization of cellular materials:** Different characterization techniques have been used to analyze the cellular materials generated, which have allowed, among other things to qualitatively and quantitatively analyze parameters of the cellular structure such as cell size, cell anisotropy, cell density or the volumetric fraction of cells in the case of bimodal structures and to analyze the fraction of open cells present in the structure. In addition to these parameters, it has been possible to study the density of the foamed samples through Archimedes' method, as well as their thermal conductivity. **Table 1.10** lists the main characterization techniques used in cellular materials. A more detailed explanation of the characterization of cellular materials can be found in Chapter 3.

| Cellular Materials Characterization | |
|---|---|
| **Characterization Techniques** | Chapters |
| **Density Determination (Archimedes)** | 3, 4, 5, 6 and 7 |
| **Open Cell Content (Pycnometry)** | 3, 4, 5, 6 and 7 |
| **Scanning Electron Microscopy (SEM)** | 3, 4, 5, 6 and 7 |
| **Extinction Coefficient** | 3 and 6 |
| **Thermal Conductivity by TPS Method** | 3 and 6 |

**Table 1.10.** Characterization techniques used in cellular materials.

**6. Analysis and interpretation of the results obtained:** The results obtained throughout the thesis have been profusely interpreted, analyzed and related to each other, in order to find a common thread that explains the composition-process-structure-properties relationship in PS-based cellular materials. The discussion and interpretation of these results can be found in Chapters 4 to 8 of this thesis.

**7. Development of a work methodology:** Once the obtained results have been interpreted and analyzed, a work methodology has been implemented that allows choosing the correct fraction and type of nucleating agent as well a the most suitable dispersion conditions. On the other hand, with this methodology it is possible to determine which parameter are having a higher influence in the

thermal properties of the foams and therefore, to modify these parameters in pursuit of a substantial improvement of the properties.

In **Figure 1.9** you can see a diagram that represents the previous points.

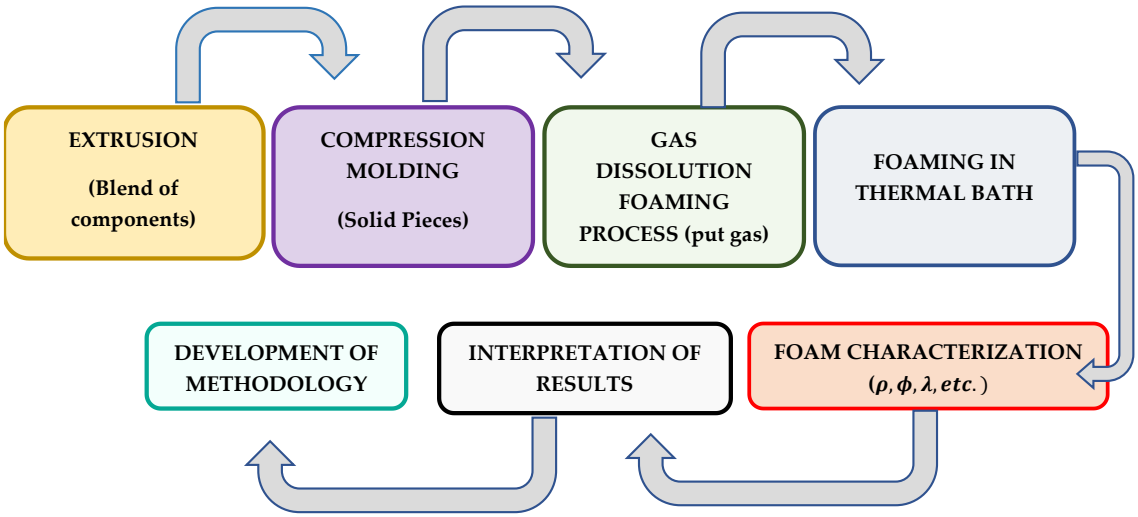


**Figure 1.9.** Scheme of the methodology followed in this thesis.

## 1.8 Bibliography


[1] H.G. Liddell, R. Scott, H.S. Jones,R. McKenzie. *A Greek-English Lexicon*. **1940,** Ninth Edition. Oxford University Press, United Kingdom.

[2] Imperial Chemical Industries LPD. *Landmarks of the Plastics Industry 1862-1962*. **1962**, Welwyn Garden City, United Kingdom.

[3] M.E. Bowden. *Chemical achievers: the human face of the chemical sciences*. **2015**, first Edition. Chemical Heritage Foundation, United States.

[4] Anonymous. *A Short Memoir of Alexander Parkes (1813–1890), Chemist and Inventor*. **1890**, printed for private circulation.

[5] C. Everton. *The History of Snooker and Billiards*. **1986**, first edition. Partridge Press, India.

[6] J.W. Hyatt. *J Ind Eng Chem*. **1914**,6(2),158-161.

[7] J.L. Nicholson G.R. Leighton. *Plastics Come of Age*. **08-01-1942**, Harper's Magazine, United States.

[8] K. Mulder, M. Knot. *Technol Soc*. **2001**;23(2),265-286.

[9] M. Demirors. *The History of Polyethylene, chapter 9 In: 100+ years of plastics, Leo Baekeland and beyond. **2011**, ACS Symposium Series, Vol. 1080*

[10] M.E. Hermes. *Enough for One Lifetime: Wallace Carothers, Inventor of Nylon*. **2005**, Chemical Heritage Foundation; United States.

[11] O. Bayer. *Angew Chemie*. **1947**;59(9),257-272.

[12] J. Scheirs, D. Priddy. *Historical Overview of Styrenic Polymers. In: Modern Styrenic Polymers: Polystyrenes and Styrenic Copolymers*. **2003**, first edition, John Wiley & Sons, United States.

[13] J. Borkin. *The Crime and Punishment of I. G. Farben*. **1978**, first edition, Free Press, United States.

[14] S. Vecchiato, J. Ahrens, A. Pellis, D. Scaini, B. Mueller, E. Herrero-Acero, G.M.Guebity.*ACS Sustain Chem Eng*. **2017**;5(8):6456-6465.

[15] G. Cecchin, G. Morini, F. Piemontesi. *Kirk-Othmer Encyclopedia of Chemical Technology*. **2003,**351-362.

[16] R.A. Auras, L.T. Lim, S.E.M. Selke, H. Tsuji. *Poly (Lactic Acid): Synthesis, Structures, Properties, Processing, and Applications*. **2010**, first edition, Wiley, New Jersey United states.

[17] F. Ullman. *Ullmann's Encyclopedia of Industrial Chemistry*. **2016**. Seventh edition. Wiley, New Jersey United states.

[18] H. Mera, T. Takata. *High-Performance Fibers. In: Ullmann's Encyclopedia of Industrial Chemistry*. **2000**. Seventh edition. Wiley, New Jersey United states.

[19] E. Frank, V. Bauch, F. Schultze-Gebhardt, K.H. Herlinger. *Fibers, 1. Survey. In: Ullmann's Encyclopedia of Industrial Chemistry*. **2000**. Seventh edition. Wiley, New Jersey, United states.

[20] E. Kishi, A. Ozaki, T. Ooshima, Y. Abe, M. Mutsuga, Y. Yamaguchi, T. Yamano. *Packag Technol Sci*. **2020**,33 (4-5),183-193.

[21] D. Eaves. *Handbook of Polymer Foams.**2004**,* first edition, Rapra Technology, Shropshire, United Kingdom.

[22] https://www.gellnerindustrial.com/applications-polymers. *Accessed November*

***2021***.

[23] E. Laguna-Gutierrez. *Understanding the Foamability of Complex Polymeric systems by Using Extensional Rheology*. **2016**, PhD Thesis, University of Valladolid, Spain.

[24] https://www.euractiv.com/section/energy-environment/news/while-global-plastic-production-is-increasing-worldwide-it-is-slowin-down-in-europe/. *Acessed November* ***2021***.

[25] R. Geyer, J.R. Jambeck, K.L. Law KL. *Sci Adv*. **2017**,3(7).

[26] G. Swift. *FEMS Microbiol Lett*. **1992**; 9(2-4):339-345.

[27] C.C. Ibeh, *Thermoplastic Materials: Properties, Manufacturing Methods, and Applications*. **2011,** first Edition. CRC press Taylor and Francis Group, Bocaraton, United States.

[28] J.Hopewell, R. Dvorak, E. Kosior. *Philos Trans R Soc B Biol Sci*. **2009**;364(1526),2115-2126.

[29] L.J. Gibson, M.F. Ashby. *Cellular solids. Structure and properties*. **2014**, second edition, Cambridge University Press, Cambridge, United Kingdom.

[30] P.S. Liu, G.F. Chen. *Porous Materials: Processing and Applications*. **2014**, first edition, Elsevier, Amsterdam, The Netherlands.

[31] M.Scheffler, P.Colombo. *Cellular Ceramics*: Structure, Manufacturing, Properties and Applications. **2005**, Wiley, New Jersey, United states.

[32] J. Martin-de Leon. *Understanding the Production Process of Nanocellular Polymers Based on PMMA Driven by Homogeneous Nucleation*. **2019**, PhD Thesis, University of Valladolid, Spain.

[33] C. Saiz-Arroyo. *Fabricación de Materiales Celulares Mejorados Basados en Poliolefinas. Procesado-Composicion-Estructura-Propiedades*. **2012**, PhD Thesis, University of Valladolid, Spain.

[34] *www.Foam-Expo.Eu. Accessed November* ***2021***.

[35] N. Mills. *Polymer Foams Handbook: Engineering and Biomechanicals Applications and Design Guide*.**2007**, first edition, Butterworth-Heinemann, Oxford, United Kingdom.

[36] S.T.Lee, C.B. Park, N.S.Ramesh. *Polymeric Foams*. **2016**, first edition, CRC press Taylor and Francis Group, Bocaraton, United States.

[37] N.L. Thomas. *J Cell Plast*. **2007**, 43(3), 237-255.

[38] M. Santiago-Calvo. *Synthesis, Foaming Kinetics and Physical Properties of Cellular Nanocomposites Based on Rigid Polyurethane*.**2019**, PhD Thesis, University of Valladolid, Spain.

[39] E. Lopez-Gonzalez. *Analysis of the Composition -Structure Properties Relationship of Open-Cell Polyolefin-Based Foams with Tailored Levels of Gas Phase Tortuosity*. **2019**, PhD Thesis, University of Valladolid, Spain.

[40] C.C. Kuo, L.C. Liu, W.C. Liang, H.C. Liu, C.M. Chen. *Compos Part B Eng*. **2015**,79,1-5.

[41] M. Sabzi, L. Jiang, M. Atai, I. Ghasemi. *J Appl Polym Sci*. **2013**, 129(4), 1734-1744.

[42] https://www.grandviewresearch.com/industry-analysis/polymer-foam-market. *Accessed November* ***2021***.

[43] https://stratongroup.com/blog/everything-you-need-to-know-about-pvc-foam-boards/. *Accessed November* ***2021***.

[44] https://www.zouchconverters.co.uk/news/2018/what-is-pvc-foam-and-what-is-it-used-for. *Accessed November* ***2021***.

[45] https://www.acmeplastics.com/Expanded-PVC-Foam.*Accessed November* ***2021***.

[46] https://www.arpro.com. *Accessed November* ***2021.***

[47] https://www.marketstudyreport.com/global-polypropylene-foams-market-size-research. *Accessed November* ***2021.***

[48] https://www.marketsandmarkets.com/Market-Reports/polyethylene-foam-market-129894004.html. *Accessed November* ***2021.***

[49] https://polyurethane.americanchemistry.com/polyurethane/Introduction-to-Polyurethanes/Applications/Rigid-Polyurethane-Foam/.*Accessed November* ***2021.***

[50] http://www.recticel.com/index.php/company/what-is-polyurethane.*Accessed November* ***2021.***

[51] https://polyurethane.americanchemistry.com/Flexible-Polyurethane-Foam/. *Accessed November* ***2021.***

[52] Y. Li, S. Ren. *Acoustic and Thermal Insulating Materials. In: Building Decorative Materials*. **2011**, first edition, Elsevier, Amsterdam, The Netherlands.

[53] M. Biron. *Composites, in: Thermosets and Composites*. **2013**, first edition, Elsevier, Amsterdam, The Netherlands.

[54] K. Pulidini, S. Mukherjee. *Report ID: GMI2063*. **2017**.

[55] J. Shen, C. Zeng, L.J. Lee. *Polymer (Guildf)*. **2005**;46(14), 5218-5224.

[56] https://engineer.decorexpro.com/en/otoplenie/uteplenie/ekstrudirovannyj-penopolistirol-kak-uteplitel.html. *Accessed November* ***2021.***

[57] N.H.R. Sulong, S.A.S. Mustapa, M.K.A. Rashid MK. *J Appl Polym Sci*. **2019**, 136 (20), 47529.

[58] S. Doroudiani, M.T. Kortschot, *J. Appl. Polym. Sci.* ***2003,*** 90, 1421–1426.

[59] M. Aksit, C. Zhao, B. Klose, K. Kreger, H.W. Schmidt, V. Altstädt. *Polymers (Basel)*. **2019**,11(2),268.

[60] G. Wypych. *Handbok of Polymers*.**2016**, second edition, Elsevier, Amsterdam, The Netherlands.

[61] H. Gausepohl, N. Nießner. Polystyrene and Styrene Copolymers. In: *Encyclopedia of Materials: Science and Technology*. **2001**, first edition, Elsevier Amsterdam, The Netherlands.

[62] H. Zhang, W.Z. Fang, Y.M. Li, W.Q.Tao. *Appl Therm Eng*. **2017**,115,528-538.

[63] M. L. Huber, A.H. Harvey. *Thermal Conductivity of Gases*. **2011**, ninety second Edition. CRC press Taylor and Francis Group, Bocaraton, United States.

[64] P. Acuña, Z. Li, M. Santiago-Calvo, F. Villafañe, M.A. Rodriguez-Perez, D.Y.Wang. *Polymers (Basel)*. **2019**;11(1):168.

[65] O.A. Almanza, M.A. Rodriguez-Perez, J.A.De Saja. *J Polym Sci Part B Polym Phys*. **2000**,38(7),993-1004.

[66] N.P. Suh. *Impact of microcellular plastics on industrial practice and academic research*. In Proceedings of the IUPAC Polymer Conference on Mission and Challenges of Polymer Science and Technology, Kyoto, Japan, 2–5 December

**2002**.

[67] F.A. Waldman.The *processing of microcellular foam*. **1982**, PhD Thesis, Massachusetts Institute of Technology (MIT), United States.

[68] J.E. Martini-Vvedensky, N.P.Shu, F.A. Waldman. *Microcellular closed cell foams and their method of manufacture*.**1982**, US 4473365A, patent.

[69] V. Kumar. N.P. Shu. *Polym Eng Sci*. **1990**;30(20), 1323-1329.

[70] K. Nadella, V. Kumar, W. Li. *Cell Polym*. **2005**, 24(2), 71-90.

[71] B. Notario, A. Ballesteros, J. Pinto, M.A. Rodríguez-Pérez. *Mater Lett*. **2016,** 168,76-79.

[72] V. Bernardo, J. Martín-de León, E. Laguna-Gutiérrez, M.A. Rodríguez-Pérez. *Eur Polym J*. **2017**,96,10-26.

[73] C.Forest, P. Chaumont,P. Cassagnau, B. Swoboda, P. Sonntag. *Prog Polym Sci*. **2015**, 41(6),122-145.

[74] B. Notario, J. Pinto, E. Solorzano, J.A. De Saja, M. Dumon, M.A. Rodriguez-Perez. *Polym (United Kingdom)*. **2015**,56,57-67.

[75] B. Notario, J. Pinto, E. Solorzano, A. Martin-Cid, M.A. Rodriguez-Perez. *Physical properties of nanocellular foams: the transition from the micro to the nano scale*. Polymer Conference international conference on Foams and Foams Technology, FOAMS 2014, New Jersey, United States, **2014**.

[76] V. Bernardo. *Production and Characterization of Nanocellular Polymers Based on Nanostructured PMMA Blends and PMMA Nanocomposites*. **2019**, PhD Thesis, University of Valladolid, Spain.

[77] S. Liu, J. Duvigneau, G.J. Vancso. *Eur Polym J*. **2015**,65,33-45.

[78] J.A. Reglero, P. Viot, M. Dumon. *J Cell Plast*. **2011**, 47(6), 535-548.

[79] E. Laguna-Gutierrez, A. Lopez-Gil, C. Saiz-Arroyo, R. Van Hooghten, P. Moldenaers, M.A. Rodriguez-Perez. *E.J Polym Res*. **2016**,23(12),251.

[80] H.E.Naguib, C.B.Park, N. Reichelt. *J Appl Polym Sci*. **2004**, 91(4), 2661-2668.

[81] R. Liao, W. Yu, C. Zhou. *Polymer (Guildf)*. **2010**;51(2),568-580.

[82] A. Ballesteros, E. Laguna-Gutierrez, P. Cimavilla-Roman, M.L. Puertas, A. Esteban-Cubillo, J. Santaren, M.A. Rodriguez-Perez. *J. Appl. Polym. Sci*. **2021,** 10, 51373.

[83] E. Laguna-Gutierrez, R. Van Hooghten, P. Moldenaers, M.A. Rodriguez-Perez. *J Appl Polym Sci*. **2015**, 132(47),1-12.

[84] R.K. Gupta RK, V. Pasanovic-Zujo, S.N. Bhattacharya. *J Nonnewton Fluid Mech*. **2005**,128(2-3), 116-125.

[85] E. Laguna-Gutierrez, R. Van Hooghten, P. Moldenaers, M.A. Rodriguez-Perez. *J Appl Polym Sci*. **2015** ,132(33).

[86] M.A. Rodriguez-Perez, J. Lobos, C.A Perez-Muñoz, J.A. De Saja, L. Gonzalez, B.M.A. Del Carpio. *Cell Polym*. **2008**;27(6):347-362.

[87] www.cellmat.es. *Accessed November **2021.***

[88] M.A. Rodriguez-Perez. *Propiedades Térmicas y Mecánicas de Espumas de Poliolefinas*. **1998**, PhD Thesis, University of Valladolid, Spain.

[89] J. Pinto. *Fabrication and Characterization of Nanocellular Polymeric Materials from Nanostructured Polymers*. **2014**, PhD Thesis, University of Valladolid, Spain.

[90] C.Yang, M. Wang, Z. Xing, Q. Zhao, M. Wang, G. Wu G. *RSC Adv*. **2018**,8(36),20061-20067.

[91] X. Han, K.W. Koelling, D.L. Tomasko, L.J. Lee. *Polym Eng Sci*. **2003**, 43(6),1206-1220.

[92] V.Kalimaknov. *Nucleation Theory*. **2013,** first edition**,** Springer,Berlin, Germany.

# Chapter 2

# Background and state of the art.

*"La historia es émula del tiempo, depósito de las acciones, testigo del pasado, ejemplo y aviso del presente, advertencia de lo por venir"*

El ingenioso hidalgo Don Quijote de la Mancha, Miguel de Cervantes.

# INDEX

## 2.1 Introduction

This chapter collects all the knowledge necessary to understand the background in which the basis of the thesis is supported.

Concepts like the definitions of cellular and microcellular polymers, the rheological behavior of molten polymers (in shear and uniaxial flows), the nucleation theory, the solid-state gas dissolution foaming process, and the thermal properties of polymeric foams, among others, are revised.

## 2.2 Cellular Polymers

The cellular materials are characterized by being composed of two different phases: a continuous gaseous phase which is dispersed into a solid matrix **(Figure 2.1).**[1] The nature itself presents multitude of examples of this kind of cellular materials (bones, balsa wood, some leaves of trees, etc.). Cellular polymers are those in which the solid phase is a polymeric matrix. The first cellular polymers were produced during the early 1920s, thanks to the production of cellular ebonite, one of the oldest rigid polymeric foams.[2]

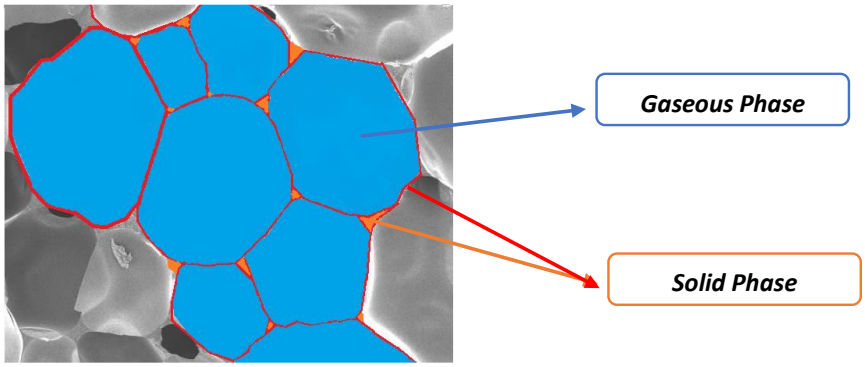


**Figure 2.1.** Micrograph of a cellular polymer. In blue color it is represented the gaseous phase. The solid phase is composed by the cell walls, which are colored in red, and the struts, which are colored in orange.

Cellular polymers have aroused a big interest in the scientific community due to the possibility of using these materials in plenty of applications and sectors. These materials are characterized by having a low density compared to their solid counterparts. Moreover, they have very interesting properties like good thermal, acoustical and electrical insulation, high energy absorption, good buoyancy, etc., which make them interesting materials for potential applications.[3-5] Even more, these properties can be extended for different polymer matrices, presenting for

example high magnetic permeability, acoustic absorption, chemical resistance, or hydrophobicity.[6-9] The possibility of producing materials presenting one or several of these properties make the cellular materials a perfect candidate to satisfy the requirements of plenty of different technological sectors like the building sector, packaging, aeronautic sector or automotive, etc.[10-12] Furthermore, the possibility of modifying the cellular structure of the cellular materials gives the possibility of designing and producing a unique material for a specific application, in other words materials on demand.

### *2.2.1 Classification and Main Characteristics*

Cellular materials can be classified following different criteria. One of the most common ways of classifying them is according to their relative density. The **relative density ($\rho_r$)** could be defined as the ratio between the density of the cellular material ($\rho_{cellular\ material}$) and the density of the polymeric solid matrix ($\rho_{polymer}$) as it is expressed in (**Equation 2.1**).

$$\rho_r = \frac{\rho_{cellular\ material}}{\rho_{polymer}} \qquad [2.1]$$

According to this parameter, cellular materials can be classified as low-density materials ($\rho_r < 0.2$), medium-density materials ($0.2 \leq \rho_r \leq 0.7$) and high-density materials ($\rho_r > 0.7$).[13] The final application, in which the cellular materials will be used, depends strongly on their final relative density. For instance, high-density materials are suitable for structural applications, whereas low-density cellular polymers are commonly used for thermal insulation applications.[14,15] One of the concepts more related with the relative density of a cellular material is **the porosity** ($\mathbf{v_f}$). The porosity is calculated following the **Equation 2.2** and it gives account of the volume fraction of the gaseous phase.

$$v_f = 1 - \rho_r \qquad [2.2]$$

Finally, concerning the relative density, another parameter that could be defined is the **expansion ratio**, which is the inverse of the relative density value (**Equation 2.3**).

$$E_r = \frac{1}{\rho_r} = \frac{\rho_{polymer}}{\rho_{Cellular\ Materials}} \qquad [2.3]$$

On the other hand, regarding to the cellular structure the cellular materials can be classified according to different parameters. The first one is related with the degree of interconnectivity between the cells. Open-cell materials are those in which the polymeric phase is only present in the cell edges also named as struts.[16] On the contrary, closed-cell materials are those in which the polymer is in both

the struts and the cell walls.[17] Finally, there is a possibility that a foam presents cells which are partially open and partially closed. These cellular materials are named as partially open cell materials. The typical structures of these materials can be seen in **Figure 2.2**.

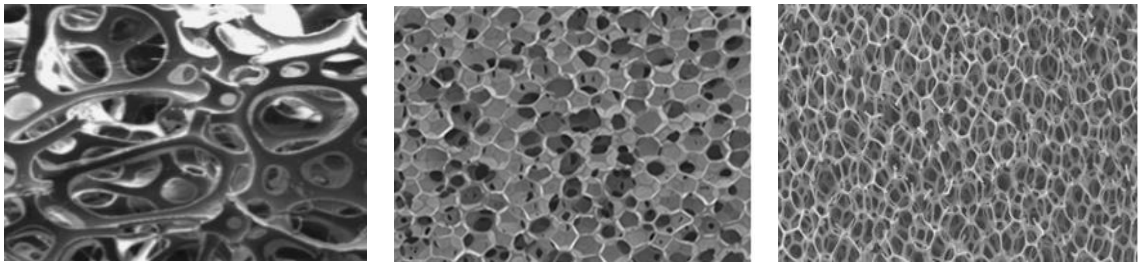

**Figure 2.2.** a) Micrograph of an open-cell cellular material. b) Micrograph of a closed-cell cellular material. c) Micrograph of a partially open cell cellular material.

Attending to the size of the cells that conform the foam it is possible to classify the cellular materials in three different ways. Macrocellular materials are those presenting cell sizes higher than 10 μm, microcellular materials are those presenting cell sizes between 10 μm and 1 μm. Finally, if a cellular material presents cell sizes lower than a few micrometers they will be named as nanocellular materials.[18]

One parameter that is strongly related with the cell size is the **cell density.** This value is defined as the number of cells per unit of volume of the cellular material. One possibility of calculating it is following the Kumar's approximation showed in **Equation 2.4**.[19]

$$N_v = \left(\frac{n}{A}\right)^{3/2} \qquad [2.4]$$

The Kumar's approximation considers, in a 2D micrograph of the cellular material, that the distribution of bubbles is isotropic. In this equation $N_v$ is the cellular density, $n$ is the number of cells observed in the image and $A$ is the area of the image. Regarding the previous classification of the cellular materials according to their cell size, the cell density for a macrocellular material varies between $10^6$ cells/cm$^3$ and $10^8$ cells/cm$^3$, in the case of a microcellular material the cell density varies between $10^8$ cells/cm$^3$ and $10^{10}$ cells/cm$^3$, and finally a material will be considered as a nanocellular material if it presents a cell density between $10^{13}$ cells/cm$^3$ and $10^{15}$ cells/cm$^3$.

The **cell nucleation density** ($N_o$) is defined as the number of nucleation points per cubic centimeter in the solid material. If it is assumed that each nucleus creates a cell in the final foam (which means that not degeneration phenomena

will appear during the foaming phase) the cell nucleation density could be defined according to **Equation 2.5**.

$$N_o = \frac{N_v}{\rho_r} \quad [2.5]$$

Where $N_v$ is the cellular density and $\rho_r$ is the relative density. Another possibility of calculating the cellular nucleation density for a polymeric cellular material is showed in **Equation 2.6**. In this equation three of the mentioned variables: relative density, cell nucleation density and cell size ($\phi$) are correlated.

$$N_0 = \frac{6}{\Pi\phi^3}\left(\frac{1}{\rho_r} - 1\right) \quad [2.6]$$

It is remarkable to mention that to obtain a material with a low relative density a high cell nucleation value is demanded. A high cell nucleation density is also required when it is pretended to reduce the cell size. For instance, in the case of an amorphous polymer like polystyrene (PS), a cell nucleation density of at least $3.5 \cdot 10^9$ nuclei/cm$^3$ is required to produce a cellular material with a relative density of 0.028 and a cell size of 10 μm.

Cell density, cell nucleation and cell size, strongly affects the final properties of the cellular material and determine their applications.[20]

The homogeneity and regularity of the cellular structure can be analyzed by considering the parameter SD/$\phi$, where SD is the standard deviation of the cell size.[21] A low value of this ratio indicates that the cellular material presents and homogeneous cellular structure and therefore, a narrow cell size distribution. There are some parameters describing the characteristics of the solid phase of the cellular structure. As it was previously mentioned the solid phase is distributed between the cell walls and the struts (see Figure 2.1). One of these parameters is the fraction of mass in the struts ($\boldsymbol{f_s}$), which is calculated as the ratio between the mass of the material which is located in the struts and the total mass of solid material (**Equation 2.7).**[22]

$$f_s = \frac{m_{struts}}{m_{struts} + m_{walls}} \quad [2.7]$$

To characterize the thickness of the solid phase that is between two cells, can be defined a parameter named as cell wall thickness ($\xi$). The cell wall thickness should be measured in the central area of the cell wall (which is usually the place where the cell wall thickness value is minimum in a cell wall). Like the cell size distribution in a foam is not perfectly homogeneous, there is a certain variability in the parameter of the cell wall thickness. Therefore, should be measured an

enough number of cell wall thicknesses to have a representative value of this parameter.

Finally, foams can be classified between rigid or flexible ones. Flexible cellular materials are those based on a flexible polymer matrix. Examples of flexible cellular materials are those based on low-density polyethylene (LDPE), ethylene vinyl acetate (EVA), ethylene butylene acrylate (EBA), etc.[23,24] On the other hand, rigid cellular materials are those composed by rigid polymeric matrices. Some examples of these polymers are polypropylene (PP), polyvinyl chloride (PVC), polystyrene (PS), etc.[25–27] The experimental procedures for measuring the cellular structural parameters are explained in detailed in Chapter 3.

## 2.3 Foaming Mechanisms

In this section the foaming mechanisms: nucleation, cell growth, degeneration and stabilization are explained in detail.

### *2.3.1. Nucleation*

Nucleation is defined as a process that generates nucleus (small bubbles) in a polymeric material due to a separation between the solid phase and the gaseous phase, which was previously introduced in the polymeric matrix.[28] Nucleation appears because of a thermodynamic instability produced, for instance, by an increase in the temperature or a release of the pressure.[29] Two mechanisms of separation of the gaseous and solid phases can appear at the same time, the spinodal decomposition and nucleation and growth.[30,31]

On the one hand, spinodal decomposition takes place at high supersaturations, at which the polymer/gas mixture is unstable.[32] This mixture undergoes spontaneous phase separation without the appearance of nucleation points. [33] This phenomenon is characterized by the vanishing of the energy barrier of nucleus formation, and so gas molecules immediately start to form clusters, which rapidly grow and coalesce.[34] The result of the spinodal decomposition is a single gas phase, or in other words, an interconnected or co-continuous cellular structure.

On the other hand, the main mechanism responsible for the phase separation in the gas dissolution foaming process is the nucleation.[18,35] The nucleation, as it has been defined in previous paragraphs, is the formation of small clusters of aggregates of gas in the polymer/gas mixture produced by a thermodynamic

instability.[36,37] Later, the gas will diffuse until the new clusters (also known as nucleus) allowing them to growth and conform the pores or cells. [38]

The formation of a nucleus requires to overcome a certain energy, as it could be seen in the following paragraphs.

Nucleation can be divided into two types: homogenous nucleation and heterogeneous nucleation, depending on which are the main responsible mechanisms.[39] The boundaries between homogenous nucleation and heterogeneous nucleation are not easy to define. Usually, if the gas is completed dissolved forming a continuous phase in a polymer, which does not present a second phase material, the process is recognized as homogenous nucleation.[18, 27, 40] On the contrary, heterogeneous nucleation occurs in the materials that present a secondary phase in the polymer, like for instance inorganic particles, which act as preferent nucleation points.[5, 40–42]

- ***Homogeneous Nucleation***

The homogeneous nucleation occurs in materials in which there are not any active nucleating agents, that is, the polymer is homogenous, or it contains additives that are not contributing to the nucleation process. These materials present just a single solid phase in which the blowing agent is the only responsible of creating the cellular structure.[43–45] According to the CNT (classical nucleation theory) the homogeneous nucleation rate, that is the number of nuclei formed per unit of volume and unit of time, could be explained as it is shown in **Equation 2.8**:

$$N_{Hom} = C_0 f_0 \exp\left(-\frac{\Delta G'_{hom}}{kT}\right) \qquad [2.8]$$

Where $C_0$ is the initial concentration of gas in the polymer, $f_0$ is the frequency factor of the gas molecules, $k$ is the Boltzmann constant, $T$ is the temperature and $\Delta G'_{hom}$ is the activation energy or Gibbs free energy barrier that could be defined as it is indicated in **Equation 2.9**:

$$\Delta G'_{hom} = \frac{16\pi\gamma^3}{3\Delta P^2} \qquad [2.9]$$

In which $\gamma$ is the surface free energy between the polymer and the blowing agent and $\Delta P$ is the pressure drop rate. To create a nucleus, it is necessary to exceed the Gibbs barrier.[36] The radius of a cluster of gas starts to grow more and more as soon as more energy is provided to the system. When it overpassed a certain limit, call free energy barrier or Gibbs barrier ($\Delta G'_{hom}$), the radius of the cluster reaches a critical radius ($r_c$) and additional molecules of gas will join this cluster

that now is a stable nucleus. On the other hand, if the energy is not high enough and the cluster does not reach the critical radius, the cluster and the gas molecules will be redistributed to other nuclei.[27]

The magnitude of the critical radius can be calculated using the **Equation 2.10**:

$$r_c = \frac{\gamma}{\Delta P} \qquad [2.10]$$

This critical radius depends on the surface tension of the mixture solid/gas and on the difference of pressure between the gas and solid phases.

**Equation 2.18** shows the dependency of the nucleation rate with variables like solubility, temperature, and pressure. The nucleation increases when the gas concentration increases. This relationship between the gas concentration and the nucleation rate has been confirmed through a bunch of numerous studies of different pure polymers.[46,47] On the other hand, the formation of nucleus will increase when the temperature of the process increases.[39] Furthermore, a higher gradient of pressure between the solid and the gaseous phase will lead to a higher nucleation rate. Moreover, the interfacial surface energy between the polymer and the gas also has an effect in the Gibbs energy barrier like it has been seen in **Equation 2.9**.[13] Therefore, by modifying the surface tension, which means in other words the viscosity of the polymer, the nucleation rate will be modified too. According to the equation proposed by Schonhorn, the surface tension of the polymer could be modelized like appears in **Equation 2.11**:

$$\gamma = A\, e^{\left(\frac{-B}{\eta_l - \eta_v}\right)} \qquad [2.11]$$

Where t $A$ is the surface tension when the viscosity is infinite, $B$ is a constant, $\eta_l$ is the liquid viscosity and $\eta_v$ the vapour viscosity. An increment of a viscosity of the polymer which means a higher difference between the liquid and vapour viscosities will lead to a higher value of the surface tension, which according to **Equation 2.9** will lead to a higher energy barrier and therefore, to a reduction of the nucleation rate.

- **Heterogeneous Nucleation**

The heterogeneous nucleation occurs in materials that present a second phase in the polymer to promote the nucleation in the interphase between the polymer and the mentioned new phase (impurities, nano o microparticles, decomposition products, organic phases, etc.)[41,42,48–50] Therefore, the surface tension of the pure polymer is altered by the presence of this second element (commonly known as nucleating agent) in the material. Particularly, the surface tension could be

reduced or increased by the second phase, which means that the Gibbs energy barrier could be also reduced or increased, respectively.[51] A simple equation to predict the surface tension of a heterogeneous system could be seen in **Equation 2.12**, where the surface tension of the heterogeneous material ($\gamma_{Het}$) could be defined as the addition of the surface tension of the polymer ($\gamma_p$) and the surface tension of the filler ($\gamma_f$) multiplied by the cosine of the wetting angle $\theta$ of the border of the two faces.

$$\gamma_{\mathrm{Het}} = \gamma_{\mathrm{p}} + \gamma_{\mathrm{f}} \cos\theta \qquad [2.12]$$

In the heterogeneous nucleation, the energy required to produce a nucleus in the interphase between the main polymer and the second phase is lower than for any other single point due to the tendency of the gas molecules to aggregate in the surface among the two materials.[8, 52] This fact facilitates the appearance of new and preferable nucleation points in the matrix. Moreover, by acting in the content of nucleating agent it is possible to modify the homogeneity of the cellular structure as well as promoting a higher number of cells in the future foam.[53] The equation (**Equation 2.13**) that rules the heterogeneous nucleation is similar as the one for the homogeneous nucleation (**Equation 2.12**), although they differ in the free energy barrier term.

$$\mathrm{N_{HET}} = \mathrm{C_1 f_1} \exp\left(\frac{-\Delta \mathrm{G'_{het}}}{\mathrm{KT}}\right) \qquad [2.13]$$

Where $C_1$ is the initial concentration of gas in the polymer matrix, $f_1$ is the frequency factor of the gas molecules, $k$ is the Boltzmann constant, $T$ is the temperature and $\Delta G'_{het}$ is the free energy barrier for the heterogeneous nucleation that should be overpassed to obtain stable nucleus.

The energy barrier for heterogeneous nucleation could be defined as it is indicated in **Equation 2.14**:

$$\mathrm{N_{HET}} = \Delta \mathrm{G'_{hom}}\, \mathrm{f}(\theta) \qquad [2.14]$$

Where $\Delta G'_{hom}$ is defined as the activation energy or Gibbs free energy in (**Equation 2.15**), meanwhile $f(\theta)$ is a function that considers the ratio between the homogeneous and the heterogeneous nucleation. This function presents values that are equal or lower than one. The physical meaning of $f(\theta)$ is to represent the wetting angle between the polymer, the second phase and the gas interphase.[54]

$$\mathrm{f}(\theta) = \frac{1}{4}(2 + \cos\theta)(1 - \cos\theta)^2 \qquad [2.15]$$

The energy necessary to produce a heterogeneous nucleation is always lower or equal than the one needed to overload the barrier for the homogenous nucleation.

On the other hand, the critical radius needed for a gas cluster to form a future stable nucleus is not modified by the presence of a second solid phase.[13] The size of the particle compared to the critical radius value, is crucial for determine the capability of the particle to work as nucleating agent. Furthermore, if the size of the particles used as nucleating agents is higher than the cell wall thickness the particles could favor the rupture of the cell walls.[55] Therefore, it is very important to control the size of the nucleating agents.

Taking these ideas into account, the cell nucleating agent selected to reduce the energy barrier to improve the cell nucleation density will depend on plenty of different variables. For instant is important to consider the affinity between the cell nucleating agent, the polymer, and the blowing agent.[41, 56–58] Previous studies reported that hybrid nanocomposites like hybrid mixtures of attapulgites with polypyrrole or metal organic frameworks (MOF), as well as silica particles present an affinity with the $CO_2$ gas and can act as efficient $CO_2$ collectors.[59–61] This fact will help to increase the concentration of gas molecules in the system which will have a strong effect in the nucleation. On the other hand, weak interactions between the nucleating agents and the polymer matrix, generally lead to a favorable nucleation, due to the reduction of the energy barrier in the interphase.[62] The processing conditions (temperature, pressure, time, etc.) determine which nucleation mechanisms, if the heterogeneous or the homogenous ones, dominate in the process. Furthermore, it is important to have nucleating agents with a regular and uniform size. On the other hand, some process like bimodality (obtention of structures with two or more predominant cell sizes) could be obtained.[63,64] Finally, the dispersion of the cell nucleating agent in the polymer matrix is a critical aspect. For an effective nucleation, the nucleating gents must be well dispersed in the polymer matrix without forming agglomerates. If nucleating agents are forming agglomerates the number of nucleation points is reduced leading to a deficient nucleation.[65]

During this thesis different types of nucleating agents have been used: inorganic nucleating agents (sepiolites) and organic nucleating agents (styrene-ethylene-butylene-styrene, SEBS). Moreover, the effects in the cellular structure produce by changing the content of the nucleating agent, the surface treatment, in the case of the nanoparticles, and the process conditions required to produce the blends polymer/nucleating agent have been deeply analyzed.

One of the objectives of this thesis is to reduce the cell size of PS foams, while maintaining their density, to improve the thermal insulation properties of this kind of materials. To fulfill this objective cell nucleation densities higher than $10^{10}$ nucleus/cm$^3$ are required. It is very difficult to reach these densities only with homogeneous nucleation. Conventional cell nucleation densities for common PS are in the order of $10^6$ cells/cm$^3$. Extreme processing conditions during the gas dissolution process (very high pressures or very low temperatures) are required to achieve these nucleation densities when working with pure polymer matrices, without nucleating agents. However, with the presence of nucleating agents, the target nucleation density could be reached without using these extreme processing conditions. When those nucleating agents are added to the polymer matrix the final cellular structure is affected by the second phase and the parameters related with it. Therefore, the cited variables (that is, the concentration of the cell nucleating agent, the dispersion of the nucleating agent in the matrix, the affinity between the nucleating agent, the polymer matrix, and the blowing agent, etc.) will control the nucleation of the system and influence dramatically on the final morphology of the cellular structure.

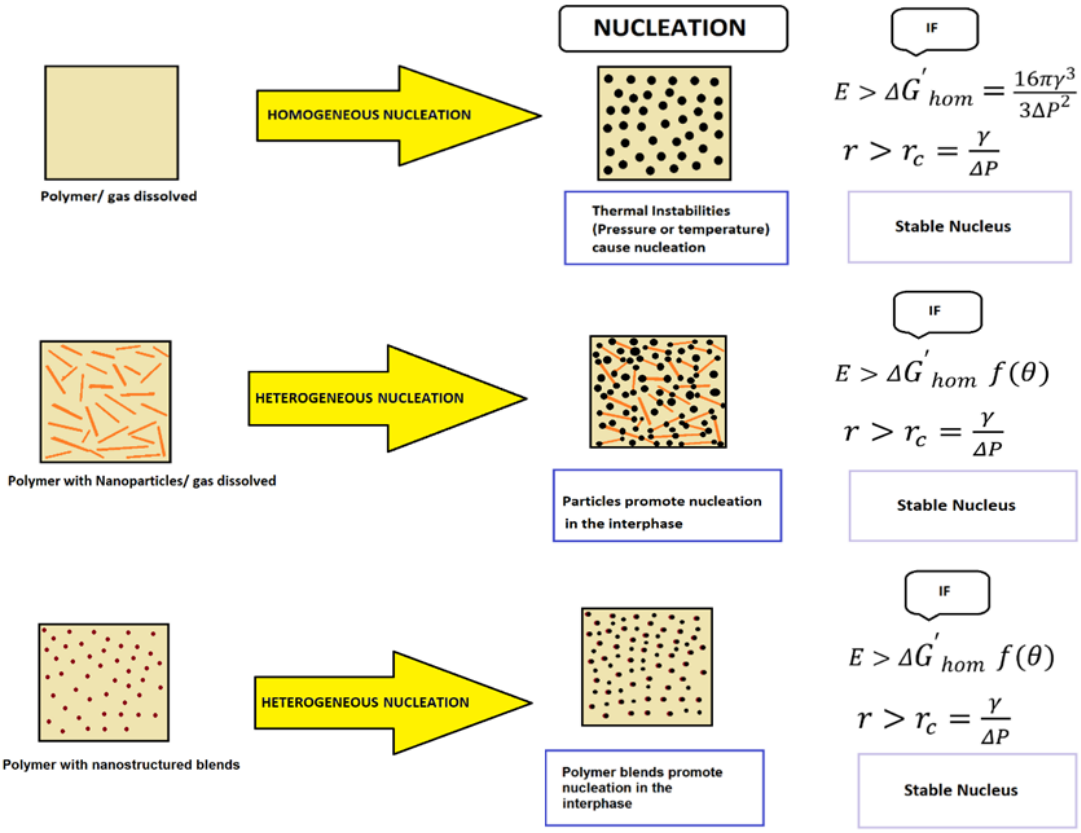


**Figure 2.3.** Schematic draw of the different nucleation processes for pure polymers, polymer nanocomposites and polymer with nanostructured blends.

**Figure 2.3** shows a scheme of the two types of the nucleation processes for a pure polymer, a nanocomposite, and a polymer containing nanostructured blends.

### *2.3.2 Cell Growth*

Once the stable nuclei have been formed, is time to provide energy to the system in order that these nucleus star to grow to generate the cells. One of the most common approximations to understand and describe the cell growth is the assumption of a cluster of gas surrounded by a Newtonian liquid with a constant viscosity.[28,37,66,67] When the polymer/gas system is heated, the gas, which is dissolved in the polymer matrix, diffuses into the nucleation points¡ allowing them to growth until the stabilization (sub section 2.6.4) occurs.

In the mentioned model, the evolution of the growth of the cell with the time could be defined as it is indicated in **Equation 2.16**:

$$\frac{dR}{dt} = \frac{R}{4\eta}\left(P_i - P_o - \frac{2\gamma}{R}\right) \qquad [2.16]$$

Where $\frac{dR}{dt}$ represents the cell growth rate, $R$ the radius of the bubble, $\eta$ the viscosity of the melt polymer, $P_i$ the pressure inside the bubble, $P_o$ the pressure outside the bubble and $\gamma$ the surface tension between the polymer and the gas interface. From **Equation 2.17** it can be concluded that the viscosity plays a major role in the growing of the cells and in the development of the cellular structure.[44, 68] A high value of the viscosity of the molten polymer will reduce the cell growth rate, if the viscosity is very high the nuclei will not have the possibility of expanding.[69,70] On the other hand, if the viscosity of the molten polymer presents a low value, the expansion rate will be higher. If this parameter is very high the polymer would not be able to withstand the rapid expansion of the bubbles. [71] This could lead to a rupture of the solid cell walls and consequently, to an increase of the degeneration phenomena, like cell coalescence, which will be analyzed in detail in next subsection (sub-section 2.3.3). [72, 73]

The ideal situation is that in which the polymer viscosity is low at the beginning of the foaming process and later, this parameter increases as the foaming process evolves. In other words, it is necessary that the polymer viscosity changes during the foaming process.[74–77] At the beginning of the foaming process a low viscosity is required to favor the initial cell growth. Later, as the polymer process evolves and the polymer is subjected to high extensional forces, the viscosity should increase allowing the solid polymer matrix to resist the extension without breaking. The change as a function of time from a low viscosity value to a high viscosity value is usually known as strain hardening behavior.[25, 75, 78–81] If this

increase in the viscosity as the extension increase does not happen or is not high enough, the polymer is not going to be able of withstanding the extensional forces and it is going to break. In this case the cellular structures are going to present large cell size, high open cell contents and they are going to be very heterogeneous.[71,72,82] In some case a densification and a collapse of the cellular structure can also occur. All these behaviors can be seen in **Figure 2.4.**

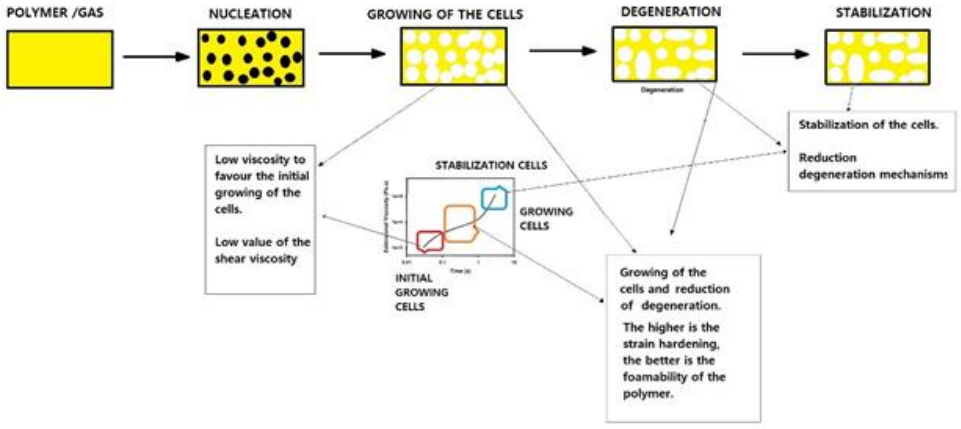


**Figure 2.4.** Schematic draw of the different foaming steps related with the extensional rheological behavior of a polymer as function of time.

Furthermore, as it was mentioned before, the viscosity of the pure polymer is reduced by the presence of the blowing agent in the system, due to the plasticization effect.[83,84] The gas absorbed by the polymer provides higher mobility to the polymeric chains due to the weakness of the entanglement of the molecules. The higher mobility of the chains leads to a reduction of the glass transition temperature ($Tg$) or the melting temperature ($Tm$), in the case of a semi-crystalline polymer. This new glass transition temperature, obtained once the gas is dissolved din the polymer matrix, is known as effective glass transition temperature.[85–87] To transmit to the nucleus, the energy necessary for the growing of the cells, it is necessary to overcome this effective glass transition temperature. In the case of PS, which is an amorphous thermoplastic polymer, a temperature higher than the effective glass transition temperature must be employed during the foaming process to allow cell growth.[88,89] Furthermore, the foaming temperature and the foaming time should be controlled carefully to avoid the appearance of some degeneration mechanisms like cell coalescence or drainage. Therefore, it is critical to known in what magnitude the glass transition temperature is reduced once the blowing agent is dissolved into the polymer matrix. Two theoretical models, the Chow model and the Chan-Yoon model can

be used for estimating the depletion of the glass transition temperature in a pure amorphous polymer like PS. [40,64]

**Equations 2.18a, 2.18b and 2.18c** represent the Chow model, where $T_g$ is the effective glass transition temperature, $T_{g0}$ is the glass transition temperature of the bulk polymer, $M_p$ is the molecular weight of the monomer of the polymer, $w$ is the weight percentage of gas dissolved in the material, $z$ is the coordination number of system polymer-gas, $M_d$ is the molecular weight of the blowing agent, R the ideal constant of the gases and $\Delta C_{p-Tg}$ the difference in the heat capacity during the glass transition.

$$\ln\left(\frac{T_g}{T_{g0}}\right) = \psi[(1-\theta)\cdot\ln(1-\theta) + \theta\ln\theta] \qquad [2.18a]$$

$$\theta = \frac{M_p \cdot w}{z \cdot M_d \cdot (1-w)} \qquad [2.18b]$$

$$\psi = \frac{z \cdot R}{M_p \cdot \Delta C_{p-Tg}} \qquad [2.18c]$$

Several authors have reported that Chow model provides precise results on the depletion of the glass transition temperatures for polymers like PS, poly (methyl methacrylate) (PMMA), polycarbonate (PC) or polyvinyl chloride (PVC) in combination with a gas blowing agent.[58,64,90] However, it is reported that the accuracy of the Chow model at high gas concentrations of gas start to fail. On the other hand, the Cha-Yoon Model (**Equation 2.19**) has also been claimed as effective for calculate the reduction of the glass transition in several polymers like PS, PC, PMMA or acrylonitrile butadiene styrene (ABS).

$$T_g = T_{g0}\ \exp\left[-(M_P)^{-1/3}(\rho_s)^{-1/4}\alpha\omega\right] \qquad [2.19]$$

In **Equation 2.19** $T_g$ is the effective glass transition temperature, $T_{g0}$ is the glass transition temperature of the bulk polymer, $M_p$ is the molecular weight of the monomer of the polymer, $\rho_s$ is the density of the bulk polymer, $w$ is the weight percentage of gas dissolved in the material and $\alpha$ is a constant of the system polymer-gas. This model presents the drawback of the lack of values in literature for the different constants of the polymer-gas system.

In the actual thesis both models will be used for the pure PS to see how the glass transition temperature is reduced after the incorporation of the blowing agent.

### *2.3.3 Degeneration phenomena of the cellular structure*

In the last stages of the cell growth different degeneration mechanisms occur, which could lead to a deterioration of the cellular structure, if they are not controlled in a suitable way. These degermation mechanisms are

coalescence, coarsening and drainage. [68,91]

- **Cell Coalescence**

Cell coalescence is a mechanism that occurs when the cell walls, which divide two growing continuous cells, break because the polymer is not able to resist the extensional forces that appear during the foaming step.[7,73,92,93] As a result, two contiguous cells become a single cell with a larger size. The combination of two small cells into one single bigger cell is thermodynamically favorable, because the surface area is reduced. On the other hand, cell coalescence increases dramatically the cell size and consequently reduces the cell density of the material. Moreover, these coalescence degeneration mechanisms could also lead to an increase of the open cell content of the cellular material.[24,94] The cell coalescence is affected by the extensional rheological behavior of the polymer matrix, and more specifically by the strain hardening, but also by the foaming temperature and by the foaming time.[95,96] Generally low foaming temperatures help to increase the melt strength of the polymer matrix and therefore, their capacity of withstand the extensional forces. On the contrary, high foaming temperatures or large foaming times usually conduct to an increase of the coalescence mechanism. An illustrative draw of this phenomena can be seen in **Figure 2.5**.

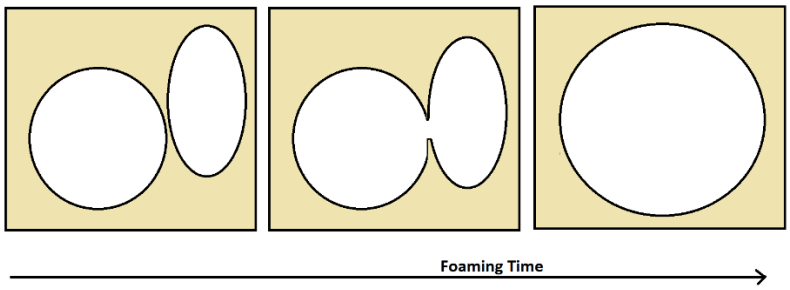


**Figure 2.5.** Schematic draw of the coalescence phenomena.

- **Coarsening**

Coarsening is defined as the diffusion of gas from the smallest cells to the biggest ones.[97–99] This fact occurs because the pressure in the large cells is lower than in the small ones. This difference of pressure motivates that the gas diffuses from the small bubbles to the big bubbles. As a result of this transfer of gas the size of the big increases and the small cells tend to disappear, which results in a reduction of the cell density. A draw of the coarsening effect can be seen in **Figure 2.6**.

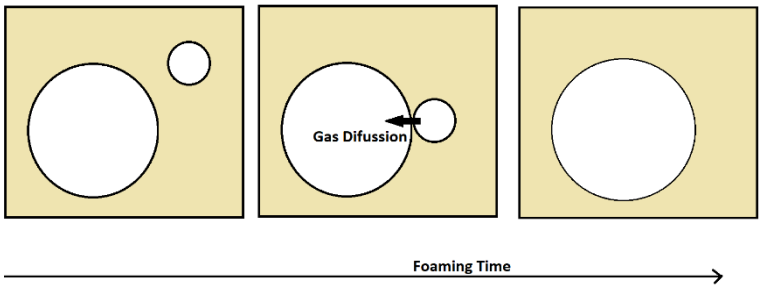


**Figure 2.6.** Schematic draw of the coarsening phenomena

- **Drainage**

Drainage occurs when the viscosity of the polymer is too low. When the polymers are heated during foaming process it tends to drain in the fine walls separating the cells.[100–102] This phenomenon is mainly due to the capillarity forces that transport the material from the cell walls to the cell edges. Consequently, the cell walls get thinner and other phenomena like coalescence and coarsening are favored. The phenomena of the drainage can be seen in **Figure 2.7**.

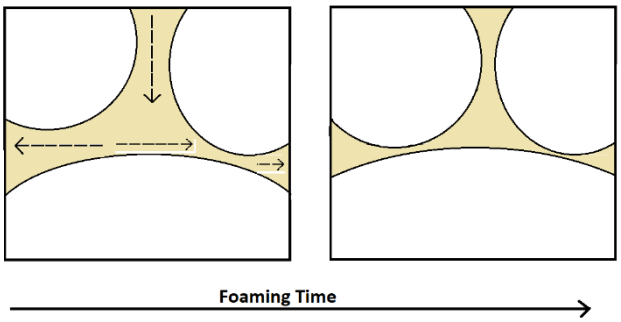


**Figure 2.7.** Schematic draw of the drainage phenomena.

### *2.3.4 Stabilization of the cellular structure*

It should be noted that the gas that has diffused into the nucleated cells eventually tends to diffuse out, to the atmosphere, because a complete separation of the two phases is thermodynamically more favorable. As the gas escapes through the thin walls, the amount of gas available for the growth of the cells decreases. As a result, if the cells do not freeze, they tend to collapse causing foam contraction. The stabilization in thermoplastic materials is performed by a rapid cooling of the sample at a temperature below the effective glass transition temperature in the case of an amorphous polymer, or until values lower than the crystallization temperature if the material is a semicrystalline one.[103] The difference between the foaming temperature and the effective glass transition temperature ($\Delta T=T-Tg$) is a key parameter to analyze the stabilization of the

cellular structure as the smaller this difference is, the quicker the stabilization of the cellular structure occurs, that is, the cellular structure has less time to degenerate during the cooling process due to the mechanisms previously mentioned. **Figure 2.8** depicts a draw that summarizes the three last steps of the foaming process.

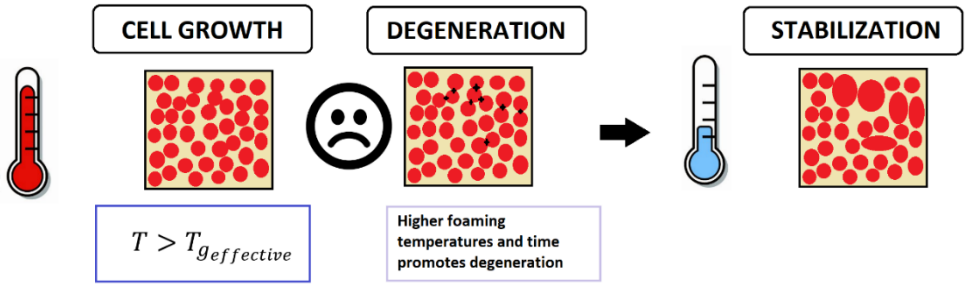


**Figure 2.8.** Schematic draw of the three last steps (cell growth, degeneration and stabilization) in the foaming of polymers.

## 2.4 Cellular Composites

The high nucleation required to reach low cell sizes, to obtain microcellular materials, demands the presence of an additional phase to promote the nucleation mechanisms. One strategy commonly employed consists of incorporating particles to the polymer matrix. [104]

These materials which combine the advantages of having a cellular structure, in which a gaseous phase, coming from a blowing agent, has been dispersed into a solid polymeric matrix, with the interesting properties that the particles provide to both the polymeric matrix and the cellular structure, are known as cellular composites.

Cellular micro-composites are cellular materials which incorporates particles with a micrometric size (microparticles). The maximum nucleation capability that microparticles could provide can be estimated following the **Equation 2.20**.

$$\frac{\text{Nucleants}}{\text{Cm}^3} = \frac{w_p \rho_c}{\rho_p V_p} \qquad [2.20]$$

In this equation $w_p$ represents the percentage of particles introduced in the system, $\rho_c$ is the density of the composites (the mixture of the solid polymer and the particles), $\rho_p$ is the density of the particles itself and $V_p$ is the volume of an individual particle. Assuming a concentration of 10 wt.% of spherical microparticles with a diameter of 1 microns and a density of 2 g/cm$^3$ (typical value

for inorganic particles) in a PS matrix with a density of 1.054 g/cm$^3$, the cell nucleation density will be in the order of $10^{12}$ nuclei/cm$^3$. [105] This value has been obtained assuming that there are not degeneration phenomena during the foaming step, which usually is not true.

In general, it is necessary to work with particles with a smaller size, that is nanoparticles, to reach the desired cell nucleation density of $3.5 \cdot 10^9$ nuclei/cm$^3$. The cellular materials incorporating nanoparticles are known as cellular nanocomposites.[24,106,107] The use of nanometric particles instead of conventional microparticles present additional advantages since they help to reduce the degeneration mechanisms because the size of these particles is lower than the cell wall thickness and therefore, they do not favor the rupture of the cell walls.[13, 108,109]

### *2.4.1 Inorganic Nucleating Agents*

Nanoparticles are materials that present at least one of their dimensions in the nanometric scale.[111,112] Concerning the type of nanoparticles, three different shapes can be found. There are one dimensional nanoparticles like nanotubes, nanoclays like sepiolites or palygorskite and nanofibers.[112–116] There are two dimensional nanoparticles like the clay platelets or the graphene.[51, 71] Finally, there are three dimensional nanoparticles like the spherical particles. Silica particles are an example of these materials.[41]

In this thesis, sepiolite particles are used as inorganic cell nucleating agents. Sepiolite is a one-dimensional particle with a needle-like shape. More information of this filler could be found in Chapter 3.

The inclusion of particles is a common strategy to improve the properties of a cellular material.[26, 119] The high surface area and the high surface to volume ratio of nanoparticles lead to a high reinforcement of the polymer matrix compared to conventional microparticles.[118] Furthermore, the nanoparticles also act in the cellular structure modifying the nucleation mechanisms, as it was mentioned before.[119] Because of these two effects of nanoparticles, the final properties of the foams are modified too. Several research works have reported the effects that nanoparticles provide to the mechanical properties or the thermal ones.[119–121] However, the final properties of the cellular nanocomposites would not depend only on the nanoparticles or the polymer matrix by itself, but also it will depend strongly on the dispersion and adhesion between the particles and the polymer. For instance, a poor dispersion of the nanoparticles, with a high presence of agglomeration points in the polymer matrix, will lead to a reduction of the final

properties of the foams.[68, 122] If the dispersion of the fillers is not suitable the final properties of the cellular composite would be even worse than the ones of the virgin polymeric cellular material. On the other hand, if the particles are well dispersed and isolated in the polymer matrix forming a percolation network, that u is touching one to each other forming a kind of net through all the polymeric structure, the final properties of the material will be enhanced significantly. [25, 62, 123]

Nanoparticles have been proved to be very efficient nucleating agents in several polymeric matrices. For a long time, talc has been the preferred nucleating agent for PS foams. [124] However, due to their micrometric dimensions, their effects on the foam structure and properties are lower than those obtained with other kind of particles like the nanometric ones. In **Table 2.1** there are collected a bunch of examples of articles in which different nanoparticles have been used and the effect that they have produced in the density and in the cellular structure of PS based cellular materials. It is remarkable to highlight some of the works, like those performed by Saraeian et al., Zeng et al. and Han et al., in which the inclusion of percentages of montmorillonites between 5 wt.% and 6 wt.%, have led to reductions of the cell size varying between 24% and 58%, improving also in some cases the fire resistance properties of the foams or the mechanical ones.[125–127] Carbon nanofibers (CNF) were also one of the most used fillers as cell nucleating agents in PS. For instance, Guo et al. and Shen et al. have reported better nucleation properties when adding just 1 wt.% of CNF particles than those obtained with a conventional talc.[116,128] Graphene oxide (GO) or thermally reduced graphene oxide (TRG) have also demonstrated their nucleation capability in the works of Li et al. and Xiao et al.[52, 129] The TRG, demonstrate more efficiency as nucleating agent than the GO, thanks to its larger surface area and its better exfoliated structure. Other nanoparticles like fullerene (FE), silica particles, attapulgite (ATP) or attapulgite/polypyrrole (ATP/PPy) have been also used as effective nucleating agents in a PS matrix.[59] Furthermore, Notario et al. demonstrated that the inclusion of 5 wt.% of natural sepiolites (N-SEP) in a PS matrix allows reducing the cell size from 70 μm of the pure PS towards 10 μm. Notario et al. also work with different types of sepiolites modified on their surfaces with quaternary ammonium salts (O-QASEP) and with silane groups (O-SGSEP). [124]

| Authors | Polymer matrix | Nucleant Agent | Amount (%) | Reduction of the Cell Size (%) | Relative Density (a.u) | $N_o$ (Cells/cm$^3$) | Saturation Conditions (psat, Tsa and tsat) |
|---|---|---|---|---|---|---|---|
| **Notario et al** | PS | N-SEP | 5 | 86 | 0.049 | $1.31\times10^{10}$ | 80 bar, 60°C, 24 hours |
| **Notario et al** | PS | O-QASEP | 1 | 56 | 0.031 | $5.76\times10^{8}$ | 80 bar, 60°C, 24 hours |
| **Notario et al** | PS | O-SGEP | 1 | 63 | 0.066 | $5.97\times10^{8}$ | 80 bar, 60°C, 24 hours |
| **Saraeian et al** | PS | MMT | 6 | 58 | 0.61 | $2.17\times10^{8}$ | 60 bar, ambient temperature, 40 hours |
| **Zeng et al** | PS | MMT | 5 | 24 | 0.76 | $1.31\times10^{8}$ | 138 bar, 120°C |
| **Han et al** | PS | MMT | 5 | 35 | 0.70 | $1.60\times10^{9}$ | Extrusion Foaming |
| **Shen et al** | PS | CNF | 1 | 70 | 0.73 | $2.78\times10^{10}$ | 138 bar, 120°C, 24 hours |
| **Guo et al** | PS | CNF | 1 | 66 | 0.047 | No data | Extrusion Foaming |
| **Yang et al** | PS | Silica Particles | 5 | 27 | 0.11 | $3.55\times10^{9}$ | 138 bar, 120°C, |
| **Li et al** | PS | GO | 15 | 65 | 0.46 | $2\times10^{9}$ | 138 bar, 120°C, 16 hours |
| **Li et al** | PS | TRG | 15 | 84 | 0.59 | $2\times10^{10}$ | 138 bar, 120°C, 16 hours |
| **Liu et al** | PS | ATP | 1 | 26 | 0.17 | $8.3\times10^{4}$ | Extrusion Foaming |
| **Liu et al** | PS | ATP/PPy | 1 | 63 | 0.49 | $1.9\times10^{6}$ | Extrusion Foaming |
| **Xiao et al** | PS | FE | 0.5 | 65 | 0.83 | $1.8\times10^{11}$ | 200 bar, 80°C, 2 hours |
| **Xiao et al** | PS | CNT | 0.5 | 62 | 0.80 | $1.6\times10^{11}$ | 200 bar, 80°C, 2 hours |
| **Xiao et al** | PS | TRG | 0.3 | 69 | 0.94 | $1.0\times10^{11}$ | 200 bar, 80°C, 2 hours |

**Table 2.1.** Examples of Nanocomposites foams based on PS. In the table appear the nucleant agents used, the amount of them introduced in the PS matrix, the percentage reduction obtained in the cell size, the relative density of the foam, the nucleation density and the conditions of the saturation conditions in the case of autoclave foaming.

The graphical representation of the reduction of the cell size achieved compared to a PS pure polymer as a function of the relative density can be seen in the Figure 2.3. In the mentioned graph it is also represented the region to be reached in this thesis by the inclusion of the nanofillers in the PS. It is important to remark that

the foams produced in this thesis have a relative density between 0.03 and 0.04. From the **Figure 2.9** it can be concluded that most of the points represented are out of the region that want to be reached for the foams produced in this thesis. Some of these materials presents higher reductions in the cell size but also a higher relative density, which could have a meaningful impact in some of the properties that will be understudy (like thermal properties).

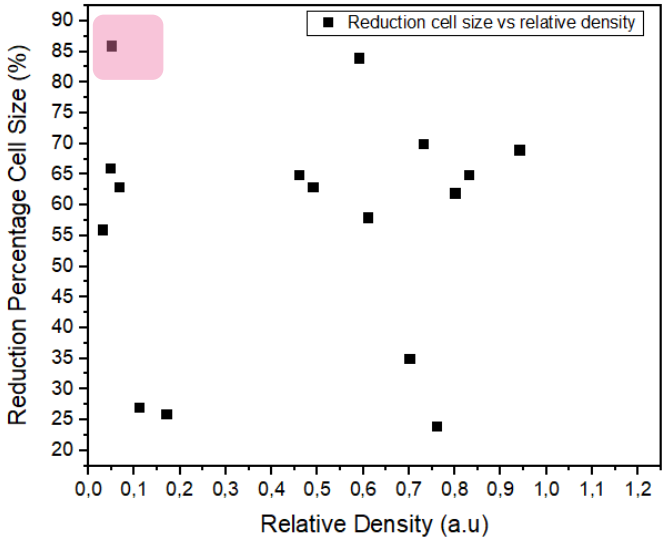


**Figure 2.9.** Graph of the percentage of reduction of the cell size as a function of the relative density for the different examples based on PS. In light pink it is market the region of interest that want to be reached during this thesis.

### *2.4.2 Organic Nucleating Agents*

Organic fillers can be also used as nucleating agents.[130] These organic agents are polymer blends or copolymers in which some of the parts of their monomeric structure create a weak junction to the main polymer and other parts are incompatible and allows the formation of domains or micelles. One of the most common polymer blends employed are the block copolymers dispersed in a polymer structure with a chemical composition like one of the parts of the block copolymer. The simplest kind of block copolymer is one in which two monomers constitute a repetitive sequence with A and B alternating along the chains. For this case, A or B will constitute the incompatible phase with the polymer and will create the micelles, and the other block will conform the compatible part. A micelle is a supramolecular structure that is constituted by the rearrangement of the copolymer's molecules. Generally, the micelles present a spherical shape with sizes that could be in the micrometric or nanometric range.[58,131] The rearrangement of the molecules will depend strongly on the process parameters. The maximum possible number of micelles per unit of volume is given by the

**Equation 2.21**, and it is calculated assuming that all the blocks of the copolymers reside in the micelles.

$$\text{Micelles}_{\text{Max}} = \frac{\text{wN}_\text{A}}{\text{M}_\text{n}\text{N}_\text{c}} \qquad [2.21]$$

Where $w$ is the weight percentage of copolymer introduced in the blend, $N_A$ is the Avogadro number, $M_n$ is the number average molecular weight of the monomer of the block copolymer, $N_c$ is the aggregation number defined as the number of the molecules of the block of the copolymer that conform one micelle. Furthermore, there is also a minimum amount of block copolymer that is needed to form micelles.[132]

As well as for inorganic particles, there is the possibility of using block copolymers in which some of the phases of the polymer work as an efficient $CO_2$ capturer for the attraction of a higher number of gas molecules during the foaming process.

Another method to obtain domains that will serve as preferable nucleation points, is the mixture between two non-compatible polymers.[93] In these systems, the polymer with the lowest proportion in the blend act as heterogeneous nucleation points in which preferably the nucleus and therefore, the cells will grow.[133,134] The size of the domains will depend on several factors like the difference in the viscosities between the two polymers and some of the process conditions of the blending. Wu et al. proposed a model for a blending of polymers in an extrusion process (see **Equation 2.22**) in which the size of the domains depends on the viscosity of the dispersed polymer $n_d$ and of the main polymer ($n_p$), the surface tension on the interphase of the materials ($\sigma$) and the shear rate of the extruder ($\dot{\gamma}$). [135]

$$\text{d} = \frac{4\sigma}{\text{n}_\text{p}\dot{\gamma}}\left(\frac{\text{n}_\text{d}}{\text{n}_\text{p}}\right)^{\pm 0.84} \qquad \begin{cases} + \, if \;\; \text{n}_\text{d}/\text{n}_\text{p} > 1 \\ - \, if \;\; \text{n}_\text{d}/\text{n}_\text{p} < 1 \end{cases} \qquad [2.22]$$

The equation has two possibilities depending on the values of the viscosity of the different phases. When both viscosities are similar, the sizes of the domains reach a minimum. Furthermore, a low surface tension among the two phases or a higher rate in the extruder will also minimize the sizes of the domains.

There is a scarce information of the use of organic phases as cell nucleating agents in PS foams. Quiang et al. demonstrated that with the inclusion of just a 1 wt.% of PDMS (polydimethylsiloxane) to a PS matrix it was possible to double the solubility of $CO_2$ with respect to that obtained with the pure PS matrix.[136] Banerjee et al. studied the influence of PS as a nucleation agent in a matrix of styrene-

butylene-ethylene (SEBS).[137] They explained that the reduction observed in the cell size is related with the foaming temperature compared to the Tg of the ethylene and styrene phases and with the content of PS introduced in the system. For a 30 wt.% of PS they reached a reduction of 60% in the cell size of the pure SEBS. Moreover, Sharudin et al. also reported the effect in the shear dynamic rheology and foaming behavior associated to adding PS to a SEBS matrix.[138] They have found that an increase in the styrene content led to an increase of the storage modulus and to a decrease of the gas permeability. Unfortunately, most of the works in which an organic phase is introduced in a polymer are performed with other polymer matrices like poly (methyl methacrylate) PMMA, with the organic phases of poly(methyl methacrylate)-poly(butyl acrylate)-poly(methyl methacrylate) copolymers known as MAM or thermoplastic polyurethane named as TPU.[139,140]

In the present work a block-copolymer SEBS, with a repetitive monomeric structure of A-B-C-A has been used in combination with PS (see Chapter 7). The mechanism of nucleation in the PS will be due to the elastomeric block, that will create domains in which the nucleus will be preferably formed. More information of the SEBS used in this work could be found in the Chapter 3, section 3.2.2.2.

## 2.5 Foaming Methods. Gas Dissolution Foaming Process

The method used during the thesis to produce the foamed materials based on PS matrix is the gas dissolution foaming process.

Gas dissolution foaming process was developed and patented in the Massachusetts Institute of Technology (MIT) in the early 80s of the last century. The process was discovered thanks to the necessity of creating a new kind of materials (microcellular foams), which present lower values of their density with a lower content of solid plastic but with similar or even higher mechanical performance than the conventional macrocellular materials. Professor Nam. P. Shu and his two master students Francis. A. Waldman and J. Martini-Vvedensky realized that by increasing the amount of cells per cubic centimeter until values close to $10^9$ cells/ cm3, which was only possible if the cell size was lower than 100 μm, it was possible to create a material with a reduced density but with similar mechanical properties as the previous materials. [17,141, 142]

Many years later, with all the experience obtained in the gas dissolution foaming processes and thanks to the development of advanced devices that allow

reaching higher conditions of pressure, lower temperatures and higher stabilization of the saturation conditions during more time, it was able to produce a new kind of materials named as nanocellular materials. These nanocellular materials are characterized by presenting a cell density between $10^{13}$cells/cm$^3$ and $10^{15}$cells/cm$^3$.[143–145] Cellular materials with nanometric cell sizes present surprisingly properties, compared to the macro or micro cellular materials, which are still being analyzed. However, these nanocellular materials have not being successfully scale up to industrial production processes, and its production remain in the laboratory scale.[13]

Regarding the process itself, gas dissolution foaming consists of several stages: saturation, depressurization, foaming and stabilization.[141,146] The gas dissolution foaming process can be carried out in two different ways, the one step process and two-step process.[51,139,147] In the case of the one step process, also known as batch foaming, the depressurization and foaming stages are combined in a single step, and they occur simultaneously. On the other hand, in the two-step process the foaming step is produced in a bath after the depressurization process as it is explained in the following paragraphs.[51]

### 1) Saturation:

The first step of the gas foaming process is the saturation step.[37,143] In this stage the polymeric material is placed in a high-pressure vessel, where the blowing agent (gas) is introduced at certain conditions of pressure and temperature, the so-called saturation pressure (Psat) and saturation temperature (Tsat).[148] The scheme of the equipment used in a usual gas dissolution foaming method is shown in **Figure 2.10**. It can be seen in this picture the first step of the process in which the sample, in light blue, is introduced in the autoclave and later, full of $CO_2$ at a certain pressure. This pressure is obtained first thanks to a bottle of gas and with the help of a pump or a booster that pressurized more the gas of the bottle if it is necessary. Furthermore, the temperature during the saturation stage (Tsat) is controlled by a temperature controller, which is connected to a heating collar that surrounds the autoclave.

Once the material is placed in the autoclave, at the mentioned conditions of pressure and temperature, the diffusion of the gas inside the materials starts to take place. $CO_2$ fills the empty space among the chain of the polymer, which is usually named as free volume. It is important to mention that when a gas fills the empty space between the polymeric chains it modifies the mobility among them. The increase in their mobility means a decrease in the viscosity of the polymer

and a reduction of the glass transition temperature (Tg) or a decrease in the crystallization and melting temperature if the polymer would be a semi-crystalline polymer.[149–151] In the case of PS, which is an amorphous polymer, the Tg is reduced until an effective glass transition temperature $Tg_{eff}$. The diffusion of the gas inside the polymer is ruled by the second Fick's diffusion law that can be seen in **Equation 2.23**. This law explains the behavior of a mass gradient through a plane sheet, taking into consideration that the diffusion coefficient is independent of the concentration of gas.[152, 153]

$$\frac{\partial C}{\partial t} = D\frac{\partial^2 C}{\partial x^2} \qquad [2.23]$$

Where $C$ is the concentration, $D$ is the diffusivity during the sorption process, $t$ is the time and $x$ the position of the sample where it is measured the concentration of gas. A particular solution of the previous differential equation, assuming only a one-dimensional diffusion along the thickness ($L$) of the material and long sorption times will be the following one (see **Equation 2.24**):

$$C = 1 - \frac{8}{\Pi^2}\exp\left(-\frac{D\Pi^2 t}{L^2}\right) \qquad [2.24]$$

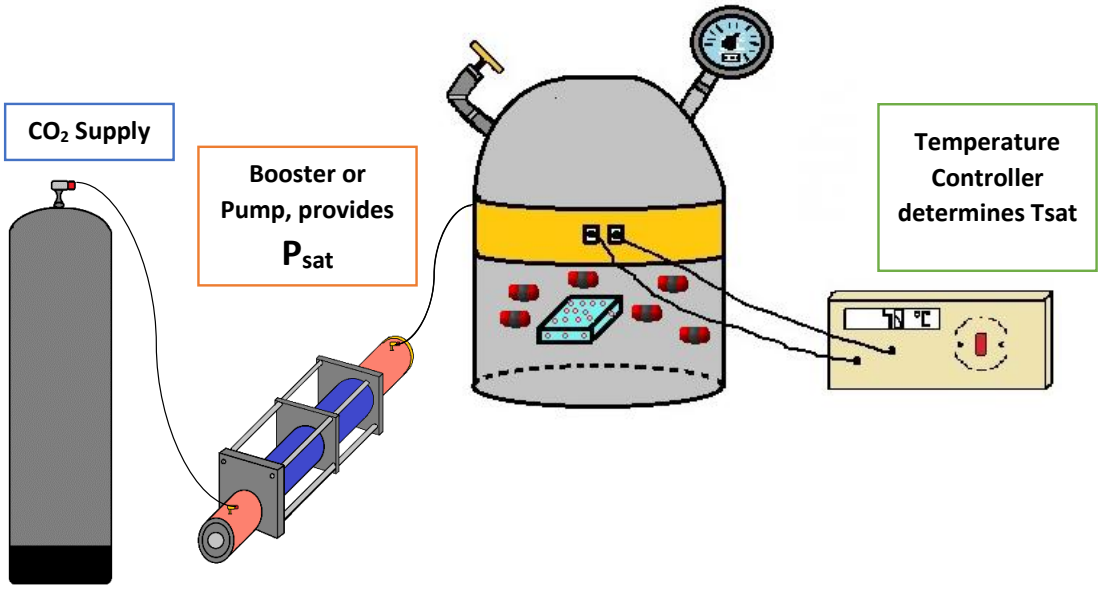


**Figure 2.10.** Scheme of the equipment used during the first step of saturation of the gas dissolution foaming process.

Once the polymer is not able to accept more percentage of gas at the same conditions of pressure and temperature it would be said that the diffusion process is completed and that it reaches its maximum solubility. The maximum solubility depends strongly on several factors like the conditions of pressure and

temperature but also on the chemical interaction between the gas and the polymer. [154–156]

Regarding the relation between the solubility and the pressure three different situations, depending on the material, are possible. Some polymers present a Henry's law relation, which means a lineal dependency of the solubility with the pressure. Also, it is possible to find a Langmuir's model in which the variation of the solubility with the pressure is exponential. Finally, there is a dual model that considers both contributions.[157,158] Even though Henry's law could be useful for some polymers and under some pressure ranges, sometimes is needed the Langmuir or the dual contribution to analyze the relation between pressure and solubility.[154]

On the other hand, the link between the temperature and the solubility of the gas in a polymer could be explained through the following Arrhenius type equation (**Equation 2.25**)

$$S = S_0 \exp\left(-\frac{\Delta Hs}{RT}\right) \qquad [2.25]$$

Where $S$ is the solubility, $S_0$ is a pre-exponential factor, $\Delta Hs$ is the enthalpy exchange, $T$ is the saturation temperature and $R$ is the ideal constant of the gases. The Arrhenius equation explains that the solubility of the gasses in a polymer decreases exponentially with an increase of the saturation temperature. Once the material is supersaturated the gas phase and the solid polymeric phase forms a continuous through all the material.[159] A scheme of the saturation process can be seen in **Figure 2.11**.

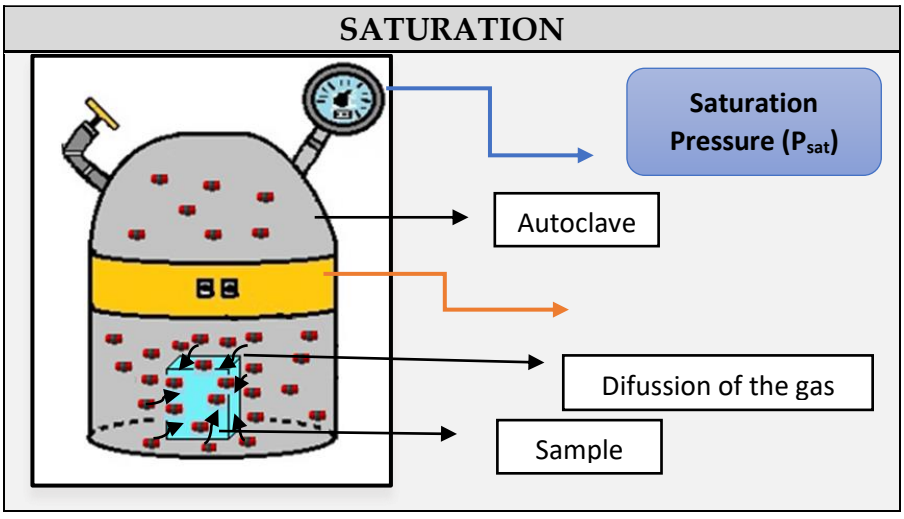


**Figure 2.11.** Schematic image of the saturation step in the gas dissolution foaming process.

### 2) Depressurization:

The second part of the process is the depressurization stage (**Figure 2.6**). During this stage the gas pressure is released at a certain depressurization speed ($V_{dep}$). The pressure drop rate, that is, the velocity at which the gas leaves the pressure vessel, is a critical factor that might affect the later foaming structure.[35,85,160] This is because the abrupt decrease in pressure generates a thermodynamic instability that could result in a nucleation process, that is the separation between the solid and the gaseous phase creating small nucleus.[161] However, until now it has not been possible to establish a complete correlation between the depressurization stage and the nucleation process. During the subsequent foaming stage, another thermodynamic instability is created by heating the polymeric sample which could also lead to the appearance of the nucleus that will conform the cell structure. Further studies must be carried out to determine which is the exact point in which the nucleus appear.[37, 162]

On the one hand, once the pressure is released the gas diffuses out of the polymer at a certain desorption rate. As a result, the surface and surrounded areas of the polymeric materials loose partially the gas that they were able to absorb during the saturation step. Therefore, in these surface regions a solid skin is formed during the foaming process.[163] The desorption rate is controlled by a parameter named as diffusivity during the desorption process.[164] The diffusivity during the desorption process depends strongly on the characteristics of the plasticized polymer-gas system and does not necessarily present similar values than the diffusivity coefficient during the sorption process. It will be named as desorption time ($t_d$), the time between the depressurization step and the foaming step. A higher desorption time will lead to the appearance of a broader solid skin in the cellular materials. A deeper explanation of the desorption phenomena will be analyzed in chapter 3, section 3.3.1.3.

It is remarkable to mention that, if the effective glass transition temperature reached due to the plasticizing effect during the saturation step is lower or equal than the saturation temperature, the sample is in a rubber state and has enough mobility to expand immediately after the pressure release.[165] If this occurs the foaming process is usually known as one single step process or batch foaming process. During the one single step process, the depressurization step and the foaming step are overlapped in one single step.

### 3) Foaming:

In this stage, if the temperature reached during the saturation step is lower than the effective glass transition temperature, the polymer remains in a glassy state, and an additional energy is required to reach a rubber state and expand the sample. This process in which the depressurization and the foaming step can be clearly identified, is called two step gas dissolution foaming process.[13,124] In the research works performed in the frame of this theses, for the foaming stage the samples were introduced in a thermal bath at certain conditions of temperature ($T_f$) and time ($t_f$). The foaming temperature maintains the polymer in a rubber state and provides the polymeric chains enough mobility to allow that the nucleation points start to grow creating the final cells of the cellular structure. The principles of the cell growth are analyzed in detail in section 2.6 of the current chapter. The foaming temperature and the foaming time should be controlled carefully to avoid the appearance of the degeneration mechanisms like coalescence, coarsening or drainage.

In the case of the batch foaming procedure or single step foaming procedure, it is possible to produce an additional foaming step, apart for the one that occurs inside the autoclave, called post-foaming. This post-foaming is usually performed to increase the homogeneity of the cellular structure. A schematic view of the two possible processes (one single step foaming process and two steps foaming process) can be seen in **Figure 2.12**.

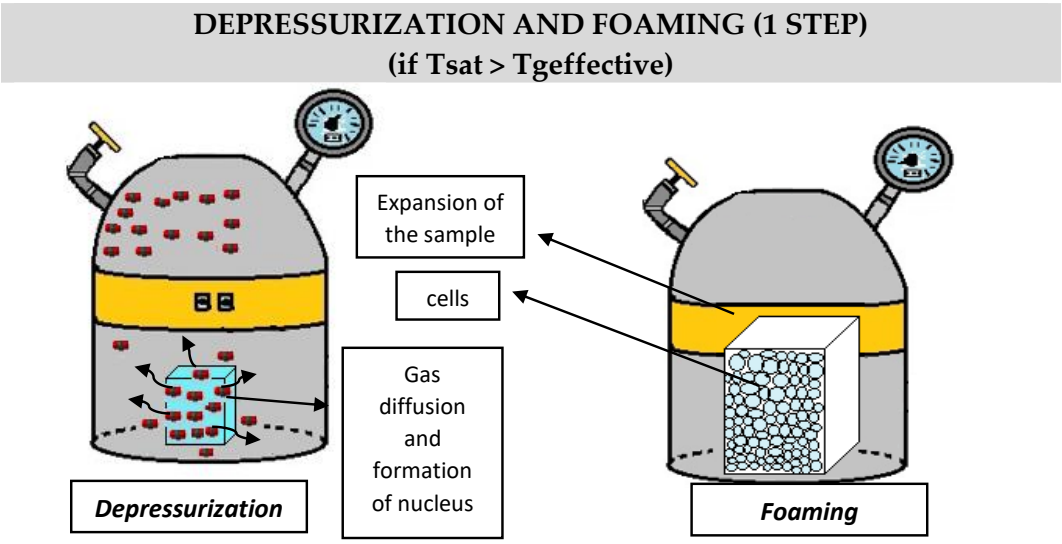

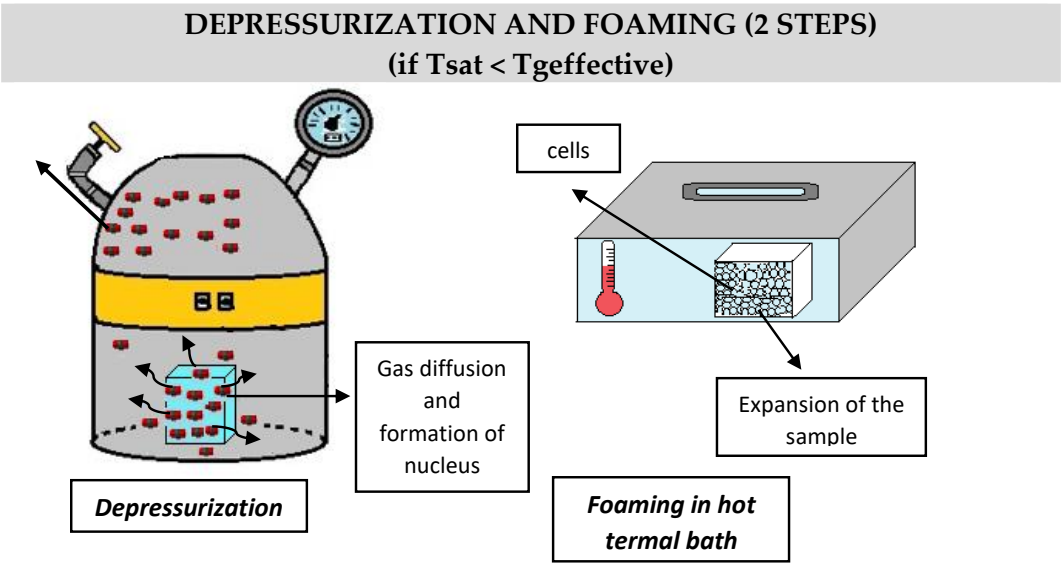


**Figure 2.12.** Schematic step of the depressurization and the foaming step for the one single step gas dissolution foaming process and for the two steps gas dissolution foaming process.

### 4) Stabilization:

Once these three previous steps have been carried out, it is critical to perform the last step: the stabilization of the cellular structure. When the material is removed from its temperature is still very high. If this temperature is not reduced at values lower than the effective glass transition temperature, the material expansion will continuous leading to the appearance of degeneration mechanisms, like cell coalescence or cell coarsening.[103,161]

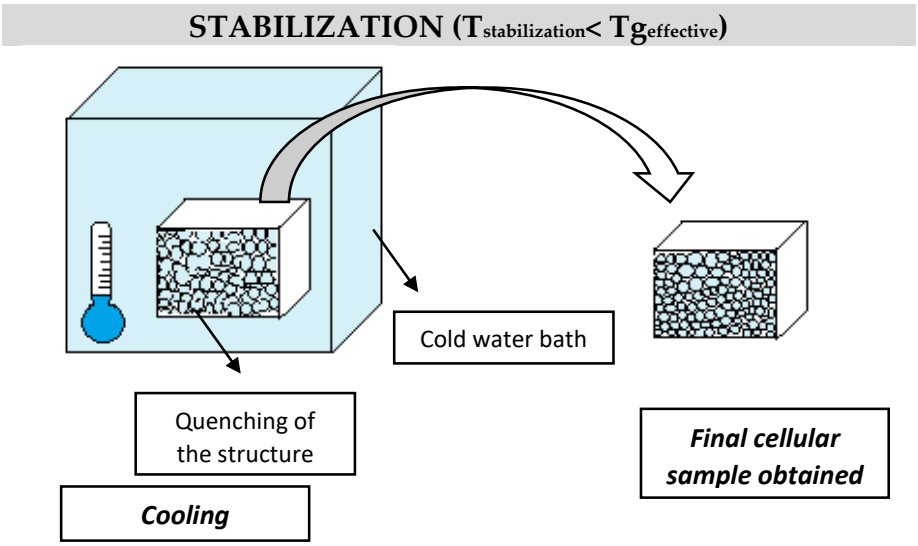


**Figure 2.13.** Schematic step of the stabilization for the gas dissolution foaming process.

Therefore, if the material is not properly stabilized it will present open cells, large cells, low nucleation densities and heterogeneous structures. Therefore, it is necessary stabilize the structure as soon as possible. In these materials the structure can be stabilized by cooling the material in a cold-water bath after being removed from the thermal oil bathroom. A schematic graph of the process can be seen in **Figure 2.13.**

## 2.6 Analysis of the Foamability

Understanding the foamability of the polymeric formulations, that is the ability of a formulation to produce optimum foams, is a key aspect to predict the structure and physical properties of different types of thermoplastic formulations without the need of producing and charactering the foams.[68]

Different parameters must be analyzed to establish a relationship between chemical composition, cellular structure, and physical properties. These parameters include the dispersion degree of the nucleating agent in the polymer matrix, the extensional and shear dynamic rheological properties of the polymeric formulation, the intrinsic thermal properties (Tg), etc.

### *2.6.1 Analysis of the Dispersion of the Nucleating Agent*

Measuring the dispersion degree of the nucleating agent in a polymeric material is not a simple task. A few years ago, the most used techniques to analyze this parameter were the methods based on the image analysis like the scanning electron microscopy (SEM), field emission scanning electron microscopy (FESEM) and transmission electron microscopy (TEM).[166,167] Although these methods can permit a qualitative analysis of the dispersion of the particles, they have significant disadvantages, mainly because there are limited to a local part of the sample. Thereby, possible micrometric defects in the structure can be undetected and the results obtained are not completely representative.[22] Moreover, the sample preparation is quite laborious, and it is necessary to measure a relevant number of scan images that represent the structure in two dimensions, which make an inefficient interpretation of the three-dimensional structure, especially when the constituent fillers are anisotropic in shape.[168] Meanwhile, scattering techniques like X-Ray diffraction (XRD) or small angle X-ray scattering (SAXS), although they are capable of providing average numerical data, are strongly model dependent and they are also valid for some specific fillers with very specific geometries.[169,170] Other methods that are linked to the

analysis of the final properties of the product, like the measurement of the mechanical modulus, thermal or electrical conductivity, offer a global view of how the nucleating agent affects the cellular structure and therefore, the physical properties and the importance of their distribution in it. Nevertheless, it is necessary to fabricate the final product to be able to measure the impact of the nucleating agent on these physical properties and the results obtained are based on indirect measurements and therefore, they are not complete accurate.[171] On the other hand, viscoelastic measurements are susceptible to changes in the nanoscale and mesoscale structures of the polymeric materials.[122] Therefore, rheology can be used as a powerful tool to evaluate the dispersion of the nucleating agents in the polymer matrix. One of the advantages of rheology is that this technique analyzes macroscopic samples and therefore, it is possible to obtain an integrated picture of the material.[167,172] However, this technique can be only used to evaluate the dispersion degree of inorganic particles. The dispersion degree of particles in a polymer can be assessed by the changes observed in the complex viscosity values of the composites in the terminal region, the variations detected in the slopes of the storage and loss modulus and the number of cross over-points detected between both moduli.[112,173,174] Also, in the current thesis, X-ray microtomography (μ-CT) has been used to characterize the dispersion degree of inorganic particles. X-ray microtomography was chosen due to their adequate non-destructive characteristics as well as their high spatial resolution, no need for specific sample preparation and the possibility to obtain data in 3D in a significant volume of sample.[22, 175]

#### *2.6.1.1 Measuring the Dispersion of the Particles by Rheology*

Polymers, from a rheological point of view, are defined as viscoelastic materials.[11,176–178] They present a behavior between an ideal solid elastic and an ideal Newtonian fluid. In **Figure 2.14** it is possible to observe the creep-recovery test response for an ideal solid elastic, an ideal Newtonian fluid and a viscoelastic material. The creep-recovery test consists in subjecting the material to a certain load during a specific time and finally remove the stress.[171] The recovery of the different materials is shown in **Figure 2.14**.

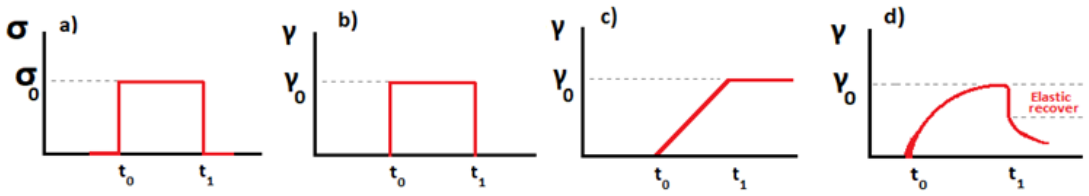


**Figure 2.14.** Response of materials to a creep-recovery test vs time. a) Definition of the test. b) Response of an ideal solid elastic material. c) Response of an ideal viscous liquid material. d) Response of a viscoelastic material.

**Figure 2.14** indicates that the ideal solid material deforms instantaneously until a certain strain value and when the load is removed the material recover its initial shape. On the other hand, the ideal viscous material is deformed progressively until it reaches a final deformation value. Later when the load is removed the material is not able to recover its original shape. Finally, the behavior of a viscoelastic material is between that of the ideal solid material and that of the ideal viscous material. The viscoelastic material deforms progressively until it reaches a final deformation value. Later, when the load is removed part of the energy used for the deformation is recover (elastic recover) and used to recover the initial shape and part of the energy is lost.

The small amplitude oscillatory shear technique allows to study the shear dynamic rheological properties of many polymers. In these tests the sample is placed between two plates (cone-plate or plate-plate, depending on the morphology).[171, 179–181] The lower plate is fixed and the upper plate is oscillating with a certain frequency of oscillation ($w$). During this test the samples suffer an oscillatory shear flow. The shear stress and the shear strain can be represented for an oscillatory test through the following equations (**Equation 2.26 and Equation 2.27**):

$$\gamma = \gamma_0 \sin(wt) \qquad [2.26]$$

$$\sigma = \sigma_0 \sin(wt + \delta) \qquad [2.27]$$

Where $\gamma$ is the shear strain, $\sigma$ is the shear stress, $\gamma_0$ is the strain amplitude and $\sigma_0$ is the shear stress amplitude and $\delta$ a phase angle shift between the stress and the strain. The shear strain rate is defined as the time derivate of the stain rate ($\dot{\gamma} = \frac{d\gamma}{dt}$) as it is represented in the **Equation 2.28**.

$$\dot{\gamma} = \gamma_0 w \cos(wt) \qquad [2.28]$$

To investigate the viscoelastic properties, the strain amplitude should be low enough to do not deform the material.[182] The small amplitude deformation generates a small shear stress that is proportional to the amplitude of the applied

strain and it changes sinusoidally with the time as it can be seen in **Figure 2.15**.[183]

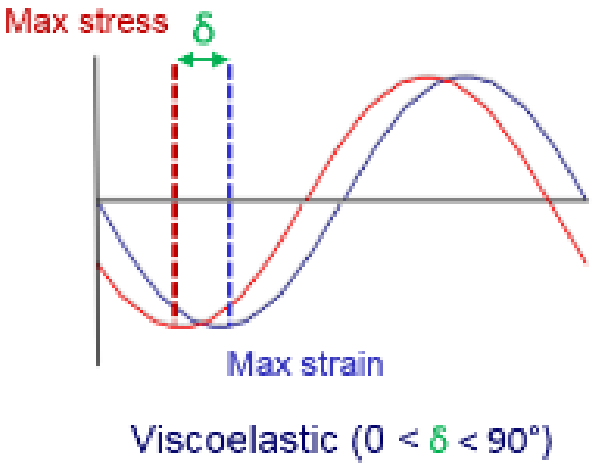


**Figure 2.15.** Sinusoidal behavior of the stress and strain for a viscoelastic material. In blue color strain curve and in red color stress curve. The phase angle between both curves varies between 0º, which represents an ideal elastic behavior, and 90° which represents an ideal viscous behavior.

For an ideal elastic solid the phase angle between the strain and stress is 0º, meanwhile for an ideal viscous the phase angle is 90º. In the case of a viscoelastic material the phase angle varies between 0º and 90º, which means that the stress shows a certain delay period compared to the strain curve.[184,185]

Apart from the (**Equation 2.26**), the stress can also be represented using the (**Equation 2.29**).

$$\sigma = \gamma_0[G'(w)\sin(wt) + G''(w)\cos(wt)] \qquad [2.29]$$

Where $G'(w)$ is the storage modulus and it is in phase with the strain, and $G''(w)$ represents the loss modulus, which is in phase with the shear rate. The storage modulus measures the quantity of energy that can be stored by the material during the shear process.[112,174,186] When the load is removed this stored energy is completely available and it acts as the driving force to compensate the previous deformation of the structure. An ideal elastic solid stores the entire energy applied during the load of the material and therefore, it recovers completely its shape once the load is removed.[171] On the other hand, the loss modulus measures the amount of energy that is dissipated and lost During the shear process part of this energy is spent in changing the structure of the tested materials when the material is flowing, and another part of this energy is spent in heating up the

material. The ideal viscous liquid loss completely l the energy and it shows and irreversible deformation that cannot be recovered.[187, 188]

The equations that represent the storage modulus and loss modulus (**Equation 2.30 and 2.31**) can be obtained from the **Equations 2.26 and 2.27**. Finally, **Equation 2.32** shows the loss tangent which is defined as the ratio between the loss modulus and the storage modulus. If the material would be a 100% elastic solid the loss tangent will be equal to 0. On the other hand, if material would be an ideal viscous one, the loss tangent will be equal to ∞. For a viscoelastic material the loss tangent value varies between both quantities $0 < \tan\delta < \infty$.

$$G' = \frac{\sigma_0}{\gamma_0}\cos\delta \qquad [2.30]$$

$$G'' = \frac{\sigma_0}{\gamma_0}\sin\delta \qquad [2.31]$$

$$\tan\delta = \frac{G''}{G'} \qquad [2.32]$$

When the harmonic functions are expressed in their complex form, the **Equation 2.33** can be obtained

$$G^* = G' + iG'' \qquad [2.33]$$

Where $G^*$ is known as complex modulus. The modulus of $G^*$ can be written as it is seen in **Equation 2.34.**

$$|G^*| = \sqrt{G'^2 + G''^2} = \frac{\sigma_0}{\gamma_0} \qquad [2.34]$$

On the other hand, the complex viscosity ($\eta^*$) is defined as it is indicated in **Equation 2.35**. complex viscosity ($\eta^*$) as it is represented in (**Equation 2.35**).

$$\eta^* = \eta' - i\eta'' = \frac{G^*}{i\omega} \qquad [2.35]$$

The real part of the complex viscosity will represent the viscous behavior or the material (**Equation 2.36**) meanwhile the imaginary part of this variable is related with the elastic behavior (**Equation 2.37**).

$$\eta' = \frac{G''}{\omega} = \frac{\sigma_0}{\omega\gamma_0}\sin\delta \qquad [2.36]$$

$$\eta'' = \frac{G'}{\omega} = \frac{\sigma_0}{\omega\gamma_0}\cos\delta \qquad [2.37]$$

The modulus of the complex viscosity can be defined as it is shown in **Equation 2.38**.

$$|\eta^*| = \sqrt{\eta'^2 + \eta''^2} = \frac{|G^*|}{\omega} \qquad [2.38]$$

Once all the parameters involved in a SAOS experiment have been defined, it is interesting to see which is the common behavior of a polymer and a polymer composite in the SAOS experiment and the procedure to obtain the dispersion degree of the fillers by using this technique.[189,190]

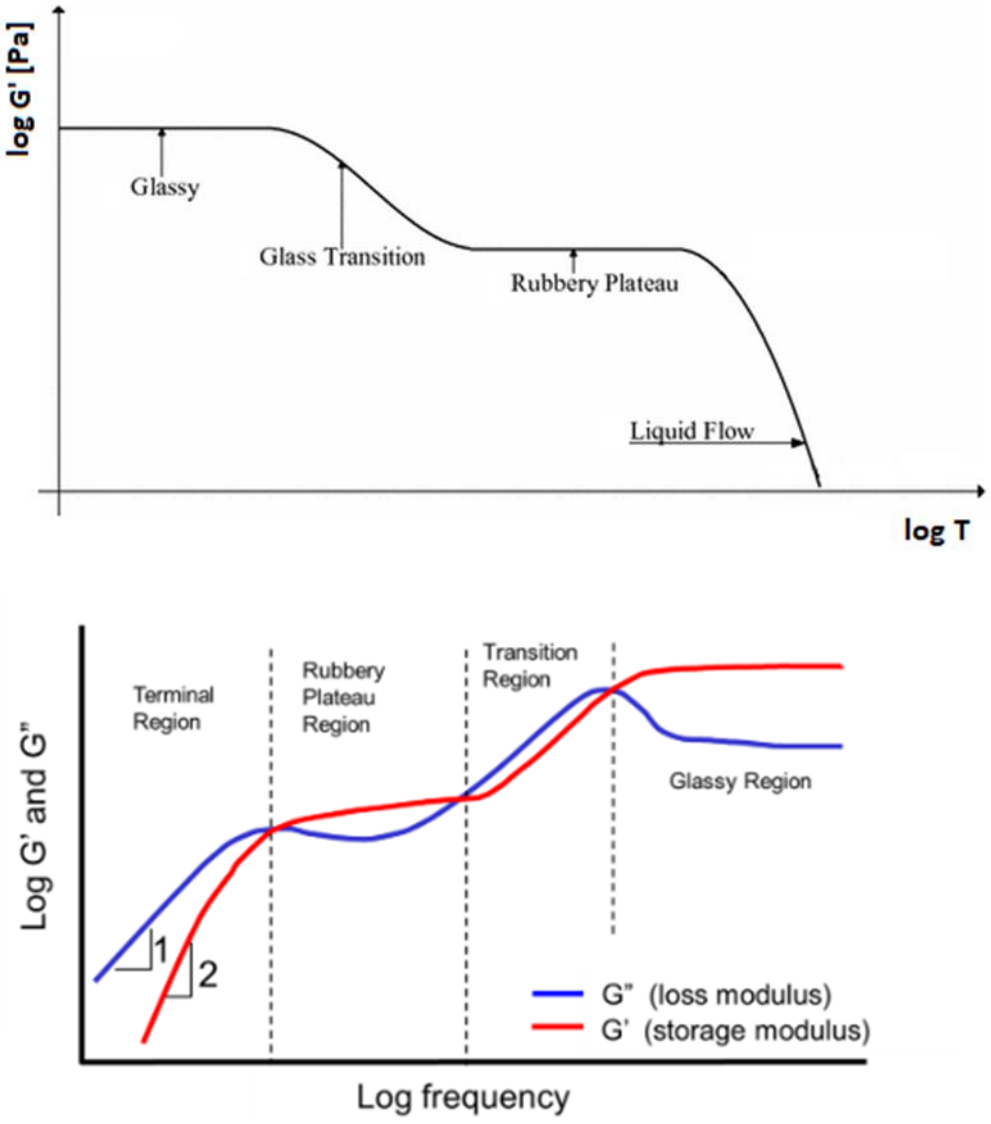


**Figure 2.16.** Rheological behavior of a polymer as a function of the temperature and as a function of the frequency.

The usual rheological behavior of polymeric material as a function of the temperature and as a function of the frequency is represented in **Figure 2.16**. At very low temperatures (below Tg), or at very high frequencies, the storage modulus is higher than the loss modulus. This region is known as glassy region. Then, when the temperature increases (above Tg), or the frequency decreases, the mobility of the polymeric chains also increases and therefore a transition takes place until reaching the so-called rubbery plateau, where the elastic behavior is

still the predominant one.[191,192] Between the glassy state and the rubbery plateau there is a transition region (Tg region) in which the loss modulus shows a maximum.[193] This behavior is produced because of the contribution of the energy required to induce an increase in the mobility of the polymeric chains.[75] Finally, when the temperature raises again the terminal flow region is achieved. In this region, the viscous modulus is higher than the elastic one. In addition, in the terminal region the viscosity remains constant and the slopes of the storage modulus and the loss modulus, versus frequency, are, in general, 2 and 1, respectively.[122,123]

In a SAOS experiments, the regions of interest that are usually analyzed are the rubbery plateau and the terminal flow region. In this frequency range it is possible to see that the curves of the loss modulus and storage modulus intersect in a point named as cross-over frequency (ωx). In polymers with a high molecular weight the cross-over point is shifted toward lower frequencies, due to the high elastic behavior of these materials in a wider range of frequencies. Furthermore, this kind of polymers present higher values of the zero-shear than the polymer with a low molecular weight.[194,195]

Shear dynamic rheology is a very interesting tool to analyze the dispersion degree of inorganic fillers, like nanoparticles, in a polymer matrix.[49,79,123,196] The incorporation of these particles leads to a modification of the behavior of the polymer matrix. Changes in the zero-shear viscosity, storage and loss modulus curves, cross frequency points, etc. are observed when the particles are incorporated to the polymer matrix.[178] For instance, as it was mentioned before, in a pure polymer matrix, the slopes of the storage modulus and the loss modulus, versus frequency, in the terminal region, are 2 and 1, respectively. Furthermore, there is a single cross-over points between these two curves in the rubber and terminal regions.[177] When particles are incorporated to the polymer matrix this behavior is modified. When the density of particles increases, this can be done by increasing the percentage of particles or by improving the dispersibility of the fillers in the material, it is possible to see that the slopes of both the storage and loss moduli in the terminal region are proportional to 1.[167] Furthermore, the value of the zero-shear viscosity increases due to the presence of fillers that provides a higher solid and elastic behavior to the material. It is even possible to detect a non-Newtonian power law behavior in the terminal region due to the presence of these particles. When the density of particles continues to increase and its value is close to the percolation density the slopes of the storage and loss moduli, in the terminal region, are proportional to 0 and

1, respectively. Furthermore, the number of cross over frequency points increase from 1 to 2.[170] Therefore, in the terminal region $G' > G''$, which indicates that the formulation presents a solid-like behavior. The fillers in a polymeric matrix are forming a percolated network when they are touching one to each other along the polymer matrix.[79] When the density of particles is higher than the percolation density an over percolated state in which $G' > G''$ in all the frequency range is detected. The effects in the rheological behavior of a polymer matrix produced by increasing the density of particles are summarized in **Figure 2.17.**[122,197]

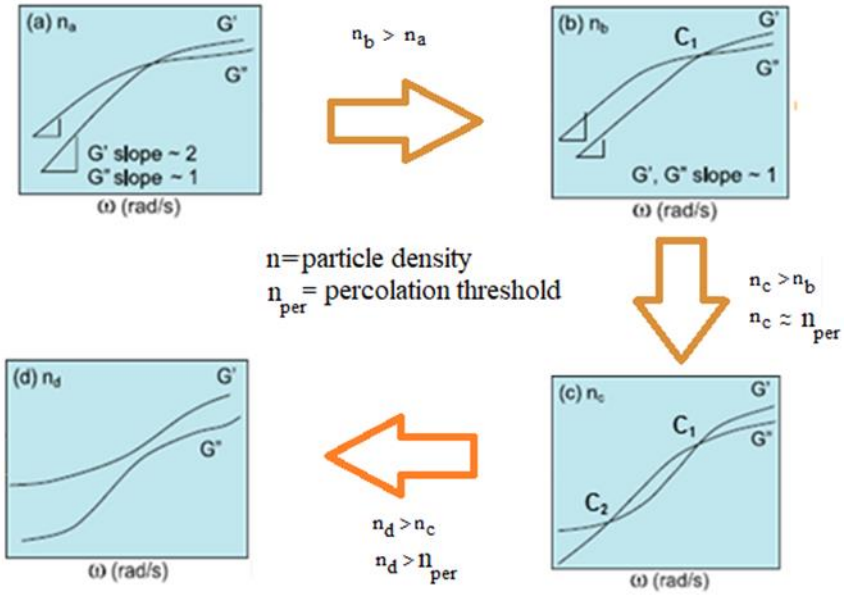


**Figure 2.17.** Representation of the behavior of the storage and loss modulus with the increment of the density of particles.

Several studies had reported that the maximum improvements due to the incorporation of the nanoparticles are obtained when they are forming a percolated network.[122,198–201] If the density of particles is higher than the percolation density the particles form agglomerates that could lead to properties that are even worse than those of the virgin polymer. Therefore, it is necessary to determine the percolation threshold for each composite to maximize the properties of the final material.[81] The value of the percolation threshold can be obtained by using Equation **2.39**.

$$G' = C(\phi_p - \phi_{pc})^n \qquad [2.39]$$

Where $C$ is a constant, $n$ is the power law exponent, $\phi_p$ is the volume fraction of particles introduced in the formulation and $\phi_{pc}$ is the percolation threshold volume fraction. To obtain this percolation threshold results it is necessary to

measure the rheological behavior of composites containing different contents of particles. The percolation threshold can be obtained by a linear regression between the curve of $log\ G'$ in the terminal region versus log of $(\phi_p - \phi_{pc})$. The dispersion degree of the sepiolites particles in the PS matrix has been analyzed using this technique.[55]

### *2.6.1.2 Measuring the Dispersion of the Particles by X-Ray Micro-Tomography*

The dispersion of the inorganic particles, sepiolites, was also measured by X-Ray Micro-Tomography (further information of the characteristics of the equipment could be found in Chapter 3).

The improvements performed in the equipment were able to make the resolution of the tomography images up to an effective pixel size of 2.5 μm. Isolated sepiolites, whose sizes are among 1-2 μm, are not detected in the tomographic analysis. However, if sepiolites are not well dispersed and they are forming agglomerates, it will be possible to detect this clusters of particles. Therefore, the samples presenting the lowest percentage of agglomerates will be the ones in which the sepiolites are better dispersed. The percentage of agglomerates was calculated using the **Equation 2.40**.

$$\text{Agglomerates (\%)} = \frac{\frac{\rho_{sep} \cdot \%V_{sep}}{\rho_{solid}}}{\%m_{sep}} \qquad [2.40]$$

Where $\rho_{sep}$ is the theoretical density of the fillers, in this case sepiolites (2.1 g/cm$^3$), $\rho_{solid}$ represents the density of the solid nanocomposite, which was measured by gas pycnometric, $\%V_{sep}$ is the fraction occupied by the agglomerates and $\%m_{sep}$ is the real mass fraction of particles in the sample.

The dispersion of the sepiolites in the PS was studied by X- Ray microtomography.

### *2.6.3 Analysis of the Viscosity of the Polymeric Formulation*

As it was previously explained the viscosity of the polymeric formulation plays a key role in the initial growth of the cells. A low viscosity is required to favor the initial growth of the cells.[202]

In this thesis the viscosity of the different formulations (those containing sepiolites and those containing SEBS) has been determinized by SAOS measurements.

The zero-shear viscosity is defined as the viscosity in the Newtonian plateau in the terminal region.[203] In **Figure 2.18** can be seen the zero-shear viscosity in the terminal region for a common pure polymer.[204]

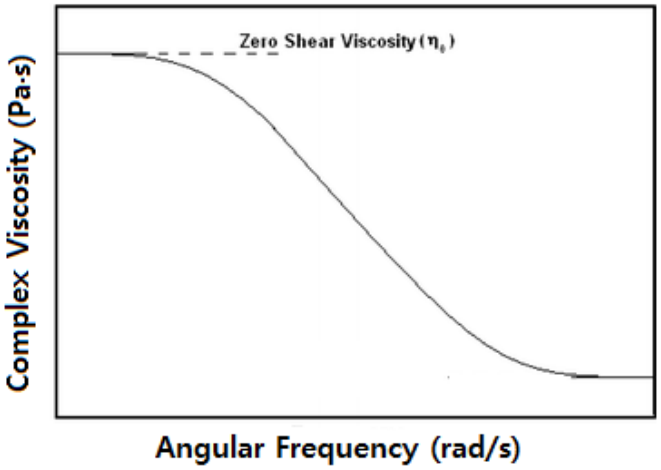


**Figure 2.18.** Representation of the complex viscosity for a material. In the image it is possible to see the zero-shear viscosity value in the terminal region of the material.

The viscosity is related with the molecular weight of the polymer matrix. The main relationship between the viscosity and the molecular are analyzed in the Mark-Houwink Sakurada equation.[205] This equation (**Equation 2.41**) explains that the zero-shear viscosity is approximately proportional (being $K_1$ the constant of proportionality, which depends on the polymer matrix) to the weight average molecular weight when it is not overpassed a critical value ($M_c$) of the mentioned average molecular weight.

$$\eta_0 = K_1 M_w \qquad [2.41]$$

For the polymers that possess low molecular weight (small molecules) there are not entanglements among their polymeric chains and therefore, the viscosity does not change with the variation of the shear rate.[194,206] The ideal viscous behavior that they present makes possible that viscosity is linearly proportional to the molecular weight of the material.

On the other hand, if the molecular weight of the polymer is higher than a critical value ($M_w > M_c$) the equation that explains the relationship between molecular weight and shear viscosity is the following one (**Equation 2.42**).

$$\eta_0 = K_1 {M_w}^{3.5} \qquad [2.42]$$

Polymers that overcome this critical value, present long chains with entanglements between them.[205] The zero-shear viscosity plateau of this materials

is produced in a lower shear rate range compared to materials with lower molecular weights. Furthermore, the viscosity experiences an abrupt increase with the increment of the molecular weight.

### *2.6.3 Analysis of the Extensional Rheological Behavior*

When the formulations are foamed during the gas dissolution foaming process, the polymeric matrix is subjected to extensional forces. Therefore, it is important to analyze how the extensional viscosity of the polymer matrix changes as the material is elongated.[55,203,207,208]

The simplest extensional flow test is the uniaxial extension, in which the material is stretched in one single direction and compressed in the other two directions. **Equations 2.43** show the velocity field in uniaxial extension, in the three directions ($v_x, v_y, v_z$).

$$v_x = \dot{\varepsilon}x \qquad [2.43a]$$

$$v_y = -\frac{1}{2}\dot{\varepsilon}y \qquad [2.43b]$$

$$v_z = -\frac{1}{2}\dot{\varepsilon}z \qquad [2.43c]$$

Where $\dot{\varepsilon}$ is a constant extensional strain rate which is applied in the $x$ direction. Another type of extensional deformation is the so-called biaxial extension, where the biaxial extension is performed in the xy plane. Finally, in the planar extensional flow the extension is produced in the x direction but there is no deformation in the y direction.[68] These three behaviors are summarized in **Figure 2.19**.

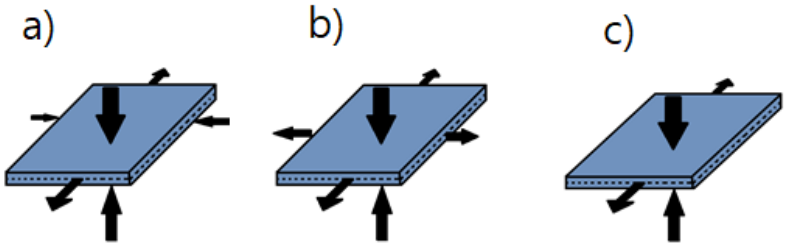


**Figure 2.19.** Types of extensional flow tests. a) Uniaxial extensional flow. b) Biaxial extensional flow. c) Planar extensional flow.

In literature biaxial and planar extension are less frequent than the uniaxial extension, due to the difficulties of the experimental conditions and the lack of equipment to perform these tests. During this thesis the uniaxial extensional rheology experiments have been performed and evaluated.

In extensional flow two magnitudes can be defined: the extensional stress ($\sigma_e$) and the extensional rate ($\dot{\varepsilon}_H$), also named as Hencky strain rate or natural strain rate. The extensional viscosity ($\eta_e$) is defined as the ratio between the stress and the strain rate (**Equation 2.44**)[11]

$$\eta_e(t) = \frac{\sigma_e(t)}{\dot{\varepsilon}_H(t)} \quad [2.44]$$

The stress is defined as the ratio between the force acting ($F(t)$) and the cross section ($A(t)$) as appears in **Equation 2.45**.

$$\sigma_e(t) = \frac{F(t)}{A(t)} \quad [2.45]$$

The cross section of the sample is modified due to the extensional forces applied in the following way (**Equation 2.46**).

$$A(t) = \frac{A_0 l_0}{l(t)} \quad [2.46]$$

Where $A_0$ is the initial cross section, $l_0$ the initial length of the material and $l(t)$ is the length of the material when the extensional force has been applied. When the materials are heated to perform the extensional test a volumetric expansion of the sample is obtained. The **Equation 2.47** can be used to calculate this expansion.

$$A(t) = A_0 \left(\frac{\rho_s}{\rho_M}\right)^{2/3} \frac{l_0}{l(t)} \quad [2.47]$$

Where $\rho_s$ is the solid-state density and $\rho_M$ is the melt density of the polymer at the temperature at which the extensional rheological test is performed. This value of the melt density can be found for some polymers in the literature or can be determined as it is seen in **Equation 2.48**, as the ratio between the melt flow rate ($MFR$), which is defined as the flow of mass per unit of time (g/10 min), and the melt volume rate ($MVR$), which is defined as the volumetric flow per unit of time ($cm^3$/10 min).[209]

$$\rho_M = \frac{MFR}{MVR} \quad [2.48]$$

The differential extensional ratio relates the change in length with the actual length as it is indicated in **Equation 2.49**.

$$d_{\varepsilon_H} = \frac{dl}{l} \quad [2.49]$$

Where $\varepsilon_H$ is the extensional strain also named as Hencky strain or natural strain. This Hencky strain is preferably used in applications in which large deformation are applied, as it can be seen in **Equation 2.50**.

$$\varepsilon_H = \int_{l_0}^{l} d_{\varepsilon_H} = \int_{l_0}^{l} \frac{dl}{l} = ln\left(\frac{l}{l_0}\right) = ln(\lambda) \quad [2.50]$$

Where $\lambda$ is known as stretching ratio, defined as the ratio between the actual length and the initial length. The Hencky strain rate and the Hencky strain are related as **Equation 2.51** indicates.

$$\varepsilon_H = \dot{\varepsilon_H} t \qquad [2.51]$$

In the present thesis a stress-controlled rheometer (AR 2000 EX from TA instruments) with an extensional fixture (SER 2 from Xpansion instruments) were used to measure the extensional rheological behavior of the different polymers. The device is based on the Meissner concept of elongate the sample in a confined space between two rotatory cylinders with clamps that turn into opposite directions with all the system heated from an integrated oven. A schematic draw of the device used for measuring the extensional viscosity can be seen in **Figure 2.20.**[177]

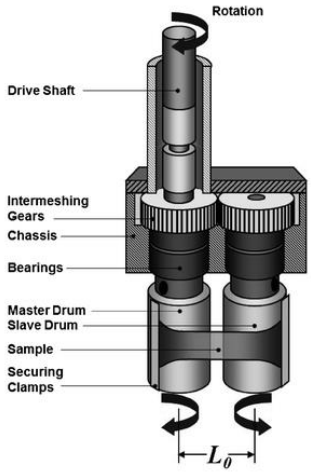


**Figure 2.20.** Scheme of the device used for measuring the extensional viscosity.

The tensile force and the Hencky strain rate are defined as following (**Equation 2.52** and **Equation 2.53**).

$$F(t) = \frac{M(t)}{D_d} \qquad [2.52]$$

$$\dot{\varepsilon_H} = \frac{\Omega(t) D_d}{l_0} \qquad [2.53]$$

Where $M(t)$ is the torque, $D_d$ is the cylinder diameter and $\Omega(t)$ is the drive shaft rotation rate.

The typical extensional rheological behavior of a polymer matrix is represented din **Figure 2.21**. The rheological behavior is usually measured at a temperature higher than the melting point in the case of semi-crystalline polymers and a temperature higher than the Tg in the case of amorphous polymers. [207,210]

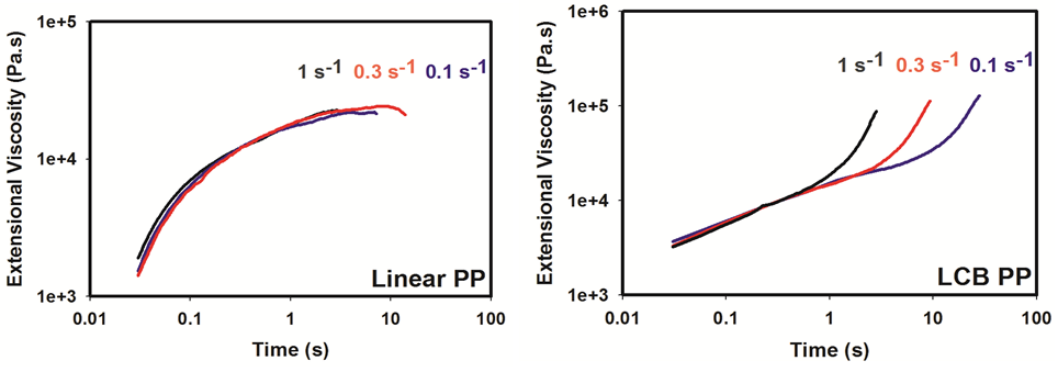


**Figure 2.21.** Graphs of the typical extensional behavior for strain- softening polymers and strain hardening polymer as a function of the time and Hencky strain rate.

The non-linearity is understanded as a deviation from the linearity viscoelastic regime (LVR). For **strain-softening** materials (figure on the left) the non-linearity appears as a steady-state level below LVR.[78,79] On the other hand, in the strain-hardening materials (figure on the right) the curves start to rise abruptly before levelling off to a steady-state Generally, the strain softening behavior is presented by linear polymers. Both, branched polymers, and linear polymers with a small amount of very high molecular weight fractions are strain-hardening polymers, that is, strain hardening polymers are those presenting a well-entangled structure regardless of their chain architecture.[75,210,211] The strain hardening behavior can be quantified by using **Equation 2.54**. For a particular value of time and Hencky strain rate, the strain hardening coefficient (S) can be calculated as:

$$S = \frac{\eta_e^+(t_0,\dot{\varepsilon}_{H0})}{\eta_{e0}^+(t_0)} \qquad [2.54]$$

Where $\eta_e^+(t_0,\dot{\varepsilon}_{H0})$ is the value of the transient extensional viscosity at a certain condition of Hencky strain rate ($\dot{\varepsilon}_{H0}$) and time ($t_0$) and $\eta_{e0}^+(t_0)$ is the value of the transient extensional viscosity in the LVR obtained at the same conditions of time and Hencky strain rate.

The scientifical explanation of the strain hardening is still not completely clear. In the beginning of 90s decade several researchers like McLeish and Larson, Laun and Munstedt, Wagner et al., Takahashi et al. or Van Ruymbeke et al. reported the necessity of branched polymers to present a strain hardening phenomenon.[212–216] In these polymers the branch points are entangled with other macromolecules forming a network and acting as anchors which prevent the backbone to retract (relaxation mechanism) after a strain step. Consequently, the backbone can readily be stretched in an extensional flow, producing strain hardening. On the other hand, the backbones of linear polymers have free ends.

Under flow these free ends allow the chain polymer to retract very quickly, and hence large stresses cannot readily build up. Consequently, these polymers do not show strain hardening.

Further studies like the ones of Liu et al., claimed that all molten polymers, regardless of their chain architecture, will exhibit strain hardening at high enough Hencky strain rates, no matter if they are branched or not.[210] The entanglement network can be strengthened in extensional rheology. They concluded that molten polymers tend to display strain hardening due to two main reasons: on the one hand, the removal of chain entanglement appears to be difficult at high rates in extension and on the other hand, the corresponding cross-sectional area shrinkage (also known as geometric condensation), which makes the system to be strengthen.

## 2.7 Properties and Applications of Cellular Composites

Insulation is the common market where PS foams play a major role.[217] For a material to be considered as a good insulator, some requirements of thermal properties must be satisfied. As it was previously indicated one of the main objectives of this thesis consist of improving the insulation behavior of PS foams by acting on their cellular structure, through the incorporation of inorganic and organic nucleating agents. Therefore, it is important to analyze the thermal conductivity of polymeric foams.

Energetic efficiency is a hot topic in the fight against the climate change.[218] A high thermal insulation seems beneficial for the building structure itself, avoiding some negative effects or damages like the ones related with frost, moisture, corrosion, etc. Moreover, it is important that the difference among the building components and the temperature indoor will be in a range of 3-4 °C. This way it is possible to obtain a save of expenses related with the heating or cooling of the indoor spaces of the houses, prevent the sweating of the houses, which causes fungus or black stains root for the wooden houses, as well as reduce the electrical heating or gas heating consumption.[219]

It is calculated that 25% of the total energy produced in the world is consumed in industrial activities, another 25% is consumed in transport issues and the remaining 50% is used for heating the apartments and the buildings itself. In other words, half of the energy available is consumed due to the lack of a goof insulation. Moreover, the actual cost of the thermal insulation with convectional

materials in a building is about 2% of the final global cost of the building.[220] Finally, with a good thermal insulator the $CO_2$ emissions associated with the greenhouse effect will be reduced by a lower consumption of energy.[221] With these facts in mind, cellular materials which present an important reduction of the weight due to their light densities as well as high thermal insulation capabilities thanks to their inner structures are ones of the most used materials to be implemented as thermal insulators.

The thermal conductivity of a cellular material ($\lambda_f$) is defined as the sum of four different terms, as it can be seen in **Equation 2.55**.

$$\lambda_f = \lambda_s + \lambda_g + \lambda_r + \lambda_c \qquad [2.55]$$

Where $\lambda_s$ is defined as the conduction through the solid phase, $\lambda_g$ is the contribution of the gas phase, $\lambda_r$ is the radiation term and $\lambda_c$ is associated to the convection in the cells. The cellular materials present a low thermal conductivity due to the low value of the conductivity of the gas inside the cells, the low quantity of solid material (which means small $\lambda_s$) and the suppression of the convection term for cell sizes lower than 4 mm.[222] For air, the conductivity of the gas phase value is 0.026 W/mK.[223] Other gases like Chlorofluorocarbons, CFC and Hydrochlorofluorocarbons, HCFC, present values between 0.09-0.015 W/mK. However, nowadays both type of gases are forbidden since the Montreal Protocol in 1989 due to their depletion in the ozone layer.[224] Therefore, different physical gases like isobutane 0.017 W/mK or carbon dioxide 0.016 W/mk are usually employed as blowing agents. Nevertheless, the diffusivity of the blowing agents out of the cellular material and the interchange between the blowing agent gas and the air outside, that could take few days to several years depend on the system, makes possible that after the evolution of the foam the final gas inside the cells will be air.[225] From the four terms cited, three if convection is suppressed, the conduction through the gaseous phase and the conduction through the solid phase terms will be related mainly with the gas used as blowing agent (or air if the time has been enough to promote the interchange of gases), the conductivity of the polymeric matrix selected, and the fractions of gaseous phase and solid phase obtained in the foam. As it can be seen in (**Equations 2.56**) and (**Equation 2.57**).

$$\lambda_g = \lambda_{gas} \cdot (1 - \rho_r) \qquad [2.56]$$

$$\lambda_s = \frac{1}{3} f_s \rho_r \lambda_{solid} \sqrt{R} + \frac{2}{3} \rho_r (1 - f_s) \lambda_{solid} R^{1/4} \qquad [2.57]$$

In the previous equations, the $\lambda_{gas}$ is the thermal conductivity of the gas that fill the cells and the $\rho_r$ is the relative density of the foam produced. Meanwhile $\lambda_{poly}$ is the thermal conductivity of the polymeric matrix (in the case of pure PS these values are between 0.156 W/mk to 0.187 W/mk), $f_s$ is the fraction of mass in the struts, that can be obtained through a local thickness image from a SEM micrograph and $R$ is the anisotropy value of the cells.

On the other hand, the radiation term, depends strongly on factors of the cellular structure like could be the cell size.[226,227] Different approximations of the radiation term had been used by several authors like Rosseland, Glicksman, Boets and Hoogendoorn, Williams and Aldao or Frank and Kingery.[228–231] For the case of microcellular foams, like the ones that are supposed to be obtained in the present work, one of the most used approximation is the Rosseland one. It has demonstrated a good degree of accuracy in some works with different polymeric matrices.[225,232] In (**Equation 2.58**) the mentioned model can be seen.

$$\lambda_r = \frac{16n^2\sigma T^3}{3K_{e,R}} \qquad [2.58]$$

Where $n$ is the effective index of refraction, $\sigma$ is the Stefan-Boltzman constant, $T$ is the temperature and $K_{e,R}$ is the Rosseland extinction coefficient.

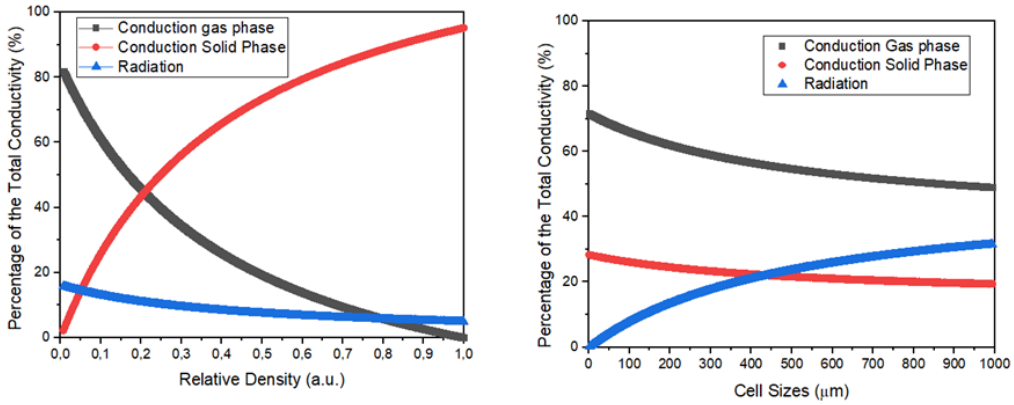


**Figure 2.22.** Contributions of the gas conduction term, solid conduction term and radiation term for a pure PS foamed material. a) Relation between the mentioned contributions and the relative density values for a cell size of 100μm. b) relation between the mentioned contributions and the cell size values for a relative density of 0.09. In both figures, effects like the change in the dispersion mechanism to the Rayleigh one or the Knudsen effect were not taken into account.

In **Figure 2.22** it can be seen how the three different contributions of the thermal conductivity changes theoretically depending on the relative density and of the cellular size for a pure PS material.

For calculating the contributions, it has been followed the same procedure as the one used in the article of Almanza et al, that used the approximation of Williams and Aldao, for the radiation contribution. Assuming a conductivity of the air of 26 mW/mk, a solid conductivity of the pure PS of 190 mW/mK, a fraction of struts of 0.25, isotropic structure, a thickness of the foam of 6 mm, a refractive index of 1.5 for PS, and a 0.04 as the absorption coefficient of the plastic.[231]

As it can be seen in Figure 2.22, the thermal conductivity values depend strongly on the density of the cellular materials. Higher densities are related with a higher contribution of the solid phase term and therefore, with a higher thermal conductivity of the foams.[233]

Considering the variations of the thermal conductivity with the cell size, an approximation to reduce the thermal conductivity would be based on reducing the cell size.[231] The strategy employed in this thesis consists of incorporating different types of nucleating agents (organic and inorganic) which led to a reduction of the cell size of the PS foams without increasing their relative density.[234]

However, it is also necessary to analyze and understand the relation between the cell size and the wavelength of the infrared (IR) radiation.[226,235] If the cell size of the foamed samples is comparable to the wavelength of the IR radiation (IR radiation presents wavelengths between 0.75 and 1000 μm) the scattering produced by the cells is the Mie scattering.[18] Meanwhile, when the sizes of the cells are reduced toward values lower than 1/10 of the wavelength, (that is between 75 nm and 100 μm) the Rayleigh scattering mechanisms are the predominant ones. In this case, the IR radiation is dispersed in a different way than in the Mie scattering. As soon as the cell size is reduced, less and less wavelengths will be scattered, and the material will not interact with the radiation. For values of the cell size similar or close to 1 μm, more than the 90% of the IR radiation will not be attenuated, the material will not absorb this radiation and the foam behaves as if it was "transparent". Therefore, in this case the thermal conductivity increases as the cell size decreases. This phenomenon is not depicted in the Figure 2.22b because the Rosseland model does not consider this phenomenon.

With the aim of investigating the variation of the radiation term with the reduction of the cell size, an in-situ FTIR spectroscopy by ATR mode was used to determine the extinction coefficient.

In the FTIR spectroscopy equipment, an IR spectrum is produced and goes through the material under study. Material can absorb, transmit or reflect the radiation depending on the interaction between the molecules of the polymeric material and the radiation of the IR waves for the different wavenumbers (the IR source produced present wavenumbers that vary between 4000 $cm^{-1}$ and 600 $cm^{-1}$). The design of the FTIR equipment and the measurement procedure is presented in detail in the Chapter 3 of the thesis.

The empirical Beer-Lambert law relates the absorption or transmittance of the light with the properties of the material under study (**Equation 2.59**).[228]

$$\tau_{n,\lambda} = e^{-K_{e\lambda} \cdot L} \qquad [2.59]$$

Where $\tau_{n,\lambda}$ represents the transmittance of the IR light for each different wavelength, $K_{e\lambda}$ is the spectral density extinction coefficient of the material for each wavelength and $L$ is the thickness of the material that is being studied. By calculating the ratio between the natural logarithm of the transmittance for all the available wavelengths and the thickness of the material it is possible to obtain a value of the spectral density extinction coefficient for each wavelength and for a specific length of the material. Later, by performing the average of the values of the spectral density extinction coefficient measured at the same wavelength but in a material with different thicknesses, it is possible to produce a spectrum with the values of the spectral extinction coefficient for each frequency as it can be seen in **Figure 2.23.**

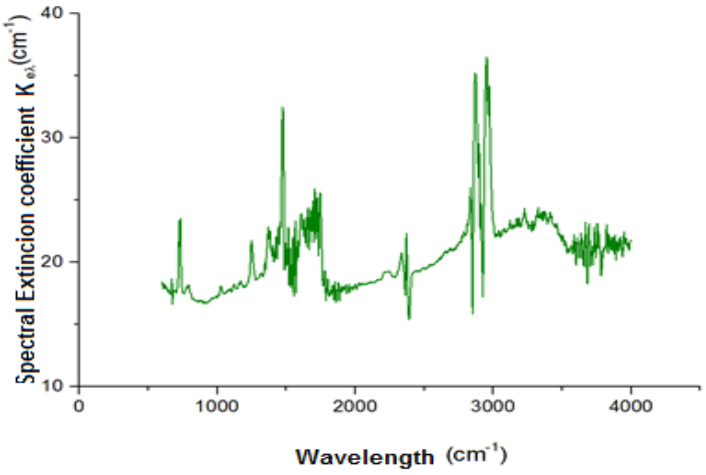


**Figure 2.23.** Graph that represents the spectral extinction coefficient as a function of the wavelength for a polymeric material.

**Equation 2.59** indicates that the radiation contribution of the thermal conductivity can be expressed as a function of a parameter named as Rosseland extinction coefficient. The obtention of the Rosseland coefficient can be calculated according to **Equations 2.60a,2.60b, 2.60c, 2.60d, 2.60e**.

$$\frac{1}{Ke,_R} = \frac{\int \frac{1}{K_{e\lambda}}\left(\frac{\partial e_{b,\lambda}}{\partial T}\right) d\lambda}{\int \left(\frac{\partial e_{b,\lambda}}{\partial T}\right) d\lambda} \quad [2.60a]$$

$$e_{b,\lambda} = \frac{c_{1L}}{\lambda^5 (\exp(c_2/T\lambda) - 1)} \quad [2.60b]$$

$$\frac{\partial}{\partial T} e_{b,\lambda} = \frac{c_{1L} c_2 \exp(c_2/T\lambda)}{\lambda^6 T^2 (\exp(c_2/T\lambda) - 1)^2} \quad [2.60c]$$

$$C_{1L} = 2hc^2 \quad [2.60d]$$

$$C_2 = \frac{hc}{k_b} \quad [2.60e]$$

Where $K_{e\lambda}$ is the spectral extinction coefficient, $T$ is the temperature at which the measurement was performed, $\lambda$ is the wavelength, $h$ is the Planck constant, $k_b$ is the Boltzmann constant and $c$ is the speed of light.

The integral depicted in the Equation 2.60a was calculated using the trapezoidal rule, in which the interval used is constituted by the two consecutives wavelengths provided by the equipment. It is expected a clear relation between both the average spectral extinction coefficient ($K_e$) and the Rosseland extinction coefficient ($K_{e,R}$) and the modification of the cellular structure, even for the regime in which the Mie scattering is changing towards the Rayleigh one, which will justify the changes observed in the values of the thermal conductivity.[18] This fact will constitute a clear proof of the relation between cellular structure and the final properties of the foams obtained.

Other mechanisms should be considered when the cell size of the foam is in the nanoscale. In this case the Knudsen effect, in which the mean free path of the gas molecules is comparable to the cell size and therefore, the collision among the gas molecules become less probably than the collision with the cell walls, led to a significantly reduction of the conduction through the gas phase term.[236] The reduction in the conduction of the gas phase is so important that the final thermal conductivity of the material is reduced in a 70% compared to the materials with micrometric cells. Although these nanocellular materials present a huge step in the reduction of the thermal conductivity, the lack of equipment necessary to produce them in an industrial scale, as well as the high densities that these foams still present, make these materials not suitable for the actual market.[40] For the

present thesis only materials with micrometric cell sizes have been produced and characterized; therefore, in these materials the Knudsen effect has not been considered.

## 2.8. Bibliography


[1] L.J. Gibson, M.F. Ashby. *Cellular solids. Structure and properties*. **2014**, second edition, Cambridge University Press, Cambridge, United Kingdom.

[2] R. B. Seymour, R.D.Deanin. *History of Polymeric Composites*.**1987**, first edition, VSP, New York, United States.

[3] J. Randrianalisoa, D. Baillis. *Comptes Rendus Phys*. **2014**, 15,(8–9),683–695.

[4] S. Doroudiani, M. T. Kortschot. *J. Appl. Polym. Sci*. **2003**, 90 (5),1421–1426.

[5] D. Eaves. *Handbook of Polymer Foams*.**2004**, first edition, Rapra Technology, Shropshire, United Kingdom.

[6] A. M. G. Silva, I. M. Pereira, T. I. Silva, M. R. Silva, R. A. Rocha, M. C. Silva, *J. Appl. Polym. Sci*. ***2021***, 138(1), 49629.

[7] R. Verdejo, R.Stämpfli,M.Alvarez-Lainez, S.Mourad, M.A.Rodriguez-Perez,P.A.Brühwiler, M.Shaffer. *Compos. Sci. Technol*.**2009**, 69(10),1564–1569.

[8] J.H. Park, S.M.Kyung, R.L.Hyeong, H.Y.Sei, B.Y.Cheng, Y.P.Seong, S.O.Chi, S.S.Young, J.K.Yeon, R.Y.Jae. *J. Sound Vib*.**2017**, 406, 224–236.

[9] J. Pinto, A. Athanassiou, D. Fragouli. *J. Phys. D. Appl. Phys*.**2016**, 49, (14) 145601.

[10] D. Feldman. *Polymeric foam materials for insulation in buildings. In: Materials for Energy Efficiency and Thermal Comfort in Buildings*. **2010**, first edition, Elsevier, Amsterdam, The Netherlands.

[11] B. A. Morris. *Rheology of Polymer Melts. In : The Science and Technology of Flexible Packaging*. **2017**, first edition, Elsevier, Amsterdam, The Netherlands.

[12] V. Mittal. *Polymer nanocomposite foams*. **2014**, first edition, CRC press Taylor and Francis Group, Bocaraton, United States.

[13] V. Bernardo. *Production and Characterization of Nanocellular Polymers Based on Nanostructured PMMA Blends and PMMA Nanocomposites*. **2019**, PhD Thesis, University of Valladolid, Spain.

[14] M.A. Rodriguez-Perez, S. Rodriguez-Llorente, J.A.De Saja. *Polym.Eng*. **1997**, 37 (6), 959-965.

[15] F. Almeida, H. Beyrichen, N. Dodamani, R. Caps, A. Müller,R. Oberhoffer. *J. Cell. Plast*.**2021**, 57 (4), 493–515.

[16] E. Lopez-Gonzalez. *Analysis of the Composition -Structure Properties Relationship of Open-Cell Polyolefin-Based Foams with Tailored Levels of Gas Phase Tortuosity*. **2019**, PhD Thesis, University of Valladolid, Spain.

[17] J. E. Martini-Vvedensky, N. P. Shu, F. A. Waldman. *Microcellular closed cell foams and their method of manufacture*. **1984**, patent 4473665-A, USA.

[18] J. Martin-de Leon. *Understanding the Production Process of Nanocellular Polymers Based on PMMA Driven by Homogeneous Nucleation*. **2019**, PhD Thesis, University of Valladolid, Spain.

[19] V.Kumar. Process Synthesis for Manufacturing Microcellular Thermoplastic Parts. **1988**, PhD Thesis, University of Massachussets (MIT).

[20] J. Pinto, E. Solorzano, M.A. Rodriguez-Perez, J.A. De Saja. *J. Cell. Plast.***2013**, 49 (6), 555-575.

[21] M. Vašina, D. C. Hughes, K. V. Horoshenkov, L. Lapčík. *Appl. Acoust.* **2006,**67 (8), 787–796

[22] S. Pérez-Tamarit, E. Solórzano, A. Hilger, I. Manke, M. A. Rodríguez-Pérez, *Eur. Polym. J.* **2018**, 109, 169–178.

[23] M. Alvarez-Lainez, M. A. Rodriguez-Perez, J. A. de Saja. *J. Polym. Sci. Part B Polym. Phys.* **2008**, 46, 212–221.

[24] G. Harikrishnan, T. U. Patro, D. V. Khakhar. *Ind. Eng. Chem. Res.* **2006**, 45 (21), 7126–7134.

[25] E. Laguna-Gutierrez, A. Lopez-Gil, C. Saiz-Arroyo, R. Van Hooghten, P. Moldenaers, and M. A. Rodriguez-Perez. *J. Polym. Res.***2016**,23,12, 251.

[26] M.Santiago-Calvo. *Synthesis, Foaming Kinetics and Physical Properties of Cellular Nanocomposites Based on Rigid Polyurethane*. **2019**, PhD Thesis, University of Valladolid, Spain.

[27] X. Han, K. W. Koelling, D. L. Tomasko, L. J. Lee. *Polym. Eng. Sci.* 2003, 43 (6), 1206–1220, 2003.

[28] V.I. Kalikmanov. *Nucleation Theory*. **2013,** first edition**,** Springer, Berlin, Germany.

[29] M. S. L. Feng. Experimental Study of Nucleation in Polystyrene/CO2 System. **2019**, PhD Thesis, University of Ohio, United States.

[30] K. Binder. *Reports Prog. Phys.* **1987**, 50 (7),783–859.

[31] A. J. Bray. *Phys. A Stat. Mech. its Appl.* **1993**, 194 (1–4), 41–52.

[32] J. W. Cahn. *Acta Metall.* **1962**, 10(3), 179–183.

[33] J. W. Cahn, J. E. Hilliard. *J. Chem. Phys.* **1958**, 28 (2),258–267.

[34] J. W. Cahn. *Acta Metall.* **1962**, 10 (10),907–913.

[35] M. M. M. Shirvan, M. H. N. Famili, A. Golbang. *Plast. Polym. Technol.* 2016, 4, 11.

[36] D. L. Tomasko, A.Burley, L.Feng, S.K.Yeh, K.Miyazono, S.N.Kumar, I.Kusaka, K.Koelling. *J. Supercrit. Fluids*. **2009**, 47 (3), 493–499.

[37] S. K. Goel, E. J. Beckman. *Polym. Eng. Sci*. **1993** ,34 (14), 1137–1147.

[38] X. F. Peng, L. Y. Liu, B. Y. Chen, H. Y. Mi, X. Jing. *Polym. Test*. **2016**, 52, 225–233.

[39] J. Martin-de Leon, V. Bernardo, M.A Rodriguez-Perez. *Materials (Basel)*.**2019**, 12 (5), 797.

[40] C. Forest, P. Chaumont, P. Cassagnau, B. Swoboda, and P. Sonntag, *Prog. Polym. Sci*.**2015**, vol. 41,122–145.

[41] J. Yang, L.Huang, Y.Zhang, F.Chen, P.Fan, M.Zhong, S.Yeh. *Ind. Eng. Chem. Res*. **2013**, 52 (39),14169–14178.

[42] Z. Liao, S.K. Yeh, C. Chu,T.Tseng, *"Critical Parameters of Generating PMMA Nanocellular Foam*. **2016**, 1816–1821.

[43] L. Verdolotti, M. R. Di Caprio, M. Lavorgna, G. G. Buonocore. *Polyurethane Nanocomposite Foams : Correlation Between Nanofillers , Porous Morphology , and Structural and Functional Properties*. **2017**, first edition, Elsevier, Amsterdam, The Netherlands.

[44] E. Laguna-Gutierrez, J. Pinto, V. Kumar, M. L. Rodriguez-Mendez, M. A. Rodriguez-Perez, *J. Cell. Plast*. **2018**, 54(2), 333–357.

[45] C. C. Ibeh, M. Bubacz. *J. Cell. Plast*. **2008**, 44(6), 493–515.

[46] Y. Sato, K. Fujiwara, T. Takikawa, S. Takishima. *Fluid Phase Equilibria*. **1999,** 162(1-2), 261–276.

[47] Y. Sato, T. Takikawa, S. Takishima, and H. Masuoka. *J.Supercrit*.**2001**,19, 187–198.

[48] L. J. Lee, C. Zeng, X. Cao, X. Han, J. Shen, G. Xu. *Compos. Sci. Technol.2005,* 65 (15–16), 2344–2363.

[49] E.Bilotti, H.R.Fischer, T.Peijs. *J. Appl. Polym. Sci*. **2007**, 107 (2),1116–1123.

[50] Y. Li, H. Ishida. *Macromolecules*.**2005**, 38 (15), 6513–6519.

[51] G. Gedler, M. Antunes, J. I. Velasco. *J. Supercrit. Fluids*. **2015**, 100, 167–174.

[52] C. Li, G.Yang, H.Den, W.Ken, Q.Zhang, F.Chen, Q.Fu. *Polym.Int*. **2021**, 62(7),4394.

[53] D. Raps, N. Hossieny, C. B. Park,V. Altstädt. *J.Polym*. **2014**, 56, 1–15.

[54] J. Shen, C. Zeng, L. J. Lee. *J.Polym*. **2005**,46, 5218–5224.

[55] E. Laguna-Gutierrez, A. Lopez-Gil, C. Saiz-Arroyo, R. Van Hooghten, P. Moldenaers, and M. A. Rodriguez-Perez, *J. Polym. Res.***2016**, 23 (12),251.

[56] Z. Martin, I. Jimenez, M. A. Gomez-Fatou, M. West, A. P. Hitchcock. *Macromolecules*. ***2011***, 44 (7),2179–2189.

[57] P.Mondal, D.V.Khakar.J.Appl.Poly.Sci.**2007**,103(5),2802-2809.

[58] J.A. Reglero, P. Viot, M. Dumon. *J. Cell. Plast*. **2011**, 47(6), 535–548.

[59] Y. Liu, L. Jian, T. Xiao,R. Liu, S. Yi, S. Zhang, L. Wang, R. Wang, Y. Ming .*Polymers (Basel)*. **2019**, 11 (6), 985.

[60] H. Wan, Y. Que, C. Chen, Z. Wu, Z. Gu, J. Meng, L. Wang, G. Guan. *Mater. Lett*.**2017**,194, 107–109.

[61] H. Shu, X. Li, Z. Zhang, *Prog. Chem*. **2008**, 20 (10), 1509–1514.

[62] M. Sabzi, L. Jiang, M. Atai, I. Ghasemi. *J. Appl. Polym. Sci*. **2013**,129 (4), 1734–1744.

[63] V. Bernardo, F. Loock, J. Martin-de Leon, N. A. Fleck, M. A. Rodriguez-Perez, *Macromol. Mater. Eng*. **2019**, 304 (7),1900041.

[64] R. Li, D.Zeng, Q.liu, Z.Jiang, T.Fang. *Polym Plast Technol Eng*.**2015**, 54(2), 37–41.

[65] M. Santiago-Calvo, S.Perez-Tamarit, P. Cimavilla-Roman,V.Blasco, C.Ruiz, R. Paris, F.Villafañez, M. A. Rodriguez-Perez. *Eur. Polym. J*. **2019**,118, 404–411.

[66] H. E. Naguib, C. B. Park, N. Reichelt. *J. Appl. Polym. Sci*. **2004**, 91 (4), 2661–2668.

[67] S. T. Lee and C. B. Park, *Foam Extrusion, Principles and Practice*, Second edi. 2014.

[68] E. Laguna-Gutierrez. *Understanding the Foamability of Complex Polymeric systems by Using Extensional Rheology*. **2016**, PhD Thesis, University of Valladolid, Spain.

[69] M. R. Holl. *Dynamic analysis, measurement, and control of cell growth in solid state polymeric foams*. **1995**, PhD Thesis, Seattle, University of Washington.

[70] E. Solorzano, S. Pardo-Alonso, J. A. De Saja, M. A. Rodriguez-Perez,. *Colloids Surfaces A Physicochem. Eng. Asp*. **2013**, 438, 167–173.

[71] M. Santiago-Calvo, V. Blasco, C. Ruiz, R. París, F. Villafañey, and M. A. Rodriguez-Perez. *Eur. Polym. J*. **2017**, 97, 230–240.

[72] K. Taki, K. Tabata, S. Kihara, M. Ohshima. *Polym. Eng. Sci*. **2006**, 46 (5), 680–690.

[73] S. Pardo-Alonso, E. Solorzano, S. Estravis, M. A. Rodriguez-Perez, J. A. De Saja. *Soft Matter*. **2012**, 8, 11262.

[74] M. Kobayashi, T. Takahashi, J. Takimoto, K. Koyama. *Polymer (Guildf)*.**1996**, 37(16), 3745–3747..

[75] H. G. H. Van Melick, L. E. Govaert, H. E. H. Meijer.*Polymer (Guildf)*.**2003**, vol. 44 (8), 2493–2502.

[76] J. Drabek, M. Zatloukal. *Phys. Fluids*. **2020**,32 (8), 083110.

[77] M. Okamoto, P.H. Nam, P. Maiti, T. Kotaka, Naoki Hasegawa, A. Usuki, *Nano Letters,* **2001,** 1(6), 295-298.

[78] T. Takahashi, W. Wu, H. Toda, J. Takimoto, T. Akatsuka, K. Koyama, *J. Nonnewton. Fluid Mech*. **1997**,68 (2–3), 259–269.

[79] R. K. Gupta, V. Pasanovic-Zujo, S. N. Bhattacharya. *J. Nonnewton. Fluid Mech*., **2005**, 128 (2–3), 116–125..

[80] Y. Zhang, H. Zhang, L. Ni, Q. Zhou, W. Guo, C. Wu. *J. Polym. Environ*. **2010**, 18, (4), 647–653.

[81] E. Laguna-Gutierrez, R. Van Hooghten, P. Moldenaers, M. A. Rodriguez-Perez, *J. Appl. Polym. Sci*. vol. **2015**, 132 (33).

[82] G. Harikrishnan, D. V. Khakhar. *Inst. Chem. Eng. AIChE*. **2010**, 56, 522–530.

[83] K. Ueberreiter, G. Kanig. *J. Colloid Sci*. **1952**, 7 (6), 569–583.

[84] *http//www. huntsman. com/polyurethanes/a/Products/Technical% 20 Present. 20overview*. Acessed November **2021**.

[85] Y. Dong Hwang , S. Woon Cha. *Polym. Test*.**2002**, 21 (3), 269–275.

[86] J. H. Gibbs, E. A. DiMarzio, *J. Chem. Phys*. **1958**,28 (3), 373–383.

[87] D. Turnbull, M. H. Cohen, *J. Chem. Phys*. **1961**, 34 (1), 120–125.

[88] M. Erber, U. Georgi, J. Müller, K. J. Eichhorn, B. Voit. *Eur. Polym. J*. 2010, 46 (12), 2240–2246.

[89] H. Yin, D. Cangialosi, A. Schönhals. *Thermochim. Acta*. **2013**,566,186–192.

[90] C. Forest, P. Chaumont, P. Cassagnau, B. Swoboda, P. Sonntag. *Polymer (Guildf)*. **2015**, 77, 1–9.

[91] C. Saiz-Arroyo. *Fabricación de Materiales Celulares Mejorados Basados en Poliolefinas. Procesado-Composicion-Estructura-Propiedades*. **2012**, PhD Thesis, University of Valladolid, Spain.

[92] P. Cimavilla-Román, S. Pérez-Tamarit, M. Santiago-Calvo, M. A. Rodríguez-Perez. *Eur. Polym. J*. **2020**,135, no.109884.

[93] J. A. Reglero, E. Cloutet, M. Dumon. *J. Appl. Polym. Sci.* **2012**, 126,38-45.

[94] X. Lu, R. Caps, J. Fricke, C. T. Alviso, R. W. Pekala. *J. Non. Cryst. Solids*. **1995**, 188 (3), 226–234.

[95] L. Madaleno, R. Pyrz,A. Crosky, L. R. Jensen, J. C. M. Rauhe, V. Dolomanova, A.M.M.V. De Barros-Timmons, J.C.C.Pinto, J.Norman. *Compos. PART A*. **2013**, 44,1–7.

[96] S. Muñoz-Pascual, C. Saiz-Arroyo, A. Vananroye, P. Moldenaers, M. A. Rodriguez-Perez. *Macromol. Mater. Eng*. **2021**, 306 (4), 2000728.

[97] S. N. S. Leung. *Mechanisms of cell nucleation, growth, and coarsening in plastic foaming: theory, simulation, and experiment*. 2009, PhD Thesis University of Toronto, Canada.

[98] Z. Zhu, D. Xu, C. B. Park, R. G. Fenton. *J. Cell. Plast*. **2005**, 41 (5), 475–486.

[99] Z. Chen, A. A. Faysal, M. Embabi, L. Yu, C. B. Park, P. C. Lee. *Polymer (Guildf)*. **2021**, 235, 124272.

[100] J. Martín-de Leon, V. Bernardo, M. Rodriguez-Perez. *Polymers (Basel)*. **2016**, 8 (7), 265.

[101] Rapra Technology, "*Cellular Polymers IV*. 4th International Conference, 5th-6th June **1997,** Held at Rapra Technology Limited, Shawbury, Shrewsbury, United Kingdom.

[102] A. Konig, U. Fehrenbacher, T. Hirth, E. Kroke. *J. Cell. Plast*. **2008**, 44 (6), 469–480.

[103] Q. B. Ho, M. Kontopoulou. *Polymer (Guildf)*. **2020**, 198, 122506.

[104] A. M.Harris, E. C.Lee. *Appl. Polym. Sci.* ***2008***,107 (4), 2246–2255.

[105] G. Wypych. *Handbok of Polymers*.**2016**, second edition, Elsevier, Amsterdam, The Netherlands.

[106] V. Bernardo, J. Martin-de Leon, M. A. Rodriguez-Perez. *Polym. Int*. **2019**, 68 (6), 1204–1214.

[107] E. Kontou, G. Anthoulis. *J. Appl. Polym. Sci*. **2007**, 105 (4), 1723–1731.

[108] Y. H. Lee, C. B. Park, K. H. Wang, M. H. Lee. *J. Cell. Plast*. 2005, 41 (5), 487–502.

[109] A. J. Crosby, J. Lee. *Polym. Rev*. 2007, 47 (2), 217–229.

[110] W. G. Zheng, Y. H. Lee, C. B. Park. *J. Appl. Polym. Sci. 2010*,117 (5), 2972–2979.

[111] G. Wang, K. L. Wang, C. J. Lu. *IOP Conf. Ser. Mater. Sci. Eng*. ***2017***,242, 012020.

[112] A. Torro-Palau, J. C. Fernandez-Garcia, A. C. Orgiles-Barcelo, M. M. Pastor-Blas, J. Martin-Martinez. *Int. J. Adhes. Adhes.* **1997**, 17 (2), 111–119.

[113] M. S. Nikolic, R. Petrovic, D. Veljovic, V. Cosovic, N. Stankovic, J. Djonlagic, *Eur. Polym. J.* **2017**, 97, 198–209.

[114] A. Alvarez, J. Santaren, A. Esteban-Cubillo, P. Aparicio, "Current industrial applications of palygorskite and sepiolite. *Dev. Clay Sci.* **2011**,3, 281–298.

[115] J. Sandler, M. S. Shaffer, T. Prasse, W. Bauhofer, K. Schulte, A.Windle. *Polymer (Guildf).***1999**, 40 (21), 5967–5971.

[116] J. Shen, X. Han, L. J. Lee. *J. Cell. Plast.* **2006**, 42 (2), 105–126.

[117] N. H. Abu-Zahra, A. M. Alian. *Polym. Plast. Technol. Eng.* **2010**, 49 (3), 237–243.

[118] J. Lobos, S. Velankar. *J. Cell. Plast.* **2016,** 52 (1), 57–88.

[119] T. Azdast, R. Hasanzadeh. *J. Cell. Plast.* **2020**, 0021955X2095930.

[120] M. Santiago-Calvo, J. Tirado-Mediavilla, J. L. Ruiz-Herrero, M. A. Rodriguez-Perez, and F. Villafañe. *Polymer (Guildf).* **2018**,150, 138–149.

[121] V. Dolomanova, J. C. M. Rauhe, L. R. Jensen, R. Pyrz, and A.M.M.V. De Barros-Timmons. *J. Cell. Plast.* ***2011***, 47 (1), 81–93.

[122] J. Zhao, A. B. Morgan, J. D. Harris. *Polymer (Guildf).* **2005**, 46 (20), 8641–8660.

[123] L. Shen, Y. Lin, Q. Du, W. Zhong, Y. Yang. *Polymer (Guildf).* **2005**, 46 (15), 5758–5766.

[124] B. Notario, D. Velasco, M. A. Rodriguez-Perez, J. Santaren, A. Alvarez, and A. Esteban-Cubillo. *Improving the cellular structure and thermal conductivity of polysyrene foams by using sepiolites*. in *International Conference on Foams,Foams Technology, FOAMS* ***2012,*** pp. 1–5.

[125] P. Saraeian, H. Tavakoli, A. Ghassemi. *J. Compos. Mater.* ***2013***, 47 (18), 2211–2217.

[126] C. Zeng, X. Han, L. J. Lee, K. W. Koelling, D. L. Tomasko. *Adv. Mater.* **2003**,15 (20), 1743–1747.

[127] X. Han, C. Zeng, L. J. Lee, K. W. Koelling, D. L. Tomasko. *Polym. Eng. Sci.* **2004**, 43 (6), 1261–1275.

[128] Z. Guo, J. Yang, M. J. Wingert, D. L. Tomasko, L. J. Lee, "of Cellular Plastics Comparison of Carbon Nanofibers," 2008, doi: 10.1177/0021955X08091450.

[129] W. Xiao, X. Liao, S. Li, J. Xiong, Q. Yang, G. Li. *Polym.Int.* **2018**, 67 (11) ,1488-1501.

[130] V. Bernardo, J.Martin- de Leon, E.Laguna-Gutierrez, T.Catelani, J.Pinto, A.Athanassiou, M.A.Rodriguez-Perez. **2018**,153, 262–270.

[131] P. Spitael, C. W. Macosko, R. B. McClurg. *Macromolecules*. **2004**, 37 (18), 6874–6882.

[132] M. D. Whitmore,T. W. Smith. *Macromolecules*. **1994**, 27 (17),4673–4683.

[133] B. H. Yokoyama, L. Li, T. Nemoto, K. Sugiyama. *Adv. Mater.* **2004**, 16 (17), 1542–1546.

[134] J. Pinto, J. A. Reglero-Ruiz, M. Dumon, and M. A. Rodriguez-Perez. *J. Supercrit. Fluids*. **2014**,94, 198–205.

[135] S. Wu. *Polym. Eng. Sci.* **1987**, 27 (5), 335–343.

[136] Q. Wu, C.B. Park, N. Zhou, W. Zhu. *J. Cell. Plast.* ***2009***, 45 (4), 303–319.

[137] R. Banerjee, S. S. Ray, A. K. Ghosh. *Int. Polym. Process.* **2017**, 32 (4), 434–445.

[138] R. Wati, B. Sharudin, M. Ohshima. *J. Appl. Polym. Sci.* **2013**.128(4), 2245–2254.

[139] M. Haurat, M. Dumon. *Molecules*.**2020**, 25(22), 5320.

[140] V. Bernardo, J. Martin-de Leon, I. Sanchez-Calderon, E. Laguna-Gutierrez, M. A. Rodriguez-Perez. *Macromol. Mater. Eng.* **2020**, 305 (1), 1900428.

[141] V.Kumar, Nam.P.Shu. *Polym. Eng. Sci.* **1990**, 30 (20), 1990.

[142] F. A. Waldman. *The Processing of Microcellular Foam*. **1982**, PhD Thesis, Massachusetts Institute of Technology (MIT), United States.

[143] D. Bao, X. Liao, T. He, Q. Yang, G. Li. *J. Polym. Res.* **2013**, 20 (11).

[144] B. Notario, J. Pinto, M. A. Rodriguez-Perez. *Polym. (United Kingdom)*.**2015**, 63, , 116–126.

[145] J. Pinto. *Fabrication and Characterization of Nanocellular Polymeric Materials from Nanostructured Polymers*. **2014**, PhD Thesis, University of Valladolid, Spain.

[146] R. Murray, J. Weller, V. Kumar. *Cell. Polym.* **2000**, 19 (6), 413–425.

[147] B. Notario, A. Ballesteros, J. Pinto, M. A. Rodriguez-Perez. *Mater. Lett.* **2016**, 168, 76–79.

[148] F. Rindfleisch, T. P. DiNoia, M. A. McHugh. *J. Phys. Chem.* ***1996***, 100 (38), 15581–15587.

[149] W. W. Brandt. *J. Phys. Chem. 1959*, 63 (7), 1080–1085.

[150] P. Alessi, A. Cortesi, I. Kikic, F. Vecchione. *J. Appl. Polym. Sci.* **2003**, 88 (9), 2189–2193.

[151] Z. Zhang, Y. P. Handa. *J. Polym. Sci. Part B Polym. Phys.* **1998**, 36 (6),977–982.

[152] K. F. Webb , A. S. Teja. *Fluid Phase Equilib.* **1999** ,158–160, 1029–1034.

[153] M. M. R. Williams. *Ann. Nucl. Energy*. 1977, 4 (4–5), 205–206.

[154] Y. A. Nizhegorodova, N. A. Belov, V. G. Berezkin, Y. P. Yampolskii. *Russ. J. Phys. Chem. A*. **2015**, 89 (3), 502–509.

[155] G. Li, J. Wang, C. B. Park. *J. Appl. Polym. Sci.* **2007**, 103(5), 2945-2953.

[156] Y. Sato, K. Fujiwara, T. Takikawa, S. Takishima, H.Masuoka. *Fluid Phase Equilibria*. **1996,** 125 (1-2), 129-138.

[157] M. Askari, "CO2/CH4. *Bulletin de la Société Royale des Sciences de Liège,* 2017, 86, 139-156.

[158] W. J. Koros, A. H. Chan, D. R. Paul. *J. Memb. Sci.* ***1977,*** 2, 165–190.

[159] B. Flaconneche, J. Martin, M. H. Klopffer. *Oil Gas Sci. Technol.* 2001, 56(3), 245–259.

[160] D. Miller, P. Chatchaisucha,V. Kumar.*Polymer (Guildf).***2009**, 50 (23), 5576–5584.

[161] S. Costeux, I. Khan, S. P. Bunker, H. K. Jeon. *J. Cell. Plast.* **2015**, 51 (2),197–221.

[162] H. Guo, V. Kumar. *Polymer (Guildf).* ***2015***,56, 46–56.

[163] K. Nadella, V. Kumar, W. Li. *Cell.Polym.*2005, 24(2),71-90.

[164] D. Li, Y. Chen, S. Yao, H. Zhang, D. Hu, and L. Zhao. *Polymers (Basel).* **2021**, 13, (9), 1494.

[165] T. P. Lodge, T. C. B. McLeish. *Macromolecules*.**2000**, 33 (14), 5278–5284.

[166] M. H. Jomaa, L. Roiba, D. S. Dhungana, J. Xiao, J.Y.Cavaille, L.Severyat, L.Lebrun, G.Diguet, K.Masenelli-Varlot. *Compos. Sci. Technol.* **2019**, 171, 103–110

[167] F. J. Galindo-Rosales, P. Moldenaers, J. Vermant. *Macromol. Mater. Eng.* **2011**, 296 (3–4), 331–340.

[168] Q. Zhang, F. Fang, X. Zhao, Y. Li, M. Zhu, D. Chen. *J. Phys. Chem. B.* **2008**, 112(40), 12606–12611.

[169] D. W. Schaefer, R. S. Justice. *Macromolecules. 2007,* 40 (24), 8501–8517.

[170] E. Laguna-Gutierrez, R. Van Hooghten, P. Moldenaers, M. Angel Rodriguez-Perez. *J. Appl. Polym. Sci.* **2015**, 132 (47), 1–12.

[171] Z. Stary, H. Münstedt.*In AIP Conference Proceedings*, **2017**, 1843 (1), 050004.

[172] D. Garcia- Lopez, J. F. Fernandez, J. C. Merino, J. Santaren, J. M. Pastor. *Compos. Sci. Technol.* **2010**, 70(10),1429–1436.

[173] J. Vlachopoulos, D. Strutt. *Rheology of Molten Polymers. In : Multilayer Flexible Packaging*. **2009**, first edition, Elsevier, Amsterdam, The Netherlands.

[174] R. Banerjee, S. S. Ray, A. K. Ghosh. *Int. Polym. Process.* **2017**, 32 (4), 434–445.

[175] S. Pardo-Alonso, E.Solorzano, L.Brabant, P.Vanderniepen, M.Dierick, L.Van Hoorebeke, M.A.Rodriguez-Perez. *Eur. Polym. J.* **2013,** 49 (5), 999–1006.

[176] S. Wu. *Polym. Eng. Sci.* 1988,28 (8),538–543.

[177] J. M. Dealy, J. Wang. *Melt Rheology and its Applications in the Plastics Industry*. **2013**, first edition, Springer, Berlin, Germany.

[178] A. Malkin, A. Y. Malkin, *Rheology Fundamentals*. **1999**, first edition, ChemTec Publishing, Toronto, Canada.

[179] F. A. Mazzeo "*Importance of Oscillatory Time Sweeps in Rheology*. TA Instruments Guide. pp. 1–4.

[180] K. M. Koki, D. K. Christopher, W. Kurt, B. M. Monon, E. Stephen. *J. Appl. Polym. Sci. 2011*, 119 (4) ,940–1951.

[181] S. Hwan Lee, E. Cho, J. Ryoun Youn. *J. Appl. Polym. Sci.* **2007**, 103 (6), 3506–3515.

[182] M. Zatloukal .*Polym. (United Kingdom)*.2016,104,258–267.

[183] https://cdn.technologynetworks.com/TN/resources/PDF/WP160620BasicIntroRheology.pdf

[184] B. Costello.*Use of Rheology to Determine the Molecular Weight Distribution of Polymers*. TA Instruments Guide. **2005**, vol 13.

[185] V. Mittal, *Characterization techniques for polymer nanocomposites*. **2012**, first edition, Wiley and Sons, New Jersey, United States.

[186] A. Usuki Y.Kojima, M.Kawasumi, A.Okada, Y.Fukushima, T.Kurauchi,O.Kamigaito. *J. Polym. Sci. Part A Polym. Chem.* **1993**, 8 (5), 1179–1184.

[187] M. J. Pastoriza-Gallego, M. Perez-Rodriguez, C. Gracia-Fernandez, and M. M. Piñeiro, *Soft Matter*.2013, 9 (48), 11690–11698.

[188] H. Münstedt, F.R. Schwarzl. *Deformation and flow of polymeric materials*. **2014,** Springer, Berlin, Germany.

[189] P. M. Wood-Adams J. M. Dealy. *Macromolecules*. **2000**, 33(20), 7481-7488.

[190] G. J. Nam, J. H. Yoo, J. W. Lee. *J. Appl. Polym. Sci.* 2005, 96 (5), 1793–1800.

[191] J. Vermant, S. Ceccia, M. K. Dolgovskij, P. L. Maffettone, C. W. Macosko. *J. Rheol. (N. Y. N. Y).* **2007**, 51 (3), 429.

[192] R. Kotsilkova. *Mech. Time-Dependent Mater.* **2002**, 6 (3), 283–300.

[193] J. Gopalakrishnan, S. K. N. Kutty. *J. Elastomers Plast.* **2013,** 47 (2), 153–169.

[194] W. Thimm, C. Friedrich, M. Marth, J. Honerkamp. *J. Rheol. (N. Y. N. Y).* **1999**, 43 (6) ,1663–1672.

[195] D. W. Mead. *J. Rheol.* **1994**, 38 (6),1797–1827.

[196] H. G. Ock, D. H. Kim, K. H. Ahn, S. J. Lee, J. M. Maia. *Eur. Polym. J.* **2016**, 76, 216–227.

[197] A. B. Morgan , J. W. Gilman. *J. Appl. Polym. Sci.* 2003, 87 (8), 1329–1338.

[198] A. Celzard, E. McRae, C. Deleuze, M. Dufort, G. Furdin, J. Marêché. *Phys. Rev. B.* **1996**, 53, 10, 6209–6214.

[199] J. Boissonade, F. Barreau, F. Carmona. *J. Phys. A. Math. Gen.* ***1983***, 16, 2777–2787.

[200] A. K. Kota, B.H.Cipriano, M.K.Duesterberg, A.L.Gershon, D.Powell, S.R.Raghavan, H.A.Bruck. *Macromolecules*. **2007**, 40 (20), 7400–7406.

[201] F. Chen, Y. Shangguan, Y. Jiang, B. Qiu, G. Luo, Q. Zheng. *Polym. (United Kingdom)*. **2015**, 65, 81–92.

[202] A. Minegishi, A. Nishioka, T. Takahashi, Y. Masubuchi, J. Takimoto, and K. Koyama.*Rheol. Acta*. **2001**, 40 (4), 329–338.

[203] A. D. Gotsis, B. L. F. Zeevenhoven, C. Tsenoglou. *J. Rheol. (N. Y. N. Y).* ***2004***, 48 (4), 895–914.

[204] F. Morea, J. O. Agnusdei, R. Zerbino. *Mater. Struct.* **2010**, 43 (4), 499–507.

[205] K. Wang, H. Huang, and J. Sheng. *J. Liq. Chromatogr. Relat. Technol.* **1998**, 21 (10), 1457–1470.

[206] B. K. Hong ,W. H. Jo. *Polymer (Guildf).* **2000**, 41 (6), 2069–2079.

[207] M. Seier, S. Stanic, T. Koch, and V.M. Archodoulaki. *Polymers (Basel).* 2020, 12 (10), 2335.

[208] M. Sugimoto, Y. Masubuchi, J. Takimoto, K. Koyama. *Macromolecules*. **2001**, 34(17), 6056–6063.

[209] E.Bowersox, D. A.Hoffman, J.Travitz. "*Assessment of the Influence of Moisture Percentage , Melt Temperature , and Residence Time on Material Degradation*," **2017**,SPE conference Proceedings, Anaheim , California,United States.

[210] G. Liu, H. Sun, S. Rangou, K. Ntetsikas, A. Avgeropoulos, S..Q. Wang. *J. Rheol. (N. Y. N. Y) 2013,* 57 (1), 89–104.

[211] M. Kobayashi, T. Takahashi, J. Takimoto, K. Koyama. *Polymer (Guildf).* **1995**, 36 (20), 3927–3933.

[212] T. C. B. McLeish, R. G. Larson. *J. Rheol. (N. Y. N. Y)* **1998**, 42 (1), 81–110.

[213] H. M. Laun and H. Münstedt. *Rheol. Acta*. **1978**, 17 (4), 415–425.

[214] M. H. Wagner, T. Raible, J. Meissner. *Rheol. Acta*. **1979**, 18 (3), 427–428.

[215] T. Takahashi, J. Takimoto, and K. Koyama. *Polym. Compos*. **1999**, 20 (3), 357–366.

[216] E. van Ruymbeke, E. B. Muliawan, S. G. Hatzikiriakos, T. Watanabe, A. Hirao, D. Vlassopoulos, *J. Rheol. (N. Y. N. Y)*. **2010**, 54 (3), 643–662.

[217] http://www.greenspec.co.uk/building-design/insulation-materials-thermal-properties/. Acessed November **2021**.

[218] https://www.euractiv.com/section/energy-environment/news/while-global-plastic-production-is-increasing-worldwide-it-is-slowin-down-in-europe/. Acessed November **2021**.

[219] https://www.dillmeierglass.com/news/components-of-an-energy-saving-building-design. Acessed November **2021**.

[220] https://www.cellubor.com/thermal-insulation. Acessed November **2021**.

[221] https://www.iea.org/topics/buildings. Acessed November **2021**.

[222] P. G. Collishaw, J. R. G. Evans. *J. Mater. Sci*. **1994**, 29 (2), 486–498.

[223] https://www.engineeringtoolbox.com/air-properties-viscosity-conductivity-heat-capacity-d_1509.html. Acessed November **2021**.

[224] R. Perkins, L. Cusco, J. Howley, A. Laesecke, S. Matthes, M. L. V. Ramires. *J. Chem. Eng. Data*. **2001**, 46 (2), 428–432.

[225] M. Santiago-Calvo, J.Tirado-Mediavilla, J.C.M.Rauhe, L.R.Jensen, J.L.Ruiz-Herrero, F.Villafañez, M.A.Rodriguez-Perez. *Eur. Polym. J*. 2018, 108, 98–106.

[226] J.R.Howell, R. Siegel, M.P.Mengu. *Thermal Radiation Heat Transfer*. **2021**, seventh edition, CRC press Taylor and Francis Group, Bocaraton, United States.

[227] C.De Micco, C.M. Aldao. *J Polym Sci Part B Polym Phys*. **2005**, 43(2),190-192.

[228] O.Almanza, M.A.Rodriguez-Perez, J.A.De Saja. *Polymer*. ***2001****, 42 (16), 7117-7126*.

[229] L.R.Glicksman . *Heat Transfer in foams. In: Low Density Cellular Plastics: Physical Basis of Behavior*. **1994**, first edition, Springer Science, The Netherlands.

[230] R.J.J. Williams, C.M. Aldao. *Polym Eng Sci*. **1983**, 23(6),293-298.

[231] O.Almanza, M.A.Rodriguez-Perez, J.A.De Saja. *Polym Int*. ***2004**, 53, 2038-20444*.

[232] S. Estravís, J. Tirado-Mediavilla, M. Santiago-Calvo, J. L. Ruiz-Herrero, F. Villafañe, M. A. Rodríguez-Pérez. *Eur. Polym. J.* **2016**, 80, 1–15.

[233] E. Solórzano, M. A. Rodriguez-Perez, J. Lazaro, J. A. De Saja. *Adv. Eng. Mater.* 2009, 11(10), 818–824.

[234] J. Schellenberg, M. Wallis. *J. Cell. Plast.*2010, 46(3), 209–222.

[235] E. Placido, M. C. Arduini-Schuster, J. Kuhn. *Infrared Phys. Technol.* 2005, 46(3), 219–231.

[236] B. Notario, J. Pinto, E. Solorzano, J.A. De Saja, M. Dumon, M.A. Rodriguez-Perez. *Polym (United Kingdom)*. **2015**,56,57-67.

# Chapter 3

## Materials, production processes and characterization techniques.

*"We are such a stuff as dreams are made on;*
*and our little life is rounded with a sleep"*
The Tempest, William Shakespeare.

*"Estamos hechos del mismo material del que*
*se tejen los sueños"*
La tempestad, William Shakespeare.

# INDEX

## 3.1 Introduction

This chapter analyzes the characteristics and properties of the pure polymer matrices and cell nucleating agents used in this work. The experimental procedures employed to produce the cellular materials and the characterization techniques employed to characterize these foamed samples are also presented in this chapter.

The characterization methods of solid and cellular materials will be referenced to their standards according to the International Organization for Standardization (ISO) or ASTM International (American Society for Testing and Materials).

## 3.2 Materials

### *3.2.1. Polystyrene*

Polystyrene (PS) is a thermoplastic amorphous polymer that was firstly produced in the 30s decade in Ludwigshafen (Ludwigshafen am Rhein, Germany) by the IG Farben company.[1] This polymer is obtained by the polymerization of styrene groups. Each of the monomers of this polymer possesses a phenyl group that is attached to a carbon atom as it can be seen in **Figure 3.1**.[2,3] The appearance of this phenyl group provides to the PS macromolecules some properties like hydrophobicity and rigidity.[4]

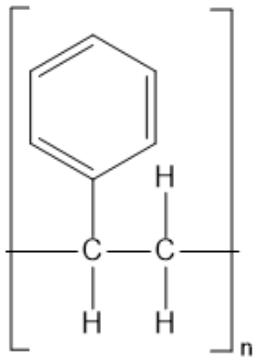


**Figure 3.1.** Schematic figure of the monomer of polystyrene.

The use of PS has been widely expanded in the polymer industry, especially for its good properties like low thermal conductivity, ease of coloring, transparency, light weight, high compressive strength, resistance to moisture and medium to high tensile strength below its glass transition temperature.[5–7] Furthermore, the price of PS, between 950 and 1050 US dollars per ton, is not very high in comparison with the price of other synthetic thermoplastic amorphous polymers

like polymethyl methacrylate (PMMA), whose price varies between 3610 and 7670 US dollars per ton, or polycarbonate (PC), whose price oscillates between 2656 and 7666 US dollars per ton. [8–10]

Due to its outstanding properties, this polymer is employed in applications and sectors such diverse as: refrigerators and air conditioners, instrument panels, some parts of televisions and computers, disposables utensils, food industry (storage and packaging), automotive pieces and building insulation, among others[11,12]. Nowadays, PS is the fourth largest, by volume, general thermoplastic in the market.[13] For example, the market for EPS (expanded polystyrene) is projected to reach 13.05 billion of American dollars by 2028.[14] The highest producers of PS in the world are BASF SE (Germany), INEOS Styrolution Group (Germany), Videolar (Brazil), Sabic (Saudi Arabia) and Formosa Plastic Corporation (Taiwan).[15] Concerning its use by region, Asia is the continent where the demand of PS is higher, followed by North America, Europe and South America.[13]

During the current thesis PS has been used as the polymer matrix to produce the cellular materials using the gas dissolution foaming process, which was explained in detail in the Chapter 2 of this manuscript.

In the thesis four different grades of PS have been employed: Edistir N2380, Edistir N3840 and Edistir N3910, all of them from Versalis (San Donato Milanese, Italy) and Styrolution 153F from INEOS Styrolution Group (Frankfurt am Main, Germany).

The characteristics of the different grades of PS are presented in the **Table 3.1**. All this information was obtained from the technical data sheets (TDS) of the different materials.

| Polystyrene | Density (g/cm$^3$) | MFR (g/10 min) at 200 ºC and 5 kg | Vicat Softening Temperature (°C) | Thermal Conductivity (W/mK) |
|---|---|---|---|---|
| **Edistir N2380** | 1.05 | 2 | 106 | 0.17 |
| **Styrolution 153F** | 1.04 | 7.5 | 101 | 0.16 |
| **Edistir N3840** | 1.05 | 10 | 88 | 0.17 |
| **Edistir N3910** | 1.05 | 27 | 83 | 0.17 |

**Table 3.1**. Main characteristics of the four PS used in the thesis: density, melt flow rate (MFR), Vicat Softening temperature and thermal conductivity of the pure PS grades.

The density, measured according to Standard ISO 1183, is quite similar for the four different PS. The melt flow rate, which is determined according to the standards ASTM D1238a and ISO 1133a, varies between 2 g/10 min and 27 g/10 min. Polymers with different MFR were selected for this thesis with the objective of analyzing the effect of this parameter in the foaming mechanisms and in the characteristics of the cellular structure of the foamed samples.

### *3.2.2 Cell Nucleating Agents*

Along the entire thesis two materials have been used as cell nucleating agents: sepiolites (inorganic nucleating agent) and styrene-ethylene-butylene-styrene (SEBS) (organic nucleating agent). These materials have been used to modify the cellular structure and therefore, the thermal properties (thermal conductivity) of the PS based foamed samples.

#### *3.2.2.1 Sepiolites*

Sepiolites are silicate acicular particles with needle-like morphologies. They are chemically conformed by magnesium silicates and they present lengths varying between 1 and 2 micrometers and thicknesses varying between 20 and 50 nanometers, as it can be seen in **Figure 3.2**. Sepiolites, whose formula is ($Si_{12}Mg_8O_{30}(OH)_4(OH_2)_4 \cdot 8H_2O$), present elements like magnesium and silicate that are combined with usual organic elements (like oxygen and hydrogen). The disposition of the chemical elements in the crystalline structure of these clays, explains the outstanding porosity of the sepiolites. Due to the zeolitic channels that conform the material, the density of these particles is lower than that of other similar clays. Moreover, these particles present a remarkable sorption capability. Furthermore, their needle like shape maximizes their surface area (c.a. 300 $m^2/g$), which makes them suitable to be used as nucleating agents in cellular materials. Moreover, the presence of silanol groups attached to the surfaces of the particles make possible the modification of their surface. The surface modification of the sepiolites could present meaningful effects in the dispersion degree of the particles in the polymers and therefore, in the final properties of the cellular materials.

Due to their interesting characteristics and properties, sepiolites are commonly employed for diverse applications like industrial absorbents for fossil fuels such as petrol (especially for oil or petrol spill in the oceans or water surfaces), production of some cements, thermal insulators, thanks to the capability of their inner channels to retain air, substitutes of the bentonite, in some cat litters or bedding for small animals or as nucleating agents among others.

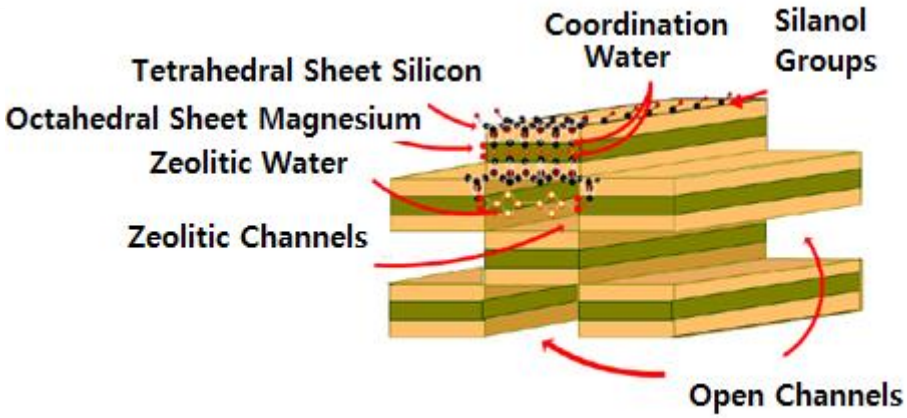


**Figure 3.2**. Image of the structure of sepiolites.

In the current thesis three different types of sepiolites with different surface treatments have been used. On the one hand, natural sepiolites (N-SEP), which have not suffered any kind of modification of their surfaces. On the other hand, two sepiolites which have been organo-modified in their surfaces. Particles superficially treated with quaternary ammonium salts, named as (O-QASEP) and particles modified with silane groups (O-SGSEP). The three sepiolites were kindly supplied by TOLSA S.A. (Madrid, Spain). The sepiolites were received in a dust way. In **Table 3.2**. some of the properties of the sepiolites used are described.

| Abbreviation | Description | Modification of the Surface | Bulk Density ($g/cm^3$) |
|---|---|---|---|
| **N-SEP** | Natural Sepiolites | No | 2.1 |
| **O-QASEP** | Sepiolites with Quaternary Ammonium Salts | Yes | 2.1 |
| **O-SGSEP** | Sepiolites with Silane Groups | Yes | 2.1 |

**Table 3.2**. Characteristics of the sepiolites used in this work.

The effects on the cellular structure and foam characteristics associated to work with different contents of clays and with different types of clays are analyzed in the Chapter 5 of the present manuscript.

### *3.2.2.2 Styrene-ethylene-butylene-styrene (SEBS)*

A copolymer is a polymer constituted by two or more monomers (heterogeneous chains). Among the different types of copolymers that can be found, random copolymers and block copolymers are the most common ones. In random copolymers the two or more monomers do not present a determined sequence in the chains. On the other hand, in block copolymers the two or more monomers constitute a repetitive sequence in which monomer A, B, C, etc., alternates along the chains in the same order.

In the present work a linear tetra-block copolymer like is the styrene-ethylene-butylene-styrene (SEBS) has been used. In **Figure 3.3** it is possible to see the chemical structure of a SEBS copolymer. In the middle part of the repetitive units the ethylene and butylene monomers can be found, meanwhile the repetitive units of styrene groups are in the outer blocks. Due to this separation between the rubber or elastomeric monomers and the styrene ones there is a good adhesion and compatibility between the SEBS and the PS, when they are blended with a common extrusion process. In addition, some domains of elastomeric phases can be formed in the PS polymer matrix due to the lack of junction between the ethylene-butylene monomers and the styrene ones. The presence of these domains or micelles, will serve as future nucleation points that will determine the characteristics of the cellular structure of the foams based on PS/SEBS.

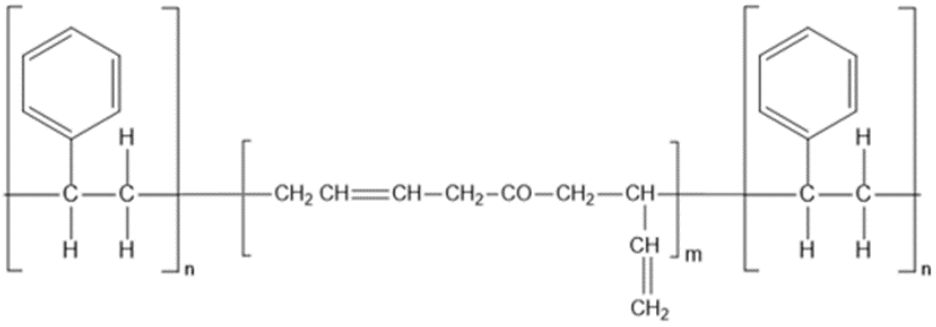


**Figure 3.3.** Schematic figure of the monomer of styrene-ethylene-butylene-styrene (SEBS).

In this work a SEBS grade of Kraton Corporation (Houston, Texas, United States) was used. In the following table (**Table 3.3)** the main characteristics of the SEBS grade selected are depicted.

| Material | MFI (g/10 min) at 230°C and 2.16 kg | Styrene/ Rubber Ratio | Viscosity in Solution (cps) |
|---|---|---|---|
| **Kraton G1643MS** | 19 | 20/80 | 210 |

**Table 3.3**. Characteristics of the grade of SEBS used in this work.

The effects on the cellular structure and foam characteristics associated to work with different contents of SEBS are analyzed in the Chapter 6 of the present manuscript.

### *3.2.3 Other materials*

#### *3.2.3.1 Antioxidant*

To avoid the degradation of the materials during the extrusion process, an antioxidant has been used. In this work the antioxidant employed was Irganox 1010 from BASF (Ludwigshafen am Rhein, Germany). This antioxidant was used in both the blends of PS with sepiolites and the blends of PS with SEBS. In the following table (**Table 3.4**) some characteristics of the Irganox 1010, which is presented in a powder form, are described.

| Material | Density (g/cm)3 | Melting Range (°C) |
|---|---|---|
| **Irganox 1010** | 1.11 | 113-126 °C |

**Table 3.4.** Characteristics of the antioxidant used in the thesis.

#### *3.2.3.2 Carbon Dioxide*

Carbon dioxide ($CO_2$) has been used as blowing agent in this thesis. The $CO_2$ gas is made up of two atoms of oxygen joined by covalent bonding to a carbon atom. At normal ambient conditions (298 K and 1 bar of pressure), $CO_2$ is in gaseous state, as it can be seen in **Figure 3.4**. During the gas dissolution process, required to produce the cellular materials based in PS, the $CO_2$ is in a supercritical state. This state is reached when the pressure is higher than 73 bars and the temperature is higher than 31 °C. In a supercritical state, a material can share the properties of gases like diffusion through a porous material (effusion) or viscosities similar to gases with the ability to dissolve materials like liquids or solids, which is a property common of liquids.

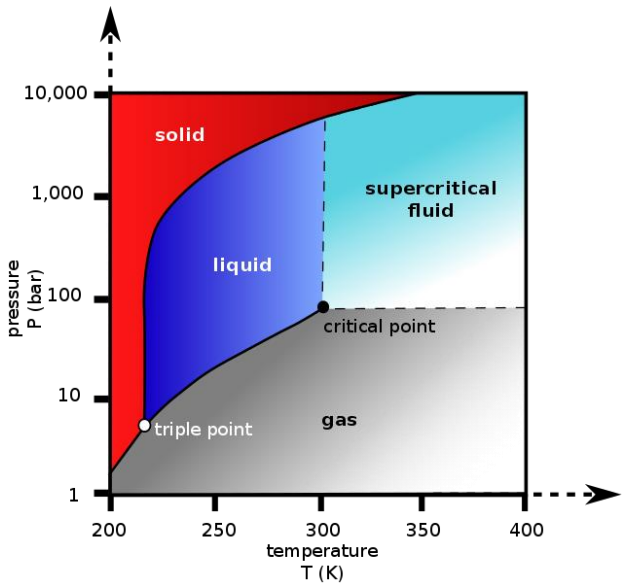


**Figure 3.4**. Phase diagram of $CO_2$.

$CO_2$ is considered an eco-friendly gas and it is replacing some of the blowing agents which have been usually employed to produce PS cellular materials like CFC and HCFC. Furthermore, the lack of necessity to take additional protective measurements, as for example in the case of flammable blowing agents like pentane, butane or isobutane, make $CO_2$ one of the most used blowing agents in the cellular materials industry.

## 3.3 Production Processes

In this section the methods used to produce the solid precursors based on PS, which are required for the foaming process and for some characterization techniques, and the cellular materials are explained. The scheme presented in **Figure 3.5** covers all the steps performed from the initial materials until the obtention of the final foamed products.

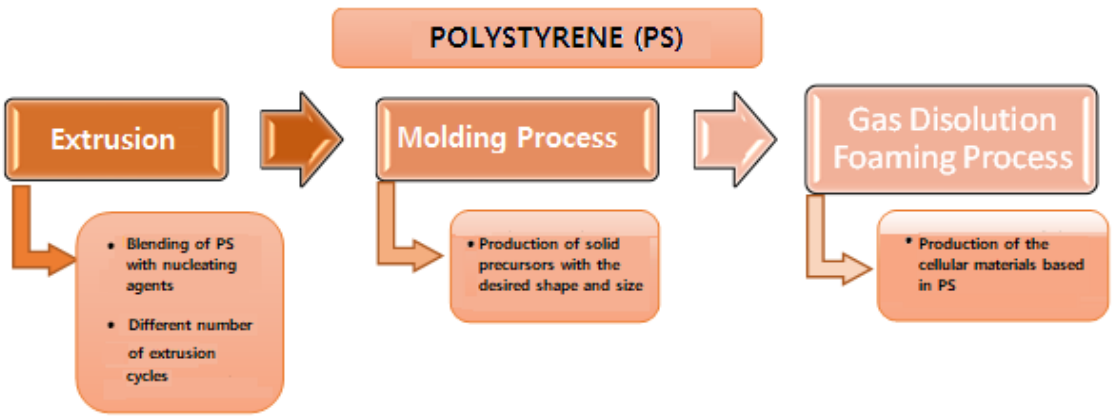


**Figure 3.5**. Scheme of the steps followed during the production processes.

The extrusion process is required to blend the PS with the different nucleating agents: sepiolites and SEBS. Furthermore, for some materials the number of extrusion cycles was incremented from one extrusion cycle to two extrusion cycles. The influence of the number of extrusion cycles was analyzed in the Chapter 5 of the thesis (section 5.2). The pellets obtained after the extrusion process, were thermoformed in a hot/cold press to produce solid precursors with the required shape and size. These solid precursors were used for the foaming process and for some characterization techniques. In the foaming process, the solid plates are introduced in an autoclave to produce the cellular materials following the gas dissolution foaming process.

### *3.3.1 Production of solid precursors*

#### *3.3.1.1 Extrusion*

A co-rotating twin screw extruder, model ZK 25T Teachline from Dr. Collin, was used for blending the PS with the cell nucleating agents (sepiolites and SEBS). The length diameter ratio (L/D) of this extruder is 24:1, with a screw diameter of 25 mm, a maximum screw speed of 200 rpm, a torque per shaft of 56 Nm, a motor capacity of 2.5 kW, and an output which can vary between 50 g/h and 5000 g/h. In **Figure 3.6** it is possible to see the extruder used along the thesis, as well as a picture of the screws and a schematic draw of the extruder with the name of the most important parts.

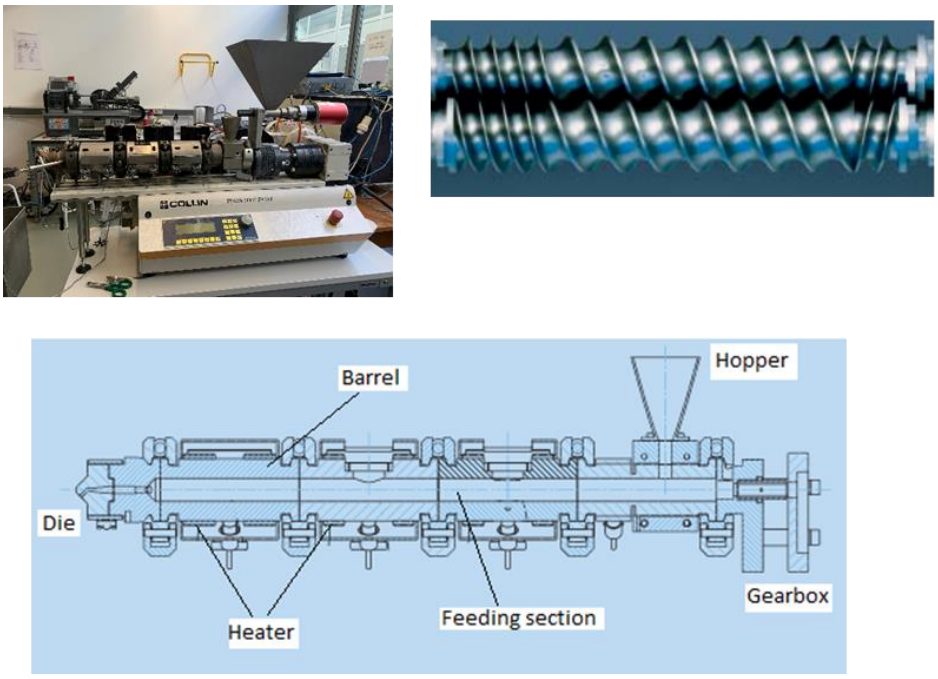


**Figure 3.6**. Images of the extruder ZK 25T Teachline from Dr. Collin, screws and schematic draw of the extruder elements.

Before materials were extruded, they were dried in a vacuum drying oven (Mod. VacioTem TV, P-Selecta) at 70 °C for 4 hours, in the case of pure PS, at 80 °C for 8 hours in the case of the different types of sepiolites and at 70 °C for 4 hours in the case of the SEBS with vacuum pressures close to 150 mbar. In principle, PS and SEBS should not require to be dried, because the water absorption at 298 K and 24 hours is lower than 0.1%, but to avoid any possible effect during the subsequent blending they were dried at temperatures below their glass transition point. On the other hand, sepiolites can store water easily; therefore, the dry process requires a slightly higher temperature and a higher number of hours. Once the samples were without moisture, they were blended in the extrusion machine. The profile of temperatures used in the extruder was the same for the two different mixtures (PS, sepiolites and antioxidant or PS, SEBS, and antioxidant). It starts with 145 °C in the feeding section, below the hopper and reaches 185 °C in the die (with a progressive increment of 10 °C in each of the 5 sections that conform the extruder). The screw speed used was 50 rpm in all the cases. The rod of blend that comes out of the die usually is cooled down in water and after that, pelletized in a pelletizer machine. This process was carried out for the formulations that contains PS and SEBS. However, the formulations containing sepiolites were cooled down in air to avoid that sepiolites could absorb part of the cooling water.

In some cases, (Chapter 5) the blends of PS and sepiolites produced in the extruder were introduced again to perform a second extrusion process with the aim of analyzing the influence of the extrusion process in the dispersion of the sepiolites. The pellets used in the second extrusion were dried in an oven for 2 hours at 60 °C at ambient pressure to remove any possible moisture in the formulation. The profile of temperatures and the screw rate used during the second extrusion cycle were the same as the ones of the first extrusion cycle.

#### *3.3.1.2 Compression Molding*

After the extrusion process, the pellets obtained were placed in a hot-cold plate press to make pieces with the desired shape for the foaming process and for the characterization procedure. The machine used for that purpose was a hot-cold press plates designed by *Talleres Remtex* (Barcelona, Spain). In **Figure 3.7** it is possible to see a picture of the press, as well as a schematic draw of how the material is in the mold. First, the pellets were dried in a vacuum oven at 60 °C and 150 mbar for at least 12 hours. Secondly, the appropriate amount of material was put in a mold, and which was covered by two solid iron plates one in the top

and the other one in the bottom. The plates and the mold were introduced in the hot plate, which is at a temperature of 235 °C. The materials were heated at this temperature for 5 min without applying any pressure. Once this step is finished and using the same temperature a pressure of 27 bar was applied for 5 minutes. Finally, the mold and the iron plates were introduced in a cold plate at ambient temperature, where the system was cooled down applying the same pressure.

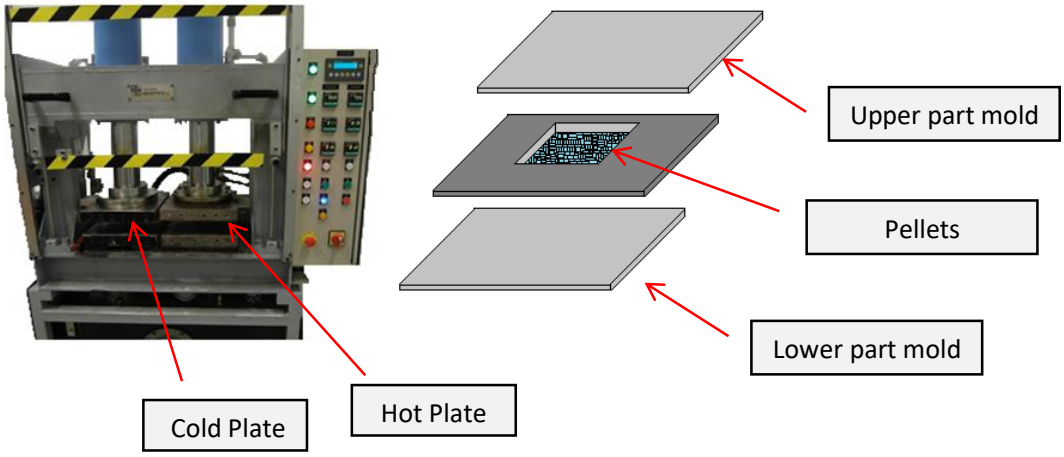


**Figure 3.7.** Image of the hot-cold plate press. Schematic design of the mold.

In the present thesis, cylindrical samples with a diameter of 150 mm and thicknesses of 2 mm were obtained. These samples were cut into small pieces of 20 x 20 x 2 (L x W x T) mm. This kind of samples were used in the gas dissolution foaming process. For the characterizations of the shear rheological properties, it was necessary to produce cylindrical samples with a diameter of 25 mm and a thickness of 1.5 mm. For the extensional rheological characterization, discs with diameters of 150 mm and thicknesses of 0.5 mm were obtained and later cut into pieces of 20 x 10 x 0.5 (L x W x T) mm.

### *3.3.1.3 Gas Dissolution Foaming Process.*

After the thermoforming process, the obtained precursors were introduced in an autoclave to produce the cellular materials. The diffusion of gas inside the samples was done controlling the temperature, pressure, and time parameters. These parameters are known as saturation temperature, saturation pressure and saturation time, respectively. After material is saturated with gas, the pressure is immediately released, and the samples are taken out of the autoclave and introduced in a thermal bath where the expansion process occurs. This period, that elapses between the release of the pressure and the introduction of the sample sin the thermal bath, is also recorded and known as desorption time. Finally, the materials that are in the thermal bath at a certain condition of

temperature (foaming temperature) are taken out at a specific time (foaming time) and cooled down as fast as possible to maintain the cellular structure. All this process can be seen in detail in Chapter 2 (section 2.4).

One of the good things of this foaming method is that it allows us to precisely control the gas uptake, sorption, and diffusivity of the polymer-gas system.

The method used during the present work to measure the gas absorbed by the polymer matrix during the saturation stage, is the gravimetric method. By using this method, the gas uptake is obtained directly by determining the weight gain by the polymer sample during the sorption stage. Basically, it consists of calculating the difference between the weight of the polymer composite at the end of the sorption process ($w_s$), when the polymer is fully saturated, and the initial weight of the composite ($w_0$). This difference divided by the initial weight of the composite provides the percentage of $CO_2$ uptake, as it can be seen in **Equation 3.1.**

$$CO_{2\ \text{Uptake}} = 100 \cdot \frac{W_s - W_0}{W_0} \qquad [3.1]$$

The value of the initial weight was taken with a precision balance, model AT261 from Mettler-Toledo (Columbus, Ohio, United States), and the value of the final weight was obtained few minutes after the depressurization of the autoclave, using the same precision balance. The ratio between the gain of mass and the initial mass provides an estimation of the gas solubility in these materials. The usual time that takes between the autoclave is depressurized and the sample is weighted is around 2 minutes. During this time the material is already losing part of the gas uptake during the saturation step. This is the reason why this measurement provides an estimation of the solubility and not a real and accurate value of this parameter. Previous works have shown that between the estimated and the real values of the gas solubility exists a difference varying between 1 wt.% and 2 wt.%.

By using the approximation of the second Fick's law, for long time diffusion processes, it is possible to study the sorption process as it can be seen in **Equation 3.2**.

$$\frac{M_t}{M_\infty} = 1 - \frac{8}{\pi^2} \exp\left(-\frac{D_s \pi^2 t}{l^2}\right) \qquad [3.2]$$

Where $M_t$ is the mass at a certain time, $M_\infty$ is the mass equilibrium value in which the material has absorbed the maximum quantity of gas for the specific conditions of time, temperature, and pressure, $t$ is the time, $l$ is the thickness of

the sample and $D_s$ is the sorption diffusion coefficient. The sorption coefficient ($D_s$) can be obtained as the slope of the graph $\ln\left(1-\frac{M_t}{M_\infty}\right)$ as a function of ($t/l^2$).

For obtaining the diffusivity of the material during the desorption process the procedure used is the following one. Samples are weighted in the precision balance before being introduced in the autoclave. After the depressurization, samples were located again in the precision balance, as fast as possible. The precision balance is now connected to a computer and the software records every second the value of the mass. By obtaining the measurements during a certain time (more than 30 minutes) it is possible to represent the diffusion curves and obtain the diffusion coefficient using the **Equation 3.3**, which is a solution of the second Fick´s law for short times.

$$\frac{M_t}{M_\infty} = -\frac{4}{l}\sqrt{\frac{D_d t_d}{\pi}} \qquad [3.3]$$

Where $M_t$ is the mass at certain time, $M_\infty$ is the mass equilibrium value in which the material has absorbed the maximum quantity of gas for the specific conditions of time, temperature, and pressure, $t_d$ is the diffusion time, $l$ is the thickness of the sample and $D_d$ is the diffusivity coefficient in the desorption process.

## 3.4 Characterization Techniques

In **Figure 3.8** it is possible to see the different characterization techniques that have been used to analyze the properties of both solid (non-foamed) and cellular materials along the entire thesis. In the case of the solid, non-foamed, formulations parameters like the density, morphology, rheological behavior, gas ($CO_2$) solubility and diffusivity and the intrinsic thermal properties were analyzed. For the cellular materials the geometrical density, open cell content, cellular structure and thermal conductivity were the characteristics and properties analyzed.

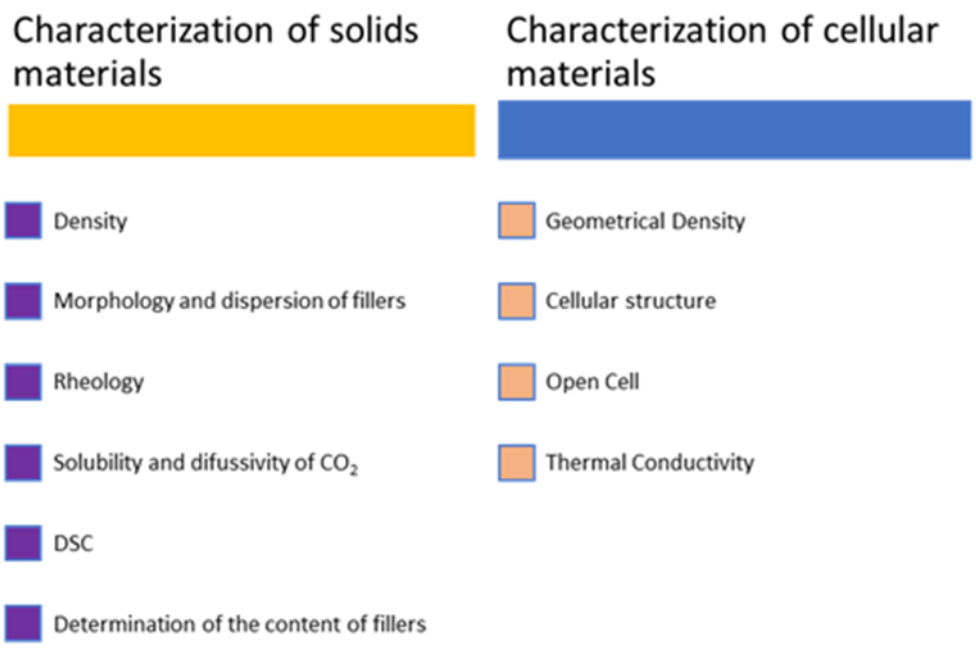


**Figure 3.8**. List of the characterization techniques applied to solids and cellular materials.

### *3.4.1 Characterization of Solid Materials*

#### *3.4.1.1 Density*

The density of the solid composites ($\rho_s$) was determined by using a gas pycnometer AccuPyc II 1340 from Micromeritics (Norcross, Georgia, USA) according to ASTM standard D1622-08. The gas pycnometer provides an accurate value of the volume of a certain material. Later, the mass of the solid sample was obtained with a precision balance, AT261 Mettler-Toledo (Columbus, Ohio, United States). The density was determined as the ratio between the mass of the sample by its corresponding volume (obtained by gas picnometry). The measurements performed in the pycnometer were done using nitrogen at a pressure of 19.5 psig (almost 1.34 bar). At least five measurements of each sample were obtained to have an accurate value of the volume of the sample.

#### *3.4.1.2 Morphology of the solid samples*

The morphology of the composites based on PS was investigated, in a qualitative way, by using scanning electron microscopy (SEM) (Flex SEM 1000 from Hitachi (chiyoda, Japan). Before, the solid samples were introduced in the SEM, they were cooled down in liquid nitrogen, fractured and covered by a thin layer of gold to make them electrically conductive. The covering of the samples with gold was performed using a sputter coating device model SCD 005 from Balzers union (Balzers, Liechtenstein).

Furthermore, X-ray micro computed tomography was used to visualize and analyze the dispersion degree of the sepiolites. The set-up employed to perform the micro-computed tomography experiments consists of a micro-focus cone-beam X-ray source L10101 from Hamamatsu (Shizuoka, Japan) with the following characteristics: spot size of 5 μm, voltage of 20-100 kV, and a current between 0 and 200 μA with a maximum output power of 20 W and a high sensitivity flat panel detector C7940DK-02 also from Hamamatsu (2240 x 2344 pixels, 50 μm of pixel size). Magnification could be defined as the ratio between the distance of the source and the detector (SDD) and the distance between the object and the source SOD, as it can be seen in **Equation 3.4.**

$$M = \frac{SDD}{SOD} \qquad [3.4]$$

In addition, a rotation stage was mounted on a linear stage, which enables movement between the source and detector and permits varying the magnification factor.[16] The linear stage was placed in a position so that the magnification value was x20 leading to a pixel size of 2.5 microns. A tube voltage of 55 kV and a current of 170 μA were selected for the measurements. The detector exposure time was 1000 ms and the rotation step was 0.3 degrees. To enhance the contrast in the reconstructed images, each projection was the result of integrating three consecutive images. An image of the device could be seen in **Figure 3.9.**

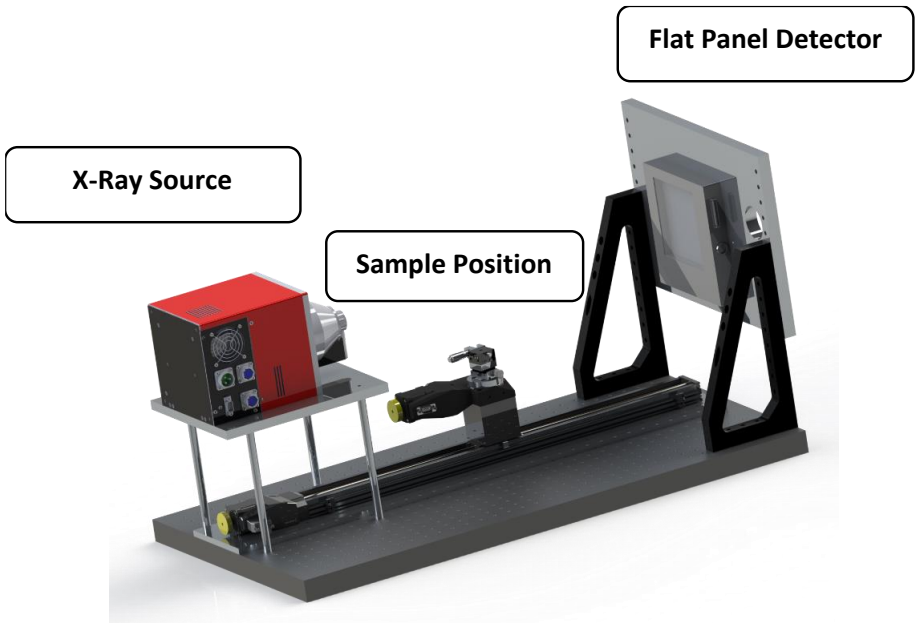


**Figure 3.9.** Image of the X-ray tomography equipment used during the thesis.

Once the projections were acquired, the reconstruction process of the tomogram was carried out using the Octopus, server/client reconstruction package.[17]

X-ray tomography has been used during the thesis to analyze the dispersion degree of the sepiolites in the PS matrix (Chapter 5). With this technique only particles with sizes higher than 2.5 μm can be detected. The isolated sepiolites used in this work present sizes which varies between 1 and 2 micrometers. Therefore, the reconstructed slices were used to analyze the number of agglomerates of particles whose sizes are higher than 2.5 μm. This method to determine the agglomerates of sepiolites has been applied in other works, like the one performed by Bernardo et al. [18]

To calculate the percentage of agglomerates, a tomographic volume of 1.25 x 2.50 x 3.50 $mm^3$ has been considered. Firstly, two consecutive 3D filters have been applied in the reconstructed slices. A 3D median filter (2 pixels of radius) has been applied to remove noise from the images and then, a 3D maximum filter (1 pixel of radius) has been computed to enhance the particles grey level intensity. Later, the particles have been binarized by means of a thresholding process based on the different level of absorption between polymer and fillers. The percentage of agglomerates in the sample has been calculated by measuring the volume fraction occupied by the agglomerates (**Equation 3.5**)

$$\text{Agglomerates (\%)} = \frac{\frac{\rho_{sep} \cdot \%V_{sep}}{\rho_{solid}}}{\%m_{sep}} \qquad [3.5]$$

Where $\rho_{sep}$ is the density of the fillers, in this case sepiolites (2.1 $g/cm^3$), and $\rho_{solid}$ represents the density of the solid nanocomposite, which was measured by gas pycnometric, $\%V_{sep}$ is the fraction occupied by the agglomerates and $\%m_{sep}$ the real mass fraction of particles in the sample.

### *3.4.1.3 Rheology*

The pure PS and the different composites, PS with sepiolites and PS with SEBS, were characterized with shear dynamic rheology and extensional rheology (more information about the background of these techniques can be found in the Chapter 2 of this manuscript). Information about the viscosity of the material, estimation of the molecular weight of the polymer (only in the case of a pure polymer) or information about the dispersion degree of the sepiolites in the polymer matrix can be obtained through the shear dynamic rheology measurements. On the other hand, with the extensional rheology measurements it is possible to obtain information about the strain hardening coefficient of the material, among others, which is related with the melt strength of the polymer.

All the shear rheology measurements were done with a stress-controlled rheometer model AR 2000 EX from TA Instruments (Lukens, Delaware, United States). Shear dynamic rheology measurements were done at a temperature of 220 °C under a nitrogen atmosphere, using parallel plates with a diameter of 25 mm and with a distance between them (gap) of 1 mm. To work in the lineal viscoelastic region for all the materials studied, a strain sweep must be performed at a fixed dynamic frequency of 1 rad·s$^{-1}$. The percentage of strain in which the materials stay in the viscoelastic regime was founded between 4-6%. Next, in the case of the composites a time sweep was performed to recover the initial state of the particle network that was partially deformed when the sample was loaded in the rheometer. The duration of the time sweep varied between 360 seconds and 600 seconds, depending on the material. Finally, the frequency sweep step was performed, in a range of angular frequencies varying between 0.01 rad s$^{-1}$ and 100 rad s$^{-1}$. From these measurements, four properties were analyzed: dynamic shear viscosity ($|\eta^*|$), storage modulus (($G'(\omega)$), loss modulus ($G''(\omega)$)) and crossover frequency ($\omega_x$). A picture of the rheometer can be seen in **Figure 3.10.**

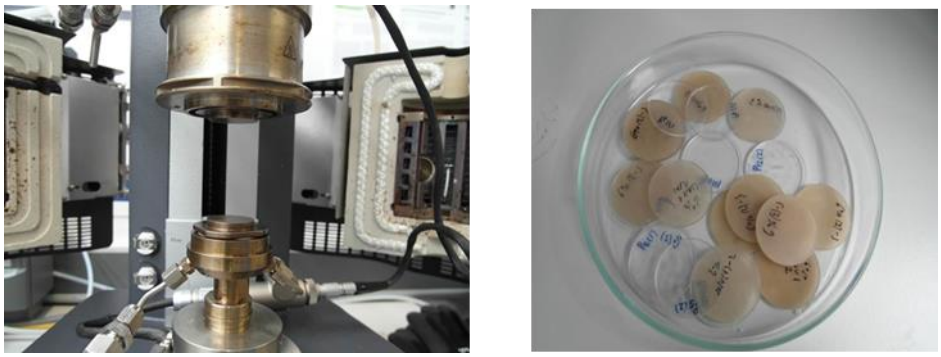

**Figure 3.10**. In the figure of the left it is possible to see the rheometer used to determine the shear dynamic rheological properties with the two parallel plates geometry. On the right picture appears the samples used in the shear dynamic rheology.

For extensional rheology, the same rheometer was employed but using in this case an extensional fixture model SER 2 from Xpansion Instruments (Spicewood, Texas, United States). In this device, the samples are clamped to two cylinders that rotate, at a fixed rate, in opposite directions applying a uniaxial stretching force to the material. The experiments were conducted at different Hencky strain rates: 0.3, 0.5 and 1 s$^{-1}$. In all the experiments the maximum Hencky strain was 2.8. In **Figure 3.11** it is possible to see a sample clamped between the two rotating drums in the extensional rheology experiment.

**Figure 3.11**. Sample during the extensional rheology experiment.

The protocol followed to perform the extensional rheology measurements is the following one:

1. ***Pre-Stretch:*** Once the machine is set at the desired temperature, the sample is located among the clamps and a pre-stretch is done to compensate the thermal expansion of the sample due to the difference between the room temperature and the experimental temperature in the rheometer. A pre-stretch rate of $5x10^{-3}$ $s^{-1}$ was used and the total Hencky strain applied during the pre-stretch was around 0.05.
2. ***Relaxation post pre-stretch:*** After the pre-stretch the sample was maintained at the same temperature without applying any stress. A time of 60 seconds was employed during the relaxation post pre-stretch.
3. ***Test:*** After the relaxation time, the extensional rheology test was performed. As it was mentioned before, three different Hencky strain rates were used (0.3, 0.5 and 1 $s^{-1}$), with a maximum Hencky strain of 2.8.

The temperature at which the extensional rheological tests were performed was 160 °C. This temperature should close to the one used during the foaming step in the gas dissolution process, in order that the results obtained during the extensional rheology measurements could be related with the foamability of the polymer matrix. Finally, to evaluate the extensional viscosity measurements it is necessary to know the density at the temperature at which the experiment is going to be performed. With that purpose on mind, the melt flow rate (MFR) and melt volume rate (MVR) were measured with an extrusion plastometer at the desired temperature (160 °C and 5 kg of load weight). The ratio between those quantities provides the density of the material at the specific temperature.

From the extensional rheology measurements, the strain hardening coefficient was obtained.

The strain hardening coefficient was obtained by extrapolating the overlapping parts of the extensional curves at different Hencky strain rates.[19] This coefficient has been determined for a time of 2.67 s and for a Hencky strain rate of 1 $s^{-1}$. A detailed explanation of how this parameter is calculated and its importance to understand the foaming process can be found in the Chapter 2 of this manuscript.

#### *3.4.1.4 Differential Scanning Calorimetry*

The glass transition temperature (Tg) of the PS and the PS composites was analyzed by differential scanning calorimetry (DSC) using a DSC 862 from Mettler Toledo (Columbus, Ohio, United States). The experimental conditions used with the PS based materials were the following ones:

- First heating from 20 ºC to 160 ºC at a heating rate of 10 ºC $min^{-1}$.
- Isotherm at a temperature of 160 ºC for 3 minutes to erase the thermal history.
- Cooling down from 160 ºC to 20 ºC at a cooling rate of 10 ºC $min^{-1}$.
- Second heating from 20 ºC to 160 ºC at a heating rate of 10ºC $min^{-1}$.

All the experiments were performed in a nitrogen atmosphere with a flux of 60 ml/min.

#### *3.4.1.5 Ashes essay*

The real percentage of fillers, sepiolites, introduced in the formulations was determined by performing an ashes essay.

The pellets obtained after the extrusion process were introduced in a ceramic crucible like those that appear in **Figure 3.12**. The crucible with the material was weighted in a precision balance, model New Classic MS from Mettler Toledo (Columbus, Ohio, United States). After they were weighted, the samples were introduced in a muffle, model Select-Horn, P-Selecta (Barcelona, Spain), at high temperatures (close to 850 ºC) for at least 90 minutes. The temperature employed must be higher than the decomposition temperature of the polymer matrix. This temperature was enough to degrade the PS and after the essay the only material that remains in the crucible was the inorganic nanoparticles (sepiolites). By weighing this residue, it was possible to calculate the real percentage of particles that was present in the formulation.

**Figure 3.12**. Ceramic crucibles used in the ashes determination essay.

### *3.4.2 Characterization of cellular materials*

#### *3.4.2.1 Density*

The density of the foamed materials ($\rho_f$) was measured using the water displacement method based on Archimedes principle according to the standard ISO 1183-1.

A density determination kit for the balance AT261 from Mettler Toledo (Columbus, Ohio, United States) was used to obtain the value of the density. Firstly, it is important to remember that in the gas dissolution foaming process a solid skin is usually generated in the samples. Therefore, it was necessary to remove this solid skin before measuring the density of the foamed materials. For that purpose, a polishing machine, model LaboPOl2-LaboForce3 from Struers (Cleveland, Ohio, United States), was used. Once the skin was removed it was possible to weigh the samples inside and outside the water and determine the foam density according to **Equation 3.6**.

$$\rho_f = \frac{w_{air}}{w_{air} - w_{water}} \cdot \rho_{water} \qquad [3.6]$$

Where $w_{air}$ is the weight of the sample in air, $w_{water}$ is the weight of the sample in water and $\rho_{water}$ is the density of the water at the temperature conditions in which the measurement was performed.

#### *3.4.2.2 Cellular Structure*

The cellular structure of the foamed samples was measured using a scanning electron microscope (SEM), model Flex SEM 1000 from Hitachi (Chiyoda, Japan). To do not deteriorate the cellular structure the samples were cut with a thin blade without applying any force. After a thin layer of the material was obtained samples were covered with gold was using a sputter coating device model SCD 005 from Balzers union (Balzers, Liechtenstein), as it was described before. To analyze the SEM micrographs a software developed by CellMat Laboratory, based in the software Fiji/Image J has been used.

The theoretical approximation that makes possible the quantification of some structural parameters like cell size, anisotropy ratio and cell density is known as Kumar Theoretical approximation.[20] This method uses the area of the image, the number of cells (selected in the image by the user), the magnification of the image and the values of the solid density and foam density. First, a binary mask was manually prepared to have a better binarization of the image. **Figure 3.13** shows a micrograph of one of the PS samples measured during the thesis and its corresponding mask required for the quantification process. Once the micrographs have been binarized, the software is able to detect the cells and perform the calculation of the different parameters. First, the program measures the dimension of each individual cell ($\phi_i$). Using these measurements, it provides the cell size distribution, the average cell size in 2 dimensions ($\overline{\phi_{2D}}$) and the standard deviation coefficient of the cell size measurements (SD). The cell sizes obtained in 2D should be transformed to a 3D value by multiplying by a correction factor. Previous works had demonstrated that this correction factor is 1.273.

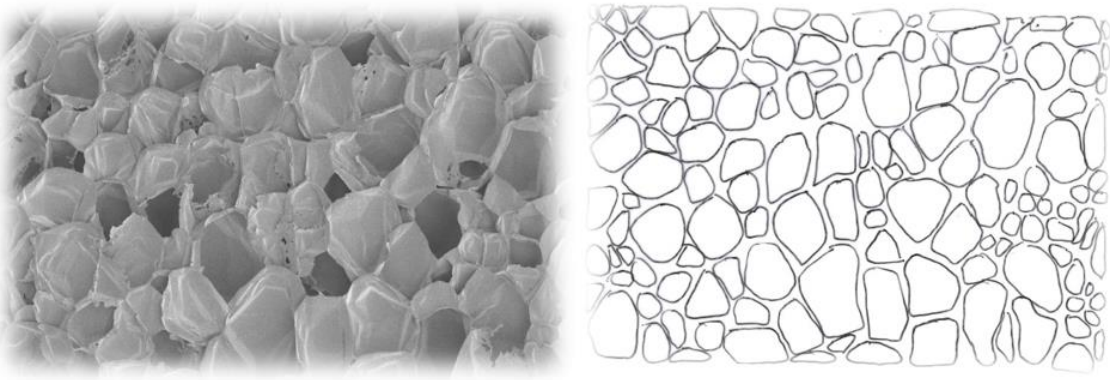

**Figure 3.13**. Figure on the left shows the SEM micrograph of a PS sample. In the figure of the right the mask required for the quantification process is depicted.

With the information provided by the software it was possible to know the values of the cell size, cell density, cell nucleation density and SD/$\phi$, parameter that accounts for the homogeneity of the cellular structure.

### *3.4.2.3 Open Cell*

The open cell content was measured with an air gas pycnometer, AccuPyc II 1340 from Micromeritics (Norcross, Georgia, USA), according to ASTM standard D6226-15. The open cell content can be calculated using the next equation (**Equation 3.7**).

$$OC(\%) = 100\left(\frac{V_{geometric} - V_{pycnometer}}{V_{geometric}}\right) \qquad [3.7]$$

Where $v_{geometric}$ is the geometric volume of the sample, $v_{pycnometer}$ is the volume of the sample obtained with the pycnometer and $p$ is the porosity calculated as $(1 - \frac{\rho_f}{\rho_s})$, where $\rho_f$ is the density of the foam and $\rho_s$ is the density of the solid matrix. The geometric volume was determined from the density results obtained by using the water displacement method. The pycnometer measurements were performed at low pressures (c.a. 4 psig) to avoid deforming the samples during the measurement.

#### *3.4.2.4 Thermal Conductivity*

The thermal conductivity of the different foamed materials was determined with a TPS (Transient Plane Source), model 2500 S (Hotdisk), following the procedures described in the standards ASTM D 5930-01 and ISO 22007-2:2015. The device can be seen in **Figure 3.14**. The measurements were performed using a sensor with a radius of 3.18 mm. Prior to the measurement it was necessary to cut the foamed samples with a saw into square pieces of 20-30 mm size and remove the solid skin with a polishing machine, model LaboPOl2-LaboForce3 from Struers (Cleveland, Ohio, United States). Once samples were ready, they were introduced covering the sensor (one sample on the top of the sensor and the other one in the bottom part of it). Later, the device and the samples were left at ambient conditions at least for 30 minutes to avoid any gradient of temperature in the system. After that, five measurements were carried out with a time span of 20 minutes among them to avoid the possible temperature drift. The time of each measurement was around 20 seconds for all samples, meanwhile the usual power was about 2.5 to 4 mW. Furthermore, the conductivity of the solid samples was also analyzed using the same device. In this case the power used was around 15 to 18 mW whereas the time was close to 30 seconds.

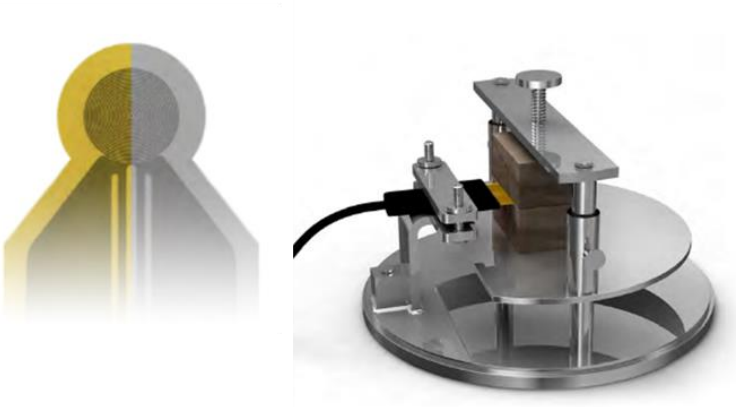

**Figure 3.14.** Sensor used for measuring the thermal conductivity of solid and cellular materials based on PS. On the right-side picture, it is possible to see the sensor already connected to the device.

## 3.5 Bibliography


[1] J. Scheirs, D.B.Priddy. *Historical Overview of Styrenic Polymers. In: Modern Styrenic Polymers: Polystyrenes and Styrenic Copolymers*. ***2003****, first edition*. John Wiley and Sons, New Jersey, United States.

[2] J.R. Wunsch. *Polystyrene - Synthesis, Production and Applications*. 2000, first edition, Smithers Rapra Publishing, Swhesbury, United Kingdom.

[3] G. Wypych. *Handbok of Polymers*.**2016**, second edition, Elsevier, Amsterdam, The Netherlands.

[4] C.Lynwood. *Polystyrene, Synthesis, Production and Applications*. 2014, first edition,Nova Publishers, New York, United States.

[5] C.Kaynak, B.M.Sipahioglu. *J Fire Sci*. **2013**, 31(4),339-355.

[6] B.Akbari, R. Bagheri. *Mech Mater*. **2016,** 103, 11-17.

[7] C.Forest, P.Chaumont, P.Cassagnau, B.Swoboda, P.Sonntag. *Prog Polym Sci*. **2015**;41,122-145.

[8] https://www.statista.com/statistics/1171105/price-polystyrene-forecast-globally/. Acessed November **2021**.

[9] https://www.plasticsinsight.com/resin-intelligence/resin-prices/pmma/. Acessed November **2021.**

[10] https://www.plasticsinsight.com/resin-intelligence/resin-prices/polycarbonate/. Acessed November **2021.**

[11] S.T.Lee, N.S.Ramesh. *Polymeric Foams, Mechanisms and Materials*. **2004**, first edition, CRC press Taylor and Francis Group, Bocaraton, United States.

[12] C. Saiz-Arroyo. *Fabricación de Materiales Celulares Mejorados Basados en Poliolefinas. Procesado-Composicion-Estructura-Propiedades*. **2012**, PhD Thesis, University of Valladolid, Spain.

[13] https://www.mordorintelligence.com/industry-reports/global-polystyrene-market-industry. Polystyrene Market. Acessed November **2021.**

[14] https://www.gminsights.com/industry-analysis/polystyrene-ps-and-expanded-polystyrene-eps-market. Acessed November **2021.**

[15] https://www.smithersrapra.com/news/2014/may/polymer-foam-market-to-consume-25-3-million-tonnes. Acessed November **2021.**

[16] S.Perez-Tamarit, E.Solórzano, A.Hilger, I.Manke, M.A.Rodriguez-Perez. *Eur Polym J*. **2018,**109,169-178.

[17] M.Dierick, B.Masschaele, L. Van de Hoorebeke. *Meas Sci Technol*. **2004**, 15(7), 1366-1370.

[18] V.Bernardo, F.Loock, J. Martin-de Leon, N.A. Fleck, M.A. Rodriguez-Perez. *Macromol Mater Eng*. **2019**,304(7), 1900041.

[19] H. Münstedt, F.R. Schwarzl. *Deformation and flow of polymeric materials*. **2014,** Springer, Berlin, Germany.

[20] J. Pinto, E. Solorzano, M.A. Rodriguez-Perez, J.A. De Saja. *J. Cell. Plast.***2013**, 49 (6), 555-575.

# Chapter 4

# Analysis of the effects of the polystyrene molecular weight in the foaming mechanisms.

*"It's a dangerous business going out of your door. You step into the Road, and if you don't keep your feet, there is no knowing where you might be swept off to"*

*The Lord of the Rings.*

*J.R.R. Tolkien.*

*"Es muy peligroso cruzar la puerta. Vas hacia el camino y si no cuidas tus pasos no sabes a donde te arrastraran"*

*El señor de los anillos.*

*J.R.R. Tolkien*

# INDEX

## 4.1 Introduction

This chapter contains the study of the influence that the molecular weight has in some structural characteristics, solubility, diffusivity parameters and the subsequent cellular structures of three different polystyrenes and PS foams. For the current study three commercial polystyrenes with different melt flow rates that are between 2 until 27 (g/10 min at 5 kg and 200ªC) and therefore different molecular weights, were used.

Structural characteristics like glass transition temperature, extensional rheological behavior or shear dynamic rheology were related with the molecular weight of the three different polymers, to see the influence of this last parameter in all of them Moreover, some theoretical models like the Flory-Fox or the Ueberreiter and Kanig ones that predict the relation of this structural characteristics with the molecular weight were also compared to the experimental results obtained.

Furthermore, the three polystyrenes were submitted to a saturation process in an autoclave using CO2 as the main blowing agent. The capabilities of the materials to absorb gas and to release it after the complete saturation were studied and related with the molecular weight. Finally, the cellular structure that was obtained in the foams was studied thanks to SEM images. The cell size, cell size homogeneity or other parameters of the cellular materials like relative density or open cell content were analyzed and related with the structural characteristics of the materials and with the solubility and diffusivity parameters.

Finally, with all the information obtained would be possible to see which grade or polymeric grades are more suitable to produce cellular materials using $CO_2$ as the main blowing agent.

Thanks to the research performed it was possible to produce an article that is presented in Section 4.2 of the actual chapter. The article is nowadays pending of being submitted to a journal.

## 4.2 Understanding how the foamability of a polystyrene matrix is affected by its molecular weight.

The section contains the publication named as: "***Understanding how the foamability of a polystyrene matrix is affected by its molecular weight***". (A. Ballesteros, E. Laguna-Gutiérrez, M.A. Rodríguez-Pérez This paper is pending to be send to a journal for its publication).

The main goal of this work is to analyze the effects of the molecular weight in the structural characteristics of the polymer, solubility, and diffusivity of the gases in the PS and the cellular structures of the materials produced. For this purpose, three different grades of PS, with different melt flow rates, have been considered: N2380 (MFR: 2g/ 10 min, 200°C, 5 kg), N3840 (MFR: 10 g/ 10 min, 200°C, 5 kg), N3910 (MFR: 27 g/ 10 min, 200°C, 5 kg). The molecular weight of the materials has been estimated by shear dynamic rheology and obtained experimentally by GPC (gel permeation chromatography). Moreover, some structural characteristics like glass transition temperature, shear rheology or extensional rheology have been measured by DSC (differential scanning calorimetry), shear rheological measurements and extensional rheological ones, respectively.

Results indicate that molecular weight has a remarkably influence in the glass transition temperature, being the material with the lowest molecular weight the one with the highest glass transition temperature. Moreover, the material with the highest molecular weight is the one with the higher shear complex viscosity and the highest extensional rheological properties (the highest strain hardening coefficient). Is important to remark the depletion observed in the strain hardening coefficient for the material with the lowest molecular weight compared to the one with the highest molecular weight.

Moreover, it was found that the material with the lowest solubility was the one with the highest sorption and diffusivity of the $CO_2$. This fact could be related with the highest free volume as it was reported by several researchers before.

Also, the depletion of the glass transition temperature by the presence of gas (plasticization effect) was studied thanks to the Chow and Cha-Yoon models. The reduction of the glass transition temperature seems similar for all the materials. However, due to the lowest initial value of the glass transition temperature in the material with the lowest molecular weight, the effective glass transition temperature reaches a value that is lower compared to the other two PS grades.

The densities are lower for the polymers with lower molecular weights, because higher expansions are allowed for this materials. Finally, the higher values of the cell sizes and the open cell content show that the material with the lowest molecular weight present a higher coalescence and do not resist so well the forces of the gases during the expansion step. This phenomenon is related with the depletion of the strain hardening mentioned before and with the difference between the effective glass transition temperature and the foaming temperatures.

In **Figure 4.1** it is possible to see the graphical abstract of this future publication.

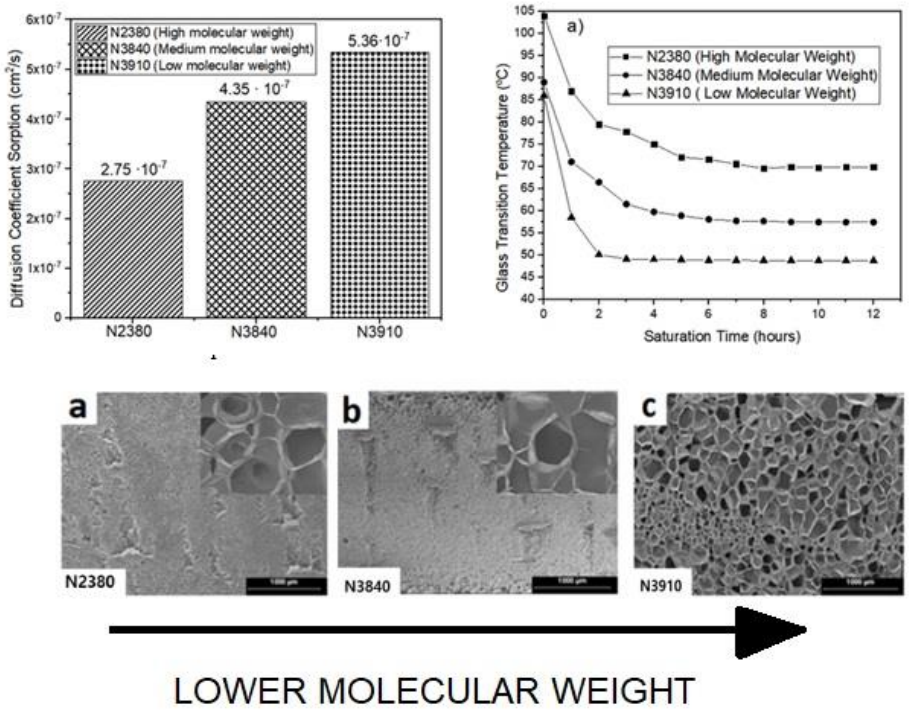


**Figure 4.1**. Graphical abstract of "Understanding how the foamability of a polystyrene matrix is affected by its molecular weight".

# Understanding how the foamability of a polystyrene matrix is affected by its molecular weight

A. Ballesteros, E. Laguna-Gutierrez, M. A. Rodriguez-Perez

***Cellular Materials Laboratory (CellMat)**, Paseo de Belén, 7, Condensed Matter Physics Department, Science Faculty, University of Valladolid, 47011, Valladolid*

***CellMat Technologies**, Edificio Parque Científico UVa, Paseo de Belén 9-A, 47011, Valladolid, Spain*

**ABSTRACT**

In the present works three different polystyrenes (PS), with different molecular weight, were foamed by a gas dissolution foaming process using CO2 as blowing agent. The main objective of this paper consists of analyzing how the molecular weight affects the foamability of the system PS/CO2. For that purpose, the solubility, diffusivity, and structural characteristics of the polymer will be studied and related with the molecular weight of the materials. It is important to analyze how the solubility and diffusivity properties condition the nucleation phenomena of the materials. Furthermore, other structural characteristics of the PS polymers like the depletion of the glass transition temperature due to plasticization effect or the extensional rheological properties could have a remarkable subsequent impact in the degeneration phenomena during the foaming stage.

The molecular weight of the polymers was estimated and determined using two different techniques: shear dynamic rheology and gel permeation chromatography. The values of the molecular weight were related with other parameters of the polymers like the glass transition temperature, and the shear dynamic and extensional rheology were measured using a differential scanning calorimetry (DSC) and a rheometer. The relations observed explain the influence of the molecular weight in those variables and were in good agreement with the models available in literature.

Furthermore, the three PS were subjected to a gas saturation process in a pressure-vessel, using CO2 as blowing agent, to later be foamed in a thermal bath. The solubilities and diffusivities were studied and related with the molecular weight. The results obtained indicate that material with the lowest molecular weight absorbs more gas, at the same conditions of temperature,

pressure, and time, than the other two PS. The gas diffusion, after the saturation process, in the PS with the lowest molecular weight is also quicker than in the other two polymers.

The plasticizing effect that occurs in the polymers, when they are saturated with the blowing agent, was also analyzed. All the materials present a similar reduction of their glass transition temperature due to the plasticizing effect. On the other hand, there is a remarkable difference in the strain hardening coefficient between the polymers. Presenting the polymer with the lowest molecular weight the one with the lower strain hardening.

Finally, the different PS were foamed in thermal baths and their cellular structures were analyzed by scanning electron microscopy (SEM). The results demonstrate that the PS with the highest molecular weight is the one showing the lowest values of the cell size and the most homogeneous cellular structure. The remarkable difference observed in the extensional rheological properties between the polymers could be related with a higher appearance of degeneration phenomena mechanisms like cell coalescence in the PS with the lowest molecular.

**KEYWORDS**

Polystyrene; molecular weight; solubility; diffusivity, cellular structure.

## 1. INTRODUCTION

Due to its excellent properties, good processability, high stiffness, and strength, non-toxicity, etc., polystyrene (PS) is a suitable candidate for plenty of applications.[1] As a result, PS is one of the most used thermoplastic polymers in sectors such diverse as food industry (storage and packaging), automotive and construction. Nowadays, PS is the fourth largest, by volume, general thermoplastic in the market. The market for PS is forecasted to grow significantly between the years 2021-2025 even with the negative impact that the COVID 19 has created .[2] Particularly, polymeric foams based on PS, like expanded PS (EPS) or extruded PS (XPS), are mainly used as thermal insulators thanks to their low thermal conductivity, light weight and resistance to moisture and medium to high tensile strength below its glass transition temperature.[3] These foams play a significant role in the growth of the insulation market, which is expected to have the strongest growth prospect over the years 2018-2023 in regions like Asia.[4]

The number of PS grades, with different physical properties, available in the current market is high. One of the properties that more differs between the different PS matrices is their molecular weight. The ability of tailor the material,

altering its molecular weight, allows changing the properties of the polymer leading to a delay of the degradation process or to an improvement of mechanical properties.[5,6] Furthermore, several structural characteristics, like the glass transition, melting or crystallization temperatures and rheological properties are influenced by the molecular weight of the materials.[7–9].

It is notorious the relation between the glass transition temperature and the molecular weight. There is an appreciable decrease in the molecular mobility of the polymer chains as a system passes through its glass transition temperature towards lower temperatures.[10] This phenomenon has led to the appearance of plenty of theoretical explanations, most of these theories are based on concomitant changes of conjugate thermodynamic variables, such as the free volume and the configurational entropy.[11–13] Free volume models explain the glass transition temperature as a critical point in which the polymer goes from a glass state, regarded as a frozen metastable state of matter, to a rubber state in which appears the molecular mobility. The current free volume theories explain that the molecular motion in the solid state of a polymer depends strongly on the "vacancies", "holes" or imperfections of the packaging of the molecules with molecular volumes between 0.02 and 0.07 $nm^3$.[11,14] Following these theories, the final conclusion obtained shown that the glass transition temperature is inversely proportional to the free volume of a polymer and therefore, it is related to the molecular weight of the polymer. One of the most notable works are those performed by Fox and Flory that exhibit a linear relation of the molecular weight with the glass transition temperature.[15,16] On the other hand, the relationship between the shear rheological properties of a material and the molecular weight can easily be seen in the Mark-Houwink Sakurada model.[17] In principle polymers with a lower zero-shear viscosity, will present a faster growing of the cells and rapid foamability. However, it is needed also that the viscosity gets modified during the foaming process towards higher values to avoid the promotion of the degeneration phenomena. Concerning the extensional rheology, Larson and Desai claim that the molecular characteristics can affect the polymeric alignment of chains, monomeric friction, high extensional rate rheology, and the strain hardening of the material (abrupt increase of extensional viscosity as time or strain increases).[18] Also, Drabek et al reported a potential dependence of the strain hardening with the molecular weight.[19] The aforementioned strain hardening effect has remarkable importance helping cell walls to withstand the deformation during the last stages of the foaming process and therefore, reducing the degeneration mechanisms (coalescence, drainage and coarsening). [20]

Moreover, the molecular weight also affects the gas solubility and diffusivity as well as the characteristics of the cellular structure of the different foams produced. Both solubility and diffusivity of a gas in a polymer matrix are vital in the nucleation and growth of bubbles during the foaming step.[21] By controlling the foaming process, it is possible to control the final properties of the foamed products. The gas solubility affects the cell nucleation mechanisms, increasing the nucleation value according to the classical nucleation theory for an homogeneous nucleation, and modifying the plasticization effect (reduction in the glass transition temperature until an effective glass transition temperature due to the presence of a blowing agent).[22] Meanwhile, the gas diffusivity also affects the cell nucleation mechanisms. A rapid diffusion of the gas could lead to a promotion of a cellular structure with non-homogeneous cell sizes, presenting different sizes between the inner cells in the core of the foams and the cells located closer to the surface of the material. The blowing agent selected in the present work is the $CO_2$ due to its good properties, like nontoxicity and non flammability, which make it a sustainable candidate to replace some other physical agents like CFC and HCFC. Many investigations have been focusing on the sorption and kinetic properties of supercritical $CO_2$ in diverse polymer matrices, such as poly(methyl methacrylate) (PMMA), polycarbonate (PC), poly(vinyl chloride) (PVC), polyethylene (PE) and PS. [23–28]

The relation between the molecular weights and the solubility and diffusivity parameters have been studied by several researchers. In particular, Shu-Kai Yeh et al have reported that the molecular weight or viscosity of PMMA is the critical parameter in generating nanocellular structures.[29] Considering three pure PMMA poly (methyl methacrylate) with different molecular weights, was the PMMA with the higher molecular weight value, the one whose foams achieve the lowest cell sizes and higher cell densities. Even though there were not seen remarkable changes in the solubility and diffusivity parameters between the PMMA materials, the changes observed in the cellular structure were explained due to the plasticization effect and the initial differences observed in the glass transition values between the polymers. On the other hand, Li et al have seen that in a crystalline material like is the POE Poly (Ethylene-co-octene) changing the copolymer compositions, and therefore the molecular weight, exhibit quite distinctive foaming behaviors. As POE molecular weight increases, there is a slightly change in the crystallization and their foams present have higher cell density and wider foaming window.[30] Moreover, Zhai et al. have found that an

increase in the POE molecular weight can significantly reduce the degeneration phenomena and increase the cell density during bubble growth, due to increment observed in the melt strength.[31] Furthermore, there have been several researchers that they have not only study the influence of the molecular weight of the pure polymer in the subsequent cellular materials, but also the importance that viscosity of polymer blends or copolymers added to the net polymer has in the cellular structural properties.[32–34]

There are different experimental techniques which can be used to determine the number average molecular weight ($M_n$) weight average molecular weight ($M_w$) and the ratio between them, known as polydispersity index ($P_D$) .[35]. Some of them are: shear dynamic rheology, NMR (nuclear magnetic resonance) for polymers with a molecular weight lower than $10^4$ g/mol, MALS (multi-angle light scattering), MALDI (matrix-assisted laser desorption mass spectroscopy), which is usually employed for proteins and biopolymers, and GPC (gel permeation chromatography).[36–39] In the present work shear dynamic rheology measurements and GPC will be used as the methods to estimate and determine, respectively, the molecular weight of the three PS. The election of these methods is based on the capability of these techniques to estimate and measure a wide range of polymers with different molecular weights. Furthermore, GPC allows obtaining both values of the molecular weight, $M_n$, $M_w$, and the polydispersity index.

As far as the author knows there is not any article in which they reported the differences observed in the solubility, diffusivity, plasticization, and the subsequent cellular structures (cell sizes, open cell contents) due to the influence of the molecular weight in a PS/$CO_2$ system. In fact, there was only found a thesis of Feng in which was reported the use of three PS with different molecular weights and check the saturation and nucleation effect for PS/$CO_2$ system in PS films with a high-speed camera.[40] They assumed that there are not cell coalescence occurring and that every nucleation point will generate a single cell, therefore that steady state nucleation rate can be identified as the slope of cell number density growth curve (cell number density vs. time). Finally, with these measurements they analyzed the scaling curves using the Sanchez-Lacombe parameters to have a tool to obtain a numerical value of the free-energy barrier for the nucleation. However, in this thesis there are not values of the sorption and diffusion coefficients as a function of the molecular weight and all the assumptions taken by Feng do not lead to a final comprehension of the cellular

structures that could be obtained and several effects like rheological ones or the plasticization effect must be considered to understand the results.

## 2. EXPERIMENTAL

### 2.1 Materials

Three commercial PS grades, recommended for foam applications, with different melt flow index (MFI) were used in the work: Edistir N2380 (MFI = 2 g/10 min), Edistir N3840 (MFI =10 g/10 min) and Edistir N3910 (MFI = 27g/10 min), all of them measured at conditions of 200 ºC and 5 kg of weight. The three PS were acquired to Versalis, Eni S.p.A (Italy). Finally, a medical grade carbon dioxide ($CO_2$) (99.9% purity) was used as blowing agent for the gas dissolution foaming experiments.

### 2.2. Fabrication of Solid Precursors

The different polymers were thermoformed in a hot-cold press to obtain materials with the desired shape and size. The compression molding process was produced at a temperature of 235 ºC and at a pressure of 27 bars. Solid samples produced in the thermoforming process present different shapes, depending on their final applications. The samples used for the foaming process were prisms with the following dimensions: 2 x 2 x 0.2 (L x W x T) cm. The samples for the extensional rheological tests were also prisms, but in this case, with the following dimensions: 2 x 1 x 0.05 (L x W x T) cm. Finally, discs with a diameter of 2.2 cm and a thickness of 0.2 cm were used for the dynamic shear rheology tests.

### 2.3. Foaming Process

The foaming of the samples was produced using the solid-state gas dissolution foaming method.[41] For this purpose, a high-pressure vessel (model PARR 4681) provided by Parr Instrument Company, with a capacity of 1 liter and capable of operating at a maximum temperature of 350 ºC and at a maximum pressure of 41 MPa has been used. The reactor is equipped with a pressure pump controller (model SFT- 10) provided by Supercritical Fluid Technologies Inc., which is controlled automatically to keep the pressure on the desired values. The pressure vessel is also equipped with a clamp heater of 1500 W where the temperature is controlled via a CAL 3300 (CAL controls) temperature controller. The previously mentioned solid-sate gas dissolution foaming process consists of two-steps.[42] Samples were firstly introduced in the pressure vessel at 8 MPa of $CO_2$ pressure for the saturation stage. Saturation temperature was 40 ºC and saturation time was varied from 1 hour to 12 hours to study the solubility and diffusivity properties of the different PS grades. After saturation, the pressure was abruptly

released. Finally, for the foaming stage, the samples that were completely saturated, after 12 hours of saturation time, were removed from the pressure vessel and introduced in a thermostatic silicon bath at a temperature of 120 ºC for 1 min. The time between the release of the pressure and the immersion in the thermal baths was around 2 min. Once materials have expanded, they were cooled down in water to stabilize the cellular structure as fast as possible to reduce degeneration mechanisms.

## 2.4 Characterization

### *2.4.1 Dynamic Shear Measurements*

A shear stress-controlled rheometer (AR 2000 EX from TA Instruments) was used to measure the dispersion degree of the different formulations. Dynamic shear measurements were conducted at a temperature of 220 ºC under a nitrogen atmosphere using 25 mm diameter parallel plates. A fixed gap of 1 mm was selected to perform the rheological measurements.

The first step, required to determine the linear viscoelastic regime, was to perform a strain sweep test at a fixed dynamic frequency (1 rad $s^{-1}$). Finally, the frequency sweep step was performed, in a range of angular frequencies varying between 0.01 rad $s^{-1}$ and 100 rad $s^{-1}$. For the measurements obtained, zero shear viscosity ($|\eta_0|$) will be used to estimate the molecular weight.

### *2.4.2 Molecular weight estimation and determination*

The number average molecular weight is defined as the ratio between the total weight of the polymer ($\sum N_i M_i$) and the total number of molecules ($\sum N_i$), as it can be seen in (**Equation 1**).

$$M_n = \frac{\sum N_i M_i}{\sum N_i} \quad [1]$$

Another possibility to quantify the mlecular weight of a polymer matrix consist on using the weight average molecular weight ($M_w$) (see **Equation 2**), which provides a more accurate measurement of the molecular weight of the material.

$$M_w = \frac{\sum N_i {M_i}^2}{\sum N_i M_i} \quad [2]$$

This parameter provides more importance to the chains with high molecular weights than to the ones with low molecular weights. Finally, another parameter used to analyze the characteristics of the molecular chains is the polydispersity index ($PD_{index}$). This variable establishes a relation between $M_n$and$M_w$, as it is indicated (**Equation 3**). If the ratio between the two parameters is higher than 1

indicates that the center of the MwD is shifted to higher values of the molecular weight, meanwhiles a ($PD_{index}$) lower than 1 indicates that the MwD is mainly defined by the chains with a low molecular weight.

$$\mathrm{PD_{index}} = \frac{\mathrm{M_w}}{\mathrm{M_n}} \quad [3]$$

The $M_n$ can be estimated thought the measurements of shear dynamic rheology using the mark Houwink -Sakurada equation (**Equation 4**)

$$\eta = \mathrm{KM_w^a} \quad [4]$$

In this equation $\eta$ is the viscosity of the polymer, $M_w$ the molecular weight of the polymer, $a$ is a coefficient and $K$ is a pre-factor that depend on the polymer-gas system. However, $K$ is a temperature dependent parameter and the possible values referred in the literature could not be obtained at the same temperature at which the rheological test is performed. Therefore, the value of $K$ needs to be adjusted accordingly. By using Arrhenius or WLF (Williams-Landel-Ferry) model it is possible to obtain this parameter for the precise temperature values. For a polymer with small chains, which do not present effective entanglements among them, viscosity is directly proportional to the molar weight, and the $a$ coefficient take values close to 1.[43] However, if the polymer present large molecules that have effective entanglements among them, the molecular weight upraise a value that is called critical value ($M_c$) and the connection between viscosity and molecular weight follows instead a relationship where $a$ takes values closed to 3.5. In this last situation viscosity increases abruptly with the molecular weight.[44]

Another way of obtaining the $M_n$ and determine the $M_w$ and the $PD_{index}$ is the gel permeation chromatography, which is based on the separation of the dissolved macromolecules of the polymer by their sizes based on their elution capabilities. In this work a gel-permeation chromatography (GPC) using a Waters Alliance GPC 2000 was used. The GPC was equipped with a tree styragel HT-type columns (HT3, HTS and HT6E) and tetrahydrofuran (THF) was used as a solvent.[45]

### *2.4.3. Extensional Rheology Measurements*

A stress controller rheometer (AR 2000 EX from TA Instruments) with an extensional fixture (SER 2, Xpansion Instruments) has been used to analyze the extensional rheological behavior of the different PS grades. In this device, the samples are clamped to two cylinders that rotate, at a fixed rate, in opposite

directions applying a uniaxial stretching force to the material. All the experiments were conducted at a temperature of 160 ºC (and at different Hencky strain rates: 0.3, 0.5 and 1 $s^{-1}$. In all the experiments the maximum Hencky strain was 2.8. Extensional viscosity can be defined as the ratio between the measured stress and the corresponding Hencky strain rate. A more detailed description of the measurement protocol can be found elsewhere.[46]

From the extensional viscosity measurements, the strain hardening coefficient (S) was obtained. This parameter (see **Equation 5**), which allows quantifying the way in which extensional viscosity increases when time or strain increase, has been obtained for three polymer matrices.

$$S = \frac{\eta_E^+(t, \dot{\varepsilon_0})}{\eta_{E0}^+(t)} \quad [5]$$

Where $(\eta_E^+(t, \dot{\varepsilon_0}))$ is the transient extensional viscosity for a determined time $(t)$ and Hencky strain rate $(\dot{\varepsilon_0})$ and $\eta_{E0}^+(t)$ is the transient extensional viscosity in the linear viscoelastic regime, which can be obtained in two different ways: as three times the time-dependent shear viscosity growth curve at very low shear rates or by extrapolating the overlapping parts of the extensional viscosity curves at different elongation rates.[47] In the present work, the second option was chosen to obtain the strain hardening coefficient. This coefficient has been determined for a time of 2.67 s and for a Hencky strain rate of 1 $s^{-1}$.

### *2.4.4 Differential Scanning Calorimetry (DSC)*

To analyze the effects of the molecular weight in the glass transition temperature ($T_g$) the thermal behavior of the polymers was characterized by DSC (Mettler, Mod. DSC 862). The experimental conditions used were the following ones:.(1) First heating step: from 20 ºC to 160 ºC at a heating rate of 10 ºC min-1; (2) Isotherm: 3 minutes at a constant temperature of 160 ºC for erasing the thermal history; (3) Cooling step: from 160 ºC to 20 ºC at a cooling rate of 10 ºC min-1 ;(4) Second heating step: from 20 ºC to 160 ºC at a heating rate of 10 ºC min-1.

### *2.4.5 Solubility and Diffusivity measurements*

The method used during the present work to measure the gas absorbed by the polymer matrix during the saturation stage, is the gravimetric method. By using this method, the gas uptake is obtained directly by determining the weight gain of a polymer sample during the sorption stage. Basically, it consists on calculating the difference between the weight of a polymer at the end of the sorption process $(W_s)$, when the polymer is fully saturated, and the initial weight of the composite

($W_0$). This difference divided by the initial weight of the composite provide the percentage of $CO_2$ uptake polymer (solubility), as it can be seen in (**Equation 6**).

$$CO_{2\,Uptake} = 100\,\frac{W_s - W_0}{W_0} \qquad [6]$$

However, when this measurement is performed the material has already lost some part of the gas due to the diffusivity process. Therefore, sample are maintained in the balance during 20 minutes for observed the lineal diffusion process. Later the weight change recorded in the balance is represented as a function of the square root of desorption time to obtain with the extrapolation the weight at time equal to zero, which is the weight of the saturated sample during depressurization.[29] On the other hand, to determine the gas diffusivity, once the material was saturated and removed from the pressure-vessel, once again the variation of its weight as a function of time was recorder, using a precision balance. Diffusion curves and diffusion coefficient were obtained thanks to this procedure.

The sorption and desorption data were applied in this study with diffusion only along the thickness direction. This was possible because the ratio of the thickness of the sample (2 mm) compared to the length of it (20 mm) is lower than 0.16.[48] According to the Fick's second law the equation to describe the diffusion of gas through a material could be expressed in the following way (**Equation 7**).

$$\frac{M_t}{M} = 1 - \frac{8}{\pi^2}\sum_{n=0}^{\infty}\frac{1}{(2n+1)^2}\exp\left(-\frac{(2n+1)^2\pi^2 Dt}{l^2}\right) \qquad [7]$$

Where $M_t$ is the sorption amount of CO2 at a specific time at certain conditions of pressure and temperature, $M$ is the equilibrium amount, $D$ is the diffusion coefficient, $t$ is the time, and $l$ is the thickness of the sample. However, equation 2 can be truncated to the first term to obtain (**Equation 8**) for the long-time diffusion process and (**Equation 9**) for the short time diffusivity, both equations are only valid when the thickness of the materials are relatively small, in the range of centimeters.[49]

$$\frac{M_s}{M_\infty} = 1 - \frac{8}{\pi^2}\exp\left(-\frac{D_s\pi^2 t}{l^2}\right) \qquad [8]$$

Where $M_s$ is the quantity of sorbed gas at the time t, $M_\infty$ is the gas equilibrium value in which material have the maximum quantity of gas for the specific conditions of time, temperature, and pressure , $D_s$ is the sorption diffusion coefficient, the time is $t$ and the thickness of the material is $l$ . For a constant

sorption diffusion coefficient $D_s$, the sorption coefficient can be obtained as the slope of the graph that plot the $\ln\left(1-\frac{M_s}{M_\infty}\right)$ as a function of $(t/l^2)$.

The gas diffusivity during the desorption process can be also analyzing by using the second Fick's law (Equation 13), using the approximation for short times or practically until the point that M(t)/M∞ equals 0.5(**Equation 9**).[50]

$$\frac{M_t}{M_\infty} = \frac{4}{l}\sqrt{\frac{D_d t_d}{\pi}} \quad [9]$$

Where $M_\infty$ is the equilibrium value in which material have the maximum quantity of gas for the specific conditions of time, temperature, and pressure, $M_t$ is the weight of the material in a certain time. $D_d$ is the desorption diffusivity coefficient at a certain condition of temperature and pressure and $t_d$ is the desorption time. The diffusion coefficient calculus is performed using the slope of the initial part of a normalized sorption plot and representing the $M_t/M_\infty$ as a function of the ${t_d}^{0.5}/l$.

### *2.4.6. Density*

The density of the solid materials was analyzed using a gas pycnometer (Accupyc II 1340 from Micromeritics). The density of the cellular materials was determined by the geometric method, that is, dividing the mass of each specimen by its corresponding geometric volume (ASTM standard D1622-08). The foamed samples used to determine the density have a cylindrical shape with a diameter close to 75 mm and a thickness of 6 mm.

The following equations (**Equation 10)** and **(Equation 11**) show the way of determining the relative density and expansion ratio. Relative density ($\rho_r$) is defined as the ratio between the density of the cellular material ($\rho_{cm}$) and the density of the solid material ($\rho_s$). On the other hand, the expansion ratio is defined as the inverse of the relative density.

$$\rho_r = \frac{\rho_{cm}}{\rho_s} \quad [10]$$

$$E = \frac{1}{\rho_r} \quad 4. \quad [11]$$

### 2.4.7. Open Cell Content

To evaluate the open cell content of the samples, according to the ASTM Standard D6226-10, a gas pycnometer Accupyc II 1340 from Micromeritics was used. The open cell content was determined using (**Equation 12**).

$$OC(\%) = 100\left(\frac{v_{geometric} - v_{pycnometer}}{V_{geometric}p}\right) \quad [12]$$

Where $v_{geometric}$ is the geometric volume of the sample, $v_{pycnometer}$ is the volume of the sample obtained with the pycnometer and $p$ is the sample's porosity calculated as $(1 - \frac{\rho_{cm}}{\rho_s})$, where $\rho_{cm}$ is the cellular material density and $\rho_s$ the solid matrix density.

### 2.4.8. Structural Characterization

The structure of the cellular materials was analyzed with a scanning electron microscope (SEM) (Jeol, Mod. JSM-820). Parameters like the average cell size ($\Phi$), the cell nucleation density ($N_0$), and the normalized standard deviation (SD/$\Phi$) were analyzed with an image processing tool based on the software Fiji/Image J.[51]

The average cell size is defined as it is indicated in Equation 13:

$$\phi = \sum_{i=1}^{n} \frac{\phi_i}{n} = \sum_{i=1}^{n} \frac{cf}{2n}(\phi_x^i + \phi_y^i) \quad [13]$$

Where $n$ is the total number of cells counted in the image, $\phi_i$ is the three-dimensional value of the cell size for a specific cell. $\phi_x^i$, $\phi_y^i$, are the length of the cells in the directions x and y, respectively, and $cf$ is a correction factor, with a value of 1.273, used to obtain a three-dimensional value of the cell size from a two-dimensional value..[51]

The cell nucleation density ($N_0$), defined as the number of cells per unit volume of the solid, was obtained using the Kumar's theoretical approximation represented in Equation 14.[42] In this formula $N_v$ is the cell density, defined as the number of cells per cubic centimeter of the foamed material, and $\rho_r$ is the relative density. More than 100 cells of different regions of each cellular material have been considered to determine this parameter.

$$N_0 = \frac{N_v}{\rho_r} \quad [14]$$

Finally, normalized standard deviation, which is defined as the ratio between the standard deviation of the cell size (SD) and the average value of the cell size (SD/$\phi$), was determined to analyze the homogeneity of the cellular structure. Low values of this parameter are related with a homogeneous cellular structure with a thin cell size distribution.

## 3. RESULTS

### 3.1. Shear Dynamic Rheology results.

The molecular weight of the three PS matrices was first estimated by dynamic shear rheology. From this experiment it was possible to analyze the changes of the complex viscosity as a function of the angular frequency (**Figure 1**). The zero-shear viscosity was also determined as the value of the viscosity in the Newtonian-plateau, at low frequencies (**Table 1**). Later, the Mark-Houwink Sakurada equation, was used to estimate the molecular weight of the different polymer matrices. The obtained values are also included in Table 1.

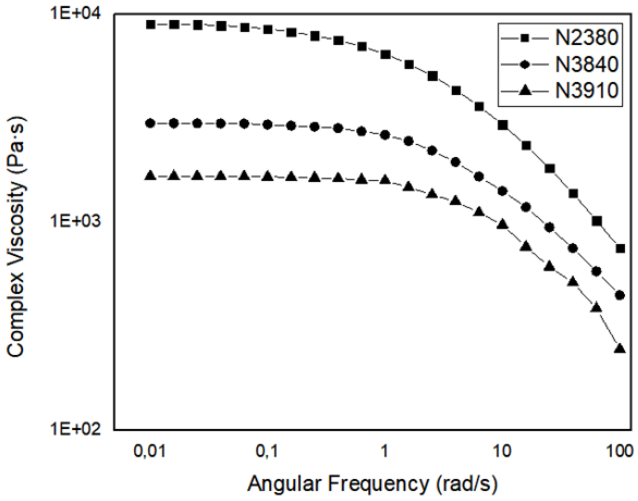


**Figure 1.** Complex viscosity as a function of the angular frequency for the three different PS.

Results indicate that the material with the lowest value of the melt flow index, Edistir N2380, presents the highest complex viscosity; meanwhile, the material N3910, the one with the highest melt flow index, presents the lowest complex viscosity. The materials therefore present a relationship between the molecular weight and the zero shear viscosity according to the Mark-Houwink Sakurada equation explained before (equation 4), in which the polymer with the highest molecular weight value should present the highest viscosity value too. It is remarkable to mention that in principle a lower viscosity value could be helpful during the growing of the cell to allow an easy expansion of the cellular structure.

Nevertheless, if viscosity due not change during the cell development could be that the degeneration phenomena play a major role in the final structure generating a structure with a notorious value of the open cell content and a non-regular cell size distribution.

### 3.2. Molecular weight determination and estimation.

On the other hand, in Table 1 it is collected the values estimated and obtained from the molecular weight of the different polymer matrices. The values were estimated using the previous results obtained in shear dynamic rheology and were also determined by GPC technique.

**Table 1.** Results obtained by dynamic shear rheology (zero-shear viscosity and molecular weight) and by GPC ($M_w$ ,$M_n$ and $PD_{Index}$).

| Sample Name | Melt Flow Index (g/10 min) | Zero-Shear Viscosity (Pa·s) | Slope of G' (Pa·s) | Slope of G'' (Pa.s) | $M_w$ obtained by GPC (g/mol) | $PD_{index}$ obtained by GPC |
|---|---|---|---|---|---|---|
| **N2380** | 2 | 9000 | 2.34 E+05 | 1.36 E+05 | 1.62 E+05 | 1.19 |
| **N3840** | 10 | 3000 | 1.56 E+05 | 1.19E+05 | 1.44 E+05 | 1.21 |
| **N3910** | 27 | 1600 | 1.08 E+05 | 1.09E+05 | 1.18 E+05 | 1.08 |

In table 1 can be seen how the trends observed with the two techniques (the shear dynamic rheology and the GPC) are the same: the molecular weight decreases as the melt flow index increases. However, the absolute values of the molecular weight depend on the technique employed to determine them. The values of the molecular weight estimated by dynamic shear rheology overestimate the values of the molecular weight obtained by GPC. This fact is especially remarkable for the polymer with the highest molecular weight (N2380). There is a difference of a 44% among the weight average molecular weight acquired by GPC and the estimation of the molecular weight by shear rheology. The estimation of the molecular weights through the shear dynamic rheology is a tool that have been used by several researches based specially in the Mead and Thimm algorithms[52,53] This method is remarkably important whenever is not possible to use other measurements based in the size exclusion methods. However, it is important to mentioned that rheology is extremely sensitive to the high molecular weight species and therefore the value obtained usually overestimated the importance of the longer chains compared to the smallest ones.[54] Providing therefore a value of the weight average molecular weight that is higher than the most accurate one obtained in the size exclusion method like is GPC. It can be understanded that for the polymer with the lowest melt flow index (higher viscosity) in which probably longer chains are founded ,compared to the other two polymers, the

importance that the rheometer provide to those chains is overestimated. This is the reason why in the future subsections the values that considered for the molecular weight are those obtained by GPC.

### 3.3. Relationship between the molecular weight and the extensional viscosity and the glass transition temperature

In this section the influence of the molecular weight in some structural characteristics of the polymers like the uniaxial extensional flow (and particularly, the strain hardening coefficient), and the experimental glass transition temperature acquired by DSC, or also theoretical glass transition temperature obtained using the Flory-Fox or Ueberreiter and Kaning models, will be analyzed.

Extensional viscosity could defined, according to the Trouton ratio, as three times the complex shear viscosity.[55] The molecular weight distribution or chain branching play a critical role in the uniaxial extensional behavior of a polymer. This fact has been tested in several materials such as PS or some polyolefins like polypropylene and polyethylene.[44,56–59] Among the properties that could be measured in a common elongational experiment, strain hardening coefficient stands out for being one of the most relevant ones as it was mentioned before.

On the other hand, it is expected a difference in the glass transition temperature according to the molecular weight. In the polymer (N2380) with a higher molecular weight it is supposed that the longer chains will need a higher temperature to start the mobility rather than the ones of the polymer with a lower value of the molecular weight (N3910). However, this glass transition temperature can also be estimated accordingly to the theoretical formula proposed by Flory-Fox ( equation 15) , in which Were $T_g$ is the glass transition temperature, $T_{g\infty}$ is the glass transition temperature of a polymer with an "infinite chain" length, according to Flory and Fox they take this value as 373 Kelvin for the PS a, $K$ is a constant that is related with the free volume of the polymer, and M is the fraction of the molecular weight of the material calculated as the ratio between the number-averaged molecular mass of the homopolymer and the number average molecular weight of the monomer. The relation between the glass transition temperature and the number average molecular weight it is a prediction by the result of the extensive experiments of Ueberreiter and Kanig. However, these equations are very dependent on the value of the molecular weight and one or other value of the parameter K can be applied or not according if the molecular weight value is higher or lower than a certain quantity. In

particular Flory and Fox proposed the equation 16 as the one working for number average molecular weights between (3E+03 until 3E+05).[60] This will be the one applied in the following study.

$$T_g = T_{g\infty} - \frac{K}{\mathrm{M}} \quad [15]$$

$$T_g = 373 - \frac{1814}{\mathrm{M}} \quad [16]$$

On the other hand in a similar equation like the one proposed Ueberreiter and Kanig report a value of the constant for $T_{g\infty}$ 361 kelvin and also different value for the constant K, because they relate more this parameter with the iso-torsion of the molecule during the glass transition generating in the end an equation that can be written as it follow (equation 17):[61]

$$\frac{1}{T_g} = 0.002801 + \frac{0.004260}{M} \quad [17]$$

**Table 2**. Structural characteristics ($M_w$ , Strain Hardening Coefficient, experimental and theoretical Tg, Length of the polymer chains and radius of gyration) of the three PS grades.

| Sample | $M_n$ (g/mol) | Strain Hardening, S | Experimental Tg (ºC) | Theoretical Tg Flory Fox (ºC) | Theoretical Tg Ueberreiter and Kanig |
|---|---|---|---|---|---|
| **N2380** | 1.36 E+05 | 4.89 | 104 | 98.62 | 83.60 |
| **N3840** | 1.19E+05 | 3.83 | 89 | 98.42 | 83.54 |
| **N3910** | 1.09E+05 | 1.16 | 86 | 98.27 | 83.49 |

The uniaxial extensional flow properties of the polymers (strain hardening coefficient) exhibit a behavior in which the material with the higher viscosity presents a higher strain hardening coefficient. According to Larson et Desai the strain hardening in a linear PP isotactic polymer decreases at very high extensional rates due to the orientation-induced reduction in friction. This is related with the facility that the chains must orientated toward the elongational alignment. For the polymer with the lowest molecular weight, this alignment will be done in a most easy way due to the presence of several chains with smaller sizes. Therefore, the results obtained are in alignment with the phenomena observed by Larson et al. The Results of the strain hardening that can be seen in table 2 indicate that the strain hardening increases as the molecular weight increases. It is quite remarkable the decrease (almost a 76%) observed in the strain hardening coefficient of the N3910 polymer compared to the N2380 polymer.

This fact could represent a serious problem during the foaming process. A low value of the strain hardening coefficient could lead to high open cell contents and heterogeneous cellular structures and even to an increase in the final foam density. On the other hand, in table 1 it is possible also to see the experimental and theoretical values of the glass transition temperature. The experimental values obtained in a common DSC experiment show a depletion of the glass transition temperature with the decrease of the molecular weight of the polymer. This behavior was also reported by Blanchard et al, in which they based their assumptions of the relation between the molecular weight and the glass transition temperature on the theoretical equation of Flory-Fox reported before (equation 15).[62] Itis explained because as soon as the length of the polymer chain increases is more difficult that it gains mobility and a higher temperature is needed for that. When comparing the results of the experimental values of the glass transition temperature, obtained by DSC, with those predicted using the Flory-Fox model or Ueberreiter and Kanig, it is possible to detect strong differences between them and the ones obtained in the DSC tests, especially for the polymers with a high melt flow index. The differences between the theoretical and experimental values were explained by Gibbs and Di-Marzio considering the low influence that the molecular weight presents in the Flory-Fox model for a same material. They argument that other factors like flexibility or mobility of the chain, bulkiness, polarity and ionicity and free volume available are overestimated in this model. [13] Furthermore, the decrement produced by the reduction in the molecular weight are similar for the Flory-Fox model and for Ueberreiter and Kanig one, the only difference is that the Flory fox model considers an initial temperature of the glass transition temperature for an infinite molecular weight of 100°C and the model proposed by Ueberreiter and Kanig select this temperature as 88°C.

### 3.4 Effect of the molecular weight on the solubility and diffusivity of CO2.

The gas uptake has been measured as a function of the saturation time, at the same conditions of pressure and temperature (8 MPa and 40º C), for three PS grades with different molecular weight. **Figure 2** indicates that the sample with the lowest molecular weight (N3910) exhibits a higher solubility than those with medium (N3840) or high molecular weight (N2380). There are plenty of factors that determine the sorption capability of a polymer. Some of the most important ones are the environmental factors during the saturation step (pressure, temperature, relative humidity, etc.), chemical affinity of the gas with the polymer, and the architecture of the polymer (morphology, orientation of the

chains, free volume, etc.). The free volume could be explained as the empty space that is founded between the chains of the polymer. Like it was reported in previous articles of Wang et al, at high pressures the gas molecules tend to occupy the available free volume remaining in the polymer.[63] Therefore, it is created a relationship between the polymer solubility and the polymer free volume: a material with a higher free volume gas has the possibility of absorbs a higher amount of gas molecules. Furthermore, Yu et al reported that the PS with that between various polystyrene with different molecular weights was the one with the longer molecular chain length the PS that present the higher glass transition temperature , and the smaller average cavity sizes ( free volume).[64] Therefore, a material with a lower molecular weight presents a higher free volume available which results in a greater capacity of absorb more gas at the same conditions. This fact could be observed in Figure 2, where it is possible to see that the polymer with the lowest molecular weight absorbs more quantity of gas at same conditions of time, temperature and pressure, than the other two polymers. Furthermore, the percentage of gas uptake at saturation conditions, that is the polymer solubility, is much higher (9.5%) for the polymer with the lowest molecular weight (N3910) than for the polymers with the medium N3840 (7.69%) and high N2380 (7.24%) molecular weight.

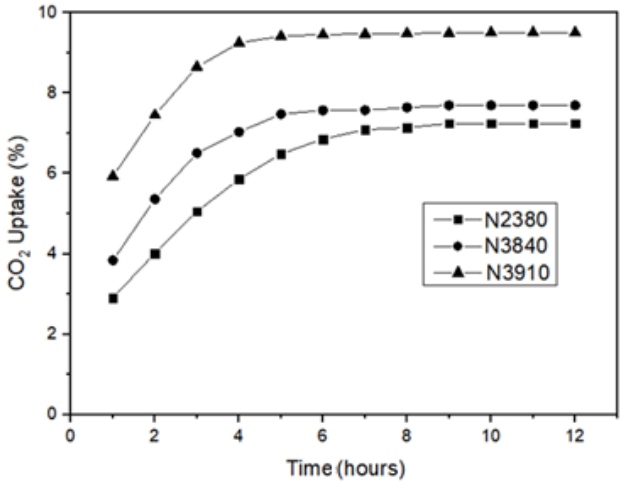


**Figure 2**. Solubility curves as a function of the saturation time for the PS matrices with different molecular weight.

Furthermore, the saturation time is also lower for the polymer with the lowest molecular weight as it could be seen in **Table 3**. The values of the solubility are also collected in Table 3.

**Table 3**. Solubility and saturation time for the three different PS**.**

| Sample | CO2 Uptake (% wt.) | Saturation Time (hours) |
|---|---|---|
| **N2380** | 7.24 | 6 hours and 40’ |
| **N3840** | 7.69 | 4 hours and 28’ |
| **N3910** | 9.50 | 3 hours and 47’ |

By using the Equation 8 it is possible to determine the gas diffusivity during the sorption process, which provides a numerical data of how easy is for the gas to penetrate in the material. **Figure 3** indicates that gas diffusivity is higher, and therefore, the gas penetrates easier, in the material with the lowest molecular weight (N3910) Than in the other two polymers (N3840 and N2380).

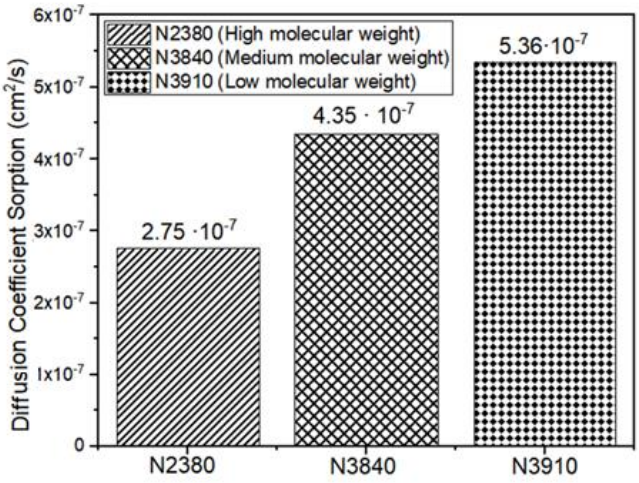


**Figure 3**. Diffusion coefficient sorption for the three PS grades.

The diffusivity curves can be obtained by recording with a precision balance the variation of the mass of the saturated polymer as a function the time. **Figure 4** shows how the materials lose gas as the desorption time increases. It is notable how the PS with the lowest molecular weight loss in 10 min around a 2% of the mass of $CO_2$ dissolved in the material, meanwhile for the other two polymers this effect is not so remarkable.

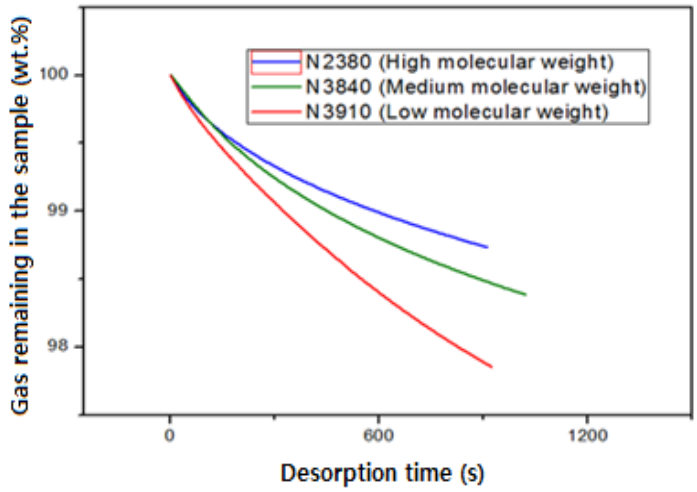


**Figure 4.** Gas remaining in the polymer vs desorption time for the three PS grades with different molecular weights.

Also, it is possible to determine the diffusion coefficient that to understand how easily the gas escapes out from the material. As it can be seen in **Figure 5** the gas diffuses out easily from the material N3910, the one with the lowest molecular weight, than for the other two polymers N3840 and N2380.

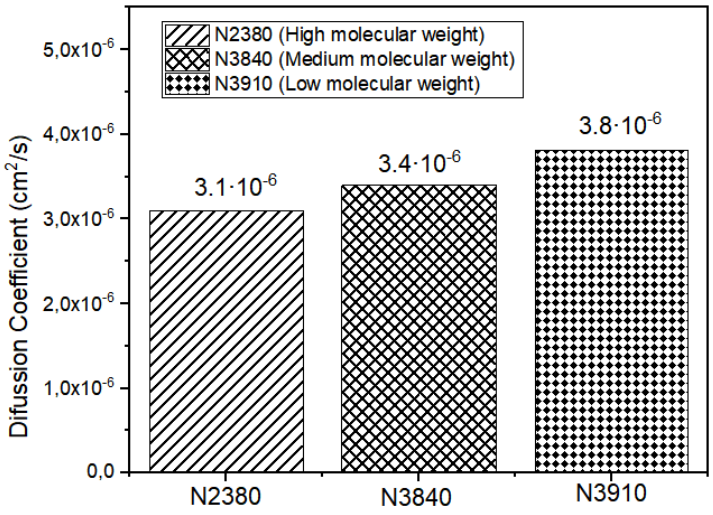


**Figure 5.** Gas Diffusivity during the desorption process for the three PS grades.

During the saturation stage the glass transition temperature decreases due to the presence of the gas (blowing agent) inside the material. This effect is usually named as plasticizing effect.[65] In the present work two different theoretical models are considered to analyze the plasticizing effect and check the relationship of this decrease and the molecular weight of the polymers. For an amorphous polymer, like PS, the most used theoretical models for predict the plasticizing effect are the Chow model and the Cha- Yoon Model.[22]

The Chow model, **Equation 18**, **Equation 18b** and **Equation 18c** represents the reduction of the glass transition temperature by the presence of gas.

$$ln\left(\frac{T_g}{T_{g0}}\right) = \psi[(1-\theta)\cdot\ln(1-\theta) + \theta\ln\theta] \quad [18a]$$

$$\theta = \frac{M_p \cdot w}{z \cdot M_d \cdot (1-w)} \quad [18b]$$

$$\psi = \frac{z \cdot R}{M_p \cdot \Delta C_{p-Tg}} \quad [18c]$$

Where $T_g$ is the effective glass transition temperature, $T_{g0}$ is the glass transition temperature of the bulk polymer, $M_p$ is the molecular weight of the monomer of the polymer, $w$ is the percentage of gas dissolved in the material, $z$ is the coordination number of the system polymer-gas, $M_d$ is the molecular weight of the blowing agent, R is the ideal gas constant and $\Delta C_{p-Tg}$ is the difference in the heat capacity during the glass transition that can been obtained by DSC.

The Chow model gives precise results related with the plasticizing effect for different diluents and for plenty of polymers, like PS, PMMA, PC, PVC, PET.[65,66] However, Chow model present the disadvantage that at high concentrations of carbon dioxide the accuracy of the model decreases.

Cha-Yoon Model is effective in polymers like PS, PC, PMMA, PETG and ABS. The actual drawbacks of this model are that the constant of the system polymer-gas is non well defined for some systems and there is not literature for the application of this model in polymer blends.

The equation of Cha-Yoon model is the following one (**Equation 19**):

$$T_g = T_{g0}\ \exp\left[-(M_P)^{-1/3}(\rho_s)^{-1/4}\alpha\omega\right] \quad [19]$$

Where $\rho_s$ is the density of the bulk polymer 1.054 g/cm$^3$ and $\alpha$ is a constant of the system polymer-gas, which for the system PS-$CO_2$ is equal to 0.7.[67]

When solving both equations for the different weight uptakes recorded it is possible to obtain two curves that represent the value of the effective glass transition temperature as a function of time (**Figure 6**).

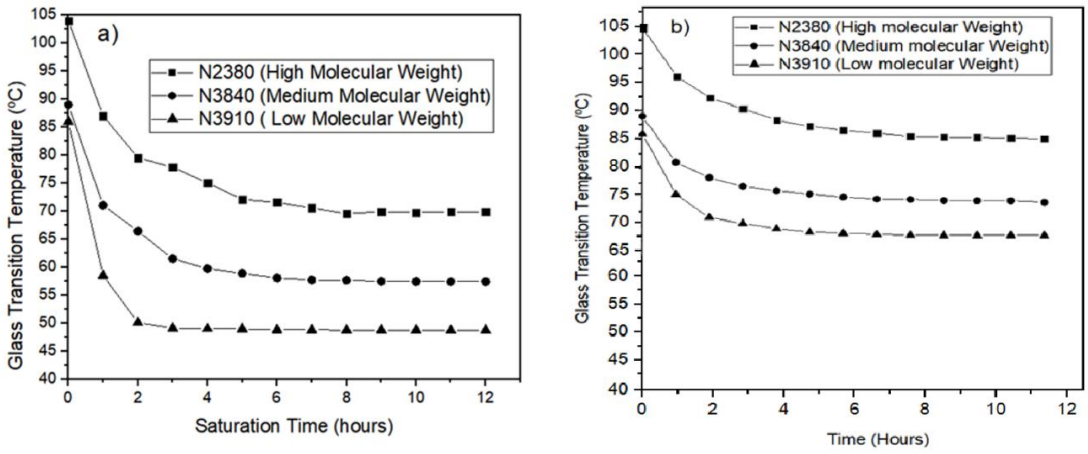


**Figure 6.** Variation of the glass transition temperature as a function of the saturation time. a) Effective glass transition temperature obtained using the Chow model as a function of the saturation time. b) Effective glass transition temperature obtained using Cha-Yoon model as a function of the saturation time.

In Figures 6a and 6b it is possible to check how the reduction of the glass transition temperature is similar for the three PS matrices. When using the Cha-Yoon model it is possible to see that the low molecular weight PS (N3910) reaches values of the glass transition temperature which are close to the saturation temperature. Consequently, when the material N3910 is removed from the high-pressure vessel it is already pre-foamed. Furthermore, in **Table 4** it is possible to see how the glass transition temperature of the PS grades changes due to the presence of $CO_2$, when they are completely saturated. The depletion of the glass transition temperature was calculated as the difference between the glass transition temperature and the effective glass transition temperature obtained by the Chow or Cha-Yoon model. In table 4 it is possible to see also, how in the Cha-Yoon model, the depletion of the glass transition temperature is faster for the low molecular weight polymers than for the other two polymers. Furthermore, the depletion of the glass transition temperature estimated by the Cha-Yoon model is higher than the one calculated using the Chow model. In the Hwang and al. publication they reported also that the Cha-Yoon model present a higher depletion of the glass transition temperature than the Chow model, they attributed this difference in the fact that the Cha-Yoon model is more appropriate for predicting a change in the glass transition temperature of polymer materials in a batch microcellular foaming process.[67]

**Table 4.** Values of the depletion of the Tg according to the Cha-Yoon model and the Chow model.

| Polymer | $M_w$ (g/mol) | Tg (°C) | Tg effective (°C) Cha-Yoon | Depletion of the Tg Cha-Yoon | Tg effective (°C) Chow | Depletion of the Tg Chow |
|---|---|---|---|---|---|---|
| **N2380** | 1.18 E+05 | 104 | 72 | 32 | 88 | 16 |
| **N3840** | 1.44 E+05 | 89 | 57 | 32 | 79 | 10 |
| **N3910** | 1.62 E+05 | 86 | 48 | 38 | 70 | 16 |

To sum up the data obtained in this subsection it seems that there is a relationship between the molecular weight and the sorption and diffusivity properties of the polymers. PS with lower molecular weight can absorb (at the same conditions of pressure, temperature, and time) more quantity of gas than PS with high molecular weight.

### 3.5 Influence of the molecular weight in the cellular structure of the foamed polymers.

In this subsection different foams are produced with the three PS matrices and their density and cellular structure are analyzed. The main objective is to determine how the foam characteristics are affected by the molecular weight of the polymer matrix.

In **Table 5**, it is possible to see the values of the density and open cell content for the three different PS foams.

**Table 5:** Values of the density and open cell content for the three different PS foamed samples.

| Sample | $M_w$ (g/mol) | Density (kg/m$^3$) | Open Cell Content (%) |
|---|---|---|---|
| **N2380** | 1.62 E+05 | 40 | 10 |
| **N3840** | 1.44 E+05 | 37 | 12 |
| **N3910** | 1.18 E+05 | 34 | 22 |

The values of the density indicate that the material with the lowest molecular weight (N3910) can expand more during the foaming process. The difference between the density of the PS with the highest molecular weight (N2380) and the PS with the lowest value of this parameter (N3910) is if around 15%. This could be related with the fact that the viscosity, measured already with the shear dynamic rheology, is lower for the material with the lowest molecular weight, which leads to an easy and rapid expansion compared to the other two PS grades. Moreover, also the higher quantity of gas that the N3910 material can acquire

(almost 2 % more of $CO_2$ uptake compared to the other polymers) could lead to a slightly higher expansion, taken into account that the time that material are diffusing before they were introduced in the thermal bath (2 min) is not enough to observed a remarkably change in the final gas concentration.

On the other hand, the open cell content presents a notable increase as soon as the molecular weight is reduced. The foam produced with the polymer with the lowest molecular weight (N3910) has an open cell content 2.2 times higher than the sample produced with the polymer with the highest molecular weight (N2380). Even the material with the lowest molecular weight, present a rapid expansion because there is not a great viscosity opposing to the grow, as we mentioned before, the strain hardening coefficient between the three polymers were quite different, as we have seen in the extensional viscosity measurements. These reduction of 76% in the strain hardening coefficient between the polymer with the lowest molecular weight compared to the one with the highest molecular weight, means that the N3910 material would not presence an increase of the viscosity during the foaming process which leads to the appearance of degeneration phenomena, like cell coalescence, that will have a remarkable impact in increasing the open cell content. Furthermore, the glass transition temperature of the low molecular weight polymer is the one with the lowest value, and when the gas perform its plasticization effect, the reduction of the Tg towards the effective glass transition temperature reach a value that is 10°C and 20°C lower than the ones of the medium and higher molecular weights polymers, respectively. Like the foaming temperature (120°C) and foaming time ( 1 min) is the same for the three polymers, this will means that the material with the lowest molecular weight will remains during this minute in a higher temperature difference between the foaming temperature and the effective glass transition temperature, than the other two PS grades. Foaming a polymer with a not proper conditions in temperature and time could lead also to the appearance of the degeneration mechanism, a most irregular cellular structure and, for instance, the increasing of the open cell content.

The inner characteristics of the cellular structure of the different foams were analyzed thanks by SEM microscopy. **Figure 7** shows the micrographs of the three PS samples.

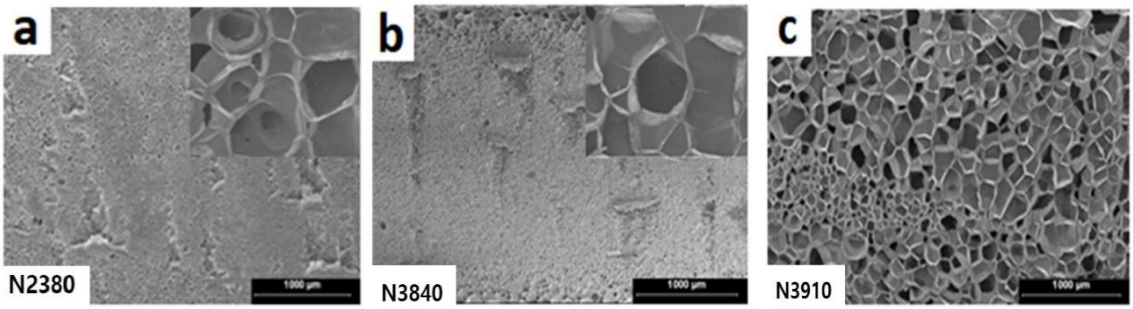


**Figure 7**. SEM micrographs of the cellular structure of the three PS foamed samples. a) Foam produced with the high molecular weight polystyrene N2380. b) Foam produced with the medium molecular weight polystyrene, Edistir N3840. c) Foam produced with the low molecular weight PS, Edistir N3910.

The sample produced with the polymer with the highest molecular weight (Figure 8a) presents the lowest cell size and the most regular and homogeneous cellular structure. By the contrary, the sample produced with the polymer with the lowest molecular weight (8c) presents the highest cell size. Furthermore, other parameters, like the cellular density, presents a similar trend. The number of cells per cubic centimeter decreases when the polymer molecular weight increases (see **Table 6**).

This result could be not an expected one if we consider the solubility and diffusivity results. As it was discussed before, the sample with the lowest molecular weight presents a higher solubility at the same conditions of temperature, pressure, and time than the other samples. Moreover, this sample also presents a slightly higher diffusivity but not so different compared to that of the other materials. Therefore, this sample should present a higher nucleation capability due to the more quantity of gas available. However, results indicate that the polymer with the lowest quantity of gas uptake is the one that presents the lowest cellular size.

Again, the explanation of the results obtained could be related with the differences observed in the extensional behavior of the three PS grades. As it was seen in the previous subsections the differences in the strain hardening coefficient among the three PS was considerable. A decrease of almost a 76% of the Strain Hardening Coefficient is perceived between the polymer with the highest molecular weight (N2380) and the polymer with the lowest molecular weight (N3910). If a polymer presents a low value of this parameter implies that the material is not able to withstand the elongational forces occurring during the expansion process. This fact leads to a rupture of the cell walls and therefore, to

an increase of the cell size. This result could explain why the foam produced with the polymer with the lowest molecular weight presents the highest cell size.

**Table 6**. Values of the cell structure characteristics for the three different based foams.

| Sample | $M_w$ (g/mol) | Cell Size (μm) | Cellular Density (Cells/cm$^3$) | Anisotropy Ratio | $SD/\theta$ |
|---|---|---|---|---|---|
| **N2380** | 1.62 E+05 | 43 ± 11 | (2.47± 0.9) ·10$^8$ | 1.02 | 0.25 |
| **N3840** | 1.44 E+05 | 88 ± 28 | (1.13 ± 0.5) ·10$^8$ | 1.06 | 0.31 |
| **N3910** | 1.18 E+05 | 264 ± 95 | (6.54 ± 0.7) ·10$^7$ | 1.05 | 0.35 |

Finally, it is also important to understand how the glass transition temperature could be affecting the cellular structure characteristics. The previous results indicated a reduction of the glass transition temperature produced by the presence of gas. The results exhibit that the lowest effective glass transition temperature was always reached by the polymer with the lowest molecular weight (N3910). This fact could mean that during the minute that the polymer is in the thermal bath at 120ºC, the gradient of temperature between the foaming temperature and the effective glass transition temperature is much higher for the polymer with the lowest molecular weight than for the other two polymers. This difference in temperatures implies that the polymer with the lowest molecular weight (N3910) stays during more time at a higher temperature compared the other materials, which results in the appearance of a higher number of degeneration mechanism by cell coalescence or coarsening. This theory is also in agreement with the values observed before in the open cell content. The sample with the lowest molecular weight (N3910) is the one presenting the highest value of the open cell content. Again, the degeneration phenomena, like cell coalescence, could play a significant role breaking the cell walls of the polymer and maximizing the open cell content.

In the Table 6 it is possible to see also how all the samples exhibit an isotropic behavior, with values of the anisotropy ratio close to 1. Finally, the standard deviation divided the cell size value, increases when the molecular weight decreases. This parameter explains that the cellular structure is more homogeneous and regular for the samples with a high molecular weight.

## 4. CONCLUSIONS

Three polystyrenes with different molecular weights have been characterized. The effect of a different molecular weight in the structural properties as well as in the solubility, diffusivity and the cellular structure have been studied. Shear

dynamic rheology and GPC were used to estimate and obtain the values of the molecular weight, respectively. The relations of some structural properties like shear dynamic rheology, extensional rheology, glass transition temperature with the molecular weight, were analyzed and seem in good agreement with some theoretical models proposed in the past. Furthermore, solubility and diffusivity properties were also studied by introducing gas in the materials in an autoclave. Polymer with the lowest molecular weight (N3910) presents the higher solubility of CO2 compared to the other two degrees. However, also the gas escapes easily from this polymer compared to the other two polystyrenes. Furthermore, the plasticizing effect that the gas has in the glass transition temperature of the three materials was also studied. The CO2 gas makes a similar reduction of temperatures for the three different polystyrenes according to the Chow and Cha-Yoon models. Nevertheless, like the material with the lowest molecular weight is the one with the lowest initial glass transition temperature, the final effective glass transition temperature is also lower for this material compared to the other two polymers. Finally, materials were foamed in a thermal bath and the cellular structure results were studied thanks to SEM micrographs. The results explain that the material with the highest molecular weight is the one that present the most homogeneous and regular cellular structure. The explanation behind this phenomenon could be found in the difference between the foaming temperature and the final effective glass transition temperature reached for the three different materials as well as from the differences observed in the strain hardening coefficient between the three different neat materials. In both theories the final effect will be the increase of the degeneration phenomena like cell coalescence that will lead to a reduction in the homogeneity of the structure and to an increase in the cell sizes for the polymers with lower molecular weight.

## 5. REFERENCES


[1] J.Maul, B.G. Frushour, J.R.Kontoff, H. Eichenauer, K.H. Ott. *Polystyrene and styrene copolymers. In: Ullmann's Encyclopedia of Industrial Chemistry*. **2016**, seventh edition. Wiley, New Jersey United states.

[2] https://www.ktvn.com/story/44434528/polystyrene-ps-market-2021-is-anticipated-to-witness-a-significant-growth-rate-during-the-forecast-period-2021-2025-with-top-20-countries-data. *Accessed November* ***2021.***

[3] C.C. Ibeh, *Thermoplastic Materials: Properties, Manufacturing Methods, and Applications*. **2011,** First Edition. CRC press Taylor and Francis Group, Bocaraton,United States.

[4] https://www.mordorintelligence.com/industry-reports/global-polystyrene-market-industry. Polystyrene Market. *Accessed November* ***2021.***

[5] G.A. Adam, J.N. Hay, I.W. Parsons, R.N. Haward. *Polymer (Guildf)*. **1976**, 17(1),51-57.

[6] R.W.Nunes, J.R Martin, J.F. Johnson. *Polym Eng Sci*. **1982**,22(4), 205-228.

[7] S.X.Lu, P. Cebe P. *J Therm Anal*. **1997**,49(1),525-533.

[8] H.M. Quackenbos. *J Appl Polym Sci*. **1980**,25(7), 1435-1442.

[9] L.W.McKeen. *Introduction to Plastics and Polymers Compositions. In: The Effect of UV Light and Weather on Plastics and Elastomers*. ***2013****, ,third edition*, Elsevier, The Netherlands.

[10] H.G.H.Van Melick, L.E. Govaert, H.E.H Meijer.*Polymer (Guildf)*. **2003**,44(8),2493-2502.

[11] I.M.Kalogeras.*Glass-Transition Phenomena in Polymer Blends. In: Encyclopedia of Polymer Blends*. 2016, first edition. Wiley, New Jersey, United states.

[12] J.H.Gibbs, E.A. DiMarzio. *J Chem Phys*. **1958**, 28(3), 373-383.

[13] E.A. DiMarzio. *Ann N Y Acad Sci*. **1981**;371.

[14] D.Turnbull, M.H. Cohen. *J Chem Phys*. **1961**, 34(1), 120-125.

[15] T.G.Fox, P.J Flory. *J Polym Sci*. **1954**,14(75), 315-319.

[16] G.Delmas, D. Patterson. *Polymer (Guildf)*. **1966**, 7(10), 513-524.

[17] K.Wang, H. Huang, J. Sheng. *J Liq Chromatogr Relat Technol*. **1998**, 21(10), 1457-1470.

[18] R.G.Larson, P.S Desai. *Annu Rev Fluid Mech*. **2015**,47(1),47-65.

[19] J. Drabek, M. Zatloukal. *Phys Fluids*. **2020**, 32(8), 083110.

[20] K.Taki, K. Tabata, S. Kihara, M. Ohshima. *Polym Eng Sci*. **2006**, 46(5), 680-690.

[21] V.I. Kalikmanov. *Nucleation Theory*. **2013,** first edition, Springer, Berlin, Germany.

[22] C. Forest, P. Chaumont, P. Cassagnau, B. Swoboda, P. Sonntag. *Prog Polym Sci*. **2015**, 41(6),122-145.

[23] S.Lin, J. Yang, J. Yan, Y. Zhao, B. Yang. *J Macromol Sci Part B*. **2010**, 49(2), 286-300.

[24] Y.Zhang, K.K. Gangwani, R.M.Lemert. *J Supercrit Fluids*. **1997**, 11(1-2), 115-134.

[25] Q.Tang, B.Yang, Y.Zhao, L. Zhao. *J Macromol Sci Part B*. **2007**, 46(2),275-284.

[26] J.J.Zhao, Y.P.Zhao, B. Yang. *J Appl Polym Sci*. **2008**;109(3), 1661-1666.

[27] O.Muth, T. Hirth, H. Vogel. *J Supercrit Fluids*. **2001**, 19(3), 299-306.

[28] Y. Sato, T. Takikawa, S. Takishima, H. Masuoka. *J Supercrit Fluids*. **2001**;19(2):187-198.

[29] S.K.Yeh, Z.E. Liao, K.C.Wang, Y.T.Ho, V.Kurniawan, P.C.Tseng, T.W.Tseng. *Polymer (Guildf)*. **2020**, 191, 122275.

[30] D.Li, Y. Chen, S.Yao, H. Zhang, D. Hu, L.Zhao. *Polymers (Basel)*. 2021;13(9):1494. doi:10.3390/polym13091494

[31] W.Zhai, J.Jiang, C.B.Park. A review on physical foaming of thermoplastic and vulcanized elastomers. *Polym Rev*. **2021**, 1-47.

[32] V. Bernardo, J. Martin-De Leon, E. Laguna-Gutierrez, T. Catelani, J. Pinto, A. Athanassiou, M.A. Rodriguez-Perez. *Polymer* **2018**, 153, 262–270.

[33] B. Notario, J. Pinto, E. Solorzano, J.A. De Saja, M. Dumon, M.A. Rodriguez-Perez. *Polym (United Kingdom)*. **2015**,56,57-67.

[34] C. Forest, P. Chaumont, P. Cassagnau, B. Swoboda, P. Sonntag. *Polymer (Guildf)*. **2015**, 77, 1-9.

[35] S.Ebnesajjad. *Introduction to Plastics. In: Chemical Resistance of Engineering Thermoplastics*. 2016, first edition, Elsevier, The Netherlands .

[36] J.C.Moore. *J Polym Sci Part A Gen Pap*. **1964,** 2(2), 835-843.

[37] T.Hara, A.Okamoto, Y.Hama, S. Okamoto. *J Polym Sci Part A-2 Polym Phys*. **1968**;6(5):961-965.

[38] N.De, M.V.A.S.Navarro, Q.Wang, P.V.Krasteva, H. Sondermann. *Methods Enzymol*. **2010**, 471,161-184.

[39] S.Umoren, M.Solomon. *J.Mater.Sci.***2016,** 1(1), 1-10.

[40] M.S.Lu Feng. Experimental Study of Nucleation in Polystyrene/CO2 System. *J.Mater.Sci.***2012,** 1(1), 45-56.

[41] S.K. Goel, E.J.Beckman. *Polym Eng Sci*. **1993**, 34(14), 1137-1147.

[42] V. Kumar. N.P. Shu. *Polym Eng Sci*. **1990**;30(20), 1323-1329.

[43] K.C.Seavey, Y.A.Liu, N.P Khare, T. Bremner, C.C.Chen. *Ind Eng Chem Res*. **2003**;42(1):5354-5362.

[44] E. Laguna-Gutierrez. *Understanding the Foamability of Complex Polymeric systems by Using Extensional Rheology*. **2016**, PhD Thesis, University of Valladolid, Spain.

[45] M.A.Milani, R. Quijada, N.R.S.Basso, A.P.Graebin, G.B.Galland. *J Polym Sci Part A Polym Chem*. **2012,** 50(17), 3598-3605.

[46] E. Laguna-Gutierrez, A. Lopez-Gil, C. Saiz-Arroyo, R. Van Hooghten, P. Moldenaers, M.A. Rodriguez-Perez. *E.J Polym Res*. **2016**,23(12),251.

[47] H.Münstedt, F.R.Schwarz. *Deformation and Flow of Polymeric Materials*. **2014** Springer: Verlag/Berlin, Germany.

[48] B.Wong, Z.Zhang, Y.P.Handa. *J Polym Sci Part B Polym Phys*. **1998**; 36(12), 2025-2032.

[49] Y.A.Nizhegorodova, N.A.Belov, V.G.Berezkin, Y.P.Yampolskii. *Russ J Phys Chem A*. **2015**, 89(3), 502-509.

[50] H.Guo, V.Kumar. *Polymer (Guildf)*. **2015**, 56,46-56.

[51] J. Pinto, E. Solorzano, M.A. Rodriguez-Perez, J.A. De Saja, *J.Cell.Plast*. **2013**, 49,555-575.

[52] D.W.Mead. *J Rheol (N Y N Y)*. **1994**, 38(6), 1797-1827.

[53] W.Thimm, C.Friedrich, M.Marth, J. Honerkamp. *J Rheol (N Y N Y)*. **1999**, 43(6), 1663-1672.

[54] B.Costello. U*se of Rheology to Determine the Molecular Weight Distribution of Polymers. In : Annual transactions of the Rheology Society ( TA instruments).* **2005**,13.

[55] A.Malkin, A.Y.Malkin. *Rheology Fundamentals*. **1994**, first edition, Chemtech Publishing, Ontario, Canada.

[56] A.Minegishi, A.Nishioka, T.Takahashi, Y.Masubuchi, J.Takimoto, K.Koyama. *Rheol Acta*. **2001**, 40(4), 329-338.

[57] H.Münstedt H. *J Rheol (N Y N Y)*. **1980**, 24(6),847-867.

[58] M.Sugimoto, Y.Masubuchi, J.Takimoto, K.Koyama. *Macromolecules*. **2001**, 34(17), 6056-6063.

[59] L.Zhong, J.Z.Liang, K. Wang. *J Macromol Sci Part B*. **2015** ,54(3), 295-305.

[60] T.G.Fox, P.J.Flory. *J Appl Phys*. **1950,**21(6), 581-591.

[61] K.Ueberreiter, G. Kanig. *J Colloid Sci*. **1952**, 7(6), 569-583.

[62] L.P.Blanchard, J.Hesse, S.L.Malhotra. *Can J Chem*. **1974**, 52(18), 3170-3175.

[63] G.Li, J.Wang, C.B.Park. *Mater. Manuf.Process*. **2006**, 115 (5), 437-443.

[64] Z.Yu, U.Yahsi, J.D.McGervey, A.M.Jamieson, R.Simha. *J Polym Sci Part B Polym Phys*. **1994**, 32(16), 2637-2644.

[65] R.Li, D.Zeng, Q.Liu, Z.Jiang. *Polym Plast Technol Eng*. **2015**, 54(2), 37-41.

66. M.R Holl, V.Kumar, J.L.Garbini, W.R.Murray. *J.Mater.Sci.***1995**, 34, 637-644.

67. Y.D.Hwang, S.W. Cha. *Polym Test*. **2002**, 21(3),269-275.

# Chapter 5

# Sepiolites as cell nucleating agents in PS foams. Analysis of the effects of sepiolites in the foaming mechanisms.

*"Porque eu sou do tamanho do que vejo e não do tamanho da minha altura"*

*Livro do Desassossego,* Fernando Pessoa,

*"Porque yo soy del tamaño de lo que veo, y no del tamaño de mi estatura"*

El libro del Desasosiego, Fernando Pessoa.

# INDEX

## 5.1 Introduction

This chapter contains two scientific works which have been already published in *Journal of Applied Polymer Science* and in *Materials Today*.

In these two works a deeply study has been performed with the objective of analyzing how the sepiolites affect the foaming mechanisms (nucleation, cell growth and cell degeneration) of PS based foams.

Three different kinds of sepiolites have been employed, natural sepiolites (N-SEP) and sepiolites superficially treated with quaternary ammonium salts (O-QASEP) and with silane groups (O-SGSEP). Sepiolites are magnesium silicates with a thickness of few nanometers and a needle-like shape. These particles possess an outstanding sorption capability, which makes them suitable for the absorption of liquids and gases. More information of these nanoparticles can be found in the Chapter 3 of this manuscript. Sepiolites were kindly supplied by the multinational company TOLSA S.A (Spain).

Sepiolites will provide a nucleation effect due to their high aspect ratios. However, this nucleation effect, which could lead to a significant reduction of the cell size and an increase of the cell density, can be only achieved if the particles are well dispersed in the polymer matrix. A bad distribution of the sepiolites in the polymer phase, with several agglomeration points, could deteriorate the final cellular structure of the foams and therefore, their properties.

These works analyze how the dispersion degree of the particles in the polymer matrix is affected by different parameters like the type of sepiolite employed (natural or organo-modified sepiolites), the content of sepiolites, and the process conditions required to produce the blends of PS and sepiolites, particularly the number of extrusion cycles. The dispersion degree was analyzed via shear dynamic rheology and X-ray micro-tomography techniques.

Other parameter that could have a significant effect in the cellular structure is the extensional rheological behavior of the polymer matrix (blend of PS and sepiolites). In this study we have also analyzed the extensional rheological behavior of the different composites to determine their strain hardening. In general, the higher the strain hardening the better for the foaming process especially when it deals on producing low density foams. Polymers presenting a high strain hardening, that is a high melt strength, can resist the expansion during the foaming process without breaking. Consequently, with this kind of polymers it is possible to reduce the degeneration mechanism and to produce

foams with higher expansion ratios, lower cell sizes, lower open cell contents and very homogeneous cellular structures.

The same composites used for the characterization of the dispersion degree and the extensional rheological behavior have been foamed by a gas dissolution process, using $CO_2$ as blowing agent. The obtained foams have been characterized in terms of density and cellular structure. Parameters like the cell size, the cell density, the anisotropy ratio, the cell size distribution, etc. have been carefully evaluated.

By performing these two works it has been possible to stablish a relationship between chemical composition, processing parameters and cellular structure.

## 5.2 Influence of the dispersion of nanoclays on the cellular structure of foams based on polystyrene

This section contains the publication named as: "***Influence of the dispersion of nanoclays on the cellular structure of foams based on polystyrene***". This paper was published in 2021 in **Journal of Applied Science** (A. Ballesteros, E. Laguna-Gutiérrez, P. Cimavilla-Román, M. L. Puertas, A. Esteban-Cubillo, J. Santaren, M. A. Rodríguez-Pérez), 138, 46, *doi:10.1002/app.51373*.

The main goal of this work is to analyze the effects of the particle's surface treatment, clay content and extrusion process in the dispersion degree of blends of PS and sepiolites as well as in the cellular structure of the foams produced from these composites. For this purpose, three different types of sepiolites have been considered: N-SEP, O-QASEP and O-SGSEP. Different formulations were produced using different contents of these sepiolites, varying between 2 wt.% and 10 wt.%. Finally, to analyze the effect of the extrusion process, the formulations were subjected to 1 and 2 extrusion cycles. The dispersion degree was determined by dynamic shear rheology and by X-ray tomography. The foams were produced by a gas dissolution foaming process using $CO_2$ as blowing agent and their cellular structure was characterized by SEM together with image analysis.

Results indicate that sepiolites treated on their surfaces with quaternary ammonium salts (O-QASEP) present a higher dispersibility in the PS matrix than the natural ones (N-SEP) or those modified with silane groups (O-SGSEP). A percolated network is obtained when using 4 wt.% of O-QASEP, 7.5 wt.% of N-

SEP and 9.0 wt.% of O-SGSEP. Regarding the extrusion process, results indicate the multiple extrusion processes have a negative effect on the molecular architecture of the polymer matrix. Moreover, an increase of the number of extrusion cycles do not lead to a better dispersion of the particles in the polymer matrix. When analyzing the cellular structure of the foamed samples it is possible to conclude that sepiolites present an outstanding nucleation capability in PS foams. When using a 6 wt.% of N-SEP, O-QASEP or O-SGSEP, the cell sizes decrease in percentages of 78%, 85% or 71%, respectively, compared to the pure PS foam. Particularly, when using 6 wt.% of O-QASEP it is possible to reduce the cell size up to values as low as 13 μm, while maintaining the foam density.

The main conclusions of this first paper are that the dispersion degree of the sepiolites in PS plays a key factor which determines the nucleation mechanisms and the characteristics of the cellular structure. Furthermore, the sepiolites modified with quaternary ammonium salts are the most adequate nucleating agents when working with A PS matrix. These particles can reduce the cell sizes up to a 85% compared to the pure polymer. In **Figure 5.1** it is possible to see the graphical abstract of this publication.

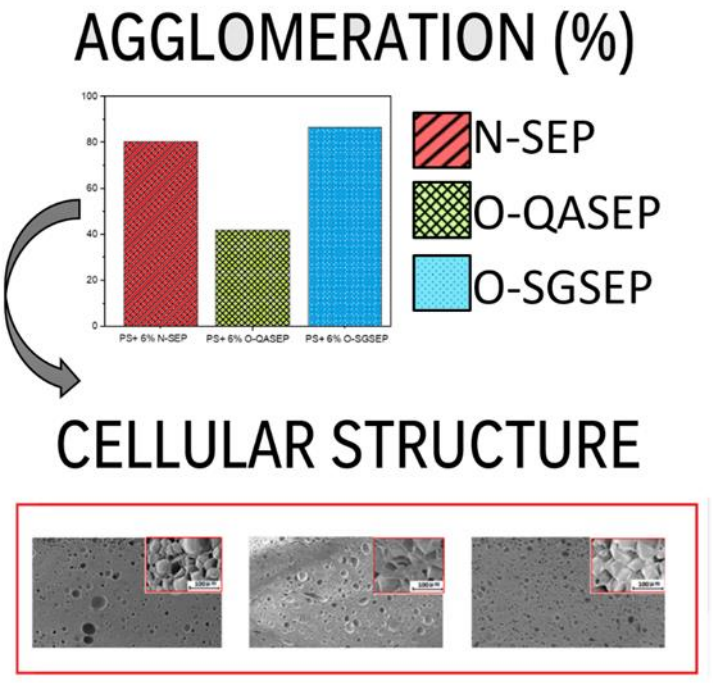


**Figure 5.1.** Graphical abstract of the work "Influence of the dispersion of nanoclays on the cellular structure of foams based on polystyrene".

# Influence of the dispersion of nanoclays on the cellular structure of foams based on polystyrene

A. Ballesteros, E. Laguna-Gutierrez, M. L. Puertas, A. Esteban- Cubillo, J. Santaren. M. A. Rodriguez-Perez

***Cellular Materials Laboratory (CellMat)**, Paseo de Belén, 7, Condensed Matter*

*Physics Department, Science Faculty, University of Valladolid, 47011, Valladolid*

***CellMat Technologies**, Edificio Parque Científico UVa, Paseo de Belén 9-A, 47011, Valladolid, Spain*

***Tolsa SA**, Ctra. Vallecas-Mejorada del Campo (M-203), Madrid.*

## ABSTRACT

In the present work blends of polystyrene (PS) with sepiolites have been produced using a melt extrusion process. The dispersion degree of the sepiolites in the PS has been analyzed by dynamic shear rheology and X-ray micro-computed tomography. Sepiolites treated with quaternary ammonium salts (O-QASEP) are better dispersed in the PS matrix than natural sepiolites (N-SEP) or sepiolites organo-modified with silane groups (O-SGSEP). A percolated network is obtained when using 6.0 wt% of O-QASEP, 8.0 wt% of N-SEP and 10.0 wt% of O-SGSEP. It has been shown that multiple extrusion processes have a negative effect on the polymer architecture. They produce a reduction in the length of the polymeric chains, and they do not lead to a better dispersion of the particles in the polymer matrix. Foams have been produced using a gas dissolution foaming process, where a strong effect of the dispersion degree on the cellular structure of the different foams was found. The effects on the cellular structure obtained by using different types of sepiolites, different contents of sepiolites and different extrusion conditions have been analyzed. The foams produced with the formulations containing O-QASEP present the lowest cell size and the most homogeneous cellular structures.

## KEYWORDS

Polystyrene; Nanocomposites; Shear Rheology; Sepiolites; X-Ray Micro-Tomography.

## 1. INTRODUCTION

Polystyrene (PS) foams are the second largest component of the foam market, after polyurethane (PU) foams, thanks to their low thermal conductivity, lightweight, high compressive strength, high resistance to moisture and medium to high tensile strength.[1, 2] Among the different varieties of PS foams expanded PS (EPS) or extruded PS (XPS) are the used as thermal insulators. The possibility of using $CO_2$ as the primary blowing agent to produce XPS foams, replacing ozone-depleting blowing agents (fluorocarbons or chlorofluorocarbons), has conferred PS foams a privileged place in the thermal insulation market.[2] For XPS foams with densities around 30 kg/m$^3$ the thermal conductivity varies between 33 and 35 mW/mK, which is still higher than the thermal conductivity of rigid PU foams (around 23–26 mW/mK, for the same density).[3]

A strategy to improve the thermal, electrical, and mechanical properties of foams consists of incorporating nanoparticles into the polymer matrix.[4-6] The blending of polymeric foams and functional nanoparticles generates a class of materials known as cellular nanocomposites. Cellular nanocomposites combine the advantages of having a cellular structure with the multifunctional effects provided by the nano-particles.[7] On the one hand, particles have an important effect on the microscale properties, improving characteristics of the cellular structure and consequently, they also have a macroscopic effect on some physical properties like thermal or mechanical ones.[5, 8] Nucleation can be modified by the presence of a small amount of well-dispersed nanoparticles leading to lower cell sizes and higher cell nucleation densities.[9] Furthermore, nanoparticles can also modify the extensional rheological properties of the polymer matrix, which have an important effect on the degeneration mechanisms and, as a consequence, on the cell size, cellular structure homogeneity and foam density.[10-12] Chen et al. demonstrated that foams with regular and homogeneous cellular structures present improved mechanical properties.[13] Moreover, it is known that thermal conductivity strongly depends on some parameters of the cellular structure such as cell size or porosity.[11] Therefore, nanoparticles could change the thermal aspects of the foams dramatically by decreasing considerably their thermal conductivity.[12]

The effects of incorporating nanoparticles into PS foams have been analyzed by several authors. Zhang et al. showed that the thermal insulation performance of PS foams was improved when introducing activated carbon nanoparticles.[14] Han et al. showed that nanoclays in a PS matrix it was possible to produce foams with lower cell sizes and higher cell densities. These cellular composites exhibited higher tensile modulus, better fire retardance, and better barrier properties than

the pure PS foam.[15] Kaynak et al. demonstrated that the inclusion of just 5% of montmorillonites combined with some usual phosphate flame retardants produced a synergistic effect leading to a reduction of the flammability of the polymer.[16] Finally, Shen et al. claimed that the incorporation of carbon nanofibers to PS foams created a protective layer around the cell walls that resulted in the enhancement of foam strength.[17]

However, research efforts are still necessary to thoroughly understand the role of nanoparticles and the importance of having a suitable dispersion to obtain the desired properties. Only when the dispersion degree of the particles in the polymeric matrix is optimal, it is possible to increase the cell density and reduce the cell diameter, with respect to the pure polymeric foams.[18]

Due to the role that nano-particles play in the microscopic and macroscopic properties it is not difficult to understand why they have aroused a large interest in the scientific community.[19-22] Most of the papers dealing with nano-particles are based on the use of particles with spherical or layered morphologies.[13] For example, montmorillonites, silica or nano-porous silica particles have been widely used in PS foams.[23-25] However, it is not simple to find in literature studies analyzing the effects that needle-like shape particles, like sepiolites, have on the final structure of foams.[21, 26-29] In fact, only one conference paper has been found. In this work, Notario et al. reported that it was possible to reduce, in a 60%, the cell size of PS foams by adding 0.5 wt% of sepiolites.[30] However, this paper does not provide a systematic study of how the dispersion degree of these particles affects the cellular structure of the foams.

Among all the needle-like shape particles available, sepiolites have been selected for this research work due to several reasons. On the one hand, sepiolites ($Si_{12}Mg_8O_{30}(OH)_4(OH_2)_4 \cdot 8H_2O$), which are natural fibrous clays, present outstanding sorption and rheological properties.[31, 32] On the other hand, the structural characteristics of sepiolites favor their dispersibility in the polymer matrix. The structure of sepiolites consists of blocks of two tetrahedral silica sheets sandwiching an octahedral sheet of magnesium oxide-hydroxide (more information about the structure of the sepiolites can be found in the work of Tian et al.[33]). The dimensions of the cross-section tunnels are about 0.36 nm × 1.1 nm. The discontinuity of the silica sheets allows the presence of a significant number of silanol (Si–OH) groups on the surface of the particles. The existence of silanol groups can enhance the interfacial interaction between the nanoparticles and the polymer and therefore, they could help to improve the dispersion of the sepiolites

in the polymeric matrix. Finally, due to their high aspect ratio (thicknesses in the nanometric scale, between 20 and 30 nm, average particle length ranging among 1 and 2 μm and large surfaces areas ~300 $m^2/g$), sepiolites are very interesting particles for being used as cell nucleating agents in thermoplastic foams. Bernardo et al. concluded that when incorporating 1.5 wt.% of sepiolites organomodified with quaternary ammonium salts in a matrix of polymethyl methacrylate (PMMA) the cell size decreases by a factor of five and the cell nucleation density increases in a factor of 160.[21] Additionally, the inclusion of sepiolites can modify several properties of the polymer matrix like the behavior of the material against fire and its mechanical and thermal properties.[34-40]

The present work aims to analyze the dispersion of different types of sepiolites in a PS matrix as well as the effect of the dispersion degree on the cellular structure of PS foams produced by a gas dissolution foaming process. This systematic study has been performed by evaluating, on the one hand, the importance of modifying the surface of sepiolites to ensure a proper interaction between the particles and polymer. For this purpose, natural sepiolites and sepiolites organo-modified with quaternary ammonium salts and silanol groups have been considered. The selection of quaternary ammonium salts and silanol groups was performed considering the results obtained in previous works in which both treatments were used to improve the interaction between these particles and a polymer matrix.[21, 41-43] On the other hand, composites containing different amounts of sepiolites have been produced to evaluate the influence of the content of sepiolites on the dispersion degree and to determine the percolation threshold. Finally, different extrusion conditions have been used to produce the PS based composites. In particular, the number of extrusion cycles has been modified. Finally, the composites produced with 6 wt% of sepiolites have been foamed by the gas dissolution foaming process. The cellular structure of these foamed samples has been analyzed and the obtained results have been related to the results obtained after the dispersion analysis.

## 2. EXPERIMENTAL

### 2.1 Materials

A commercial PS, recommended for foam applications, (INEOS, Styrolution PS153F) with a melt flow index of 7.5 g/10 min (200°C/5 kg) and a glass transition temperature (Tg) of 102°C was used as polymer matrix. Three kinds of sepiolites, kindly supplied by Tolsa S.A. (Madrid, Spain), were used in this work. They can be distinguished between non-organically modified sepiolites (labeled as N-

SEP), sepiolites organically modified with quaternary ammonium salts (O-QASEP) and sepiolites organically modified with silanol groups (O-SGSEP). An antioxidant (BASF, Irganox 1010) was also used to reduce thermal degradation during the extrusion stage.

### 2.2 Production Process

A wet milling process was used to obtain separated sepiolites from the starting sheaf-form in which particles appear naturally. The procedure of the wet milling and surface treatment of the particles was performed as it was described in a previous work.[43]

Before the extrusion process, the materials were dried in a vacuum oven (Mod. VacioTem TV, P-Selecta) at 70°C for 4 h, in the case of pure PS, and at 80°C for 8 h in the case of the different types of sepiolites. The mixing of the polymer with the sepiolites was carried out in a twin-screw extruder (Collin ZK 25 T with L/D of 24) following a temperature profile that goes from 145 to 185°C (at the die of the extruder) and with a screw rate of 50 rpm. Some amount of this material was re-extruded, once again, under the same conditions, to analyze how the number of extrusion cycles affects the dispersion of the sepiolites in the PS matrix. The pure PS was also submitted to different extrusion cycles to analyze how the rheological behavior of the polymer is affected by the extrusion process. The different formulations produced in this work are shown in **Table 1**. Formulations containing 2, 6, 8, and 10 wt.% of the different types of sepiolites were fabricated to evaluate the effects of changing the content of the particles in their dispersibility.

**Table 1**. Formulations produced and characterized during the present study.

| Sample Name | Content of Polymer (wt.%) | Content of Sepiolites (wt.%) | Content of Antioxidant (wt.%) |
|---|---|---|---|
| **Pure PS** | 99.5 | 0.0 | 0.5 |
| **PS+2% N-SEP** | 97.5 | 2.0 | 0.5 |
| **PS+2% O-QASEP** | 97.5 | 2.0 | 0.5 |
| **PS+2% O-SGSEP** | 97.5 | 2.0 | 0.5 |
| **PS+6% N-SEP** | 93.5 | 6.0 | 0.5 |
| **PS+6% O-QASEP** | 93.5 | 6.0 | 0.5 |
| **PS+6% O-SGSEP** | 93.5 | 6.0 | 0.5 |
| **PS+8% N-SEP** | 91.5 | 8.0 | 0.5 |
| **PS+8% O-QASEP** | 91.5 | 8.0 | 0.5 |
| **PS+8% O-SGSEP** | 91.5 | 8.0 | 0.5 |

| | | | |
|---|---|---|---|
| **PS+10% N-SEP** | 89.5 | 10.0 | 0.5 |
| **PS+10% O-QASEP** | 89.5 | 10.0 | 0.5 |
| **PS+10% O-SGSEP** | 89.5 | 10.0 | 0.5 |

*Note*: All formulations have been subjected to one and two extrusion cycles.

The different formulations were later thermoformed in a hot-cold plate press to obtain materials with the desired shape and size. The compression molding process was carried out at a temperature of 235°C and at a pressure of 27 bars.

The foaming of the samples was carried out using the solid-state gas dissolution foaming method.[44] For this purpose, a high-pressure vessel (model PARR 4681), provided by Parr Instrument Company, with a capacity of 1 L and capable of operating at a maximum temperature of 350°C and at a maximum pressure of 41 MPa was used. The reactor is equipped with a pressure pump controller (model SFT-10), provided by Supercritical Fluid Technologies Inc., which is controlled automatically to keep the pressure on the desired values. The pressure vessel is also equipped with a clamp heater of 1500 W where the temperature is controlled via a CAL 3300 (from CAL controls) temperature controller. The foaming process was performed in two steps.[45] Samples were firstly introduced in the pressure vessel at 8 MPa of $CO_2$ pressure for the saturation stage. The saturation temperature was 40°C and the saturation time was 24 h. It was experimentally proved that this time is enough to achieve full saturation of $CO_2$ in PS at the conditions under study. After saturation, the pressure was abruptly released. Finally, for the foaming stage, samples were removed from the pressure vessel and introduced in a thermostatic silicon bath at 120°C for 1 min. The time between the release of the pressure and the immersion in the thermal bath was 2 min. Once the materials were expanded, they were cooled down in water to stabilize their cellular structure.

## 2.3 Characterization

### *2.3.1 Dynamic Shear Measurements*

A shear stress-controlled rheometer (AR 2000 EX from TA Instruments) was used to measure the dispersion degree of the different formulations. Dynamic shear measurements were conducted at a temperature of 220°C, under a nitrogen atmosphere, and using 25 mm diameter parallel plates. A fixed gap of 1 mm was selected to perform the rheological measurements.

First a strain sweep test, at a fixed dynamic frequency (1 rad $s^{-1}$), was performed to determine the linear viscoelastic regime of the different nanocomposites. Later,

a time sweep was performed to recover the initial state of the particle network, which was partially deformed when the sample was loaded in the rheometer. The duration of the time sweep varied between 360 and 600 s, depending on the material. Finally, the frequency sweep step was performed, in a range of angular frequencies varying between 0.01 and 100 rad $s^{-1}$. From these measurements, four parameters were analyzed: dynamic shear viscosity ($|\eta^*|$), storage modulus ($G'(\omega)$), loss modulus ($G''(\omega)$), and crossover frequency ($\omega_x$). Furthermore, the Mark-Houwink Sakurada equation, which relates the complex viscosity with the molecular weight, was used to estimate the molecular weight of the polymer matrix.[46]

### *2.3.2 X-Ray Micro-Computed Tomography*

The set-up employed to perform the micro-computed tomography experiments consisted of a micro-focus cone-beam X-ray source L10101 from Hamamatsu (spot size: 5 μm, voltage: 20–100 kV, current: 0–200 μA) with a maximum output power of 20 W and a high sensitivity flat panel detector C7940DK-02 also from Hamamatsu (2240 × 2344 pixels, 50 μm of pixel size). In addition, a rotation stage was mounted on a linear stage which enables movement between the source and detector and permits varying the magnification factor.[47]

The linear stage was placed in a position so that the magnification value was ×20, leading to a pixel size of 2.5 μm. A tube voltage of 55 kV and a current of 170 μA were selected for the measurements. The detector exposure time was 1000 ms and the rotation step was 0.3°. To enhance the contrast in the reconstructed images, each projection was the result of integrating three consecutive images.

Once all the projections were acquired, the reconstruction process of the tomogram was carried out using Octopus, server/client reconstruction package.[48]

Due to the limited spatial resolution of the tomographic system (2.5 μm), the reconstructed slices can be used to analyze the number of agglomerates of particles present in the solid PS nanocomposites. The isolated sepiolites present sizes that are between 1 and 2 μm and with this X-ray experiment only particles with sizes higher than this 2.5 μm can be detected. Therefore, the particles observed in this experiment are agglomerations of the primary sepiolites particles. This method to determine the agglomerates of sepiolites has been applied in other works, like the one performed by Bernardo et al.[49]

To calculate the number of agglomerates of particles, a tomographic volume of 1.25 × 2.50 × 3.50 $mm^3$ has been considered. Firstly, two consecutive 3D filters

have been applied in the reconstructed slices. In addition, a 3D median filter (two pixels of radius) has been applied to remove noise from the images and later, a 3D maximum filter (one pixel of radius) has been computed to enhance the particles gray level intensity. Then, the particles have been binarized by means of a thresholding process based on the different level of absorption between polymer and fillers. The percentage of agglomerates in the sample has been calculated according to (**Equation (1)),** by measuring the volume fraction occupied by the agglomerates ($\%V_{sep}$) and considering the real mass fraction of particles in the sample (($\%m_{sep}$).

$$\text{Agglomerates (\%)} = \frac{\frac{\rho_{sep} \cdot \%V_{sep}}{\rho_{solid}}}{\%m_{sep}} \quad [1]$$

where ($\rho_{sep}$) is the theoretical density of the sepiolites (2.1 g/cm$^3$) and ($\rho_{solid}$) represents the density of the solid nanocomposite, which was measured by gas pycnometry.

### *2.3.3 Gas Uptake*

The gravimetric method has been used to measure the gas absorbed during the saturation stage. By using this method, the gas absorbed is obtained directly from determining the weight gain by the polymer sample during the sorption stage. It consists of calculating the ratio between the difference in the sample weight before and after the saturation process and the initial weight of the composite. This ratio provides the percentage of the CO2 absorbed by the composite, as can be seen in (**Equation (2)).**

$$CO_2\text{Uptake} = \frac{W_s - W_0}{W_0} \quad [2]$$

where $W_s$ is the weight after saturation and $W_0$ is the initial weight.

### *2.3.4 Density*

The density of the solid precursors was analyzed using a gas pycnometer (Accupyc II 1340 from Micromeritics). The density of the cellular materials, which were produced using the gas dissolution foaming process, was determined by the geometric method, that is, dividing the corresponding mass of each specimen by its geometric volume (ASTM standard D1622-08). The foamed samples used to determine the density have a cylindrical shape with a diameter of 7.5 cm and a thickness of 6 mm. The following equations (**Equations (3) and (4)**) show the way of determining the relative density ($\rho_r$) and expansion ratio (E). Relative density is defined as the ratio between the density of the foam ($\rho_{foam}$) and the

density of the bulk solid material ($\rho_{solid}$). On the other hand, the expansion ratio is defined as the inverse of the relative density.

$$\rho_r = \frac{\rho_{foam}}{\rho_{solid}} \quad [3]$$

$$\mathrm{E} = \frac{1}{\rho_r} \quad [4]$$

### 2.3.5 Open Cell Content

To evaluate the open cell content of the samples, according to the Standard ASTM D6226-10, see (**Equation 5**), a gas pycnometer Accupyc II 1340 from Micromeritics was used.

$$OC(\%) = 100\left(\frac{v_{geometric} - v_{pycnometer}}{p.V_{geometric}}\right) \quad [5]$$

where $v_{geometric}$ is the geometric volume of the sample, $v_{pycnometer}$ is the volume of the sample obtained with the pycnometer and $p$ is the porosity calculated as $(1 - \frac{\rho_{foam}}{\rho_{solid}})$.

### 2.3.6 Cellular Structure

The structure of the cellular materials, produced by gas dissolution foaming, was analyzed with a scanning electron microscope (SEM) (Jeol, Mod. JSM-820). Parameters such as the average cell size (Φ), and the cell nucleation density ($N_0$) were analyzed with an image processing tool based on the software Fiji/Image J.50 More than 100 cells of different regions of each cellular material have been considered to determine these parameters.

The average cell size is defined as it is indicated in (**Equation 6**).

$$\phi = \sum_{i=1}^{n} \frac{\phi_i}{n} = \sum_{i=1}^{n} \frac{cf}{2n}(\phi_x^i + \phi_y^i) \quad [6]$$

Where $n$ is the total number of cells counted in the image, $\phi_i$ is the three-dimensional value of the cell size for and specific cell. $\phi_x^i$ and $\phi_y^i$ are the chord lengths of the cells in the directions x and y, respectively and $cf$ is a correction factor used to convert the two-dimensional value of the cell size to a three-dimensional value. As it was indicated in the work of Pinto et al. a value of 1.273, has been selected for the mentioned correction factor.[50]

The cell nucleation density ( $N_0$), defined as the number of cells per unit volume of the solid, was obtained using the Kumar's theoretical approximation represented in (**Equation 7**).[45] In this formula ($N_v$) is the cell density, defined as the number of cells per cubic centimeter of the foamed material, and ($\rho_r$) is the relative density (see **Equation 3**).

$$N_0 = \frac{N_v}{\rho_r} \quad [7]$$

In this work, the cellular materials containing sepiolites present a bimodal structure showing small cells, combined with large cells, those with a size higher than 200 μm. Although, the number of large cells is lower than the number of small cells, the volume occupied by the large cells is not negligible. For this reason, to quantify the observed bimodality the relative volume fraction occupied by the small cells is defined as it is indicated in (**Equation 8**).

$$v_s = 100 \cdot \frac{A_t - A_l}{A_t} \quad [8]$$

where $A_l$ is the observed area occupied by the large cells in the SEM images and $A_t$ the total area of the image. In the pure PS foams, which do not present a bimodal structure, this parameter was not calculated, and it was considered as zero.

Finally, the ratio between the standard deviation of the cell size (SD) and the average value of the cell size ($SD/\phi$), allows analyzing the homogeneity of the cellular structure. Low values of this parameter are related to a homogeneous cellular structure with a narrow cell size distribution.

Only the small cells were considered for the determination of the different parameters: cell size, cell nucleation density and $SD/\phi$.

## 3. RESULTS

### 3.1 Analysis of the dispersion degree by shear rheology

The values of the zero-shear viscosity, the slopes of the storage modulus and loss modulus and the number of crossover points between the curves corresponding to the loss and storage moduli have been analyzed for the different formulations.

#### *3.1.1. Effect of the Types of Particles*

In this section, the study is focused on materials produced with different types of sepiolites: N-SEP, O-QASEP, and O-SGSEP. Therefore, for comparative purposes, the content of particles has been fixed (6 wt.%) as well as the production conditions (one single extrusion cycle).

**Figure 1** shows the behavior of the complex viscosity ($|\eta^*|$), the storage modulus $G'(\omega)$, and the loss modulus $G''(\omega)$, as a function of the angular frequency for the pure PS and for the three types of composites. Figure 1(a) shows an increase in the complex viscosity values of the formulations containing sepiolites with respect to the pure PS. This increment is chiefly remarkable in the formulation containing O-QASEP. Moreover, in this composite the Newtonian plateau,

observed with the other materials at low frequencies, disappears and the behavior corresponds to that of a non-Newtonian power law material.

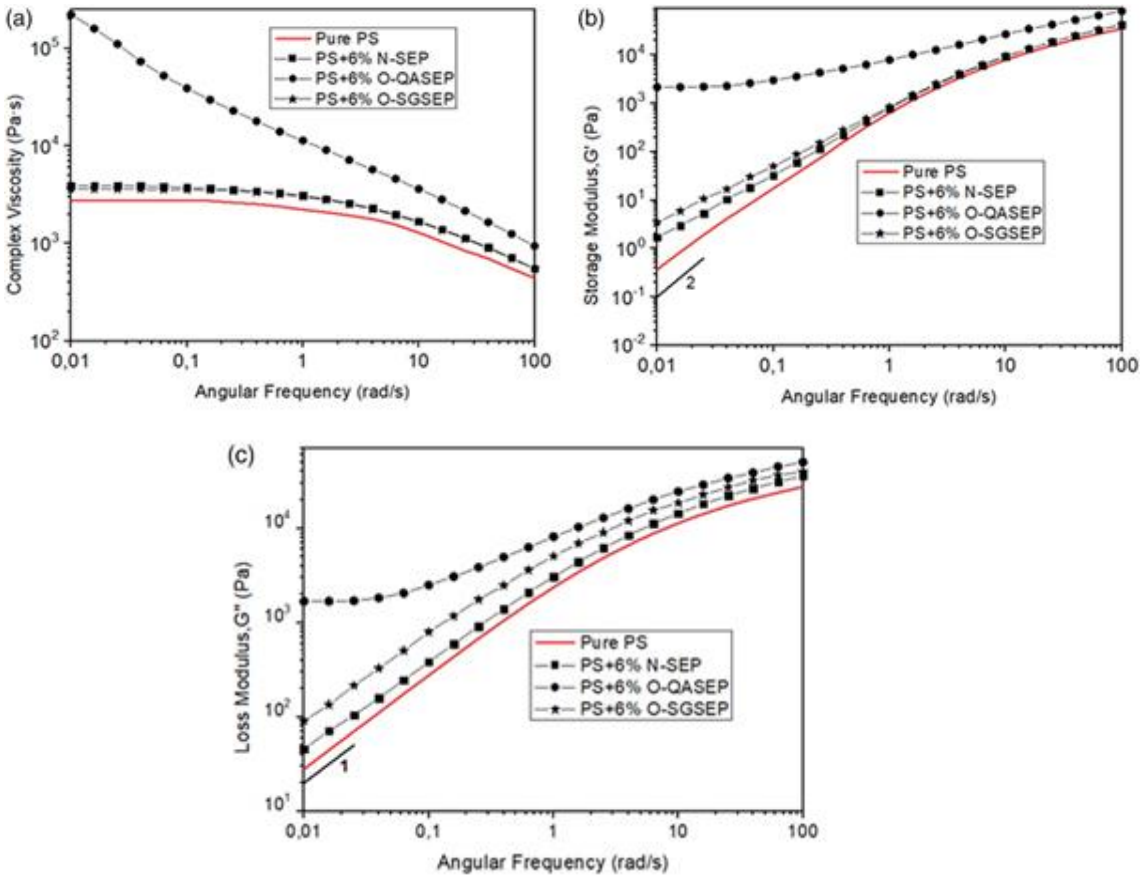


**Figure 1.** Viscoelastic properties for the pure PS and the different composites produced with a fixed content of sepiolites (6 wt.%). All formulations were produced using one single extrusion cycle. (a) Complex viscosity versus angular frequency. (b) Storage modulus versus angular frequency. (c) Loss modulus versus angular frequency. Common slopes values for a pure polymer are also shown in (b, c).

For the materials presenting a Newtonian-plateau, the zero-shear viscosity ($\eta_0$) is determined as the value of the viscosity in the Newtonian-plateau. The results of zero-shear viscosity are collected in **Table 2**. Results indicate that the composites present a higher zero-shear viscosity than the pure PS.

**Table 2**. Linear viscoelastic properties of the pure PS and the different composites containing 6 wt.% of different types of sepiolites, all of them subjected to a single extrusion process.

| Sample Name | Zero Shear Viscosity, $\eta_0$ (Pa·s) | Slope of G' (Pa·s) | Slope of G'' (Pa.s) | Crossover Frequency, $\omega_x$ (rad/s) |
|---|---|---|---|---|
| **PURE PS** | 2905 | 1.78 | 0.96 | 42.29 |
| **PS+6% N-SEP** | 3839 | 1.27 | 0.95 | 41.18 |

| | | | | |
|---|---|---|---|---|
| **PS+6% O-QASEP** | NON-NEWTONIAN | 0.67 | 0.75 | 3.67/28.67 |
| **PS+6% O-SGSEP** | 3498 | 1.32 | 0.92 | 42.16 |

Storage modulus $G'(\omega)$ is altered by variations in the molecular structure of polymers. At low frequencies, in the area called terminal region, where the longest relaxation times play a major role, the storage modulus is usually proportional to the square of the frequency $G' \propto w^2$.[51] To quantify the changes in the storage modulus, the slopes of the $G'$curves in the terminal region (between 0.01 and 0.1 rad/s) were measured. The obtained results are collected in Table 2. For the pristine polymer, it is expected that the slope of $G'$presents a value close to 2. As soon as the density of particles increases, the slope should approach to 1. Finally, when the formulations are reaching the percolation state or they are completely percolated, the slope of $G'$should present values approaching to 0.[52] It is important to mention that the density of particles can increase due to two main reasons. On the one hand, the density of particles increases if the content of particles introduced in the polymeric matrix increases. On the other hand, the density of particles increases if the content of particles is fixed but the particles are dispersed in a more efficient way. Therefore, in systems in which the number of particles is fixed, a reduction of the slope of $G'$ is related with an increment of the dispersion degree. Figure 1(b) shows the differences between the curves of the formulations containing particles and that of the pure polymer. These differences are mainly remarkable in the slopes of the curves in the terminal region, which are clearly reduced in the systems containing particles. A reduction of 29% of the slope of $G'$is achieved when adding 6 wt.% of N-SEP. Meanwhile, a reduction of the slopes of $G'$ of 62% and 26% is obtained when adding 6 wt.% of O-QASEP and 6 wt.% of O-SGSEP, respectively. Furthermore, as it is indicated in Table 2, the slope of $G'$corresponding to the composite containing 6 wt.% of O-QASEP particles presents a value close to 0, which indicates that, for this kind of sepiolites, this content is close to the percolation threshold.

On the other hand, the loss modulus, $G''(\omega)$, of a pure polymer should be proportional to the frequency in the terminal region $G'' \propto w$.[51] The effect of the type of particles in the loss modulus is shown in **Figure 2(**c). The slopes of $G''$ in the terminal region have been also calculated and the obtained values are shown in Table 2. The slopes of $G''$ for the systems containing N-SEP or O-SGSEP are like that of the pure polymer. However, the value for the material containing O-QASEP is much lower. A reduction of 21% is reported indicating, once again, a much better dispersion of this type of particles in the PS matrix.

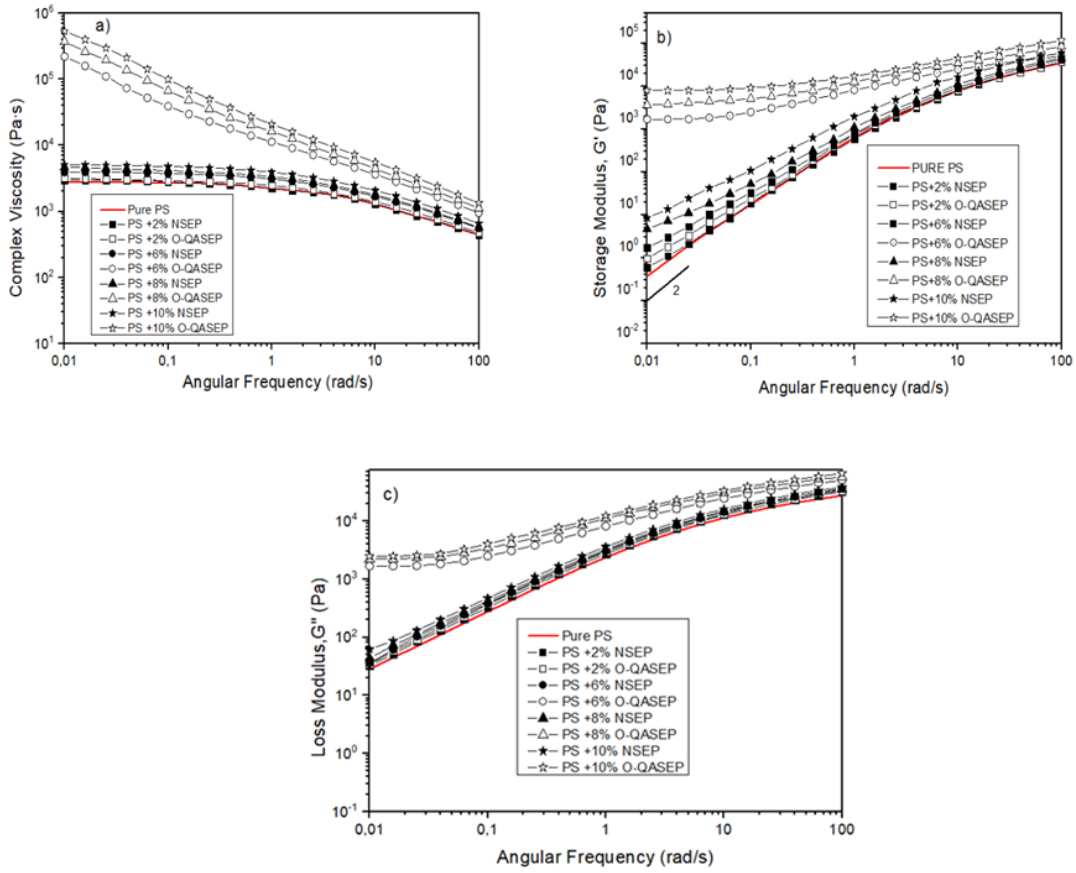


**Figure 2:** Viscoelastic properties for the pure PS and the blends of the polymer with different contents of N-SEP and O-QASEP. All the formulations were produced with one extrusion cycle. (a) Complex viscosity versus angular frequency. (b) Storage modulus versus angular frequency. (c) Loss modulus versus angular frequency. Common slopes values for a pure polymer are also shown in figures (b) and (c).

The crossover frequency ($w_x$) has been also measured (see Table 2). This parameter is defined as the frequency at which the storage modulus $G'(\omega)$ and the loss modulus $G''(\omega)$ intersect. The presence of one single crossover point indicates that the material is not already percolated.[52] On the other hand, the presence of two crossover points indicates that the density of particles is close to the percolation threshold. Finally, a spectrum in which no crossover points appear implies that the density of particles is higher than the percolation threshold.[52] The data collected in Table 2 show that the composites produced with 6 wt.% of N-SEP and with 6 wt.% of O-SGSEP only show a single crossover point, which indicates that in these materials a network structure has not been formed. Meanwhile, for the material produced with 6 wt.% of O-QASEP two crossover points have been obtained, which indicates that this composite presents a percolated structure.

Furthermore, the crossover frequencies of the storage and loss modulus curves shift to lower frequencies thanks to the inclusion of particles. This behavior indicates that the composites remain in a solid-like behavior for a wider region of frequencies. In other words, the dynamic oscillatory shear measurements indicate that the incorporation of sepiolites to a PS matrix modifies the long-time relaxation behavior of the polymer by increasing the relaxation time due to the formation of a three-dimensional network structure.[53] Kotsilkova et al. suggested in their work that longer relaxation times indicate that the structure of the nanocomposite is creating a significant energetic barrier against the molecular motion during the shear flow.[54]

With all the information collected it is possible to conclude that only the formulation containing 6 wt.% of O-QASEP is already percolated. Moreover, the rheological results also indicate that O-QASEP presents a much better dispersion degree. On the other hand, the formulations containing N-SEP and O-SGSEP exhibit a rheological behavior that is like that of the pure PS matrix, which indicates a poor dispersion of these particles in the polymer matrix.

### *3.1.2. Effect of the Content of Particles*

This section analyzes the effects on the rheological behavior produced by changing the content of particles. The percentages of particles introduced in the polymer are the following ones: 2, 6, 8, and 10 wt.%. All the data showed in this section belongs to blends produced in a single extrusion process.

Figure 2 (a) shows the effect of changing the content of particles on the complex viscosity. Only the particles which lead to the most promising results have been included in this figure, On the other hand, in **Table 3**, the data corresponding to the three types of particles are reported: N-SEP, O-QASEP, and O-SGSEP. For blends containing N-SEP, the complex viscosity slightly increases as the content of particles increases. For example, the zero-shear viscosity increases 0.3% and 32%, with respect to the pure PS, when incorporating 2 and 6 wt.% of N-SEP, respectively. However, the presence of a non-Newtonian power law behavior in the terminal region is only observed when high amounts of particles are introduced in the system (8 and 10 wt.%). On the other hand, the inclusion of O-QASEP, in percentages similar or higher than 6 wt.%, leads to a significant modification of the structure of the material. Finally, with the O-SGSEP particles the viscosity increases 0.2%, 20%, and 62%, compared to the neat material, when introducing 2, 6, and 8 wt.% of particles, respectively. Therefore, it is necessary to incorporate contents close to 10 wt.% to create a percolated network when

using these O-SGSEP particles. Due to the change perceived from a Newtonian to a non-Newtonian power law regime in the terminal region of complex viscosity and with the data collected in Table 3, it is possible to assert that the percolation state is reached when incorporating 6 wt% of O-QASEP, 8 wt% of N-SEP and 10 wt% of O-SGSEP.

**Table 3.** Linear viscoelastic properties of the pure PS and the composites containing 2, 6, 8, and 10 wt% of N-SEP, O-QASEP, and O-SGSEP

| Sample Name | Zero Shear Viscosity, $\eta_0$ (Pa·s) | Slope of G' (Pa·s) | Slope of G'' (Pa.s) | Crossover Frequency, $\omega_x$ (rad/s) |
|---|---|---|---|---|
| **PURE PS** | 2905 | 1.78 | 0.96 | 42.29 |
| **PS+2% N-SEP** | 2916 | 1.48 | 0.97 | 42.26 |
| **PS+2% O-QASEP** | 2943 | 0.82 | 0.94 | 41.15 |
| **PS+2% O-SGSEP** | 2912 | 1.52 | 0.98 | 42.89 |
| **PS+6% N-SEP** | 3839 | 1.27 | 0.95 | 41.18 |
| **PS+6% O-QASEP** | NON-NEWTONIAN | 0.67 | 0.75 | 3.67/28.67 |
| **PS+6% O-SGSEP** | 3498 | 1.32 | 0.92 | 42.16 |
| **PS+8% N-SEP** | NON-NEWTONIAN | 0.57 | 0.67 | 2.16/25.67 |
| **PS+8% O-QASEP** | NON-NEWTONIAN | 0.16 | 0.44 | No Crossover Points |
| **PS+8% O-SGSEP** | 4726 | 1.15 | 0.89 | 39.24 |
| **PS+10% N-SEP** | NON-NEWTONIAN | 0.07 | 0.42 | No Crossover Points |
| **PS+10% O-QASEP** | NON-NEWTONIAN | 0.05 | 0.39 | NO CROSSOVER POINTS |
| **PS+10% O-SGSEP** | Non-Newtonian | 0.46 | 0.54 | 2.15/23.14 |

*Note*: The composites were subjected to a single extrusion process.

Both the storage modulus, $G'(\omega)$, and loss modulus, $G''(\omega)$ increase when the content of particles increases, as it can be seen in Figure 2(b,c), respectively. From the values of the slopes of $G'$and $G''$, collected in Table 3, it is possible to conclude that the slopes decrease when the content of particles increases. For instance, a reduction of the slopes of $G'$of 53%, 62%, 91% and 97%, with respect to the pure PS, is reached for the formulations containing 2, 6, 8, and 10 wt.% of O-QASEP, respectively. Furthermore, the slopes of the two moduli, in the terminal region, of the samples presenting a Newtonian plateau (2 and 6 wt.% of N-SEP, 2 wt.% of O-QASEP and 2, 6, and 8 wt.% of O-SGSEP) are closed to 1. Moreover, the storage modulus and loss modulus of these last formulations intersect in a single crossover point, which indicates that in these materials a percolated network structure has not been formed. On the contrary, the formulations containing

contents similar or higher than 6 wt.% of O-QASEP, 8 wt.% of N-SEP and 10 wt.% of O-SGSEP present slopes of $G'$ and $G''$ that approach to 0.

The theoretical percolation threshold ($\phi_{per}$) has been determined. To obtain this parameter the following (**Equation 9**) has been used.[55]

$$G' = C(\phi_c - \phi_{per})^n \quad [9]$$

where $C$ is a constant, $n$ is a power law exponent, $\phi_c$ is the clay volume fraction, $\phi_{per}$ is the percolation threshold volume fraction and $G'$ is the value of the storage modulus at low frequencies. The value of $\phi_{per}$ is obtained by fitting to a linear regression the curve $\log(G')$ versus $\log(\phi - \phi_{per})$ . This procedure is done for different values of $\phi_{per}$. This equation can be used only in the proximities of the percolation threshold.[56] Finally, the value of $\phi_{per}$ for which the best fit is obtained is considered as the percolation threshold of the composite. In the system that contains O-QASEP particles a value of the percolation threshold of 4.0 wt% was obtained. This value was 7.5 wt% for the system containing N-SEP and 9.0 wt.% for the system containing O-SGSEP.

Finally, it is essential to mention that the crossover points between $G'$ and $G''$ change from 1 single point to 2 points or even to 0 points depending on the type and content of particles. Table 3 summarizes this behavior. The formulations containing 2 and 6 wt.% of N-SEP, 2 wt.% of O-QASEP and 2, 6, and 8 wt.% of O-SGSEP present only a single crossover point, which indicates that in these formulations the percolation threshold is not reached. Meanwhile, the formulations containing 8 wt.% of N-SEP, 6 wt.% of O-QASEP and 10 wt.% of O-SGSEP present two crossover points and hence, it can be concluded that they are close to the percolation threshold. Finally, the materials containing 10 wt.% of N-SEP and 8 and 10 wt.% of O-QASEP do not present any crossover point, which indicates that these contents of particles are higher than the percolation threshold. Furthermore, when the particles are introduced in the polymer it is also possible to observe a shifting effect of the crossover point to lower frequencies. It is remarkable the shifting of 13.62 rad/s in the case of the formulation containing 6 wt.% of O-QASEP.

### *3.1.3. Effect of the Extrusion Process*

In this section, the effects on the dispersion degree associated to produce the composites by using one or two extrusion cycles are analyzed. Moreover, these effects have been also studied in the pure PS to analyze the importance of comparing materials with the same thermo-mechanical history.

Figure 3 shows the complex viscosity ($|\eta^*|$), the storage modulus ($G'(\omega)$) and the loss modulus ($G''(\omega)$) for the pure PS after zero (raw material as received), one and two extrusion cycles. **Figure 3(a)** shows the effect of the number of extrusion cycles on the complex viscosity. The material with the highest value of the zero-shear viscosity ($\eta_0$) is the one that has not been extruded. The zero-shear viscosity of the non-extruded pure PS material is 5% and 10% higher than that of the PS after one and two extrusion cycles, respectively (see **Table 4**). On the other hand, no important differences are detected between the curves of $G'$ and $G''$, for the three PS samples.

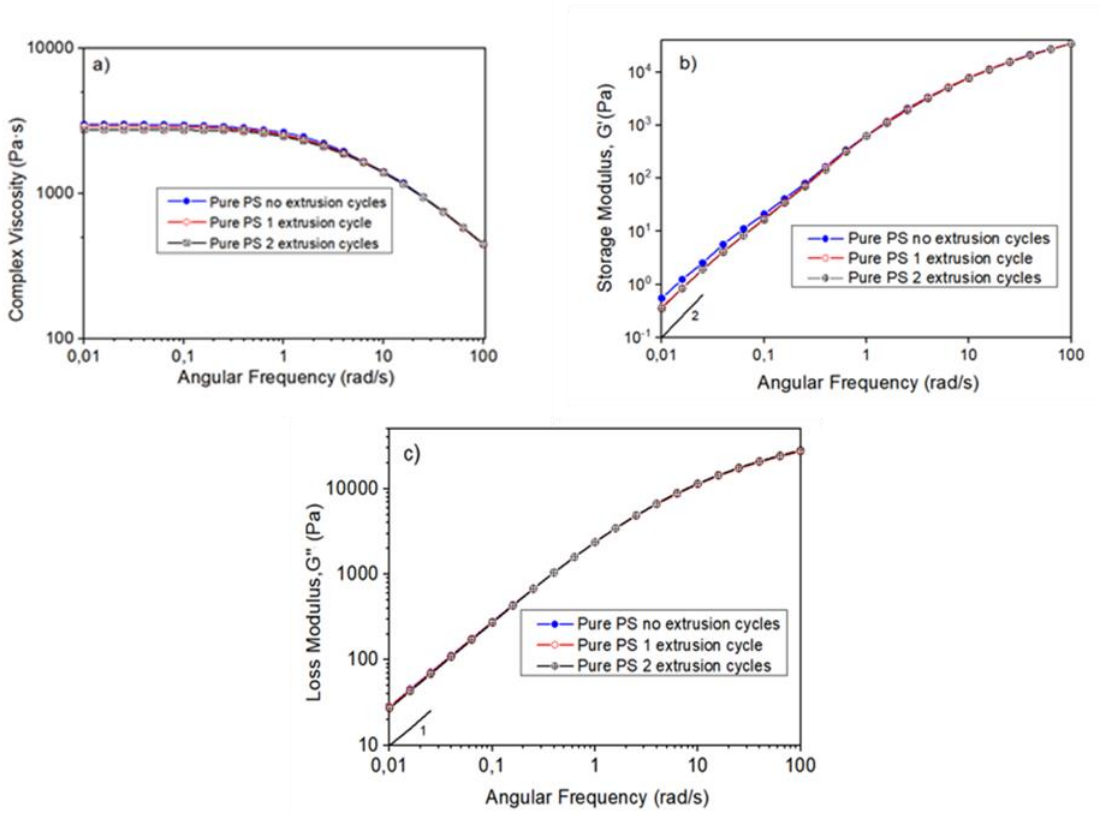


**Figure 3.** Viscoelastic properties for the pure PS subjected to different extrusion cycles. (a) Complex viscosity vs. angular frequency. (b) Storage modulus vs. angular frequency. (c) Loss of modulus vs. angular frequency. Common slopes values for a pure polymer are also shown in figures (b) and (c).

**Table 4.** Linear viscoelastic properties of pure PS subjected to a different number of extrusion cycles.

| Sample Name | Zero Shear Viscosity, $\eta_0$ (Pa·s) | Slope of G' (Pa·s) | slope of G'' (Pa·s) | Crossover Frequency $\omega_x$ (rad/s) | Molecular weight (g/mol) |
|---|---|---|---|---|---|
| **PURE PS NO EXTRUSION CYCLES** | 3076 | 1.72 | 0.96 | 41.01 | 1.56 E+05 |
| **PURE PS 1 EXTRUSION CYCLE** | 2905 | 1.78 | 0.96 | 42.29 | 1.55 E+05 |
| **PURE PS 2 EXTRUSION CYCLES** | 2751 | 1.78 | 0.96 | 43.19 | 1.53 E+05 |

Only in the terminal region, a slight difference is detected (see Figure 3(b,c)). The numerical values of the slopes in the terminal region are depicted in Table 4. Results indicate that the slopes are lower for the non-extruded pure polymer than for the ones subjected to one and two extrusion cycles. An increase of a 3% in the slope of $G'$ is obtained when the material goes from 0 extrusion cycles to one or two extrusion cycles. This fact could indicate a possible deterioration of the molecular structure of the pure polymer due to the extrusion process. Results also indicate that when increasing the number of extrusions cycles the crossover point is shifted to higher frequencies. This variation in the frequency of the crossover points indicates that the material presents a lower solid-like behavior.

Typically, an increase in the molecular weight and in the molecular weight distribution results in an increment of the zero-shear viscosity value, in a reduction of the slopes of $G'(\omega)$ and $G''(\omega)$ and in an increment of the shear thinning behavior.[57] In the present study, when the number of extrusion cycles increases, the complex viscosity decreases, the values of the slopes of $G'(\omega)$ and $G''(\omega)$ increase and the shear thinning behavior also decreases. Furthermore, the molecular weight values, estimated by using the Mark-Houwink Sakurada equation, exhibit a slight reduction when the formulation is subjected to a higher number of extrusion cycles. Therefore, these results could be indicating that some degradation of the polymer molecular structure could occur during the extrusion process leading to a reduction of the lengths of the polymeric chains.

Although it was proven that a major number of extrusion cycles lead to some degradation of the pure polymer, in the case of the composites an increase in the number of extrusion cycles could lead to a better dispersion of the sepiolites in the polymer matrix. However, this increase in the number of extrusion cycles could also produce a re-agglomeration of the particles deteriorating their dispersion. To determine which of the two options is dominating the behavior of these composites, formulations containing 2, 6, 8, and 10 wt.% of the three

different kind of sepiolites (N-SEP, O-QASEP, and O-SGSEP) were extruded one and two times and their rheological behavior was analyzed. With the aim of including figures in which data could be easily analyzed, **Figure 4** only shows the data corresponding to O-QASEP. The trends for the other materials were similar and all the data for all the materials are reported in the **Table 5**.

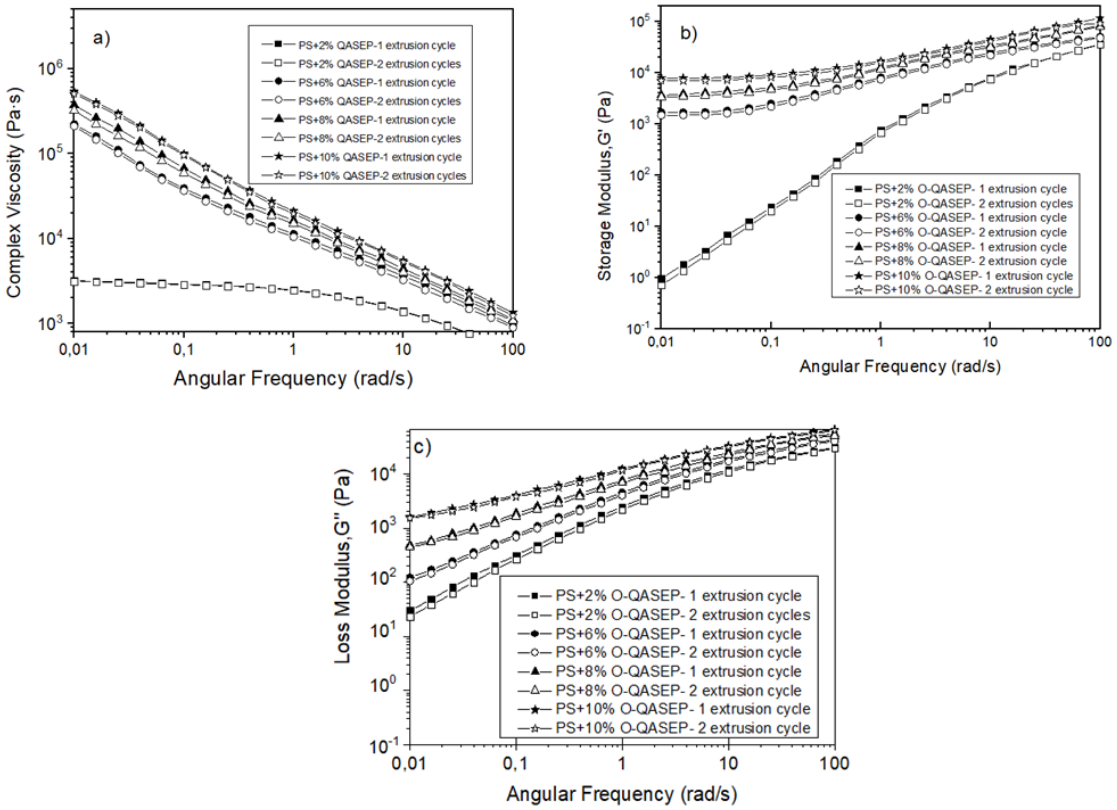


**Figure 4.** Viscoelastic properties of the formulations based on PS and O-QASEP subjected to different extrusion cycles. (a) Complex viscosity vs. angular frequency. (b) Storage modulus vs. angular frequency. (c) Loss modulus vs. angular frequency. Common slopes values for a pure polymer are also shown in Figures (b) and (c).

**Table 5**. Linear viscoelastic properties of the formulations subjected to a different number of extrusion cycles.

| Sample Name | Zero Shear Viscosity, $\eta_0$ (Pa·s) | Slope of G' (Pa·s) | Slope of G'' (Pa·s) | Crossover Frequency, $\omega_x$ (rad/s) |
|---|---|---|---|---|
| **PS+2% N-SEP 1 extrusion cycle** | 2916 | 1.48 | 0.97 | 42.26 |
| **PS+2% N-SEP 2 extrusion cycle** | 2805 | 1.56 | 0.98 | 42.67 |
| **PS+2%O-QASEP 1 extrusion cycle** | 2943 | 0.82 | 0.94 | 41.15 |
| **PS+2%O-QASEP 2 extrusion cycle** | 2826 | 0.89 | 0.97 | 42.63 |

| | | | | |
|---|---|---|---|---|
| **PS+2%O-SGSEP 1 extrusion cycle** | 2912 | 1.52 | 0.98 | 42.89 |
| **PS+2%O-SGSEP 2 extrusion cycle** | 2793 | 1.68 | 0.98 | 43.16 |
| **PS+6% N-SEP 1 extrusion cycle** | 3839 | 1.27 | 0.95 | 41.18 |
| **PS+6% N-SEP 2 extrusion cycle** | 3989 | 1.31 | 0.98 | 42.66 |
| **PS+6%O-QASEP 1 extrusion cycle** | NON-NEWTONIAN | 0.67 | 0.75 | 3.67/28.67 |
| **PS+6%O-QASEP 2 extrusion cycle** | NON-NEWTONIAN | 0.67 | 0.74 | 5.98//30.01 |
| **PS+6%O-SGSEP 1 extrusion cycle** | 3498 | 1.32 | 0.92 | 42.16 |
| **PS+6%O-SGSEP 2 extrusion cycle** | 3654 | 1.33 | 0.96 | 42.88 |
| **PS+8% N-SEP 1 extrusion cycle** | NON-NEWTONIAN | 0.57 | 0.67 | 2.16/25.67 |
| **PS+8% N-SEP 2 extrusion cycle** | NON-NEWTONIAN | 0.59 | 0.70 | 2.51/26.18 |
| **PS+8%O-QASEP 1 extrusion cycle** | NON-NEWTONIAN | 0.16 | 0.44 | NO CROSSOVER POINTS |
| **PS+8%O-QASEP 2 extrusion cycle** | NON-NEWTONIAN | 0.18 | 0.48 | No Crossover Points |
| **PS+8%O-SGSEP 1 extrusion cycle** | 4726 | 1.15 | 0.89 | 39.24 |
| **PS+8%O-SGSEP 2 extrusion cycle** | 4922 | 1.20 | 0.92 | 40.71 |
| **PS+10% N-SEP 1 extrusion cycle** | NON-NEWTONIAN | 0.07 | 0.42 | NO CROSSOVER POINTS |
| **PS+10% N-SEP 2 extrusion cycle** | NON-NEWTONIAN | 0.08 | 0.43 | No Crossover Points |
| **PS+10%O-QASEP 1 extrusion cycle** | NON-NEWTONIAN | 0.05 | 0.39 | NO CROSSOVER POINTS |
| **PS+10%O-QASEP 2 extrusion cycle** | NON-NEWTONIAN | 0.051 | 0.41 | No Crossover Points |
| **PS+10%O-SGSEP 1 extrusion cycle** | NON-NEWTONIAN | 0.46 | 0.54 | 2.15/23.14 |
| **PS+10%O-SGSEP 2 extrusion cycle** | NON-NEWTONIAN | 0.49 | 0.57 | 2.59/24.67 |

In both Figure 4 and Table 5, it is possible to check how the complex viscosity decreases when the number of extrusion cycles increases. For example, the reductions detected in the zero-shear viscosity due to the increment from one to two extrusion cycles for the formulations with 2 wt.% of N-SEP, O-QASEP and O-SGSEP are 4 wt.% in all cases. For the formulations with 6 wt.% of N-SEP, O-SGSEP, and O-SGSEP this value is also 4%. In the previous section it was observed that for the pure PS, the reduction of the zero-shear viscosity between

one and two extrusion cycles was 5%. Therefore, this reduction is very similar to the reduction detected in the polymer composites (4%). This behavior combined with the increase of the slopes of $G'$ and $G''$ when changing from one to two extrusion cycles allow concluding that the main effect associated to increase the number of extrusion cycles is a deterioration of the molecular structure of the polymer matrix due to the high shear forces that are produced during the extrusion process. Another important conclusion of this analysis is that a higher number of extrusion cycles does not help to reach a better dispersion of the sepiolites in the PS matrix.

### 3.2 Analysis of the dispersion degree by X-Ray Microtomography

In this work, another complementary technique has been employed to analyze the dispersion degree. With that purpose in mind, the formulations containing 6 wt% of the three different kinds of particles subjected to a single extrusion process, have been analyzed by X-ray microtomography. The reason for selecting these formulations is that these materials showed substantial differences in the shear dynamic rheology tests (see Figure 1 and Table 2).

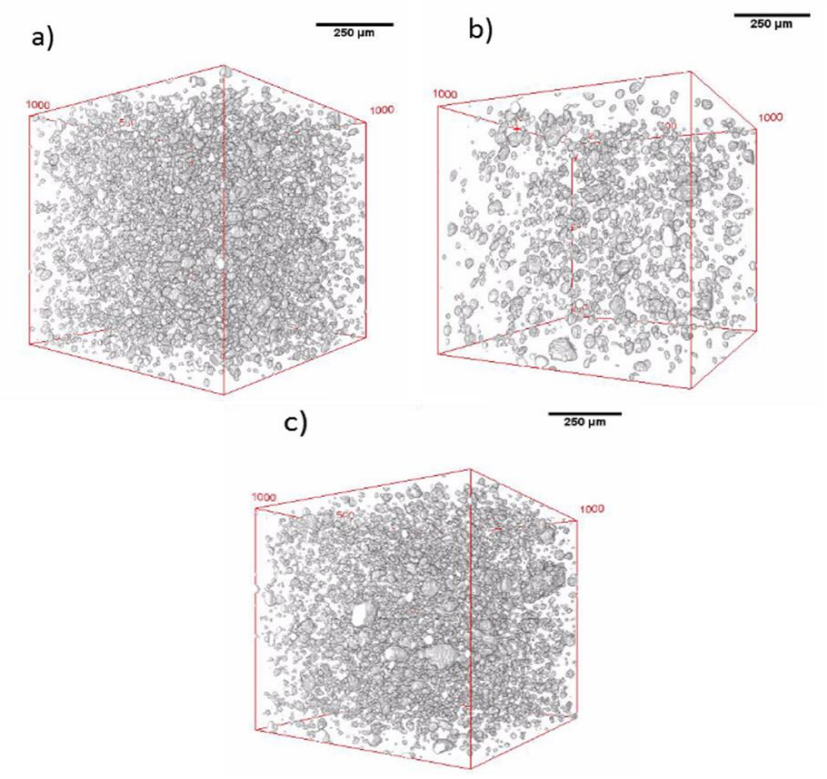


**Figure 5.** Reconstruction of the microtomography analysis for the formulations produced with 6 wt.% of the different types of particles. The formulations were subjected to a single extrusion process. (a) PS+6% N-SEP. (b) PS+6% O-QASEP. (c) PS+6% O-SGSEP.

**Figure 5** shows tomography reconstructions of the three samples. The number of particles detected is clearly lower in the composite containing 6 wt.% of O-QASEP. Furthermore, the set of agglomerates detected in the materials with 6 wt.% of N-SEP and 6 wt.% of O-SGSEP presents a higher dimension compared to the one of the nanocomposite containing O-QASEP. As it was previously mentioned, the minimum particle size detected by the X-ray device employed is 2.5 μm and therefore, the particles detected are in fact agglomerations of individual sepiolite particles.

This behavior is a clear explanation of the different dispersion capability of the three types of particles in the polymer matrix. **Figure 6** exhibits the quantitative analysis of the percentage of agglomeration of these particles, which was calculated using Equation 1.

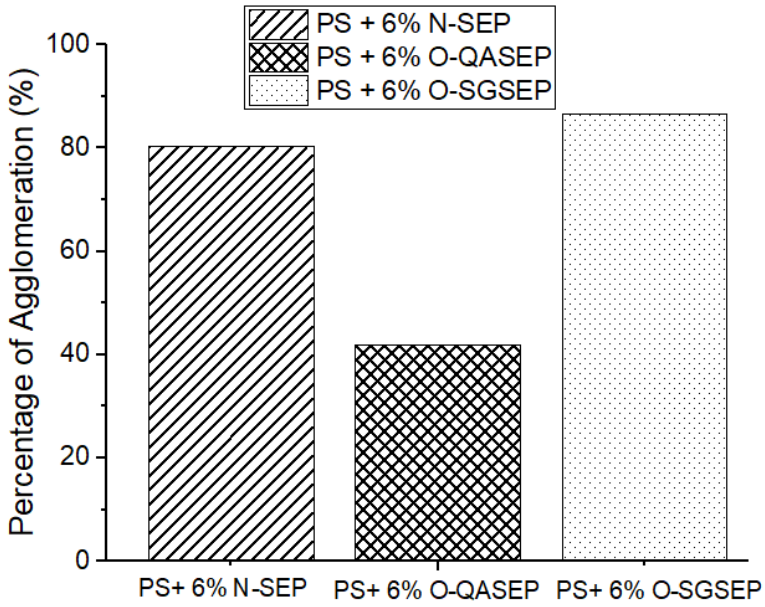


**Figure 6.** Percentage of agglomerates for the three formulations produced with the PS and 6 wt.% of particles, subjected to a single extrusion cycle.

The percentage of agglomeration, that is, the percentage of particles that are agglomerated forming agglomeration clusters bigger than 2.5 μm, is lower for the formulation containing 6 wt.% of O-QASEP (41.96%) than for the materials with 6 wt.% of N-SEP and 6 wt.% of O-SGSEP (80.41% and 86.86%, respectively). A higher percentage of agglomeration implies a worse dispersion of the particles in the material. Therefore, the results obtained by X-ray microtomography agree with the data obtained in the shear dynamic rheology experiments.

### 3.3 Analysis of the PS based foams

This section deals with the analysis of the foaming behavior and the characteristics of the cellular structure of foams produced with the formulations containing 6 wt.% of the three different types of particles. Moreover, the relationships between the dispersion degree of the particles and the cellular structure are analyzed.

### *3.3.1. Gas Uptake, Density, and expansion ratio*

The results obtained for the gas uptake, the relative density, and the expansion ratio of the cellular materials produced via gas dissolution foaming are collected in **Table 6**. These data indicate that the incorporation of sepiolites allows increasing the gas absorbed compared to the pure polymer. The presence of inner channels, which are able to store inside gas, together with the organo-modification that sepiolites present could make possible a higher affinity between the gas and the particles leading to a higher absorption of $CO_2$, compared to the formulations without nanoclays.[58] On the other hand, the relative densities and the expansion ratios are quite similar to those of the pure polymer. This fact implies that the differences in viscosity observed in the shear dynamic rheology tests do not have a significant effect in the expansion ratio of the materials. In addition, the effect of extruding the materials once or twice is not affecting the solubility and the expansion ratio.

**Table 6**. Gas uptake, density, and expansion ratio of the cellular materials produced by the gas dissolution foaming process.

| Sample Name | Gas Uptake (wt. %) | Relative Density | Expansion Ratio |
|---|---|---|---|
| **PURE PS 1 EXTRUSION CYCLE** | 7.69 ± 0.18 | 0.0317 ± 0.007 | 31.92 ± 1.06 |
| **PURE PS 2 EXTRUSION CYCLES** | 7.67± 0.16 | 0.0319 ± 0.005 | 31.34 ± 1.04 |
| **PS+6% N-SEP 1 EXTRUSION CYCLE** | 8.19 ± 0.38 | 0.0303 ± 0.0063 | 33.00 ± 1.21 |
| **PS+6% N-SEP 2 EXTRUSION CYCLES** | 8.18 ± 0.41 | 0.0309 ± 0.0086 | 32.32 ± 1.19 |
| **PS+6%O-QASEP 1 EXTRUSION CYCLE** | 8.22 ± 0.48 | 0.0301 ± 0.0024 | 33.24 ± 0.77 |
| **PS+6%O-QASEP 2 EXTRUSION CYCLES** | 8.19 ± 0.52 | 0.0301 ± 0.0051 | 33.18 ± 0.76 |
| **PS+6%O-SGSEP 1 EXTRUSION CYCLE** | 8.15 ± 0.74 | 0.0311 ± 0.0040 | 32.08 ± 1.04 |
| **PS+6%O-SGSEP 2 EXTRUSION CYCLES** | 8.14 ± 0.66 | 0.0312 ± 0.0066 | 32.02 ± 1.16 |

*3.3.2. Cellular Structure*

SEM micrographs of the cellular materials produced with the pure PS and with the composites containing a fixed content (6 wt.%) of the different types of sepiolites are shown in **Figure 7**. Several conclusions can be extracted from the qualitative and quantitative analysis of the SEM micrographs. On the one hand, when sepiolites are introduced in the PS polymer, a bi-modal behavior is detected. As it can be seen in **Table 7** the volume fraction of small cells represents more than the 70% of the total volume. The large agglomerates of particles make possible the appearance of the large cells. Furthermore, as it can be seen in Table 7, the nucleation effect of sepiolites plays an essential role in the cellular structure. The cell size of the foams produced from the composites is always lower than the cell size of the foams produced from the pure PS. The lowest cell sizes are detected in the foams produced from the composites containing O-QASEP. Cell sizes as low as 13 μm have been obtained in these materials. Therefore, it seems that there is a strong connection between the dispersion degree of the particles in the polymer matrix and their effectivity as nucleating agents. The cell size of the composites subjected to only one extrusion cycle is reduced in a 78%, 85%, and 72%, with respect to that of the polymer matrix, when using N-SEP, O-QASEP, and O-SGSEP, respectively. In the case of the composites subjected to two extrusion cycles, the cell size is reduced in a 71%, 78%, and 68%, with respect to that of the polymer matrix, when using N-SEP, O-QASEP, and O-SGSEP, respectively. In all the cases the cell size is higher in the samples subjected to two extrusion cycles than in the samples subjected to one extrusion cycle. This result confirms that the increment of the extrusion cycles does not improve the dispersion of the particles and therefore, the cellular structure is not improved. As the density of these materials is very similar, there is a relationship between cell size and cell nucleation density. The higher the cell size the lower the cell nucleation density. The highest value of cell nucleation density is detected in the foam containing 6 wt% of O-QASEP subjected to one extrusion cycle. The cell nucleation density of this material is 80 times higher than that of the foam produced with the pure PS.

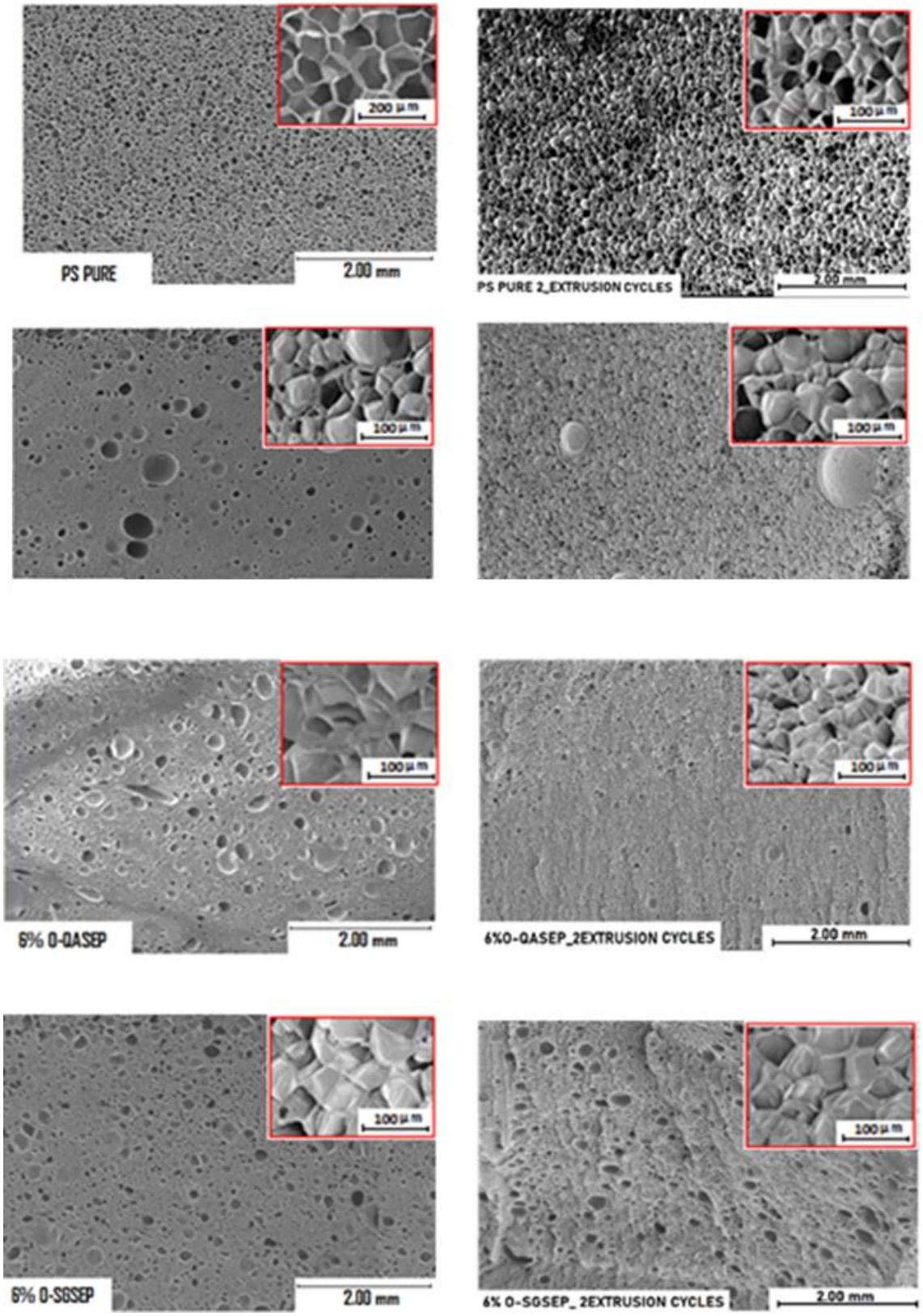


**Figure 7.** SEM images of the foamed samples produced with the pure PS and with the composites containing the different types of sepiolites.

**Table 7.** Cell size, cell nucleation density, volume fraction of large cells, and SD/ϕ of the pure PS and the composites containing 6 wt.% of the different sepiolites, subjected to one and two extrusion cycles.

| Sample Name | Cell Size (μm) | Cell Nucleation Density (nuclei/cm$^3$) | Volumetric Fraction of Large Cells | SD/$\phi$ |
|---|---|---|---|---|
| **PURE PS 1 EXTRUSION CYCLE** | 88.40 ± 28.12 | (4.82 ± 0.5) ·10$^6$ | 0.00 | 0.31 |
| **PURE PS 2 EXTRUSION CYCLES** | 101.15 ± 34.27 | (4.74 ± 0.2) ·10$^6$ | 0.00 | 0.33 |
| **PS+6% N-SEP 1 EXTRUSION CYCLE** | 19.14 ± 5.06 | (3.73± 0.4) ·10$^8$ | 0.21 | 0.26 |
| **PS+6% N-SEP 2 EXTRUSION CYCLE** | 29.32 ± 8.09 | (3.06± 0.4) ·10$^8$ | 0.18 | 0.30 |
| **PS+6%O-QASEP 1 EXTRUSION CYCLE** | 13.01 ± 2.69 | (3.85± 0.1) ·10$^8$ | 0.18 | 0.20 |
| **PS+6%O-QASEP 2 EXTRUSION CYCLE** | 22.18 ± 4.79 | (3.61± 0.2) ·10$^8$ | 0.15 | 0.21 |
| **PS+6%O-SGSEP 1 EXTRUSION CYCLE** | 24.88 ± 4.65 | (3.43± 0.7) ·10$^8$ | 0.24 | 0.18 |
| **PS+6%O-SGSEP 2 EXTRUSION CYCLE** | 32.64 ± 7.41 | (2.86± 0.9) ·10$^8$ | 0.20 | 0.20 |

When analyzing the relationships between the dispersion degree of the particles in the PS matrix and the characteristics of the cellular structure it is possible to conclude that the samples with the lowest percentage of aggregates, those produced with the O-QASEP, present the lowest cell sizes and the highest cell nucleation densities. This fact could indicate that the main nucleation of the small cells is related to the isolated sepiolites rather than with the agglomerations of particles.

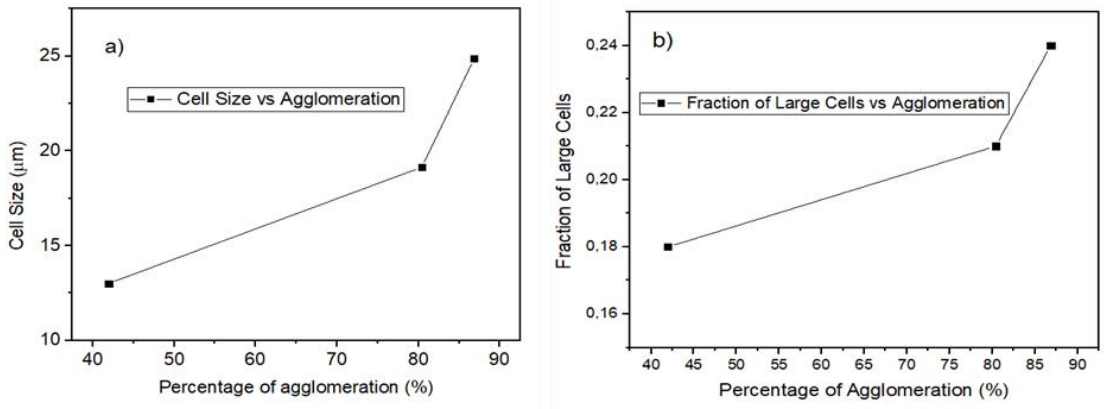


**Figure 8.** (a) Relation between the cell size and the percentage of agglomeration for formulations containing 6 wt.% of sepiolites subjected to a single extrusion process. (b) Relation between the fraction of large cells and the percentage of agglomeration for materials containing 6 wt.% of sepiolites subjected to a single extrusion process.

In **Figure 8(a)** it is possible to see the relation between the cell size and the percentage of agglomeration for the formulations that contain 6 wt.% of sepiolites subjected to a single extrusion process.

Regarding the data corresponding to the volumetric fraction of small cells depicted in Table 7, it is possible to see how samples with O-QASEP present higher percentages of small cells than the other cellular composites. This fact could be related with the better dispersibility observed of this kind of particles in the PS matrix. In other words, the bimodal behavior that appears with the sepiolites depends strongly on the agglomeration of these nanoclays. This behavior is confirmed with the Figure 8(b), which represents the relation between the presence of large cells and the percentage of agglomeration. The higher the agglomeration ratio the higher the number of large cells that appear in the cellular structure. Finally, the ratio of the SD divided by the cell size ($\phi$) gives information about the homogeneity of the cellular structure. The lower the value of $SD/\phi$ the more homogeneous the cellular structure. Results indicate that, when the largest cells are not considered, the structures of the foams containing sepiolites are more homogeneous than the structure of the foams produced with the pure PS. In addition, the foams produced with the formulations subjected to one extrusion cycle are also more homogeneous than the foams produced with the formulations subjected to two extrusion cycles, which agrees with the results obtained in the rheological study.

## 4.CONCLUSIONS

Blends of PS with sepiolites have been prepared and characterized. The effects on the dispersion degree of the particles in the PS matrix associated to modify the type of particles (N-SEP, O-QASEP, O-SGSEP), the content of particles (2, 6, 8, and 10 wt.%) and the process conditions (one and two extrusion cycles) have been analyzed in this research by using two different techniques: dynamic shear rheology and X-ray micro-computed tomography. Shear dynamic rheology results show that the O-QASEP particles are the ones with the best dispersibility. The increment detected in the complex viscosity values of the formulations containing O-QASEP and the reductions observed in the values of the slopes of G′ and G″ curves are more pronounced than those observed for the other particles. Furthermore, rheological results indicate that in the formulations containing 6 wt.% of O-QASEP a percolated structure has been formed; whereas it is necessary to incorporate 8 wt.% of N-SEP and 10 wt.% of O-SGSEP to achieve the percolation state. Moreover, the conclusions reached with the shear dynamic

rheology measurements are corroborated with the X-ray micro-tomography results.

An increase of the number of extrusion cycles lead to a deterioration of the molecular structure of the PS matrix due to the high shear forces that are produced during the extrusion process. Furthermore, by increasing the number of extrusion cycles it is not possible to achieve a better dispersion of the particles in the polymer matrix.

Finally, the pure PS and the composites containing 6 wt.% of sepiolites have been foamed and their cellular structure has been characterized. Results indicate that sepiolites are strong nucleating agents for PS foams Cell sizes were reduced up to 80% and cell densities were increased by 80 times. Moreover, the dispersion degree of the particles in the PS has an important effect on the cellular structure characteristics. The formulation with the best dispersion of particles (6 wt.% O-QASEP) presents the lowest cell size, the highest cell density, and a very homogeneous cellular structure. In addition, the foams produced with the formulations subjected to two extrusion cycles present worse cellular structures than their counterparts subjected only to one extrusion cycle.

## ACKNOWLEDGMENTS

Financial assistance from the Junta of Castile and Leon (VA202P20) and Spanish Ministry of Science, Innovation and Universities (RTI2018-098749-B-I00) and the "Ente Público Regional de la Energía de Castilla y León" (EREN) are gratefully acknowledged.

## REFERENCES

[1] D.L. Tomasko, A. Burley, L. Feng, S.K. Yeh, K. Miyazono, S. Nirmal-Kumar,I.Kusaka. K. Koelling, *J. Supercrit. Fluids*. **2009**, 47, 493–499.

[2] C.C. Ibeh, *Thermoplastic Materials: Properties, Manufacturing Methods, and Applications*. **2011,** First Edition. CRC press Taylor and Francis Group, Bocaraton,United States.

[3] Insulation materials and their thermal properties. Greenspec, *http:// www.greenspec.co.uk/building-desing/insulation-materials-thermal-properties/*,**2018**, Accessed 5 March 2021

[4] A.K. Kota, B.H. Cipriano, M.K. Duesterberg, A.L. Gershon, D. Powell, S.R. Raghavan,

H. A. Bruck, *Macromolecules*. **2007**,40, 7400–7406.

[5] V. Dolomanova, J.C.M. Rauhe, L.R. Jensen, R. Pyrz, A.B. Timmons, J. Cell. Plast. **2011**,47,81–93.

[6] H. Mauroy, T.S. Plivelic, J.-P. Suuronen, F.S. Hage, J.O. Fossum, K.D. Knudsen, *Appl. Clay Sci*. **2015**,108, 19–27.

[7] L.J. Lee, C. Zeng, X. Cao, X. Han, J. Shen, G. Xu, *Compos. Sci. Technol.* ***2005***, 65,2344–

23637.

[8] Y. Kojima, A. Usuki, M. Kawasumi, A. Okada, Y. Fukushima, T. Kurauchi, O. Kamigaito, *J. Mater. Res*. **1993**,8, 1185–1189.

[9] M. Santiago-Calvo, J. Tirado-Mediavilla, J.C. Rauhe, L.R. Jensen, J.L. Ruiz-Herrero, F.

Villafañe, M.A. Rodriguez-Perez, *Eur. Polym. J.* ***2018***, 108, 98–106.

[10] J.U. Park, J.L. Kim, D.H. Kim, K.H. Ahn, S.J. Lee, K.S. Cho, *Macromol. Res.* ***2006***, 14,

318–323.

[11] S. Doroudiani, M.T. Kortschot, *J. Appl. Polym. Sci.* ***2003***, 90, 1421–1426.

[12] M. Okamoto, P.H. Nam, P. Maiti, T. Kotaka, Naoki Hasegawa, A. Usuki, *Nano Letters,* **2001,**1 ,6, 295-298.

[13] Y. Chen, R. Das, M. Battley, *Int. J. Solids Struct*. **2015**, 52, 150–164.

[14] C. Zhang, B. Zhu, L.J. Lee, *Polymer (Guildf)*. **2011,**52,1847-1855.

[15] X. Han, C. Zeng, L.J. Lee, K.W. Koelling, D.L. Tomasko, *Polym. Eng. Sci.* **2003**, 43, 1261–1275.

[16] C. Kaynak, B.M. Sipahioglu, *J. Fire Sci.* **2013**, 31 ,339–355.

[17] J. Shen, X. Han, L.J. Lee, *J. Cell. Plast*. **2006**, 42, 105–126.

[18] Y.H. Lee, C.B. Park, K.H. Wang, M.H. Lee, *J. Cell. Plast*. **2005**,41, 487–502.

[19] G. Wang, K.L. Wang, C.J. Lu, *IOP Conf. Ser. Mater. Sci. Eng*. **2017**,242, 012020.

[20] W.G. Zheng, Y.H. Lee, C.B. Park, *J. Appl. Polym. Sci*. **2010**, 117, 2972–2979.

[21] V. Bernardo, J. Martín-de Leon, E. Laguna-Gutierrez, M.A. Rodriguez-Perez, *Eur. Polym. J*. **2017** ,96,10–26

[22] G. Hu, F. Feng, *Polym. Technol. Mater*. **2020**, 59, 1407–1416.

[23] S. Bourbigot, J.W. Gilman, C.A. Wilkie, *Polym. Degrad. Stab.****2004***, 84, 483–492.

[24] E. Kontou, G. Anthoulis, *J. Appl. Polym. Sci.* ***2007***, 105, 1723–1731.

[25] J. Yang, L. Huang, Y. Zhang, F. Chen, M. Zhong, *J. Appl. Polym. Sci.* **2013**, 130,4308–4317.

[26] J. Martín-de Leon, V. Bernardo, M.A. Rodriguez-Perez, *Materials (Basel)*. **2019**,12, 797.

[27] M. Frydrych, C. Wan, R. Stengler, K.U. O.Kelly, B. Chen, *J. Mater. Chem*. **2011**, 21 , 9103–9111.

[28] F. Wang, J.S. Liang, Q.G. Tang, *Key Eng. Mater*. **2012**, 512-515, 280–283.

[29] V. Bernardo, J. Martin-de Leon, M.A. Rodriguez-Perez, *Polym. Int.* **2019**,68, 1204–1214.

[30] B. Notario, D. Velasco, M.A. Rodriguez-Perez, J. Santaren, A. Alvarez, A. Esteban-Cubillo, *Int. Conf. Foam. Technol. Foam. 2012, Barcelona (Spain).* **2012,** 1–5

[31] F. Bergaya, B.K. Theng, G. Lagaly, *Handbook of Clay Science,volume 1.* First Edition. Elsevier, **2006.**

[32] A. Singer, E. Galán Huertos, *Developments in Palygorskite-Sepiolite Research: A New Outlook on These Nanomaterials.*First Edition.Elsevier; **2011**.

[33] G. Tian, G. Han, F. Wang, J. Liang. *Sepiolite Nanomaterials: Structure, Properties and Functional Applications. In: Nanomaterials from Clay Minerals.* Elsevier; **2019**:135-201

[34] J. Zhang, S. de Juan, A. Esteban-Cubillo, J. Santarén, D.-Y. Wang, *Chinese J. Chem.* **2015**, 33, 285–291.

[35] N.H. Huang, Z.J. Chen, J.Q. Wang, P. Wei, *Express Polym. Lett.* **2010**,4,743–752.

[36] D. Killeen, M. Frydrych, B. Chen, *Mater. Sci. Eng. C.* **2012**,32,749–757.

[37] Y. Zheng, Y. Zheng, *J. Appl. Polym. Sci.* **2006**, 99, 2163–2166.

[38] M. Liu, M. Pu, H. Ma, *Compos. Sci. Technol.* **2012**,72,1508–1514.

[39] S. Xie, S. Zhang, F. Wang, M. Yang, R. Séguéla, J.-M. Lefebvre, *Compos. Sci. Technol.* **2007**, 67, 2334–2341.

[40] D. Garcia-Lopez, J.F. Fernandez, J.C. Merino, J. Santaren, J.M. Pastor, *Compos. Sci. Technol.* **2010**,70,1429–1436.

[41] E.M. Araujo, A.M. D Leite, R.A. da Paz, V da N. Medeiros, T.J. A Melo, H de L. Lira. *Materials (Basel).* **2011**;4,1956-1966.

[42] Y. Yin, Z. Hong, X. Tian, Q. Zhu, H. Wang, W. Gao. *Polym Bull.* **2018**;75,2151-2166.

[43] N. García, J. Guzmán, E. Benito, A. Esteban-Cubillo, E. Aguilar, J. Santarén, P. Tiemblo, *Langmuir*. **2011,**27,3952–3959.

[44] S.K. Goel, E.J. Beckman, *Polym. Eng. Sci.**1993,*** 34, 1137–1147.

[45] V.Kumar, Nam.P.Shu, *Polym. Eng. Sci.**1990,*** 30.

[46] K. Wang, H. Huang, J. Sheng. *J Liq Chromatogr Relat Technol.* **1998**;21,1457-1470.

[47] S. Perez-Tamarit, E. Solorzano, A. Hilger, I. Manke, M.A. Rodriguez-Perez, *Eur. Polym. J.* **2018**,109, 169–178.

[48] M. Dierick, B. Masschaele, L. Van Hoorebeke, *Meas. Sci. Technol.* **2004**, 15, 1366–1370.

[49] V. Bernardo, F. Loock, J. Martin-de Leon, N.A. Fleck, M.A. Rodriguez-Perez, *Macromol. Mater. Eng*. **2019**, 304, 1900041

[50] J. Pinto, E. Solorzano, M.A. Rodriguez-Perez, J.A. De Saja, *J.Cell.Plast*. **2013**, 49,.555-575.

[51] E. Laguna-Gutierrez, R. Van Hooghten, P. Moldenaers, M. A. Rodriguez-Perez, *J. Appl. Polym. Sci*.2015, 132, 1–12.

[52] J. Zhao, A.B. Morgan, J.D. Harris, *Polymer (Guildf).**2005***, 46, 8641–8660.

[53] S. Hwan Lee, E. Cho, J. Ryoun Youn, *J. Appl. Polym. Sci.* **2007**,103,3506–3515.

[54] R. Kotsilkova, *Mech. Time-Dependent Mater.* **2002**,6, 283–300

[55] J. Vermant, S. Ceccia, M.K. Dolgovskij, P.L. Maffettone, C.W. Macosko, *J. Rheol. (N. Y. N. Y)*. **2007**,51,429-450.

[56]M.J. Pastoriza-Gallego, M. Pérez-Rodríguez, C. Gracia-Fernández, M.M. Piñeiro, *Soft Matter*. 2013,9, 11690–11698.

[57]G.J. Nam, J.H. Yoo, J.W. Lee, *J. Appl. Polym. Sci.* **2005**, 96, 1793–1800.

[58]J.A. Cecilia, E. Vilarrasa-García, C.L. Cavalcante, D.C.S. Azevedo, F. Franco, E. Rodríguez-Castellón, *J. Environ. Chem. Eng*. **2018**, 6, 4573–4587.

## 5.3 Polystrene /sepiolites nanocomposite foams: Relationship between composition, particle dispersion, extensional rheology and cellular structure

This section contains the publication: "***Polystyrene/sepiolites nanocomposite foams: Relationship between composition, particle dispersion, extensional rheology and cellular structure***" published in 2021 in Materials Today Communications (A. Ballesteros, E. Laguna-Gutierrez, M. L. Puertas, A. Esteban-Cubillo, J. Santaren, M. A. Rodriguez-Perez), 29, 102850, *doi: 10.1016/j.mtcomm.2021.102850*.

The main goal of this work is to analyze how the cellular structure of (PS)/sepiolites nanocomposite foams is affected by the extensional rheological behavior of the polymer matrix. The dispersion of the sepiolites in the polymer matrix has been also considered in this work. . Three types of particles were used: N-SEP, O-QASEP and O-SGSEP. Moreover, different composites have been produced varying the amount of particles (between 2 wt.% and 10 wt.%).

The results obtained indicate that the strain hardening decreases as soon as the particles are introduced in the polymer matrix. However, not all the particles affect the extensional rheological properties in the same way. N-SEP lead to a lower reduction of the strain hardening than the organo-modified particles. On the other hand, there is a difference in the particles ability to be dispersed in the PS matrix. A higher dispersion degree was obtained with the O-QASEP than with the N-SEP or with the O-SGSEP.

The different composites have been foamed by a gas dissolution foaming process. The density and cellular structure of the different foams have been characterized. The obtained results show that these particles act as very effective cell nucleating agents, especially those which are well dispersed int eh PS matrix (O-QASEP). The foams presenting the most interesting cellular structures (lower cell sizes, higher cell densities and most regular and homogeneous structures) are those produced with the formulations containing O-QASEP. When introducing these particles, it is possible to reduce the cell size from values close to 90 μm, in the case of the pure PS, to values close to 10 μm. Furthermore, it has been found a relationship between the strain hardening and the open cell content. The open cell content decreases as the strain hardening increases. In general, in these materials, the cellular structure is more affected by the dispersion degree of the

particles in the polymer matrix, and therefore, by the nucleating mechanisms, than by the extensional rheological properties of the formulation, which control the degeneration mechanisms. In **Figure 5.2** it is possible to see the graphical abstract of this publication.

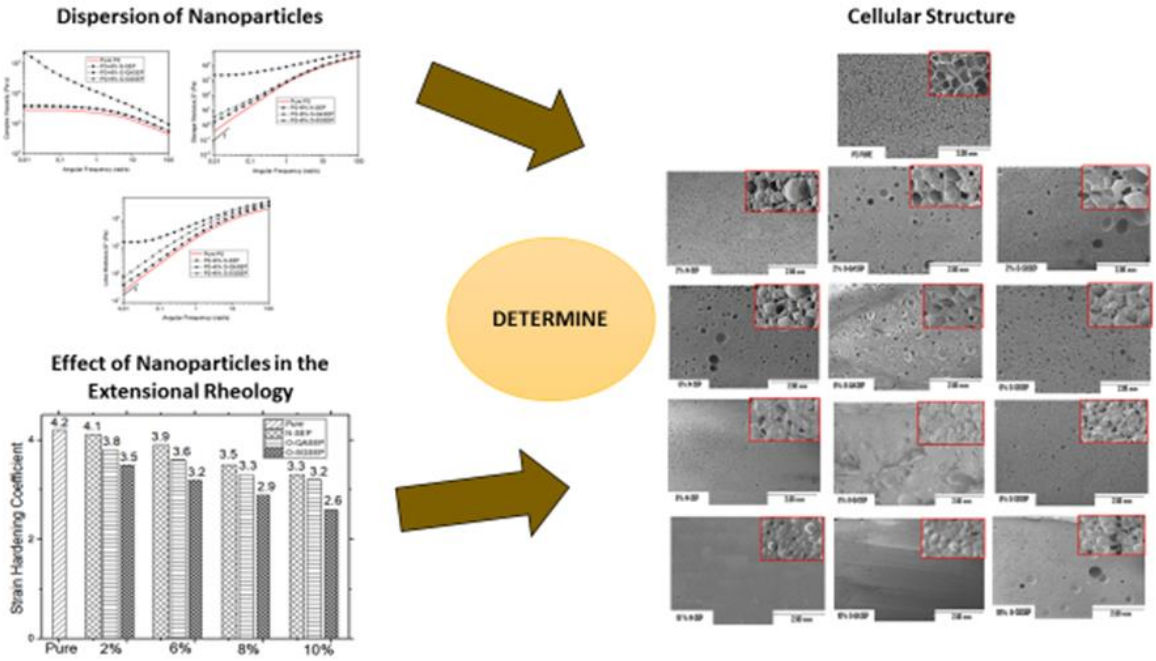


**Figure 5.2.** Graphical abstract of the work "Polystyrene/sepiolites nanocomposites foams: Relationship between composition, particle dispersion, extensional rheology, and cellular structure".

# Polystyrene/sepiolites nanocomposite foams: Relationship between composition, particle dispersion, extensional rheological, and cellular structure.

A. Ballesteros, E. Laguna-Gutierrez, M. L. Puertas, A. Esteban- Cubillo, J. Santaren. M. A. Rodriguez-Perez

***Cellular Materials Laboratory (CellMat)**, Paseo de Belén, 7, Condensed Matter Physics Department, Science Faculty, University of Valladolid, 47011, Valladolid*

***CellMat Technologies**, Edificio Parque Científico UVa, Paseo de Belén 9-A, 47011, Valladolid, Spain*

***Tolsa SA**, Ctra. Vallecas-Mejorada del Campo (M-203), Madrid.*

**HIGHLIGHTS**

•Blends of PS with natural and treated sepiolites have been produced.

•Extensional rheological properties and dispersion degree of PS/SEP was measured.

•Nanocomposite materials were foamed by the gas dissolution foaming process.

•Strong relationships founded between dispersion of sepiolites and cellular structure.

•Extensional Rheology determine the appearance of degeneration phenomena.

## ABSTRACT

The main objective of this work is to analyze how the cellular structure of foamed polystyrene based (PS) nanocomposites, produced by gas dissolution foaming, is affected by the extensional rheological behavior of the polymer matrix and by the dispersion degree of the particles. These composites have been produced with different types of natural and organomodified sepiolites and with different contents of these particles. The extensional behavior and the dispersion degree were characterized by extensional and shear dynamic rheology, respectively. The results obtained indicate that the extensional rheological behavior controls the foam degeneration mechanisms; meanwhile, the way in which the particles are dispersed in the PS matrix controls the nucleation mechanisms. Results also indicate that, in these systems, the characteristics of the cellular structure are mainly defined by the way in which nucleation occurs. Therefore, improving the dispersion degree is a key approach to reduce the cell size by 90%, with respect to the pure polymer.

**KEYWORDS**

Cellular nanocomposites; Extensional rheology; Sepiolites

## 1. INTRODUCTION

One procedure to improve the thermal and also the electrical and mechanical properties of foams consists of incorporating nanoparticles into the polymer matrix.[1-3] These foams, produced from polymer nanocomposites, are known as cellular nanocomposites. These materials combine the advantages of having a cellular structure with the beneficial effects provided by the nanoparticles.[4] Nanoparticles act in two different ways. On the one hand, nanoparticles can modify the characteristics of the cellular structure, and, on the other hand, nanoparticles can improve the morphology and properties of the solid polymer matrix present in the cell walls. A small amount of well-dispersed nanoparticles will act as nucleation sites modifying the cellular structure and leading to lower cell sizes and higher cell nucleation densities.[5] Nanoparticles can also modify the extensional rheological properties of the polymer matrix, which have an important effect on the degeneration mechanisms and, as a consequence, on the cell size, cellular structure homogeneity and foam density.[6-8]

Polystyrene (PS) has been selected for this work because the foams based on this polymer are the most used in the foam market, after polyurethane (PU) foams. They are commonly employed as thermal insulators thanks to their low thermal conductivity.[9,10]

It is well known that the thermal conductivity strongly depends on some parameters of the cellular structure such as cell size or porosity.[11] The incorporation of nanoparticles is an interesting strategy to improve the thermal properties of the foams in a significant way, by modifying the characteristics of the cellular structure.[12] The effects of incorporating nanoparticles into a PS matrix, intended for foaming applications, have been evaluated in previous works. Zhang et al. showed that the introduction of activated carbon (AC) nanoparticles makes it possible to improve the thermal insulation performance of PS foams.[12] Han et al. showed that the inclusion of nanoclays in a PS matrix leads to a reduction of the cell size and to an increase of the cell density. Moreover, the cellular nanocomposites exhibited higher tensile modulus, improved fire retardance, and better barrier properties.[13] Fei et al. demonstrated that the inclusion of lignin into PS in contents between 10 wt% and 50 wt% helped to control the cell size and cell density of the foamed samples and also increased their maximum sound absorption coefficient, at normal incidence, in

values higher than 0.9.[14] Finally, Shen et al. claimed that the use of carbon nanofibers in PS foams created a protective layer around the cell walls that resulted in the enhancement of the foam strength.[15]

Most of the works dealing with nanoparticles are based on the use of spherical or layered particles.[13] Particles like montmorillonites, silica or nano-porous silica have been extensively used for the production of cellular PS based composites.[16-18] However, it is not easy to find in literature studies analyzing the effects that needle-like shape particles, like sepiolites, could have on the final cellular structure of PS foams. [19-24] In fact, there is not plenty of literature that studies the use of sepiolites to modify the cellular structure of PS foams. The only publication we have detected on this topic is the one performed by Notario et al. [25] The authors reported that it is possible to reduce the cell size of PS foams by 60% just by adding 0.5 wt% of sepiolites. However, this work does not report an exhaustive and systematic study of how the dispersion degree of these particles as well as the extensional rheological behavior of the solid polymer composite affect the cellular structure of the foams.

Sepiolites are natural clays with a needle-like shape, with thicknesses in the nanometric scale, between 10 and 12 nm, large surfaces areas ca. 300 $m^2/g$, densities close to 2.1 $g/cm^3$ and high aspect ratios. The structure of sepiolites consists of blocks of two tetrahedral silica sheets sandwiching an octahedral sheet of magnesium oxide hydroxide. The dimensions of the cross-section tunnels are about 0.36 nm x 1.1 nm. The discontinuity of the silica sheets allows the presence of a significant number of silanol (Si-OH) groups on the surface of the particles. These silanol groups can enhance the interfacial interaction between the nanoparticles and the polymer and therefore, improve the dispersion of sepiolites in the polymeric matrix. These properties make sepiolites suitable for being properly dispersed in different kinds of polymers. Bernardo et al. have analyzed the role of sepiolites as nucleating agents in a polymethyl methacrylate (PMMA) matrix. They found that it was possible to decrease the cell size by a factor of 5 by incorporating 1.5% of sepiolites.[19] Furthermore, sepiolites can also have a decisive influence on some properties of the polymer matrix like in the flammability behavior, mechanical or thermal properties. For instance, sepiolites could work as fire- retardant agents in polymers when they are combined with other additives like decabromodiphenyl ether (DBDPE) or antimony trioxide (ATO).[26] Huang et al. reported that sepiolites have a synergetic effect with some intumescent flame retardant agents and that they could improve the performance of a material based on polypropylene (PP)

thanks to the barrier effect that they produce and the capability of these particles to increase the char residue formation.[27] Mechanical properties are also modified by the inclusion of sepiolites.[28] In particular, Zheng et al. proved that by incorporating 1 wt% of sepiolites in epoxy nanocomposites it was possible to double the flexural strength and multiplying by a factor 5 the impact strength. [29] Finally, thermal properties, like thermal stability, are also altered when sepiolites are incorporated into the polymer matrix.[30,31] Garcia-Lopez et al. show that by incorporating 6% of sepiolites to a polyamide 6, it was possible to increase the heat deflection temperature up to 2.5 times, compared to the one of the pure polymer.[32]

All these improvements in the structure and properties of solid polymers induced by sepiolites are interesting; however, in the case of polymeric foams, these properties are conditioned by the way in which the extensional rheological behavior of the polymer matrix is modified by the incorporation of these particles and by the way in which the particles are dispersed in the polymer matrix. To produce foams with high expansion ratios and homogeneous cellular structures with low cell sizes it is necessary that the extensional viscosity of the polymer matrix increases as the polymer is elongated, due to the extensional forces occurring during the foaming process. [33,34] In the initial moments of cell growth, it is desired that viscosity takes low values to permit bubbles to grow. Later, as the polymer is stretched due to the cell growth, a high extensional viscosity is required. This way, the polymer matrix can resist the foam expansion without breaking. This behavior, that is, this abrupt increase of extensional viscosity as time or strain increases is usually known as strain hardening.[35-37] The aforementioned effect has remarkable importance in helping cell walls to withstand the deformation during the last stages of the foaming process and therefore, to reduce the degeneration mechanisms (coalescence, drainage and coarsening).[38] Some authors have investigated the influence of nanoparticles in the uniaxial extensional flow with diverse results. A considerable number of authors have reported and alignment of the nanoparticles in the uniaxial extensional flow, increasing the melt strength of the polymers or inducing strain hardening to the melt. [39-41] Contrary to this theory, Okamoto et al. declared that the strain hardening is a result of the perpendicular disposition of particles to the direction of the force. [8] The effect of the clay content on the strain hardening has also been analyzed. Kotsilkova et al. observed an increase in the strain hardening in PMMA with the inclusion of high contents of smectite particles (between 10% and 15%).[42] Nevertheless, Gupta et al. mentioned that the presence of silicate

layers (contents of bentonite between 2.5% and 5%) in ethylene-vinyl acetate (EVA) might induce solid-like behavior and increase the extensional viscosity, compared to the unfilled material, due to the reorganization of the clay layers during the extensional process.[43] However, this increase in the extensional viscosity takes part until a certain value of the Hencky strain, beyond this point the contribution of the polymer chains dominates over the contribution of the particles. Finally, Laguna-Gutierrez et al. reported that on some occasions the strain hardening could be strongly decreased by the presence of particles.[39] This is a behavior that several authors have also reported.[44-47] They have considered that particles can interfere with the occurrence of the strain hardening phenomenon since they are partially converting the extensional flow in the surrounding polymer into shear flow.

On the other hand, it is also crucial to understand how the dispersion degree of the particles in the polymer matrix affects the final properties of the foamed sample. The relation between the dispersion of the particles and the nucleation process during the foaming step is remarkable.[4] The nucleation mechanisms can be modified and controlled by the inclusion of particles which can work as heterogeneous nucleation sites in which the energy nucleation barrier, defined as the minimum energy necessary to start the nucleation process, is reduced.[48] However, only when the dispersion degree of the particles in the polymer matrix is optimal, it is possible to increase the cell density and reduce the cell diameter, compared to the virgin material.[49] Furthermore, the final properties of the foamed samples are affected by the characteristics of the cellular structure, which, in turn, are conditioned by the dispersion degree.[50] As a consequence, plenty of strategies have been proposed to accomplish a good dispersion of the fillers, among others: ultra-sonication of particles, high shear mixing processes or the functionalization of the particles.[39,50-52]

An excellent dispersion of particles over the polymer and hence, a god nucleating effect can be achieved. However, if particles modify the extensional behavior of the material in the wrong way (that is, particles lead to a reduction of the polymer strain hardening), the degeneration phenomena would appear, and the improvements obtained in the cellular structure could be lost. Therefore, the main objective of this work is to analyze how the extensional rheological behavior of the PS matrix is affected by the incorporation of sepiolites as well as to understand the relationships between extensional rheology, dispersion degree and cellular structure. This new knowledge will allow determining which of these two parameters (extensional behavior or dispersion) has more influence

when it comes to achieving an optimum cellular structure and will provide the opportunity of having a more exhaustive control over the foaming process and therefore, about the structure and properties of foamed nanocomposites based on PS and sepiolites.

## 2. EXPERIMENTAL

### 2.1 Materials

A commercial PS recommended for foam applications (INEOS, Styrolution PS153F) with a melt flow index of 7.5 g/10 min (200 ºC/5 kg) and a glass transition temperature (Tg) of 102 ºC was used as polymer matrix. Three kinds of sepiolites kindly supplied by Tolsa S.A. (Madrid, Spain) were used in this work: natural sepiolites (N-SEP), sepiolites organically modified with quaternary ammonium salts (O-QASEP) and sepiolites organically modified with silanol groups (O-SGSEP). The wet milling process and the organo-modification of the particles were reported in a previous work.[53]

An antioxidant (BASF, Irganox 1010) is also used to avoid thermal degradation during the extrusion stage. Finally, a medical-grade carbon dioxide ($CO_2$) (99.9% purity) was used as a blowing agent for the gas dissolution foaming experiments.

### 2.2 Production Processes

Before materials were processed, they were dried in a vacuum drying oven (Mod. VacioTem TV, P-Selecta) at 70 ºC for 4 h, in the case of pure PS, and at 80 ºC for 8 h, in the case of the different types of sepiolites. The mixing of the polymer with the sepiolites was carried out in a twin-screw extruder (Collin ZK 25 T with L/D of 24) using a temperature profile that goes from 145 ºC to 185 ºC (at the die of the extruder) and with a screw rate of 50 rpm. The different formulations produced in this study are shown in **Table 1**. Formulations containing 0 wt.%, 2 wt.%, 6 wt.%, 8 wt.% and 10 wt.% of sepiolites were produced.

**Table 1.** Summary of the formulations produced during the present study.

| *Sample Name* | *Content of Polymer (wt%)* | *Content of Sepiolites (wt%)* | *Content of Antioxidant (wt%)* |
|---|---|---|---|
| **PURE PS** | 99.5 | 0.0 | 0.5 |
| **PS + 2% N-SEP** | 97.5 | 2.0 | 0.5 |
| **PS + 2% O-QASEP** | 97.5 | 2.0 | 0.5 |
| **PS + 2% O-SGSEP** | 97.5 | 2.0 | 0.5 |
| **PS + 6% N-SEP** | 93.5 | 6.0 | 0.5 |

| | | | |
|---|---|---|---|
| **PS + 6% O-QASEP** | 93.5 | 6.0 | 0.5 |
| **PS + 6% O-SGSEP** | 93.5 | 6.0 | 0.5 |
| **PS + 8% N-SEP** | 91.5 | 8.0 | 0.5 |
| **PS + 8% O-QASEP** | 91.5 | 8.0 | 0.5 |
| **PS + 8% O-SGSEP** | 91.5 | 8.0 | 0.5 |
| **PS + 10% N-SEP** | 89.5 | 10.0 | 0.5 |
| **PS + 10% O-QASEP** | 89.5 | 10.0 | 0.5 |
| **PS + 10% O-SGSEP** | 89.5 | 10.0 | 0.5 |

The different nanocomposites were then thermoformed in a hot plate press to obtain materials with the desired shape and size. The compression molding process was performed at a temperature of 235 ºC and at a pressure of 27 bars. Samples with different dimensions were produced for the different tests. Rectangular prisms with the following dimensions: 20 × 10 × 0.5 (L x W x T) mm were produced for the extensional rheological characterization. Moreover, cylindrical samples with a radius of 11 mm and a thickness of 2 mm were produced to perform the shear dynamic measurements. Finally, samples with diameters of 150 mm and thicknesses of 2 mm were also produced by compression molding. From these samples different specimens with the following dimensions: 20 × 20 × 2 (L x W x T) mm were obtained for the foaming tests.

### 2.3 Foaming Process

The foaming of the samples was carried out using the solid-state gas dissolution foaming method.[54] For this purpose, a high-pressure vessel, PARR 4681 from Parr Instrument Company, with a capacity of 1 l and capable of operating at a maximum temperature of 350 ºC and at a maximum pressure of 41 MPa, was used. This reactor is equipped with a pressure pump controller, SFT- 10 from Supercritical Fluid Technologies Inc., which is controlled automatically to keep a constant pressure. The pressure vessel is also equipped with a clamp heater of 1500 W where the temperature is controlled via a temperature controller (CAL 3300 from CAL controls). The previously mentioned solid-state gas dissolution foaming process consists of two steps.[55] Samples were firstly introduced in the pressure vessel at 8 MPa of $CO_2$ pressure for the saturation stage. The saturation temperature was 40 ºC and the saturation time was 24 h. It was proved that these conditions are enough to achieve full saturation of $CO_2$ in the PS based materials. After saturation, the pressure was abruptly released. Finally, for the foaming stage, samples were removed from the pressure vessel

and introduced in a thermostatic silicon bath at 120 ºC for 1 min. The time between the release of the pressure and the immersion in the thermal bath was 2 min. Once the materials have expanded, they were cooled in water to stabilize the cellular structure.

## 2.4 Characterization

### *2.4.1 Extensional Rheology*

A stress-controlled rheometer (AR 2000 EX from TA Instruments) with an extensional fixture (SER 2, Xpansion Instruments) was used to analyze the extensional rheological behavior of the different solid, non-foamed, composites. In this device, the samples are clamped to two cylinders that rotate, at a fixed rate, in opposite directions applying a uniaxial stretching force to the material. All the experiments were conducted at a temperature of 160 ºC and at different Hencky strain rates: 0.3, 0.5 and 1 $s^{-1}$. In all the experiments the maximum Hencky strain was 2.8. Extensional viscosity can be defined as the ratio between the measured stress and the corresponding Hencky strain rate. A more detailed description of the measurement protocol can be found elsewhere.[39]

From the extensional viscosity measurements, the strain hardening coefficient (S) was obtained. This parameter (see **Equation 1**), which allows quantifying the way in which the extensional viscosity increases when time or strain increases, has been obtained for the different formulations.

$$S = \eta_E^+(t, \dot{\varepsilon_0})/\eta_{E0}^+(t) \qquad [1]$$

Where $(\eta_E^+(t, \dot{\varepsilon_0}))$ is the transient extensional viscosity for a determined time $(t)$ and Hencky strain rate $(\dot{\varepsilon_0})$ and $\eta_{E0}^+(t)$ is the transient extensional viscosity in the linear viscoelastic regime, which can be obtained in two different ways: as three times the time-dependent shear viscosity growth curve at very low shear rates or by extrapolating the overlapping parts of the extensional curves at different elongation rates.[56] In the present work, the second option was chosen to obtain the strain hardening coefficient. This coefficient has been determined for a time of 2.67 s and for a Hencky strain rate of 1 $s^{-1}$.

### *2.4.2. Shear rheology*

A shear stress-controlled rheometer (AR 2000 EX from TA Instruments) was used to measure the dispersion degree of the different solid, non-foamed, formulations. Dynamic shear measurements were conducted at a temperature of 220 ºC under a nitrogen atmosphere using 25 mm diameter parallel plates. A fixed gap of 1 mm was selected to perform the rheological measurements.

The first step was to perform a strain sweep test at a fixed dynamic frequency (1 rad $s^{-1}$) to determine the linear viscoelastic regime of the different nanocomposites. Then, a time sweep was performed to recover the initial state of the particle network that was partially deformed when the sample was loaded in the rheometer. The duration of the time sweep varied between 360 s and 600 s, depending on the material. Finally, the frequency sweep step was performed, in a range of angular frequencies varying between 0.01 rad $s^{-1}$ and 100 rad $s^{-1}$. From these measurements, four properties were analyzed: dynamic shear viscosity ($\eta^*$), storage modulus ($G'(\omega)$), loss modulus ($G''(\omega)$) and crossover frequency ($\omega x$).

### *2.4.3. Gas uptake*

The method used during the present work to measure the gas absorbed by the polymer matrix, during the saturation stage, was the gravimetric method. By using this method, the gas uptake ($CO_2$ Uptake) was obtained directly by determining the weight gained by the polymer sample during the sorption stage. This parameter was determined according to **Equation 2**.

$$CO_{2\ Uptake} = \frac{W_s - W_0}{W_0} \qquad [2]$$

Where $W_s$ is the weight of the polymer composite after the saturation stage, when the polymer matrix is fully saturated, and $W_0$ is the initial weight of the sample before being introduced in the pressure vessel. The time between the depressurization of the pressure vessel and the weight of the sample was around 2 min. These measurements are only an estimation of the solubility and they have been used to establish a comparison between the behavior of the different samples.

### *2.4.4. Density*

The density of the solid materials was analyzed using a gas pycnometer (Accupyc II 1340 from Micromeritics). The density of the foamed materials was determined by the geometric method, that is, dividing the corresponding mass of each specimen by its geometric volume (ASTM standard D1622–08).

The following equations ( **Equation 3**) and (**Equation 4**) show the way of determining the relative density and expansion ratio. Relative density ($\rho_r$) is defined as the ratio between the density of the foam ($\rho_{foam}$) and the density of the bulk solid material ($\rho_{solid}$). On the other hand, the expansion ratio ($E$) is defined as the inverse of the relative density ($\rho_r$).

$$\rho_r = \rho_{foam}/\rho_{solid} \quad [3]$$

$$E = 1/\rho_r \quad [4]$$

### 2.4.5. Open Cell Content

To evaluate the open cell content (OC) of the different foamed samples, according to the Standard ASTM D6226–10, a gas pycnometer, Accupyc II 1340 from Micromeritics, was used. To obtain the open cell content **Equation 5** was employed.

$$OC(\%) = \frac{100(V_{geometric} - V_{pycnometer})}{V_{geometric} \cdot p} \quad [5]$$

Where $V_{geometric}$ is the geometric volume of the sample, vpycnometer is the volume of the sample obtained with the pycnometer and p is the porosity calculated as ($1-\rho_{foam}/\rho_{solid}$), where $\rho_{foam}$ is the density of the foam and $\rho_{solid}$ is the density of the solid matrix.

### 2.4.6. Structural characterization

The structure of the cellular materials was analyzed with a scanning electron microscope (SEM) (Jeol, Mod. JSM-820). Parameters such as the average cell size ($\Phi$), the cell nucleation density (N0), the relative volume fraction occupied by the small cells (vs) and the homogeneity of the cellular structure (SD/$\Phi$) were analyzed with an image processing tool based on the software Fiji/Image J [57]. More than 100 cells of different regions of each cellular material have been analyzed to determine these parameters.

The average cell size is defined as it is indicated in **Equation 6**.

$$\phi = \sum_{i=1}^{n} \phi_i/n = \sum_{i=1}^{n} cf/2n\,(\phi_x^i + \phi_y^i) \quad [6]$$

Where $n$ is the total number of cells counted in the image, ϕi is the three-dimensional value of the cell size for and specific cell. $\phi_x^i$, $\phi_y^i$, are the length of the cells in the directions x and y, respectively, and $cf$ is a correction factor used to correct the two-dimensional value of the cell size to a three-dimensional value of this parameter. As it was indicated in the work of Pinto et al. a value of 1.273 has been selected for the mentioned correction factor. [57]

The cell nucleation density $N_0$, defined as the number of cells per unit volume of the solid, was obtained using the Kumar's theoretical approximation as it is indicated in **Equation 7.** [55] In this formula $N_V$ is the cell density, defined as the number of cells per cubic centimeter of the foamed material, and ϱr is the relative density.

$$N_0 = N_V/\rho_r \qquad [7]$$

In this work, the cellular materials containing sepiolites present a bimodal structure: small cells, combined with large cells (cells that present sizes higher than 200 μm). Even though the number of large cells is quite low compared to the one of the small cells, the volume that the large cells occupy it is not negligible. For this reason, to quantify the observed bimodality the relative volume fraction occupied by the large cells (vl) is defined as it is indicated in **Equation 8**.

$$V_l = 1 - 100(A_t - A_l/A_t) \qquad [8]$$

Where $A_l$ is the area occupied by the large cells in the SEM images and $A_t$ is the total area of the image. In the pure PS foams, which do not present a bimodal structure, this parameter was not calculated, and it is considered as zero.

Finally, the ratio between the standard deviation of the cell size distribution (SD) and the average value of the cell size (SD/Φ) allows analyzing the homogeneity of the cellular structure. Low values of this parameter are related with an homogeneous cellular structure with a narrow cell size distribution.

## 3. RESULTS

### *3.1. Extensional rheology*

In this section, the effects on the extensional viscosity produced by changing the type and the percentage of sepiolites are evaluated.

**Figure 1** shows the values of the transient extensional viscosity as a function of time for the virgin PS and for the composites containing 2 wt.%, 6 wt.%, 8 w.t% and 10 wt.% of N-SEP, O-QASEP and O-SGSEP. Curves have been multiplied by a factor (included in the figure) to make possible the comparison of the different materials in a single figure.

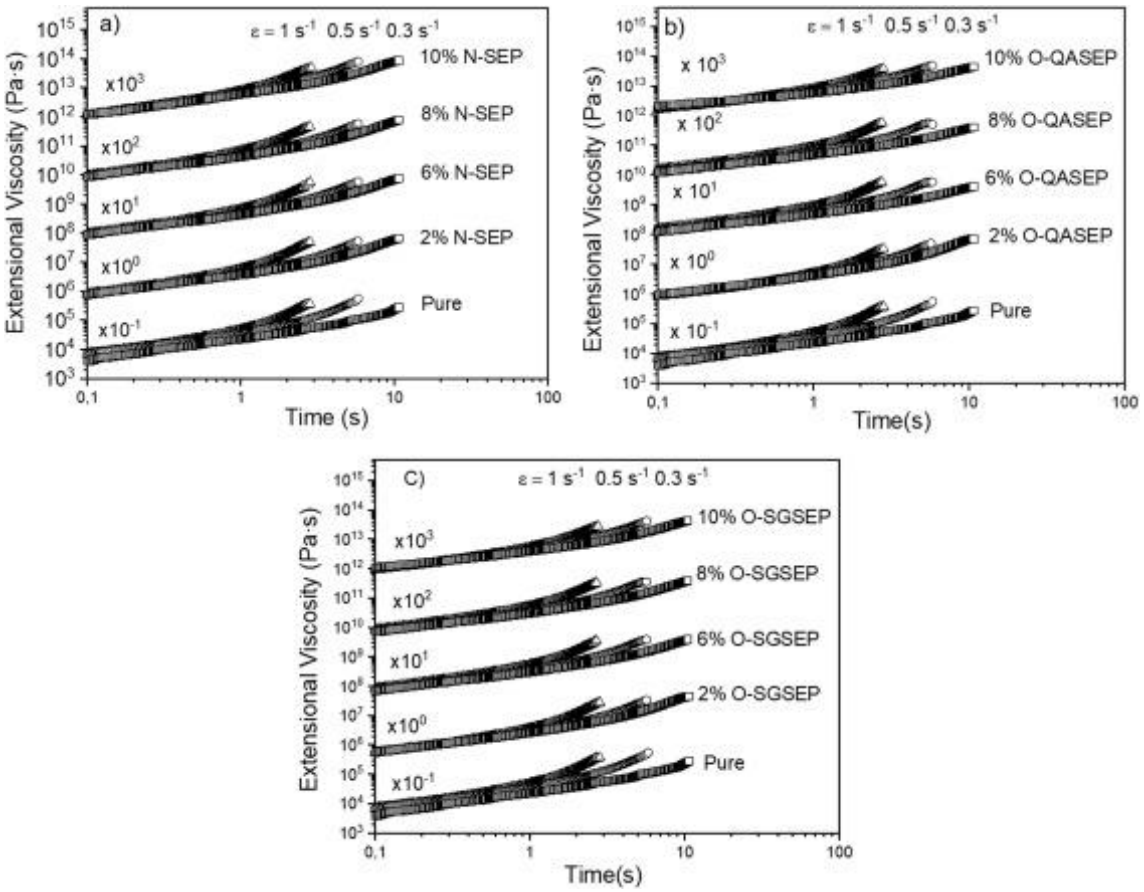


**Figure 1.** Extensional viscosity behavior of the composites containing different amounts of particles. a) PS based composites containing different contents of N-SEP. b) PS based composites containing different contents of O-QASEP. c) PS based composites containing different contents of O-SGSEP.

Results indicate that all the formulations exhibit strain hardening. It is possible to appreciate slight differences in the way in which strain hardening occurs depending on the type of particles employed. The pure PS and the formulation containing N-SEP present a more abrupt strain hardening than that presented by the formulations containing treated particles (O-QASEP and O-SGSEP). Furthermore, the obtained results indicate that the strain hardening of the polymer composites is always lower than the strain hardening of the pure PS. This phenomenon is especially remarkable for the formulations with high percentages of sepiolites (10 wt.%). In order to quantify this behavior and evaluate how the strain hardening changes as the content of particles increases, the strain hardening coefficient of the different formulations has been quantified using Equation 1 and the obtained results are depicted in **Figure 2**.

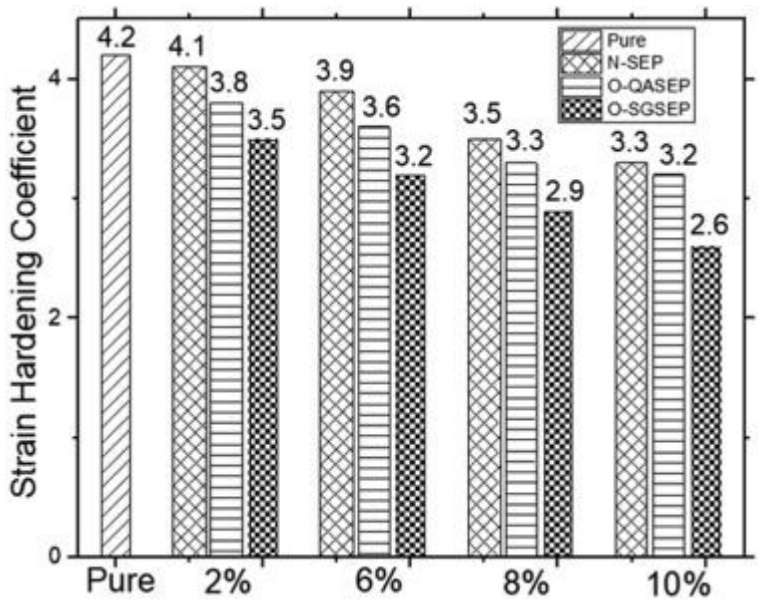


**Figure 2**. Strain hardening coefficient obtained for the pure PS and for the composites containing different contents of N-SEP, O-QASEP and O-SGSEP. This parameter has been determined for a time of 2.67 s and for a Hencky strain rate of 1 s−1.

Figure 2 shows the value of the strain hardening coefficient of the different formulations. As it was previously indicated, this coefficient has been determined for a time of 2.67 s and for a Hencky strain rate of 1 $s^{-1}$. The pure PS presents the highest strain hardening coefficient (value of 4.2). The incorporation of sepiolites leads to a reduction of the strain hardening coefficient, independently of the type of particles employed. However, the magnitude in which the strain hardening decreases depends on the type of particles. The strain hardening of the formulations produced with the O-QASEP and with the O-SGSEP is always lower than the strain hardening of the formulations produced with the N-SEP, being the strain hardening of the composites produced with the O-SGSEP the lowest one. For instance, at the same percentage of particles, 6 wt.%, for example, when adding N-SEP a reduction of the strain hardening close to 7 %, with respect to that of pure PS, is detected. When adding the same amount of O-QASEP and O-SGSEP the reduction increases up to 14.0% and up to 22.0%, respectively.

Considering the results obtained in the literature, there are several theories to explain the results obtained in this work. The reduction detected in the strain hardening as the clay content increases could be explained considering that this kind of needle-like shape nanoparticles cannot be aligned in the uniaxial extensional flow direction.[16,42] Another theory is that based on the work of Gupta et al. [28] They indicated that the polymeric composites behave like solid-like

materials when their structures are percolated or close to percolation. In this state, they detected a decrease of the strain hardening under uniaxial extensional forces. In the present study a remarkable decrease in the strain hardening occurs when the clay content increases. It is important to remark that the formation of a percolated network structure becomes favored when particles with a large aspect ratio, like sepiolites, are introduced in the system. When this percolated network is obtained the properties of the composite are notoriously affected. Other works proposed that the introduction of particles partially converts the extensional flow in the surrounding polymer into a shear flow. As a consequence, the strain hardening can be strongly decreased by the presence of particles. [45-48,58]

### *3.2. Shear rheology*

The dispersion degree of the particles in the polymer matrix has been analyzed by means of shear dynamic rheology measurements considering the formulations containing 6 wt.% of particles.

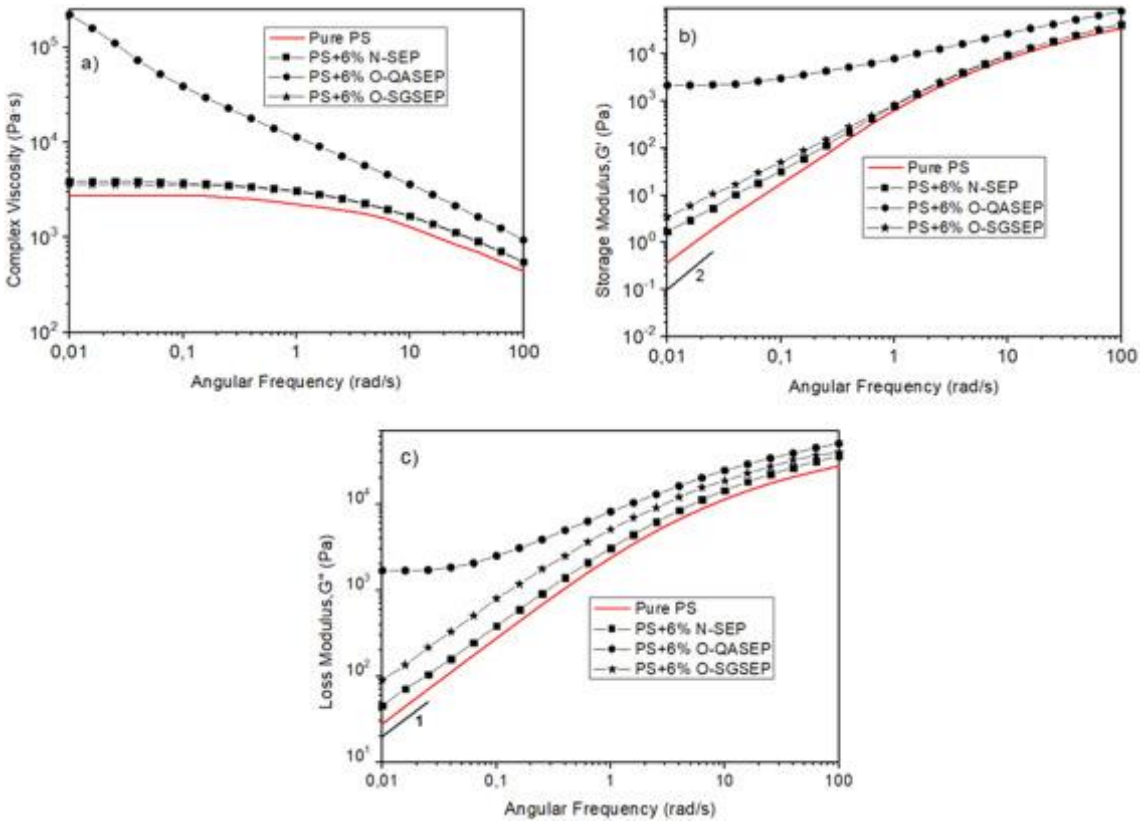


**Figure 3.** Viscoelastic properties of the pure PS and the different composites produced with a fixed content of sepiolites (6 wt.%). (a) Complex viscosity vs. angular frequency. (b) Storage modulus vs. angular frequency. (c) Loss modulus vs. angular frequency. Common slopes values for a pure polymer are also shown in Figure 3(b) and (c).

**Figure 3** shows the behavior of the complex viscosity (η*) (**Figure 3(a)**), the storage modulus (G′(ω)) (**Figure 3(b)),** and loss modulus (G″(ω)) (**Figure 3(c))** as a function of the angular frequency for the pure PS matrix and the three types of composites under study. Figure 3(a) shows that the composites present a higher viscosity than the pure PS matrix. This increment is chiefly remarkable for the formulation containing O-QASEP. Moreover, in this composite the Newtonian behavior observed at low frequencies in the other materials disappears and the behavior corresponds to that of a non-Newtonian power-law material.

For the materials presenting a Newtonian plateau, the zero-shear viscosity ($\eta_0$) has been obtained as the value of the viscosity in the Newtonian plateau. The results of zero-shear viscosity are collected in **Table 2**.

**Table 2.** Linear viscoelastic properties of the pure PS and the different composites containing a 6 wt% of different types of sepiolites.

| *Sample Name* | *Zero Shear Viscosity $\eta_0$ (Pa·s)* | *Slope of G' (Pa·s)* | *Slope of G'' (Pa·s)* | *Cross Over Frequency, $\omega_x$ (rad/s)* |
|---|---|---|---|---|
| **PURE PS** | 2905 | 1.78 | 0.96 | 42.29 |
| **PS + 6% N-SEP** | 3839 | 1.27 | 0.95 | 41.18 |
| **PS + 6% O-QASEP** | NON-NEWTONIAN | 0.67 | 0.75 | 3.67/28.67 |
| **PS + 6% O-SGSEP** | 3498 | 1.32 | 0.92 | 42.16 |

Storage modulus (G′(ω)) is altered by variations in the molecular structure of polymers. At low frequencies, in the area known as terminal region, where the longest relaxation times play a major role, the storage modulus of pure polymers is proportional to the square of the frequency $G' \propto \omega^2$.[58] In other words, for a pure polymer it is expected that the slope of G′ presents a value close to 2. To quantify the changes in the storage modulus, caused by the incorporation of particles, the slopes of the G′ curves in the terminal region (between 0.01 and 0.1 rad $s^{-1}$) were measured. The obtained results are collected in Table 2. As soon as the density of particles per unit volume increases, the values of the slope should approach to 1. When the formulations reach a percolation state, the slope of G′ should present values close to 0.[60] It is important to mention that the density of particles could increase due to two main reasons: an increase in the percentage of particles introduced in the polymeric matrix or in the case of a fixed content of particles, like in this case, an increase of the dispersion degree of the particles in the polymer matrix. Figure 3(b) shows the differences between the curves of the

formulations that contain particles and that of the pure polymer. The slopes of the curves in the terminal region are clearly reduced in the systems containing particles. A reduction of 28% of the slope of G′ is achieved when adding 6 wt% of N-SEP. Meanwhile, a decrease of the slope of 62% and 26% is obtained when adding 6 wt% of O-QASEP and 6% of O-SGSEP, respectively. Furthermore, as it is indicated in Table 2, the slope of G′ corresponding to the composite containing 6 wt.% of O-QASEP particles presents a value close to 0, which indicates that these particles are better dispersed than the others.

On the other hand, the loss modulus,G″(ω) of a pure polymer should be proportional to the frequency in the terminal region G″∝ω.[58] In other words, for a pure polymer it is expected that the slope of G″ presents a value close to 1. The effect of the type of particles in the loss modulus is shown in Figure 3(c). The slopes of G″ in the terminal region have been also calculated and the values obtained are shown in Table 2. The slopes of G″ for the systems containing N-SEP and O-SGSEP are similar to that of the pure polymer. On the other hand, the slope of the composite containing O-QASEP is lower. A reduction of 21% is reported, which once again indicates a much better dispersion of this type of particles in the PS matrix. The crossover frequency (ωx) has been also measured (see Table 2). This parameter is defined as the frequency at which the storage modulus G′ω and the loss modulus G″(ω) intersect. The presence of one single crossover point indicates that material is not already percolated.[59] On the other hand, the presence of two crossover points indicates that the density of particles is close to the percolation threshold. Finally, a spectrum in which no crossover points appear implies that the density of particles is higher than the percolation threshold.[59] Results indicate that the composites produced with 6 wt% of N-SEP and with 6 wt% of O-SGSEP only show a single crossover point, which means that in these materials a network structure has not been formed. Meanwhile, for the material produced with 6 wt.% of O-QASEP two crossover points have been obtained, which indicates that this composite presents a percolated structure.

The rheological results indicate that O-QASEP presents a much better dispersion degree than the other two particles. On the other hand, the formulations containing O-SGSEP and N-SEP exhibit a rheological behavior very similar to that of the pure PS matrix, which indicates a poor dispersion of the particles in the polymer matrix.

### *3.3. Gas uptake and foam density*

This section analyzes how the incorporation of sepiolites affects the gas uptake by the polymer matrix as well as the density, and cellular structure of the foamed materials produced gas dissolution foaming. Moreover, the obtained results are related with those obtained after the analysis of both extensional and shear rheological properties.

The results obtained for gas uptake, relative density, and expansion ratio are collected in **Table 3**.

**Table 3.** Gas uptake during the sorption process, relative density and expansion ratio of the cellular materials produced by gas dissolution foaming.

| Sample Name | Gas Uptake (%wt.) | Relative Density | Expansion Ratio |
|---|---|---|---|
| **Pure PS** | 7.69 ± 0.18 | 0.031 ± 0.007 | 31.92 ± 1.06 |
| **PS + 2% N-SEP** | 7.86 ± 0.24 | 0.030 ± 0.008 | 33.00 ± 0.82 |
| **PS + 2% O-QASEP** | 7.93 ± 0.39 | 0.027 ± 0.004 | 35.83 ± 0.93 |
| **PS + 2% O-SGSEP** | 7.90 ± 0.16 | 0.029 ± 0.001 | 34.36 ± 1.06 |
| **PS + 6% N-SEP** | 8.19 ± 0.38 | 0.030 ± 0.006 | 33.00 ± 1.21 |
| **PS + 6% O-QASEP** | 8.22 ± 0.48 | 0.030 ± 0.002 | 33.24 ± 0.77 |
| **PS + 6% O-SGSEP** | 8.15 ± 0.76 | 0.031 ± 0.004 | 32.08 ± 1.04 |
| **PS + 8% N-SEP** | 8.34 ± 0.18 | 0.031 ± 0.005 | 31.46 ± 1.31 |
| **PS + 8% O-QASEP** | 8.38 ± 0.26 | 0.030 ± 0.007 | 32.66 ± 0.96 |
| **PS + 8% O-SGSEP** | 8.18 ± 0.49 | 0.033 ± 0.006 | 30.02 ± 0.66 |
| **PS + 10% N-SEP** | 8.13 ± 0.55 | 0.033 ± 0.001 | 29.46 ± 0.58 |
| **PS + 10% O-QASEP** | 8.25 ± 0.58 | 0.032 ± 0.002 | 30.76 ± 1.01 |
| **PS + 10% O-SGSEP** | 8.03 ± 0.16 | 0.035 ± 0.006 | 28.36 ± 0.79 |

**Figure 4** shows the effect of the content of particles on the gas uptake. The different formulations present a similar behavior independently of the type of particles employed (with or without surface treatment). An increase of the gas uptake is detected when the amount of sepiolites increases up to values close to the 8 wt.%. This result indicates that due to the incorporation of sepiolites the material can absorb more gas ($CO_2$). The explanation of this behavior could be that sepiolites are $CO_2$-philic particles. This type of trend has been detected in other systems. For instance, Yidong et al. incorporated attapulgite nanoparticles into a PS polymer and they detected an increase in the percentage of $CO_2$ absorbed by the material. [60] The reason behind this behavior could be that the presence of functional groups, like the hydroxyl groups (-OH) located in the

surface of the sepiolites, could have a strong interaction with the $CO_2$ molecules. [61] Also, even when the particles were dried to remove moisture, some water could be still trapped in the clay, which could help to increase the absorption of the blowing agent. [62]

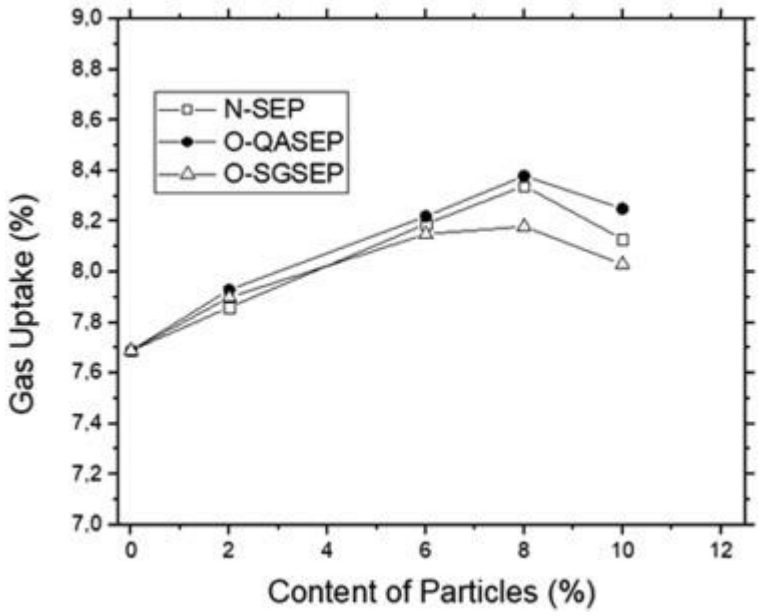


**Figure 4**. Percentage of gas uptake as a function of the content of particles.

However, when the particle content is higher than 8 wt.% a decrease in the gas uptake is detected. One possible explanation for this change in the trend could be related to a change in the diffusivity when high contents of particles are introduced in the polymer matrix (that is, when the content of particles is close to the percolation threshold). If this occurs, as the gas uptake was measured at a fixed time (2 min) after releasing the pressure, it could happen that a significant amount of the $CO_2$ would have left the sample at the time of measurement.

The results also indicate that the composites containing O-QASEP present higher values of the gas uptake than the other materials. As it was previously shown these are the particles that better dispersed into the polymer matrix. This result could mean that when particles are agglomerated the chemical bonding interaction between the gas and the nanoparticles is less effective than when the particles are well dispersed. However, further studies would be required to check this hypothesis. In the composites, the amount of gas available for foaming is higher and this fact could have a significant effect on parameters like foam density, cell size, and cell nucleation density.

**Figure 5** shows the relationship between the relative density of the cellular materials and the content of sepiolites introduced in the system.

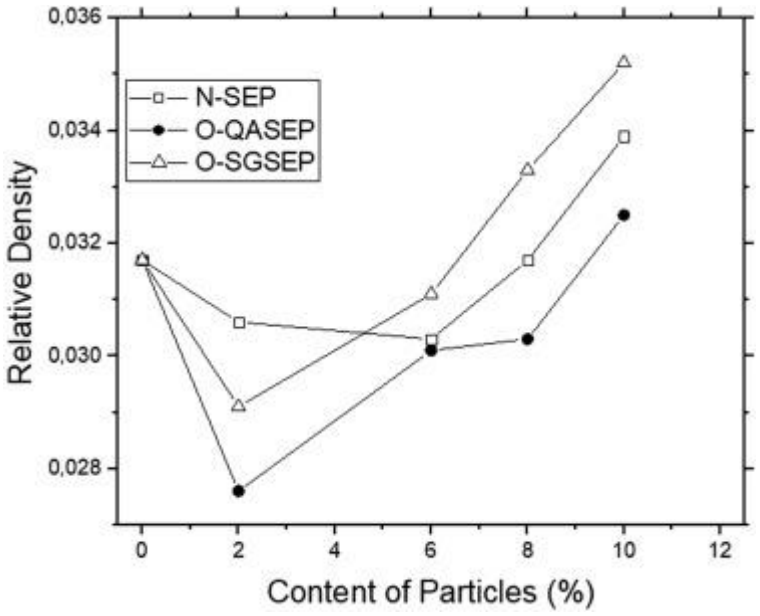


**Figure 5**. Relative density vs the content of particles.

The behavior of the relative density is similar, independently of the type of particle considered. It is possible to see that the curve presents a minimum. It was expected that as soon as the percentage of particles increases the density of the material decreases since a higher amount of gas is introduced in the system (see Figure 4). The relationship between the increase in the gas uptake and the reduction of the foam density has been reported before. [63] This trend is detected when working with contents of particles lower than 2 wt.%. Moreover, it is also possible to see that there is a relationship between the gas uptake by each system and the foam density. For a content of particles of 2 wt.% the sample containing N-SEP presents the lowest gas uptake and the highest density. On the contrary, the sample containing O-QASEP presents the highest gas uptake and the lowest density. However, an opposite trend is detected when adding higher content of particles. In this case, the density increases as the amount of particles increases. When the content of particles introduced increases the viscosity of the materials also suffers a notorious increment. Consequently, the polymer finds the expansion more difficult despite having a higher concentration of gas. Therefore, the capability of the material to expand more thanks to the high content of the gas is playing against the increment of viscosity that sepiolites provide to the polymeric structure and therefore, a minimum is detected in the curve density vs. content of particles.

### *3.4. Open Cell Content*

The open cell content of the different cellular materials has been also measured. The influence that this parameter has on the properties of the cellular materials has been widely studied. Generally, materials with high open cell contents exhibit poor mechanical properties, low thermal insulation capability, and improved acoustic absorption capacity. [64, 65] **Figure 6(a)** shows the open cell content values as a function of the percentage of particles. Additionally, **Figure 6(b)** presents the strain hardening coefficient as a function of the content of particles.

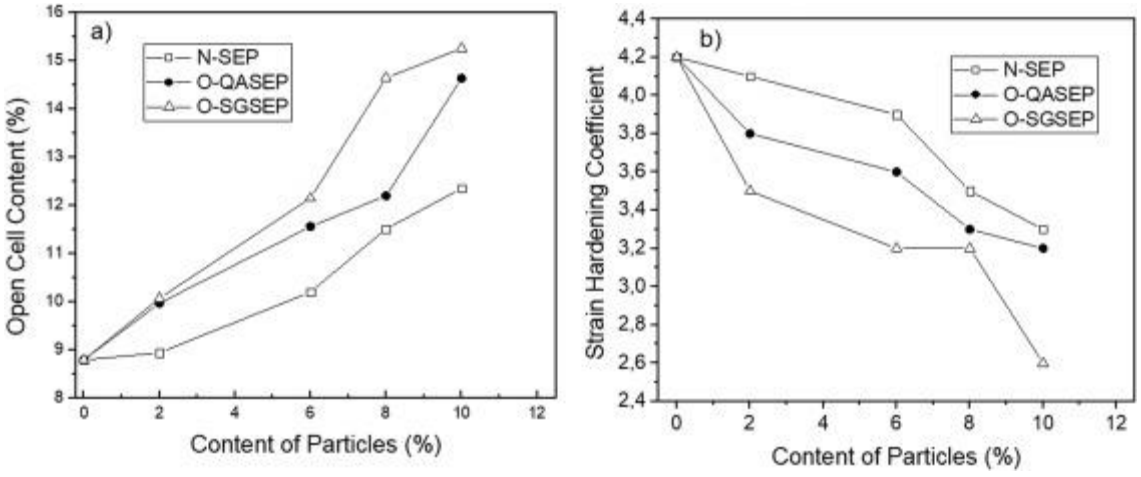


**Fig. 6**. (a) Open cell content as a function of the content of particles. (b) Strain hardening coefficient as a function of the content of particles.

Results show that all the foamed samples present a low value of the open cell content, varying between 9% and 15%. From Fig. 6(a) it can be concluded that the open cell content increases when the percentage of particles increases. Moreover, the same behavior occurs for the three types of particles. Results depicted in Fig. 6(b) indicates that when the content of particles increases the strain hardening coefficient is reduced. When a low-density cellular material is produced, the polymer contained in the cell walls is subjected to high extensional forces. If the polymer is not able to resist the extension, the thin cell walls break leading to an increase of the open cell content. In other words, the materials with a high strain hardening, that is, those containing low contents of particles, can resist the elongational forces occurring during the foaming process without breaking. As a result, the foams produced from these materials present low open cell contents. The decrease of the strain hardening (and therefore, the increase in the open cell content) detected when the amount of particles increases has been analyzed by several authors. [39]

Figure 6(a) also indicates that the foams containing N-SEP present the lowest values of the open cell content. By the contrary, the samples containing O-SGSE present the highest values of this parameter. This result could be explained considering, once again, Figure 6(b), in which it is possible to see that the formulations containing N-SEP present the highest values of the strain hardening coefficient while the formulations containing O-SGSEP present the lowest values of this parameter. Therefore, there is a close relationship between the strain hardening behavior of the different formulations and the open cell content of the foamed materials.

### *3.5. Cellular Structure*

SEM micrographs of the cellular materials produced with the pure PS and with the different composites are depicted in **Figure 7**. Several conclusions can be extracted from the qualitative observation of these images. On the one hand, the pure polymer displays a monomodal cellular structure. However, when sepiolites are introduced in the PS matrix, a bi-modal behavior is promoted. As it can be seen in **Table 4** the volume fraction of large cells represents near 20% of the material. The large agglomerates of particles make possible the appearance of these large cells. The foams produced with the composites containing O-QASEP, which were the particles with the highest dispersion capability, present the lowest volumetric fraction of large cells. By the contrary, the foams produced with N-SEP and O-SGSEP, with a poor dispersion capability, show the highest volumetric fraction of big cells. Furthermore, the volume fraction of the large cells increases as the content of sepiolites increases. Nevertheless, apart from creating a bimodal structure, the sepiolites also play an essential role in the nucleation mechanisms. The foams produced with the sepiolite-based present cellular structures with lower cell sizes than those produced with pure PS.

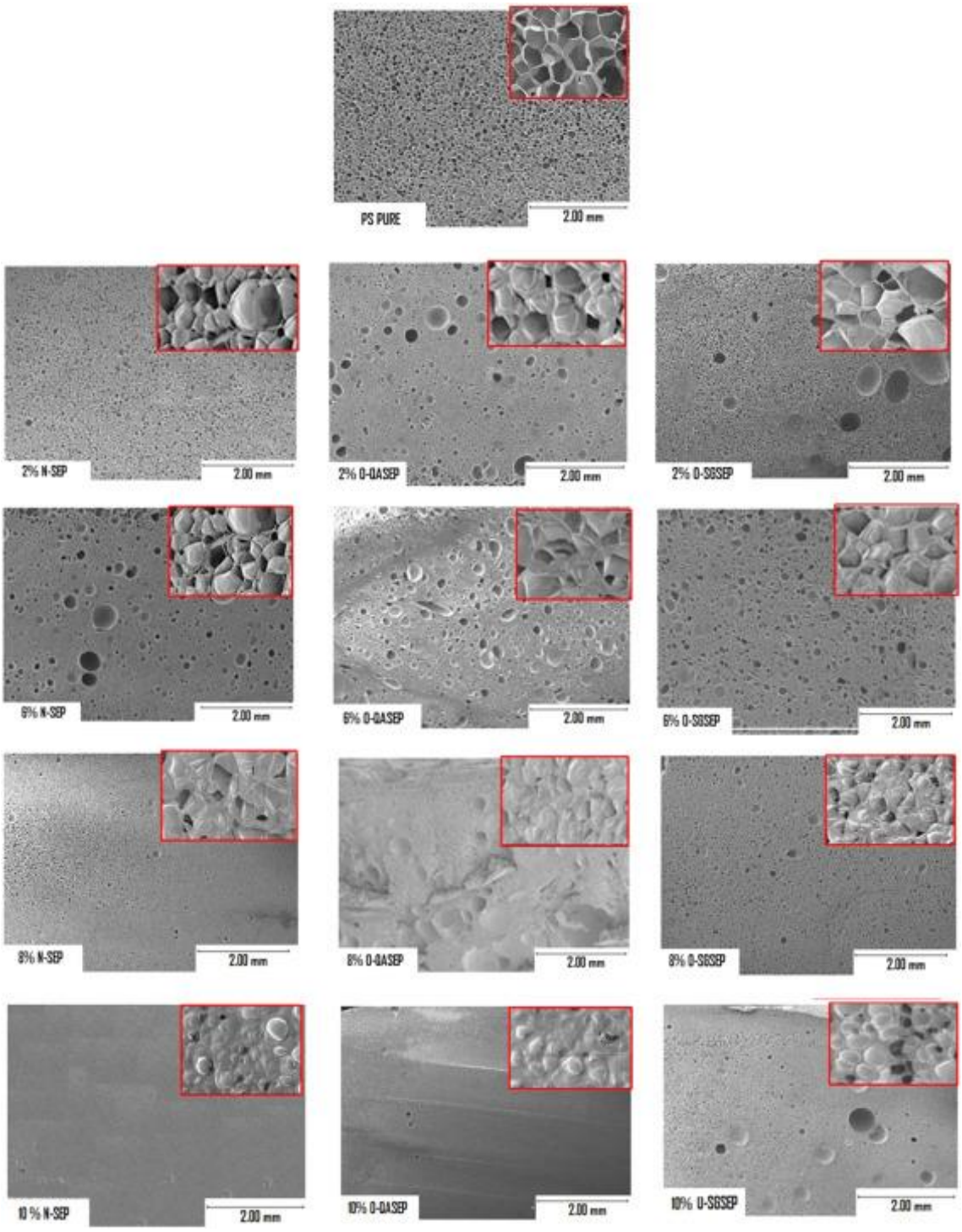


**Figure 7.** SEM micrographs of the different foams. In a rectangle in the right upper side of each micrograph an image with a higher magnification is presented.

**Table 4.** Cell size, cell nucleation density, volumetric fraction of big cell and SD/φ of the cellular materials produced by the gas dissolution foaming process.

| Sample Name | *Cell Size (μm)* | *Cell Nucleation Density (nuclei/cm3)* | *Volumetric Fraction of Big Cells* | *SD/φ* |
|---|---|---|---|---|
| **Pure PS** | 88.40 ± 28.12 | (4.82 ± 0.52) X10$^{6}$ | 0 | 0.31 |
| **PS + 2% N-SEP** | 25.52 ± 3.88 | (3.46 ± 0.34) X10$^{8}$ | 0.18 | 0.15 |
| **PS + 2% O-QASEP** | 15.92 ± 1.75 | (3.82 ± 0.15) X10$^{8}$ | 0.15 | 0.10 |
| **PS + 2% O-SGSEP** | 30.30 ± 3.42 | (3.33 ± 0.56) X10$^{8}$ | 0.22 | 0.11 |
| **PS + 6% N-SEP** | 19.14 ± 5.06 | (3.73 ± 0.43) X10$^{8}$ | 0.21 | 0.26 |
| **PS + 6% O-QASEP** | 13.01 ± 2.69 | (3.85 ± 0.12) X10$^{8}$ | 0.18 | 0.20 |
| **PS + 6% O-SGSEP** | 24.88 ± 4.65 | (3.43 ± 0.70) X10$^{8}$ | 0.24 | 0.18 |
| **PS + 8% N-SEP** | 11.67 ± 2.93 | (4.06 ± 0.36) X10$^{8}$ | 0.23 | 0.25 |
| **PS + 8% O-QASEP** | 9.22 ± 1.30 | (4.15 ± 0.82) X10$^{8}$ | 0.21 | 0.14 |
| **PS + 8% O-SGSEP** | 17.14 ± 5.40 | (3.75 ± 0.21) X10$^{8}$ | 0.26 | 0.31 |
| **PS + 10% N-SEP** | 12.97 ± 3.69 | (4.02 ± 0.90) X10$^{8}$ | 0.26 | 0.28 |
| **PS + 10% O-QASEP** | 9.63 ± 1.36 | (4.13 ± 1.07) X10$^{8}$ | 0.24 | 0.14 |
| **PS + 10% O-SGSEP** | 17.03 ± 4.02 | (3.78 ± 0.11) X10$^{8}$ | 0.29 | 0.23 |

From previous sections, it was extracted that the best dispersion degree was achieved with the O-QASEP. This result has an important effect on the cellular structure. Several works have demonstrated that the cell nucleation density strongly depends on the dispersion degree of the particles.[39, 66] Moreover, higher cell nucleation densities are obtained with the polymeric systems that present an efficient dispersion. Nonetheless, extensional rheological parameters, like the strain hardening coefficient, are also critical to control the cell degeneration mechanisms by coalescence. [39] Therefore, both parameters, the dispersion degree and the strain hardening coefficient could have a critical effect on the cellular structure characteristics. Taking these ideas into account, several parameters accounting for the cellular structure such as cell size, the cell nucleation density and cell size distribution (SD/φ) have been analyzed in detail (see Table 4).

Results depicted in Table 4 and in **Figure 8(a)** indicates that the cell size decreases when the percentage of particles increases. It is possible to obtain reductions in the cell size of 85%, 89% and 80%, with respect to the pure PS, when using 10 wt% of N-SEP, O-QASEP and O-SGSEP, respectively. That is, the foams with the lowest values of cell size are those containing O-QASEP while the foams with the highest values of the cell size are those containing O-SGSEP. These results indicate that in these polymeric systems there is a strong influence of the

dispersion degree on the nucleation mechanisms and hence, in the cell size. The formulations presenting the higher dispersion degrees are those who lead to foams with the lowest cell sizes while the formulations presenting the lowest dispersion degrees are those who lead to foams with the highest cell sizes. Moreover, in **Figure 8(b)** the relationship between the cell size and the strain hardening coefficient is represented. The cell size increases when the strain hardening coefficient increases. If the main factor controlling the cellular structure was the extensional rheological behavior of the formulations, as soon as the strain hardening coefficient increases, the cell size of the materials should decrease. However, in this case, is the other way around. This fact constitutes another proof that, in these systems, the nucleation mechanisms are the key factor controlling the cellular structure. These results demonstrate that, in these PS/sepiolites systems, the dispersion of particles is crucial to reach homogeneous cellular structures with low values of the cell size and high cell nucleation densities.

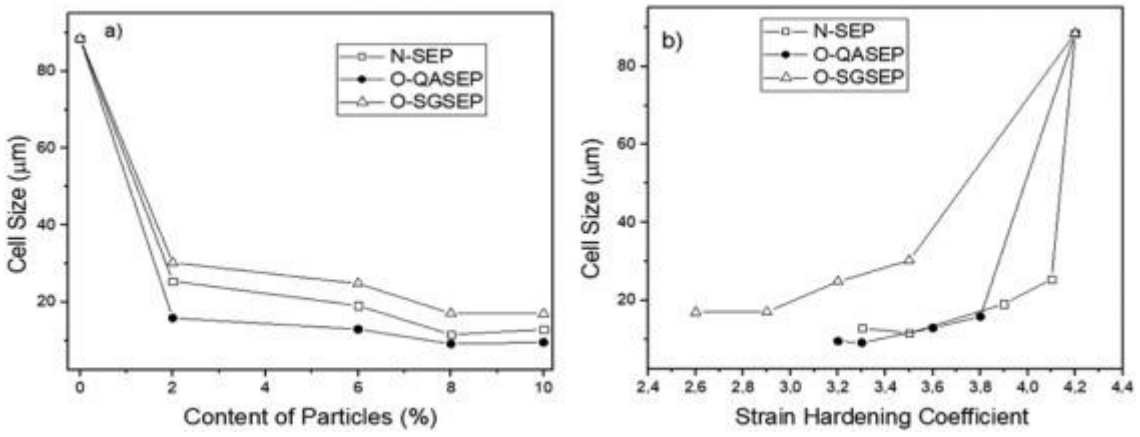


**Fig. 8**. (a) Correlation between the cell size and the content of particles. (b) Cell size of the cellular materials as a function of the strain hardening coefficient.

Cell nucleation density follows a similar trend than the cell size (see **Figure 9**). As soon as sepiolites are introduced in the system an abrupt increase of the cell nucleation density is produced. Moreover, the cell nucleation density increases as the content of particles increases. Independently on the content of particles, the composite containing O-QASEP exhibits the highest cell nucleation density.

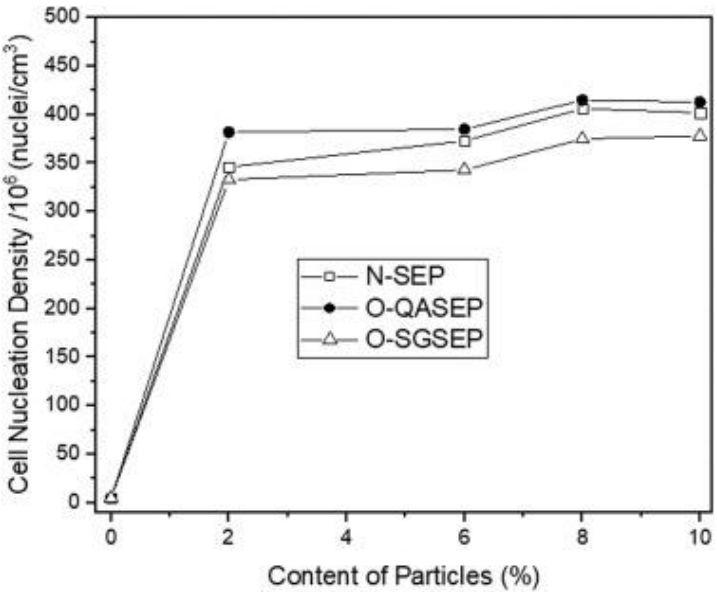


**Figure 9.** Correlation between the content of particles introduced in the system and the cell nucleation density.

Finally, the homogeneity of the cellular structures is gathered in the SD/Φ parameter. Results included in Table 4 show that as soon as low percentages of sepiolites (close to 2%) are introduced in the PS matrix the cell size distributions become more homogeneous. This is something that could be explained considering the capability of the sepiolites to act as nucleants leading to finer and more homogeneous cellular structures. However, when a large content of particles is introduced (close to 10 wt.%), it is possible to see an increase in the value of SD/Φ, which indicates that the cellular structure is not as homogeneous as that of the foams containing low amounts of particles. This could be indicating that if the amount of particles is very high, they trend to agglomerate and as a consequence, the obtained cellular structure is more heterogeneous.

## 4. CONCLUSIONS

Blends of PS with different contents of sepiolites (2, 6, 8 and 10 wt.%) both non-treated (N-SEP) and superficially treated with quaternary ammonium salts (O-QASEP) and with silane groups (O-SGSEP) have been prepared and foamed by gas dissolution foaming using CO2 as blowing agent. The extensional rheological properties of the solid (non-foamed) composites have been analyzed as well as the dispersion degree of the particles in the PS matrix with the objective to analyze how the characteristics of the cellular structure are affected by these two parameters.

Extensional rheology results demonstrate that the strain hardening decreases as the clay content increases. Moreover, the composites produced with N-SEP

presents the highest values of the strain hardening, while the lowest values are detected in the composites produced with the O-QASEP. A relationship between the strain hardening and the open cell content has been detected. The samples presenting the lowest values of the open cell content are those presenting the highest values of the strain hardening. In all the systems, the open cell content is always lower than 15%.

The dispersion degree of the particles in the PS matrix has been characterized by shear rheology. The obtained results indicate that O-QASEP present a much better dispersion degree than the other two particles. The way in which the particles are dispersed in the PS matrix has an important effect on the cellular structure. The highest reductions in the cell size, with respect to the foams produced with the virgin PP, are detected in the foams produced with the composites containing O-QASEP. A reduction of the cell size of approximately 90% and an increase in the cell nucleation density of around 90 times is obtained when adding 8 wt.% of O-QASEP.

From these results, it is possible to conclude that in these polymeric systems the degeneration mechanisms, which are conditioned by the extensional rheological behavior of the polymer matrix, are more intensive in the samples containing clays and they have an important effect in the open cell content. However, nucleation mechanisms, which in turn mainly depend on how the particles are dispersed in the PS matrix, are the key factor controlling the cellular structure (cell size, cell homogeneity and cell nucleation density). Therefore, in these systems to obtain a reduction in the cell size it is necessary to start from a formulation in which the particles are perfectly dispersed in the polymer matrix without forming agglomerates.

## Acknowledgments

Financial assistance from the Junta of Castile and Leon (VA202P20) and Spanish Ministry of Science, Innovation and Universities (RTI2018-098749-B-I00) and the "Ente Público Regional de la Energía de Castilla y León" (EREN) are gratefully acknowledged.

## Apendix A: Supplementary Material

**Table.** Linear viscoelastic properties of the pure PS and all the composites produced using sepiolites.

| Sample Name | Zero Shear Viscosity, $\eta_0$ (Pa·s) | Slope of G' (Pa·s) | Slope of G'' (Pa.s) | Crossover Frequency, $\omega_x$ (rad/s) |
|---|---|---|---|---|
| **Pure PS** | 2905 | 1.78 | 0.96 | 42.29 |
| **PS+2% N-SEP** | 2916 | 1.48 | 0.97 | 42.26 |
| **PS+2% O-QASEP** | 2943 | 0.82 | 0.94 | 41.15 |
| **PS+2% O-SGSEP** | 2912 | 1.52 | 0.98 | 42.89 |
| **PS+6% N-SEP** | 3839 | 1.27 | 0.95 | 41.18 |
| **PS+6% O-QASEP** | Non-Newtonian | 0.67 | 0.75 | 3.67/28.67 |
| **PS+6% O-SGSEP** | 3498 | 1.32 | 0.92 | 42.16 |
| **PS+8% N-SEP** | Non-Newtonian | 0.57 | 0.67 | 2.16/25.67 |
| **PS+8% O-QASEP** | Non-Newtonian | 0.16 | 0.44 | No Crossover Points |
| **PS+8% O-SGSEP** | 4726 | 1.15 | 0.89 | 39.24 |
| **PS+10% N-SEP** | Non-Newtonian | 0.07 | 0.42 | No Crossover Points |
| **PS+10% O-QASEP** | Non-Newtonian | 0.05 | 0.39 | No Crossover Points |
| **PS+10% O-SGSEP** | Non-Newtonian | 0.46 | 0.54 | 2.15/23.14 |

## 5. REFERENCES


[1] A.K. Kota, B.H. Cipriano, M.K. Duesterberg. *Macromolecules*. **2007**, 40 (20), 7400–7406.

[2] V. Dolomanova, J.C.M. Rauhe, L.R. Jensen, R. Pyrz, A.B. Timmons.*J. Cell.Plast*. **2011**, 47 (1),81-93.

[3] H. Mauroy, T.S. Plivelic, J.P. Suuronen, F.S. Hage, J.O. Fossum, K.D. Knudsen. *Appl. Clay Sci.* **2015,** 108, 19-27.

[4] L.J. Lee, C. Zeng, X. Cao, X. Han, J. Shen, G. Xu. *Compos Sci. Technol*. **2005,** 65 (15–16 SPEC. ISS.), 2344-2363.

[5] M. Santiago-Calvo, J. Tirado-Mediavilla, J.C. Rauhe, L.R. Jensen, J.L. Ruiz-Herrero, F. Villafañez, M.A. Rodriguez-Perez. *Eur. Polym. J*. **2018,** 108,98-106.

[6] J.U. Park, J.L. Kim, D.H. Kim, K.H. Ahn, S.J. Lee, K.S. Cho.*Macromol.Res*. **2006**,4 (3) 318-323.

[7] S. Doroudiani, M.T. Kortschot. *J. Appl. Polym. Sci.* **2003,** 90 (5), 1421-1426.

[8] M. Okamoto, P.H. Nam, P. Maiti, T. Kotaka, Hasegawa Naoki, A. Usuki.*Nano Lett*.**2001,** 1, 295-298.

[9] C.C. Ibeh. *Thermoplastic materials: properties, manufacturing methods, and applications*.***2011***.CRC Press, Boca Raton, United States.

[10] https://www.thecowboychannel.com/story/43663399/polystyrene-market-2021-is-estimated-to-clock-a-modest-cagr-of-26nbspduring-the-forecast-period-2021-2026-with-top-countries-data. **Accessed 2021.**

[11] Y. Chen, R. Das, M. Battley. *Int. J. Solids Struct.***2015,** 52(2005),150-164.

[12] C. Zhang, B. Zhu, L.J. Lee. *Polymer,.***2011,** 52(2005),1847-1855.

[13] X. Han, C. Zeng, L.J. Lee, K.W. Koelling, D.L. Tomasko.*Polym.Eng.Sci.* ***2003,*** 43 (6), 1261-1275.

[14] Y. Fei, W. Fang, Z. Mingqiang, J. Jiangming. *Polymer*. **2019**,11,106.

[15] J. Shen, X. Han, L.J. Lee. *J. Cell. Plast.* **2006**,42, 105-126.

[16] S. Bourbigot, J.W. Gilman, C.A. Wilkie. *Polym. Degrad. Stab*. **2004**, 84 (3),483-492.

[17] E. Kontou, G. Anthoulis. *J. Appl. Polym. Sci.* **2007**, 105 (4), 1723-1731.

[18] J. Yang, L. Huang, Y. Zhang, F. Chen, M. Zhong.*J.Appl.Polym.Sci.***2013**, 130 (6), 4308-4317.

[19] V. Bernardo, J. Martin-deLeon, E. Laguna-Gutierrez, M.A. Rodriguez-Perez.*Eur. Polym. J*. **2017**, 96, 10-26.

[20] M.S. Nikolic, R. Petrovic, D. Veljovic, V. Cosovic, N. Stankovic, J. Djonlagic.*Eur. Polym. J*. **2017**, 97, 198-209.

[21] P. Lu. *Polym. Plast. Technol. Eng*. ***2011,*** 50 (15), 1541-1545.

[22] M. Alexandre, P. Dubois. *Mater. Sci. Eng. R. Rep*. ***2000,*** 28, (1-2),1-63.

[23] N.A. Mohd Zaini, H. Ismail, A. Rusli. *Polym. Plast. Technol. Eng*. **2017**, 56 (15), 1665-1679.

[24] V. Bernardo, J. Martin-de Leon, M.A. Rodriguez-Perez. *Polym. Int.* ***2019,*** 68, 1204-1214.

[25] B.Notario, D.Velasco, A. Esteban-Cubillo, J.Santarén, M.A. Rodriguez-Perez. *FOAMS* **2012**, 1–5, 68, 1204-1214.

[26] J. Zhang, S. de Juan, A. Esteban-Cubillo, J. Santarén, D.Y. Wang. *Chin. J. Chem.* 2015, 33 (2),285-291.

[27] N.H. Huang, Z.J. Chen, J.Q. Wang, P. Wei. *Express Polym. Lett*. **2010**, 4, (12), 743-752.

[28] D. Killeen, M. Frydrych, B. Chen. *Mater. Sci. Eng. C.***2012**, 32 (4), 749-757.

[29] Y. Zheng, Y. Zheng. *J. Appl. Polym. Sci.* **2006**,99 (5), 2163-2166.

[30] M. Liu, M. Pu, H. Ma. *Compos Sci. Technol.* **2012**, 72 (13),1508-1514.

[31] S. Xie, S. Zhang, F. Wang, M. Yang, R. Seguela, J.M. Lefebvre. *Compos Sci.Technol.* **2007**, 67 (11–12), 2334-2341.

[32] D. Garcia-Lopez, J.F. Fernandez, J.C. Merino, J. Santaren, J.M. Pastor. *Compos Sci. Technol.* **2010**, 70 (10), 1429-1436.

[33] G.J. Nam, J.H. Yoo, J.W. Lee. *J. Appl. Polym. Sci.* ***2005,*** 96,1793-1800.

[34] H.G.H. Van Melick, L.E. Govaert, H.E.H. Meijer. *Polymer*. **2003**, 44,2493-2502.

[35] P.M. Wood-Adams, J.M. Dealy. *Macromolecules*. **2000**, 33 (20), 7481-7488.

[36] U. ParkJ, L.K. Jeong, D.H. Kim, K.H. Ahn, S.J. Lee, K.S. Cho. *Macromol. Res.* **2006**, 14, 318-323.

[37] B.A. Morris. *Rheology of Polymer Melts. The Science and Technology of Flexible Packagin*. **2017,** Elsevier, Amsterdam, The Netherlands.

[38] K. Taki, K. Tabata, S. Kihara, M. Ohshima. *Polym. Eng. Sci.***2006**, 46,680-690.

[39] E. Laguna-Gutierrez, A. Lopez-Gil, C. Saiz-Arroyo, R. Van Hooghteen, P. Moldenaers, M.A. Rodriguez-Perez. *J. Polym. Res.***2016**, 23, 251.

[40] M. Kobayashi, T. Takahashi, J. Takimot, K. Koyama. *Polymer*.**1995**, 36,3927-3933.

[41] M. Koki, D.K. Christopher, W.K. Kurt, M. Monon, E.B. Stephen. *J. Appl. Polym. Sci.* **2011**, 119, 1940-1951.

[42] R. Kotsilkova. *Mech. Time Depend. Mater.***2002**, 6,283-300.

[43] R.K. Gupta, V. Pasanovic-Zujo, S.N. Bhattacharya.*J.Nonnewton.Fluid Mech.***2005** 128,116-125.

[44] L.A. Utracki, P. Sammut. Polym. Eng. Sci.**1990**, 30,1019-1026.

[45] T. Takahashi, W. Wu, H. Toda, J.I. Takimoto, T. Akatsuka, K. Koayama. *J. Nonnewton. Fluid Mech.***1997**, 68 (1997),259-269.

[46] M. Kobayashi, T. Takahashi, J.I. Takimoto, K. Koyama. Polym. (Guildf). **1996**, 37, 3745-3747.

[47] J.F. Le Meins, P. Moldenaers, J. Mewis. *Rheol. Acta.***2003**, 42, 184-190.

[48] V.I. Kalikmanov. *Nucleation Theory*. **2013,** first edition**,** Springer, Berlin, Germany.

[49] Y.H. Lee, C.B. Park, K.H. Wang, M.H. Lee. *J. Cell. Plast.***2005**, 41, 487-502.

[50] J.A. De Lima, F.F. Camilo, R. Faez, S.A. Cruz. *Appl. Clay Sci.***2017**, 143, 234-240.

[51] J. Sandler, M.S.P. Shaffer, T. Prasse, W. Bauhofer, K. Schulte, A.H. Windle. *Polymer*.**1999**, 40, 5967-5971.

[52] E. Bilotti, H.R. Fischer, T. Peijs. *J. Appl. Polym. Sci.***2007**, 107, 1116-1123.

[53] N. García, J. Guzman, E. Benito, A. Esteban Cubillo, E. Aguilar, J. Santaren, P. Tiemblo. *Langmuir*.**2011**, 27, 3952-3959.

[54] S.K. Goel, E.J. Beckman. *Polym. Eng. Sci.* **1993**, 34, 1137-1147.

[55] V. Kumar, P. Nam, A. Shu. *Polym. Eng. Sci.* **1990**, 30, 1323-1329.

[56] H. Münstedt, F.R. Schwarzl. *Deformation and flow of polymeric materials*. **2014,** Springer, Berlin, Germany.

[57] J. Pinto, E. Solorzano, M.A. Rodriguez-Perez, J.A. De Saja. *J. Cell. Plast.***2013**, 49 (6), 555-575.

[58] E. Laguna-Gutierrez, R. Van Hooghten, P. Moldenaers, M.A. Rodriguez-Perez. *J. Appl. Polym. Sci.***2015**, 132, 1-12.

[59] J. Zhao, A.B. Morgan, J.D. Harris. *Polymer*. **2005**, 46, 8641-8660.

[60] Y. Liu, L. Jian, T. Xiao, R. Liu, S. Yi, S. Zhang, L. Wang, R. Wang, Y. Min. *Polymers*. **2019**, 11, 985.

[61] H. Wan, Y. Que, C. Chen, Z. Wu. *Mater. Lett.***2017**, 194, 107-109.

[62] N.H. Abu-Zahra, A.M. Alian. *Polym. Plast. Technol. Eng.***2010**,49,237-243.

[63] E. Di Maio, G. Mensitieri, S. Iannace, L. Nicolais, W. Li, R.W. Flumerfelt Polym. Eng. Sci.**2005**, 45, 432-441.

[64] M. Alvarez-Lainez, M.A. Rodríguez-Perez, J.A. De Saja. *J. Polym. Sci. Part B Polym. Phys*.2008, 46, 212-221.

[65] M.A. Rodriguez-Perez, M. Alvarez-Lainez, J.A. De Saja. *Appl. Polym. Sci.**2009***, 114, 1176-1186.

[66] E. Solórzano, M.A. Rodriguez-Perez, J. Lazaro, J.A. De Saja. *Adv. Eng. Mater.* **2009**, 11, 818-824.

# Chapter 6

# Analysis of the thermal conductivity of foams based on PS and sepiolites. Effect of the cell size in the thermal conductivity.

*"La verdadera ciencia enseña, sobre todo, a dudar y a ser ignorante"*

*Miguel de Unamuno*

# INDEX

## 6.1 Introduction

In the present chapter are shown the results obtained in the thermal conductivity measurements of the foamed composites produced by the gas dissolution foaming technique. The composites are the same as the one reported in the chapter 5 (produced with three different types of sepiolites and distinct percentage of them). Once the thermal conductivity was measured by the transient plane source method (TPS), the thermal conductivity results are correlated with the cellular structures obtained as well as with the dispersion degree of the particles measured in the chapter 5. Furthermore, measurements of the FTIR (Fourier-Transform infrared spectroscopy) were performed to analyze in detail the influence of the radiation term in the thermal conductivity.

## 6.2 Optimum cell size to reduce the thermal conductivity of foams based on polystyrene/sepiolite nanocomposites.

The section contains the publication named as: "*Optimum cell size to reduce the thermal conductivity of foams based on polystyrene/sepiolite nanocomposites.*" published in 2021 in xxxx (A. Ballesteros, E. Laguna-Gutierrez, M.L. Puertas, A. Esteban-Cubillo, J. Santaren, M.A. Rodriguez-Perez) xxxxxxxxxx (doi).

The main objective of the article is understanding the relation between the cellular structure of the foams and the thermal properties. For that objective, the formulations employed in the chapter 5 will be used again. Furthermore, these formulations present the advantage that an exhaustive study of the dispersion, as well as the extensional rheological behavior has been realized previously. These wo parameters were correlated with the cellular structures obtained. Now in this point, is time to see if there is found another relationship between cellular structure and thermal properties in the foams of PS/SEP.

For the thermal conductivity was needed that samples are the most homogeneous and flat as possible. For that purpose, samples were cut and polished, removed their skin, after they were foamed. Once the measurements of the thermal conductivity are obtained by the TPS method. Same samples were submitted to an FTIR analysis to see if it is possible to relate the thermal radiation contribution with the cellular structure of the materials.

The results shown that the thermal conductivity is reduced when the cell size decrease. However, this reduction observed is only valid when the cell size is in a range of values that are higher than 40 μm. For values lower than this magnitude, the thermal conductivity increases again. A possible explanation of this behavior is because the cell size of the materials is in the border of the Mie scattering and changing towards the Rayleigh one. In the Rayleigh scattering the infrared radiation would be dispersed in a different way related with the cell size. Which means that the light with smaller wavelengths (bluish colors) is greater scattered than those with higher wavelengths (reddish colors) and in the case of the infrared light materials behaves almost transparent for this radiation. Furthermore, apart for the thermal conductivity the FTIR spectrum decay for the materials with cell sizes lower than 40 μm, meaning that the material is no longer able to absorb the same amount of radiation and confirms the measurements of the thermal conductivity taken in the TPS method. The graphical abstract of the article can be found in figure 6.1

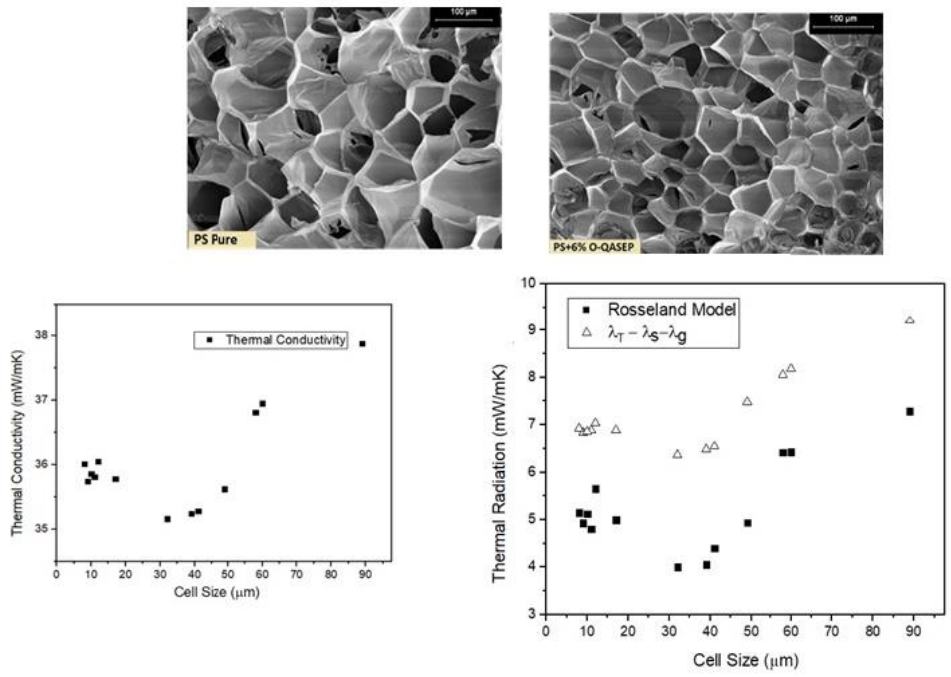


**Figure 6.1.** Graphical abstract of "*Optimum cell size to reduce the thermal conductivity of foams based on polystyrene/sepiolite nanocomposites*".

# Optimum cell size to reduce the thermal conductivity of foams based on polystyrene/sepiolite nanocomposites

A. Ballesteros, E. Laguna-Gutierrez, M. L. Puertas, A. Esteban- Cubillo, J. Santaren. M. A. Rodriguez-Perez

***Cellular Materials Laboratory (CellMat)**, Paseo de Belén, 7, Condensed Matter*

*Physics Department, Science Faculty, University of Valladolid, 47011, Valladolid*

***CellMat Technologies**, Edificio Parque Científico UVa, Paseo de Belén 9-A, 47011, Valladolid, Spain*

***Tolsa SA**, Ctra. Vallecas-Mejorada del Campo (M-203), Madrid.*

## ABSTRACT

The thermal conductivity of cellular nanocomposites based on polystyrene and sepiolites (PS/SEP) has been characterized and related with the parameters accounting for the cellular structure. For this purpose, the thermal conductivity of a high number of PS/SEP foams with different cell sizes, ranging from 90 μm to 9 μm, and similar densities was measured via the transient plane source (TPS) method. The results obtained indicate that thermal conductivity as a function of the cell size presents a minimum for a value of the cell size close to 40 microns. This result has been explained by analyzing the extinction coefficient of these materials by means of FTIR spectroscopy. The extinction coefficient presents a maximum for a value of the cell size of 40 microns. When the values of the cell size vary between 100 microns and 40 microns the extinction coefficient increases as the cell size decreases meaning that the material is more able to scatter the infrared (IR) radiation. However, for values of the cell size lower than 40 microns the extinction coefficient decreases as the cell size decreases, which indicates that these foams start to be more transparent to the IR radiation.

## KEYWORDS

Polystyrene, sepiolites, thermal conductivity, extinction coefficient

## 1. INTRODUCTION

The thermal conductivity of a cellular polymer is the sum of four contributions, as it can be seen in **Equation 1**.[1,2]

$$\lambda_f = \lambda_s + \lambda_g + \lambda_r + \lambda_c \qquad [1]$$

Where $\lambda_s$ is the conduction through the solid phase (polymer matrix), $\lambda_g$is the conduction across the gas phase, $\lambda_r$ is the thermal radiation term and $\lambda_c$ represents the convection within the cells, which can be omitted if the cell size is lower than 2 mm.[3]

Therefore, cellular materials present the advantage of having very low thermal conductivities in comparison with their solid counterparts due to two main reasons.[4] On the one hand, the low conductivity by conduction of gasses. For instance, this value is 26 mW/mK in the case of air. On the other hand, due to the small amount of solid phase that these materials present, due to its low relative density, which led to a reduction of the term $\lambda_s$. As a consequence, these materials are commonly use as primary materials for thermal insulation.[5] For example, polystyrene (PS) foams are one of the most commonly used materials for thermal insulation applications, especially in the building sector.[6]

These PS foams are characterized by having cell sizes in the micrometric range.[7] In this kind of materials the conduction through the solid phase, see **Equation 2**, depends on parameters like the relative density ($\rho_r$), which is defined as the ratio between the density of the cellular material ($\rho_{cm}$) and the density of the solid matrix ($\rho_s$), the thermal conductivity of the solid polymer matrix ($\lambda_{solid}$), the cell anisotropy ratio ($R$), and the fraction of mass in the struts ($f_s$).[4]

$$\lambda_s = \frac{1}{3} f_s \rho_r \lambda_{solid} \sqrt{R} + \frac{2}{3} \rho_r (1 - f_s) \lambda_{solid} R^{1/4} \qquad [2]$$

The conduction through the gas phase depends on the relative density and on the thermal conductivity of the gaseous phase ($\lambda_{gas}$), as it is indicated in **Equation 3**.[8]

$$\lambda_g = \lambda_{gas} (1 - \rho_r) \qquad [3]$$

Finally, , the radiation term, which is related with the infrared energy that the material is able to absorb or scatter in a certain region of frequencies (infrared wavelength going from 700 nm to 1 mm), has been modelized by several authors.[9,10] In the present work the Rosseland approximation has been considered (**see Equation 4)**.

$$\lambda_r = \frac{16 n^2 \sigma T^3}{3 K_{e,R}} \qquad [4]$$

Where, $n$ is the effective index of refraction, usually taken as 1 for the foamed systems, $\sigma$ is the constant of Stefan-Boltzmann and $K_{e,R}$ is the Rosseland extinction coefficient.[11]

Many authors, who have analyzed the behavior of cellular materials based on different polymeric matrices, have shown that a reduction of the cell size, for a constant relative density, led to a significant decrease of the thermal conductivity of the foams.[3,12–14]. The variation of the cell size could involve the change of the fraction of mass in the struts, which will have an effect in the solid conduction term or a change in the radiation contribution.[15]. Arduini-Schuste et al, have attributed the decrement observed in the thermal conductivity by the attenuation of the thermal radiation, as an increase in the extinction coefficient term, due to a scatter and absorption processes produced by the cells.[16] On the other hand, the Mie theory tells that wavelength of the curve, in this case the infrared radiation curve, is independent when the size of the scatterer centers (the distance between the struts in this case) is bigger than wavelength. However, if the distance between the scattering centers is much smaller , ten times smaller, than the IR radiation wavelength the dependency between the thermal radiation with the cellular sizes can be different and foams behave as "transparent materials" for the IR radiation. In the case of foams with cell sizes that approach to values lower than 10 times the wavelength of the infrared radiation, the main method of scattering will be the Rayleigh one and not the Mie scattering. In the Rayleigh scattering the infrared radiation would be dispersed in a diverse way concerning the cell sizes. [17,18] Which means that the light with smaller wavelengths (bluish colors) is greater scattered than those with higher wavelengths (reddish colors) and in the case of the infrared light, becomes almost transparent and not scattered by the cellular material. This fact is especially remarkable in nanocellular foams when the cell sizes reach values lower than 200 nm. The decrease of the heat conduction transfer through the gas phase, due to the Knudsen effect, make the nanocellular foams one of the most promising insulators of the future.[19] However, the lack of technologies to produce at industrial scale these nanocellular foams and the high densities that these materials still present make microcellular foams still being the most used ones as thermal insulators.[20]

Therefore, it seems that, in low density foams, there is an appropriate range of cell sizes in which the thermal radiation is reduced when the cell sizes are decreasing as well.

Controlling in a precise way the cell size of cellular materials with similar relative densities is a key factor to obtain a reduction of the thermal conductivity due to the depletion of the radiation term. The incorporation of nanoparticles is a promising strategy to improve the cellular structure, by increasing the cell nucleation density and therefore, reducing the cell size.[21,22] Previous works have demonstrated that sepiolites work as strong nucleation agents in cellular materials based on PS.[23]

In the present work a set of cellular materials based on blends of PS and sepiolites, with similar relative densities, with the same anisotropy ratio and with different cell sizes (varying between 8 and 100 microns), have been produced. Later, a systematic study has been performed to analyze how the thermal conductivity depends on the cell size. A modeling of the thermal conductivity, considering the different terms, has been done and a confirmation of the phenomena of the variation of the thermal conductivity with the cellular size has been performed by the measurement of the extinction coefficient.

## 2. EXPERIMENTAL

A commercial PS matrix, recommended for foam applications (INEOS, Styrolution PS153F), with a melt flow index of 7.5 g/10 min (200 ºC/5 kg) and a glass transition temperature (Tg) of 102 ºC was used in this work. Moreover, three kinds of sepiolites kindly supplied by Tolsa S.A. (Madrid, Spain) were employed: non-organically modified sepiolites (N-SEP), sepiolites organically modified with quaternary ammonium salts (O-QASEP) and sepiolites organically modified with silanol groups (O-SGSEP). An antioxidant (BASF, Irganox 1010) was also used during the extrusion process to avoid the thermal degradation of the polymer matrix. Finally, carbon dioxide (CO2) (99.9% purity) was used as blowing agent for the foaming of the PS composites.

Prior to the extrusion process the materials were dried in a vacuum drying oven (Mod. VacioTem TV, P-Selecta) at 70 ºC for 4 hours, in the case of pure PS, and at 80 ºC for 8 hours in the case of the different types of sepiolites. The mixing of the polymer with the sepiolites was carried out in a twin-screw extruder (Collin ZK 25T with L/D of 24) following a temperature profile that goes from 145 ºC to 185 ºC (at the die of the extruder) and with a screw rate of 50 rpm. Different formulations were produced adding 2 wt.%, 6 wt.%, 8 wt.% and 10 wt.% of the three different types of sepiolites (N-SEP, O-QASEP and O-SGSEP) to the PS matrix. After extrusion the materials were thermoformed in a hot-cold plate press

(at 235ºC and 27 bar) to produce solid precursor with the following dimensions: 2 x 2 x 0.2 cm (L x W x T). These precursors were used during the foaming step.

The production of the foamed materials was performed using the gas dissolution foaming procedure. First, the samples were introduced in a pressure vessel where the blowing agent (CO2) was dissolved into the polymer matrix. The saturation step was performed using a pressure of 7 MPa and a temperature of 40 ºC for 8 hours.[23] Once the samples were completely saturated the pressure vessel was depressurized and the samples were introduced in a thermostatic oil silicone bath for 1 minute at 120 ºC to allow their expansion. The solid skin of the foamed samples was removed using a polishing machine (LaboPO12-Laboforce3, Struers).

The density of the cellular materials was determined by the geometric method, that is, dividing the corresponding mass of each specimen by its geometric volume (ASTM D1622-08).

The cellular structure of the foams was characterized by scanning electron microscopy (SEM Jeol, Mod. JSM-820). Later, the average cell size ($\Phi$) was obtained with an image processing tool based on the software Fiji/Image J.[24]

The thermal conductivity of both the foamed samples and the solid composites was measured using the transient plane soured (TPS) method at room temperature (23 ºC).[8] The thermal conductivity of the foamed samples was measured one month after their production. This way it can be considered that the O2, used as blowing agent has been exchanged by air, and therefore, the gas inside the cells is air with a thermal conductivity of 26.24 mW/mK.

The extinction coefficient was determined by Fourier transform infrared spectroscopy (FTIR). To determine the extinction coefficient, the foamed samples were cut into thin sheets with thicknesses varying between 0.5 mm and 2 mm. Infrared spectra were collected with a Bruker Tensor 27 FTIR spectrometer. First, the backgrounds were registered to eliminate $H_2O$ and $CO_2$ contributions. Later, transmittance spectra were obtained considering the samples with different thicknesses. The transmittance ($\tau_{n,\lambda}$) was determined as the ratio between the intensity transmitted through the sample ($I_\lambda(x)$) and the incident intensity ($I_{\lambda\,0}(x)$) (**Equation 5**).

$$\tau_{n,\lambda} = \frac{I_\lambda(x)}{I_{\lambda\,0}(x)} \qquad [5]$$

The spectral extinction coefficient ($K_{e,\lambda}$) for thin samples can be obtained using the Beer-Lambert law, which indicates that there is a relation between the

transmittance values ($\tau_{n,\lambda}$), the thickness of the sheet ($L$) and the extinction coefficient of the sample ($K_{e,\lambda}$), which depend on the nature of the material (see **Equation 6**).

$$\tau_{n,\lambda} = e^{\left(-\int_0^L K_{e,\lambda}\, dx\right)} \qquad [6]$$

For homogeneous samples, under the assumption that $K_{e,\lambda}$ is independent of x, it is possible to write the following equation (**Equation 7**)

$$K_{e,\lambda} = \frac{-\ln(\tau_{n,\lambda})}{L} \qquad [7]$$

By means of a linear regression ($\ln(\tau_{n,\lambda})$ vs. L), the spectral extinction coefficient ($K_{e,\lambda}$) can be obtained for each wavelength ($K_{e,\lambda}$). To obtain a single value of the extinction coefficient it is possible to use Rosseland approximation, which is valid when the medium absorbs, and its scatter is isotropic. Under these conditions, the Rosseland extinction coefficient ($K_{eR}$) can be determined according to (**Equations 8, 9 and 10**).

$$\frac{1}{K_{eR}} = \frac{\int_{\Delta\lambda} \frac{1}{K_{e,\lambda}} \left(\frac{\partial e_{b,\lambda}}{\partial T}\right) d\lambda}{\int_{\Delta\lambda} \left(\frac{\partial e_{b,\lambda}}{\partial T}\right) d\lambda} \qquad [8]$$

$$e_{b,\lambda} = \frac{c_1}{\lambda^5 \left(e^{\left(C_2/T\lambda\right)} - 1\right)} \qquad [9]$$

$$\frac{\partial}{\partial T} e_{b,\lambda} = \frac{C_1 C_2 e^{\left(C_2/T\lambda\right)}}{\lambda^6 T^2 \left(e^{\left(C_2/T\lambda\right)} - 1\right)^2} \qquad [10]$$

Were $T$ is the temperature, and $C_1$ and $C_2$ are the first radiation constant and the second radiation constant, respectively.

## 3. RESULTS

**Figure 1** shows an example of how the addition of nanoparticles modify the cell size. This figure also indicates that the anisotropy ratio does not vary significantly between the two formulations. In **Table 1** the values of the relative density, cell size and anisotropy ratio of the different cellular materials produced are depicted.

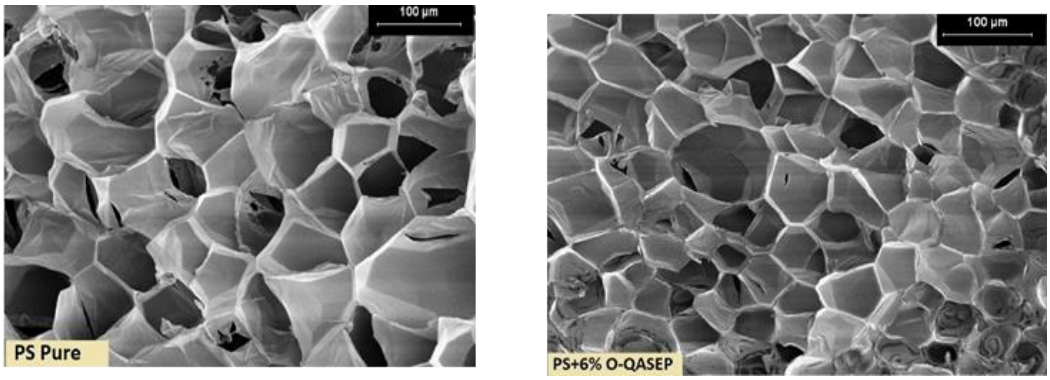


**Figure 1.** SEM microscopies of the pure PS foamed sample (left) and the foamed sample containing 6 wt.% of O-QASEP (right).

**Table 1.** Relative density, cell size and anisotropy ratio of the different foamed samples.

| Sample Name | Relative Density | Cell size (µm) | Anisotropy |
|---|---|---|---|
| **PURE PS** | 0.030 ± 0.006 | 89 ± 26 | 1.14 ± 0.03 |
| **PS+2% N-SEP** | 0.031 ± 0.008 | 60 ± 11 | 1.14 ± 0.06 |
| **PS+2% O-QASEP** | 0.031 ± 0.004 | 49 ± 9 | 1.11 ± 0.01 |
| **PS+2% O-SGSEP** | 0.031 ± 0.001 | 58 ± 12 | 1.12 ± 0.02 |
| **PS+6% N-SEP** | 0.031 ± 0.006 | 39 ± 11 | 1.16 ± 0.02 |
| **PS+6% O-QASEP** | 0.031 ± 0.001 | 32 ± 9 | 1.19 ± 0.03 |
| **PS+6% O-SGSEP** | 0.032 ± 0.004 | 41± 12 | 1.21 ± 0.01 |
| **PS+8% N-SEP** | 0.032 ± 0.006 | 11 ± 4 | 1.18 ± 0.04 |
| **PS+8% O-QASEP** | 0.032 ± 0.008 | 9 ± 2 | 1.16 ± 0.07 |
| **PS+8% O-SGSEP** | 0.033 ± 0.007 | 17 ± 6 | 1.18 ± 0.08 |
| **PS+10% N-SEP** | 0.034 ± 0.002 | 10 ± 3 | 1.17 ± 0.05 |
| **PS+10% O-QASEP** | 0.033 ± 0.003 | 8 ± 1 | 1.19 ± 0.04 |
| **PS+10% O-SGSEP** | 0.036 ± 0.007 | 12 ± 5 | 1.14 ± 0.02 |

Results depicted in Table 1 indicates that all the foamed samples present a similar relative density. In general, the values of the relative density slightly increase when the content of particles increases; however, the differences detected are not very high. Moreover, no significant differences are detected in terms of anisotropy ratio. This fact is important to make possible a comparison of the thermal conductivity values obtained for the different foams and isolate the effects associated with having foams with different cell size. Table 1 also indicates that the foams present significant differences in the cell size. This parameter varies between values close to 90 µm, for the pure PS, and values close to 10 µm for the formulations containing the highest amount of sepiolites (10 wt.%).

**Figure 2** shows the variation of the thermal conductivity, determined with the TPS method, as a function of the cell size. When the cell size varies between 90 μm and 40 μm a decrease in the thermal conductivity is detected. However, when the cell size varies between 40 μm and 10 μm an increase in the thermal conductivity is observed. The IR radiation is that band in the electromagnetic radiation spectrum with wavelengths above red visible light, between 780 nm and 1 mm. In the case of foams with cell sizes close to values lower than 10 times the wavelength of the infrared radiation (that is, cell sizes varying between 78 nm and 100 μm) the main method of scattering is the Rayleigh one, which means that the light with smaller wavelengths (bluish colors) is greater scattered than those with higher wavelengths (reddish colors) and in the case of the infrared light, start to become almost transparent and not scattered by the cellular material.

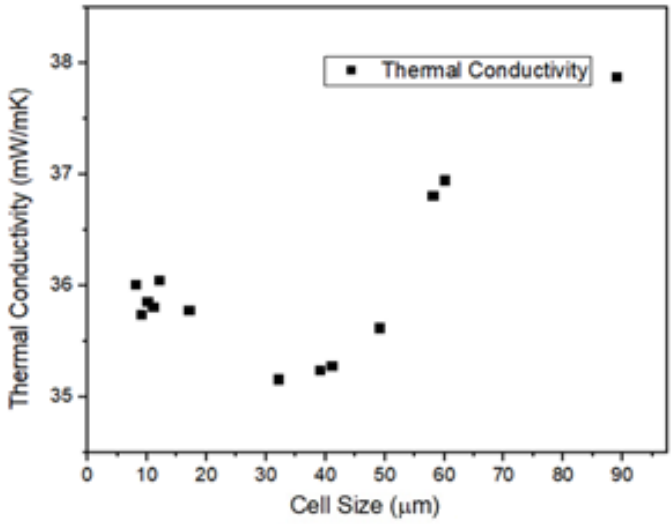


**Figure 2**. Thermal conductivity, experimentally determined, as a function of the cell size.

The thermal conductivity has been modeled according to Equations 1-3. This way it is possible to analyze the variation with the cell size of the conduction through the solid phase and the conduction through the gas phase. The obtained results are depicted in Figure 3a and 3b.

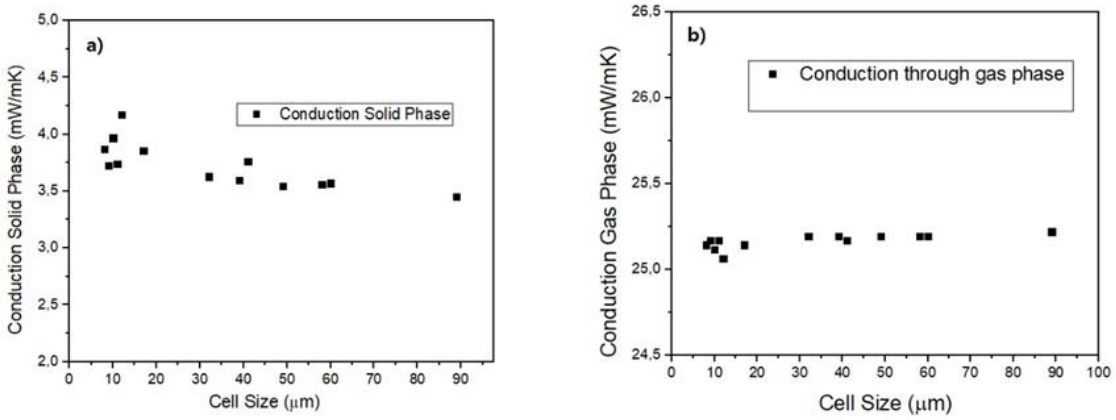


**Figure 3a.** Thermal conductivity through the solid phase, theoretically calculated, as a function of the cell size. **Figure 3b.** Thermal conductivity through the gaseous phase, theoretically calculated, as a function of the cell size.

Figure 3a shows the variation of the conduction through the solid phase as a function of the cell size. On the one hand, this term depends on the relative density of the foamed samples and on the anisotropy ratio, which were similar in all the materials analyzed (see Table 1). On the other hand, this term also depends on the thermal conductivity of the solid phase, this parameter has been experimentally determined and the obtained results are depicted in **Table 2**. It is possible to see that the thermal conductivity of the solid phase increases due to the presence of sepiolites. Similar values are obtained independently on the type of sepiolite used. Finally, this parameter also depends on the fraction of mass in the struts. A constant value of the fraction of mass in the struts has been considered in this work (0.25), which is a value in agreement with low density microcellular foams.[5] Results indicate that the thermal conduction through the solid phase decreases as the cell size increases. This phenomenon cannot explain the minimum detected in the thermal conductivity when the cell size varies between 9 μm and 90 μm. On the other hand, even there is an increment of 0.5 mW/mK in the thermal solid conduction phase between the cell size ranges from 40 micrometers to 10 micrometers due to the increase of the thermal conductivity of the solid composites (see table 2). This fact could not explain the variation observed in the global thermal conductivity for these range of foams. In the total thermal conductivity, the change observed in the values at that range of cell sizes is more than 1.2 mW/mK so cannot be explained due to the increase observed in the thermal solid conductivity mechanism only.

On the other hand, the gas trapped in the cells, after the diffusion of the $CO_2$, is air, with a thermal conductivity of 26.24 mW/mK at room temperature (298 K).

Furthermore, the foamed materials present a similar relative density. Consequently, the conduction through the gas phase does not change substantially with the cell size as it is indicated in Figure 3b.

**Table 2**. Thermal conductivity of the solid composites.

| Sample Name | $\lambda_{solid}(mW/mK)$ |
|---|---|
| **PURE PS** | 189.9 |
| **PS+2% N-SEP** | 190.2 |
| **PS+2% O-QASEP** | 190.4 |
| **PS+2% O-SGSEP** | 190.5 |
| **PS+6% N-SEP** | 190.6 |
| **PS+6% O-QASEP** | 190.8 |
| **PS+6% O-SGSEP** | 190.7 |
| **PS+8% N-SEP** | 191.0 |
| **PS+8% O-QASEP** | 191.2 |
| **PS+8% O-SGSEP** | 191.1 |
| **PS+10% N-SEP** | 191.3 |
| **PS+10% O-QASEP** | 191.2 |
| **PS+10% O-SGSEP** | 191.4 |

The radiation term has been obtained following two alternative routes. On the one hand, by using the Equation 4. In this case it was necessary to determine the Rosseland extinction coefficient of the different samples by FTIR spectroscopy. The variation of the extinction coefficient as a function of the cell size is depicted in **Figure 4.** This parameter presents a maximum for a value of the cell size close to 40 μm. When the values of the cell size vary between 100 μm and 40 μm the extinction coefficient increases, which indicates that the material absorbs the infrared radiation more easily. However, when the cell size varies between 40 μm and 10 μm the extinction coefficient decreases. This result indicates that foams start to be more transparent to the infrared radiation.

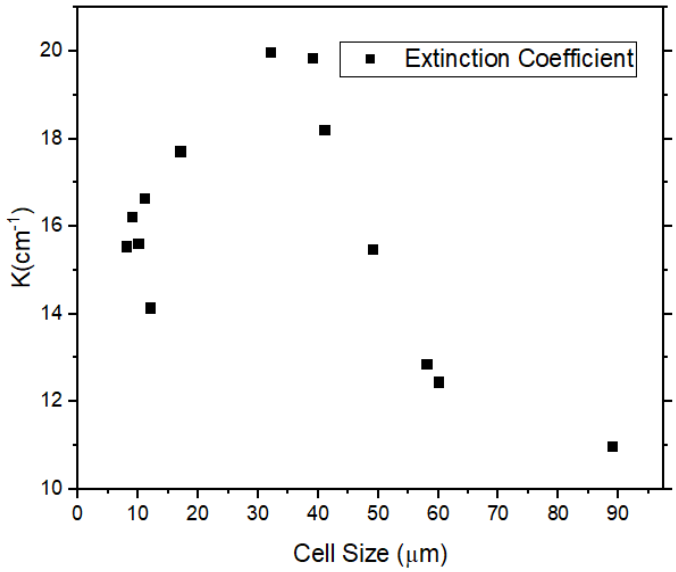


**Figure 4.** Values of the Rosseland extinction coefficient as a function of the cell size.

Once the Rosseland extinction coefficient was determined, the Rosseland approximation (Equation 4) was used to determine the radiation term of the thermal conductivity. The results obtained are depicted in **Figure 5**.

On the other hand, the radiation term has been also obtained by subtracting from the thermal conductivity of the foam the terms of conduction trough the solid and gaseous phases. The obtained results are also depicted in Figure 5.

Independently on the procedure used to determine the radiation term it is possible to see that the radiation term presents a minimum for a value of the cell size close to 40 μm. Moreover, there is a slight difference between the two curves obtained by the two different methods, which indicates that the hypothesis of considering a fraction of mass in the struts of 0.25 to perform the different calculus is a good approximation.

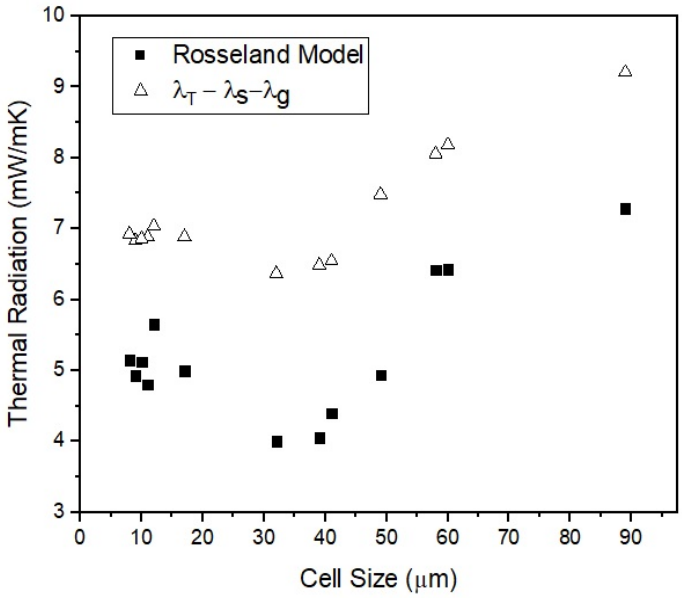


**Figure 5.** Thermal radiation values obtained by applying the Rosseland model and by subtracting from the global thermal conductivity the contributions of the solid and gaseous phases.

## 4. CONCLUSIONS

In this paper the thermal conductivity is measured for a series of cellular nanocomposites based in PS/SEP and related with the cellular structures that present these materials. The data reported exhibit a reduction of the thermal conductivity in the range from 90 μm until 30 μm. This result could be correlated seen the increase in the extinction coefficient at the same rage of cell sizes. This trend of the decreasing of the thermal conductivity with the cell size has been reported in several previous publications. Also, is also possible to see an increase for values of the cell size lower than 35 μm in the extinction coefficient. However, at a certain vale close to 35 μm the thermal conductivity starts to increase again. Again, the same effect, a decrease in the extinction coefficient, is reported in the FTIR experiment. Both behaviors constitute a proof that in PS there is a selected range of micrometric sizes where the thermal conductivity is minimum

## 5. REFERENCES

[1] D. Feldman. *Polymeric foam materials for insulation in buildings. In: Materials for Energy Efficiency and Thermal Comfort in Buildings*. **2010**, CRC press Taylor and Francis Group, Bocaraton, United States.

[2] T. Azdast, R. Hasanzadeh. *J Cell Plast*. **2021**, 57 (5),769-797.

[3] N.C.Hilyard, A.Cunningham . *Low Density Cellular Plastics: Physical Basis of Behavior*. **1994**, first edition, Springer Science, The Netherlands.

[4] L.R.Glicksman . *Heat Transfer in foams. In: Low Density Cellular Plastics: Physical Basis of Behavior*. **1994**, first edition, Springer Science, The Netherlands.

[5] O.Almanza, M.A.Rodriguez-Perez, J.A.De Saja. *J Polym Sci Part B. **2000**, 38 (7), 993-1004.*

[6] Y. Li, S. Ren. *Acoustic and Thermal Insulating Materials. In: Building Decorative Materials*. **2011**, first edition, Elsevier, Amsterdam, The Netherlands.

[7] X. Han, K.W. Koelling, D.L. Tomasko, L.J. Lee. *Polym Eng Sci*. **2003**, 43(6),1206-1220.

[8] E.Placido, M.C. Arduini-Schuster, J. Kuhn. *Infrared Phys Technol*. **2005**, 46(3), 219-231.

[9] O.Almanza, M.A.Rodriguez-Perez, J.A.De Saja. *Polymer. **2001**, 42 (16), 7117-7126.*

[10] R.J.J. Williams, C.M. Aldao. *Polym Eng Sci*. **1983**, 23(6),293-298.

[11] J.R.Howell, R. Siegel, M.P.Mengu. *Thermal Radiation Heat Transfer*. **2021**, seventh edition, CRC press Taylor and Francis Group, Bocaraton, United States.

[12] M. Alvarez-Lainez, M.A. Rodríguez-Perez, J.A. De Saja. *J. Polym. Sci. Part B Polym. Phys*.**2008**, 46, 212-221.

[13] J.Schellenberg, M. Wallis. *J Cell Plast*. **2010**,46(3), 209-222.

[14] T.Widya, C.W. Macosko. *J Macromol Sci Part B*. **2005**, 44(6), 897-908.

[15] C.De Micco, C.M. Aldao. *J Polym Sci Part B Polym Phys*. **2005**, 43(2),190-192.

[16] M.Arduini-Schuster, J. Manara, C. Vo. *Int J Therm Sci*. **2015**, 98, 156-164.

[17] J.Martín-de León,J.L. Pura, V. Bernardo, M.A. Rodríguez-Pérez. *Polymer (Guildf)*. 2019,170,16-23.

[18] F.Almeida, H. Beyrichen, N. Dodamani, R. Caps, A. Müller, R. Oberhoffer. *J Cell Plast*. **2021**;57,(4), 493-515.

[19] B. Notario, J. Pinto, E. Solorzano, J.A. De Saja, M. Dumon, M.A. Rodriguez-Perez. *Polym (United Kingdom)*. **2015**,56,57-67.

[20] C. Forest, P. Chaumont, P. Cassagnau, B. Swoboda, P. Sonntag. *Prog Polym Sci*. **2015**, 41(6),122-145.

[21] B. Lecouvet B, J.G.Gutierrez, M. Sclavons, C.Bailly C. *Polym Degrad Stab*. **2011**,96(2), 226-235.

[22] V. Dolomanova, J.C.M. Rauhe, L.R. Jensen, R. Pyrz, A.B. Timmons, J. Cell. Plast. **2011**,47,81–93.

[23] A. Ballesteros, E. Laguna-Gutierrez, P. Cimavilla-Roman, M.L. Puertas, A. Esteban-Cubillo, J. Santaren, M.A. Rodriguez-Perez. *J. Appl. Polym. Sci.* **2021,** 10, 51373.

[24] J. Pinto, E. Solorzano, M.A. Rodriguez-Perez, J.A. De Saja. *J. Cell. Plast.***2013**, 49 (6), 555-575.

# Chapter 7

# SEBS as cell nucleating agents in PS foams. Analysis of the effects of SEBS in the foaming mechanisms.

"Facilius per partes in cognitionem totius aduccimur"
Lucio Anneo Séneca.

"Por partes conseguiremos entender mejor el todo"
Lucio Anneo Séneca.

# INDEX

## 7.1 Introduction

This section contains the publication named as: "SEBS as an Effective Nucleating Agent for Polystyrene Foams" published in Polymers (A. Ballesteros, E. Laguna-Gutierrez, M. A. Rodriguez-Perez), 13 (21), 3836.

In this work a deeply study is performed with the aim of analyzing how the foaming mechanisms of a PS foam are affected by the incorporation of a SEBS tri-block copolymer.

SEBS is a tri-block-copolymer formed by monomers of styrene, ethylene, and butylene. SEBS is a thermoplastic elastomer which presents a rubber behavior. SEBS was chosen as nucleating agent due to the interesting chemistry that this organic phase presents. On the one hand, the styrenic part of the SEBS presents a good interaction with the PS matrix, which makes easier the compatibility and dispersion of this elastomeric phase in the polymer. On the other hand, the ethylene- butylene part does not show this affinity and it creates domains in which the cells will grow preferably. Therefore, this is a mechanism to modify the nucleation. Furthermore, the butylene part presents a high affinity for the $CO_2$ gas used as blowing agent, which is interesting to improve the gas concentration in the polymer matrix during the saturation step.

Different contents of SEBS (varying between 0.25 wt.% and 10 wt.%) have been introduced in the PS matrix. The dispersion of the SEBS particles in the PS matrix has been analyzed by means of scanning electron microscopy. A proper quantity of well distributed particles will provide a beneficial nucleation effect in the PS. However, a bad distribution this secondary phase will lead to properties even lower than those of the pure PS matrix.

Both the shear dynamic and the extensional rheological behavior of the composites was characterized, to understand how the cell growth and cell degeneration mechanisms are influenced by the incorporation of SEBS. Furthermore, the variation of the glass transition temperature (Tg) was measured by DSC.

Later, different cellular materials were produced using the previously analyzed composites. The foams were produced by gas dissolution foaming using $CO_2$ as blowing agent.

Finally, the density and cellular structure of these foamed materials were analyzed to determine parameters like the cell size, cell density, etc.

The obtained results indicate that the shear viscosity, the extensional viscosity, and the strain hardening decrease as the content of SEBS increases. Therefore, a deterioration of the cellular structure is observed when working with contents of SEBS higher than 3 wt.%.

In Figure 7.1 it is possible to see the graphical abstract of the mentioned article.

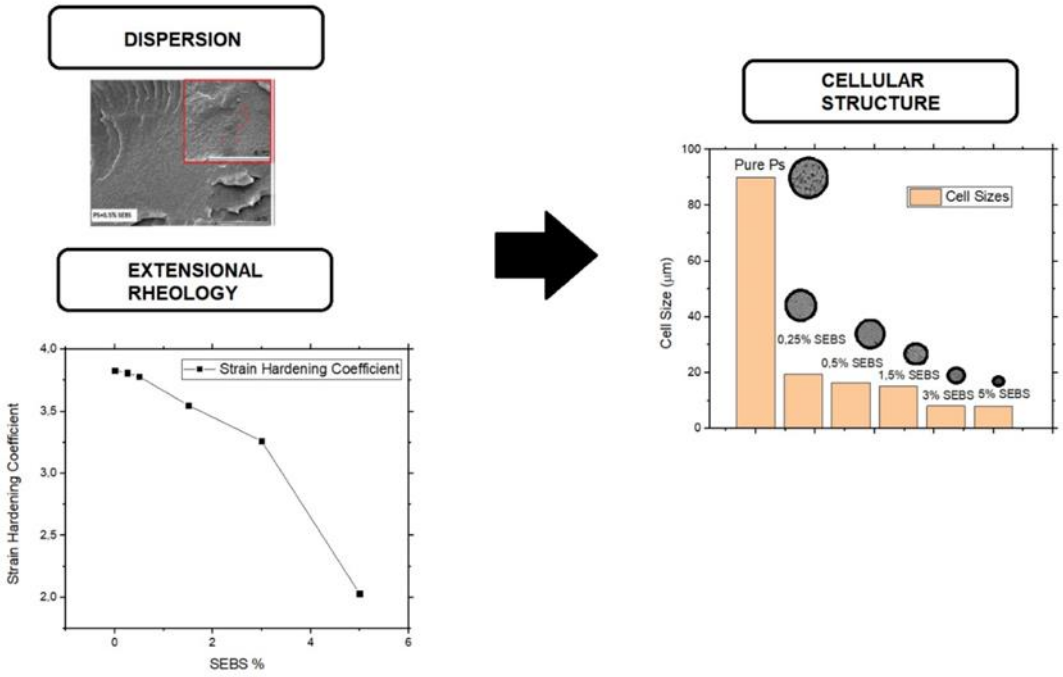


**Figure 7.1**. Graphical abstract of "SEBS as an Effective Nucleating Agent for Polystyrene Foams".

# SEBS as an Effective Nucleating Agent for Polystyrene Foams.

A. Ballesteros, E. Laguna-Gutiérrez, M. A. Rodríguez-Pérez.

***Cellular Materials Laboratory (CellMat)**, Paseo de Belén, 7, Condensed Matter Physics Department, Science Faculty, University of Valladolid, 47011, Valladolid*

***CellMat Technologies**, Edificio Parque Científico UVa, Paseo de Belén 9-A, 47011, Valladolid, Spain.*

## ABSTRACT

Different percentages of an elastomeric phase of styrene-ethylene-butylene-styrene (SEBS) were added to a polystyrene (PS) matrix to evaluate its nucleating effect in PS foams. It has been demonstrated that a minimum quantity of SEBS produces a high nucleation effect on the cellular materials produced. In particular, the results show that by adding 2% of SEBS it is possible to reduce the cell size by 10 times while maintaining the density and open cell content of the foamed materials. The influence of this polymeric phase on the glass transition temperature (Tg), shear and extensional rheological properties has been studied to understand the foaming behavior. Results indicate a slightly increase in the Tg and a decrease of the shear viscosity, extensional viscosity, and strain hardening coefficient as the percentage of SEBS increases. Consequently, an increase in density and a deterioration of the cellular structure is detected for SEBS amounts higher than 3%.

## KEYWORDS

Organic phases; SEBS; rheology; Cellular materials; Polystyrene.

## 1. INTRODUCTION

Elastomeric phases, like thermoplastic elastomers (TPEs), which present the elastic behavior of rubbery materials and the re-processability of the thermoplastic polymers, have aroused the interest of the scientific community in the last years.[1] Among all the TPE available, the tri-block copolymers have been used widely. Some examples of them are the: poly(methyl methacrylate)-poly(butyl acrylate)-poly(methyl methacrylate) copolymers, also known as MAM, the styrene-butylene-styrene (SBS) or the styrene-ethylene-butylene-styrene (SEBS). This last material presents a high resistance to degradation, which

makes it interesting for blending with common thermoplastic materials like polypropylene (PP) or polystyrene (PS).[2] The incorporation of this organic phases in common thermoplastic polymers has been reported by several researchers with successfully results when it deals on modifying the impact properties of the solid polymer matrix. For instance, Sang et al. reported that by adding 13 wt.% of SEBS to a PS matrix it was possible to improve the impact strength up to 4.4 times compared to the one of the pure PS.[3] Furthermore, Lindsey et al. showed that the inclusion of 20% SEBS in blends of high-density polyethylene (HDPE) with PS increases in a 100% the impact behavior of the blends, with the drawback of reducing the tensile strength and the elastic modulus.[4] Finally, Banerjee et al. reported that it was possible to reinforce the mechanical properties of a SEBS matrix by introducing a certain amount of PS. They also reported that the rheological behavior was modified. An increase in the PS content resulted in the lowering of the shear viscosity and energy requirement for mixing, indicating an easier flow and a more sustainable processing.[1]

However, the use of these elastomeric organic phases to improve the cell nucleation of common polymers during the foaming process has not been deeply studied. In general terms, the addition of a second phase creates interfaces in the polymer/gas mixture, and these surfaces induce wetting, that is, gas molecules tend to aggregate at the foreign surface. Then, the nucleation process tends to take place in these pre-existing surfaces. This process is called heterogeneous nucleation. The nucleation rate (NHET), for heterogeneous nucleation, is given by **Equation 1.**[5]

$$N_{HET} = C_1 f_1 \, exp\left(\frac{-\Delta G'_{het}}{KT}\right) \qquad [1]$$

where C1 is the concentration of gas in the polymer, f1 is the frequency factor of the gas molecules, k is the Boltzmann constant, T is the temperature and $\Delta G'_{het}$ is the free energy barrier for the heterogeneous nucleation that should be overpassed to obtain stable nucleus.

The paucity of literature focused on studying the effects, in the foaming mechanisms, associated to incorporate a TPE phase to a thermoplastic polymer matrix could be due to the difficulties associated with the selection of the proper organic phases. There are two key aspects that must be considered to obtain an improvement of the heterogeneous nucleation and therefore, of the foaming behavior. On the one hand, the elastomeric phase must be properly dispersed in the polymer matrix and on the other hand, the elastomeric phase must have a

high affinity with the blowing agent used during the foaming process.[6] It is well known that dispersion plays a key role that determine the final properties of the cellular materials. In fact, a poor dispersion could deteriorate the final properties of the cellular materials to values even lower than those obtained with the virgin polymers.[7] The main advantage of using secondary organic phases, like TPE, to promote nucleation is that it is possible to design systems that "self-assemble" during melt blending creating a morphology with an excellent dispersion of very small domains of the secondary phase. However, this only can be achieved when using materials with a proper chemistry between the phases and an adequate viscosity.

Some examples in the literature focused on using organic phases in cellular materials have been found. MAM or thermoplastic polyurethane (TPU) have been used successfully as nucleating agents in poly (methyl methacrylate) (PMMA) while polydimethylsiloxane (PDMS) has been used in PP and in PS. Bernardo et al. have demonstrated that by adding 10 wt.% of a MAM copolymer to a PMMA matrix it was possible to reduce the cell size in a 93%, with respect to the pure PMMA.[8] Bernardo et al. have also demonstrated that the addition of 2 wt.% of TPU allows reducing the cell size of PMMA foams in an 80%.[9] Haurat et al. reported the results obtained using two different additives core-shell (CS) particles based on PBA (poly (butyl acrylate)) and PMMA and MAM in a PMMA polymer matrix. Results indicate that a liquid-core CS presents advantages for a decrease in density, even at room temperature foaming. On another side, in a PMMA/20 wt% MAM blend, through a quasi-one-step batch foaming, a "porous to nonporous" transition is observed on thick samples. Such a sharp porosity gradient (from nonporous transparent areas to porous opaque areas within the same sample) would reveal a lower limit of pore size at around 50 nm in a batch classical process in "mild conditions".[10] Qingfeng et al. reported a remarkable increase in the cell density of PP foams by the inclusion of a 5.2 wt.% of PDMS [5]. Quiang et al. demonstrated that with the inclusion of just a 1 wt.% of PDMS to a PS matrix it was possible to double the solubility of $CO_2$ with respect to that obtained in the pure PS matrix.[11] Banerjee et al. have studied the use of PS (10 wt.%,30 wt.% and 50 wt.%) as nucleation agent for the SEBS polymer. They observed an increase in the complex viscosity of the solid composites as the content of PS increased. They also reported that when the materials were foamed at temperatures closed to the glass transition (Tg) of the PS, the rheological characteristics of the material ruled the expansion ratio and the shrinkage. On the other hand, when the foaming temperatures were lower than the Tg of the PS but

higher than that of the ethylene-butylene phase, the PS act as a nucleation agent for the SEBS material. In this situation a 30 wt.% of PS leads to a reduction of the cell size of a 60%, with respect to the pure SEBS. Higher contents of PS (50 wt.%) generates a co-continuous phase in the material resulting in an increase of the cell size.[12]

Finally, Sharudin et al. have also reported the effect in the shear dynamic rheology and foaming behavior associated to adding PS to a SEBS matrix. They have found that an increase in the styrene content led to an increase of the storage modulus and to a decrease of the gas permeability. As a result, the shrinkage of the foam was controlled, and stable microcellular elastomer foams were obtained.[13]

After the literature search and as far as the author knows, there are not works that analyze the use of SEBS as a nucleation agent in a cellular material based on PS.

Taking all the previous ideas into account, in this work different contents of SEBS, varying between 0.25 wt.% and 10 wt.%, have been added to a PS matrix with the objective of improving the cell nucleation mechanisms. A significant reduction of the cell size can be only achieved if the system presents a proper dispersion of the elastomeric phases (ethylene-butylene) and a good interaction with the gas used as blowing agent (CO2).

The reduction of the cell size due to the improvement of the cell nucleation mechanisms and the improvement of the homogeneity of the cellular structure could have positive effects in the physical properties of the foamed samples by reducing the thermal conductivity and improving the mechanical properties.[14] This is a very interesting result considering one of the main applications of PS foams as thermal insulators in the construction sector.[15] Furthermore, this work is the first one, as far as the authors known, that analyzes the effects of the SEBS as cell nucleating agent in PS foams.

## 2. MATERIALS AND METHODS

A commercial polystyrene (PS) recommended for foam applications (Edistir N3840 from Versalis) with a melt flow index of 10 g/10 min (200 °C/5 kg), a density of 1.05 g/cm$^3$ and a glass transition temperature (Tg) of 89 °C was used as polymer matrix. A commercial SEBS (Kraton G1643MS from Kraton Corporation, Texas, United States) with a melt flow index of 17.6 g/10 min (200

°C/5 kg), a density of 0.91 g/cm$^3$ and a styrene content of 20% was used as secondary phase to produce the PS-SEBS blends. Before materials were processed, they were dried in a vacuum drying oven (Mod. VacioTem TV, P-Selecta, Barcelona, Spain) at 70 °C for 4 h.

The mixing of the PS with the SEBS was carried out in a twin-screw extruder (Collin ZK 25 T with L/D of 24) following a temperature profile that goes from 145 °C to 185 °C (at the die) and with a screw rate of 50 rpm. Different formulations were produced adding 0.25 wt.%, 0.5 wt.%, 1.5 wt.%, 3 wt.%, 5 wt.% and 10 wt.% of SEBS to the PS matrix. After extrusion the materials were pelletized and then, thermoformed in a hot-cold press (at 235 °C and 27 bar) obtaining materials with the desired shape and size 2 × 2 × 0.2 cm (L × W × T) for the foaming experiments.

The glass transition temperature (Tg) of the pure PS and the materials containing SEBS was analyzed by differential scanning calorimetry (DSC) using a DSC 3 + from Mettler Toledo. A heating step from 20 °C to 160 °C at a heating rate of 10 °C min$^{-1}$ was considered in this experiment. The measurements were performed in a nitrogen atmosphere with a flux of 60 mL/min.

The shear dynamic rheology was measured using a stress-controlled rheometer (AR 2000 EX from TA Instruments). Dynamic shear measurements were performed at a temperature of 220 °C, under a nitrogen atmosphere, and using parallel plates with a diameter of 25 mm. A fixed gap of 1 mm was selected to perform the rheological measurements. First, a strain sweep test, at a fixed dynamic frequency (1 rad s$^{-1}$), was performed to determine the linear viscoelastic regime of the different blends. It was found that the strain employed should be 3%. Later, a time sweep was performed to recover the initial state of the material, which was partially deformed when the sample was loaded in the rheometer. The duration of the time sweep varied between 360 and 600 s, depending on the material. Finally, the frequency sweep step was performed in a range of angular frequencies varying between 0.01 and 100 rad s$^{-1}$. From these measurements, four parameters were analyzed: the dynamic shear viscosity in the terminal region, also known as zero shear viscosity ($|\eta*|$), the slopes of the storage and loss modulus ($G'$ and $G''$) in the terminal region and the cross over points among the two curves ($G'$ and $G''$). The same rheometer but in this case with an extensional fixture (SER 2 from Xpansion Instruments) was used to analyze the extensional rheological behavior of the different formulations. In this device, the samples were clamped to two cylinders that rotate, at a fixed rate, in opposite directions

applying a uniaxial stretching force to the material. All the experiments were conducted at a temperature of 160 °C and at different Hencky strain rates: 0.3, 0.5 and 1 $s^{-1}$. In all the experiments the maximum Hencky strain was 2.8. From these experiments the extensional viscosity was obtained as the ratio between the measured stress and the corresponding Hencky strain rate. A more detailed description of the measurement protocol can be found elsewhere.[7] From the extensional viscosity measurements, the strain hardening coefficient (S) was obtained. This parameter (see **Equation 2**), which allows quantifying the way in which the extensional viscosity increases when time or strain increase, has been obtained for the different formulations.

$$S = \eta_E^+(t, \dot{\varepsilon_0})/\eta_{E0}^+(t) \quad [2]$$

where $(\eta_E^+(t, \dot{\varepsilon_0}))$ is the transient extensional viscosity for a determined time $(t)$ and Hencky strain rate $(\dot{\varepsilon_0})$ and $\eta_{E0}^+(t)$ is the transient extensional viscosity in the linear viscoelastic regime, which can be obtained in two different ways: as three times the time-dependent shear viscosity growth curve at very low shear rates or by extrapolating the overlapping parts of the extensional curves at different elongation rates.[16] In the present work, the second option was chosen to obtain the strain hardening coefficient. This coefficient has been determined for a time of 2.67 s and for a Hencky strain rate of 1 $s^{-1}$.

The morphology of the solid (non-foamed) PS-SEBS blends was analyzed by scanning electron microscopy (SEM). First, the materials were frozen in liquid nitrogen and afterwards fractured. The surface of fracture was made conductive by sputtering deposition of a thin layer of gold and later, SEM micrographs were obtained by using a FlexSEM 1000 from Hitachi (Hitachi, Japan).

Foams were produced using the gas dissolution foaming process using a saturation pressure of 8 MPa and a saturation temperature of 40 °C for 8 h. $CO_2$ was used as blowing agent.[17] Once the samples were removed from the pressure vessel, they were introduced in a thermostatic oil silicone bath for 1 min at 120 °C to produce the expansion of the different materials.

Before characterizing the cellular materials, the solid skin of the foamed samples was removed using a polishing machine model LaboPOl2-LaboForce3 from Struers. Then, the density of the cellular materials without skin was determined (ASTM standard D1622-08). In addition, the open cell content was measured using a gas pycnometer according to the standard ASTM D6226 and using nitrogen as the gas for the measurement.

The cellular structure of the foamed samples was characterized by SEM using the same microscope and a similar procedure to prepare the samples to that employed with the solid materials. Parameters such as the average cell size (Φ), the cell nucleation density ($N_0$) and the standard deviation of the cellular structure (SD) were measured using an image processing tool based on the software Fiji/Image J.[18]

## 3. RESULTS AND DISCUSSIONS

To improve the nucleation mechanisms during the foaming process with the aim of improving the cell nucleation density and reducing the cell size, the dispersion of the secondary phase (SEBS) in the PS matrix should be as better as possible. Thus, an important step in this work was to determine if the elastomeric phase is well dispersed in the polymer matrix. The dispersion degree has been analyzed qualitatively through scanning electronic microscopy.

SEM images of the solid (non-foamed) composites are shown in **Figure 1**. In these micrographs it is possible to detect two different phases, the PS matrix and the SEBS domains. The domains have a spherical shape, and they are properly dispersed in the PS matrix with diameters varying between 0.2 and 0.5 μm. Examples of the SEBS domains have been marked with circles in the SEM images to favor their observation. The SEBS domains tend to agglomerate as SEBS content increases. It is remarkable that for contents higher than 3 wt.% of SEBS domains are bigger as can be seen in the SEM micrographs. This fact could indicate that there is an optimal content of SEBS that allows to maximize its dispersion in the PS matrix.

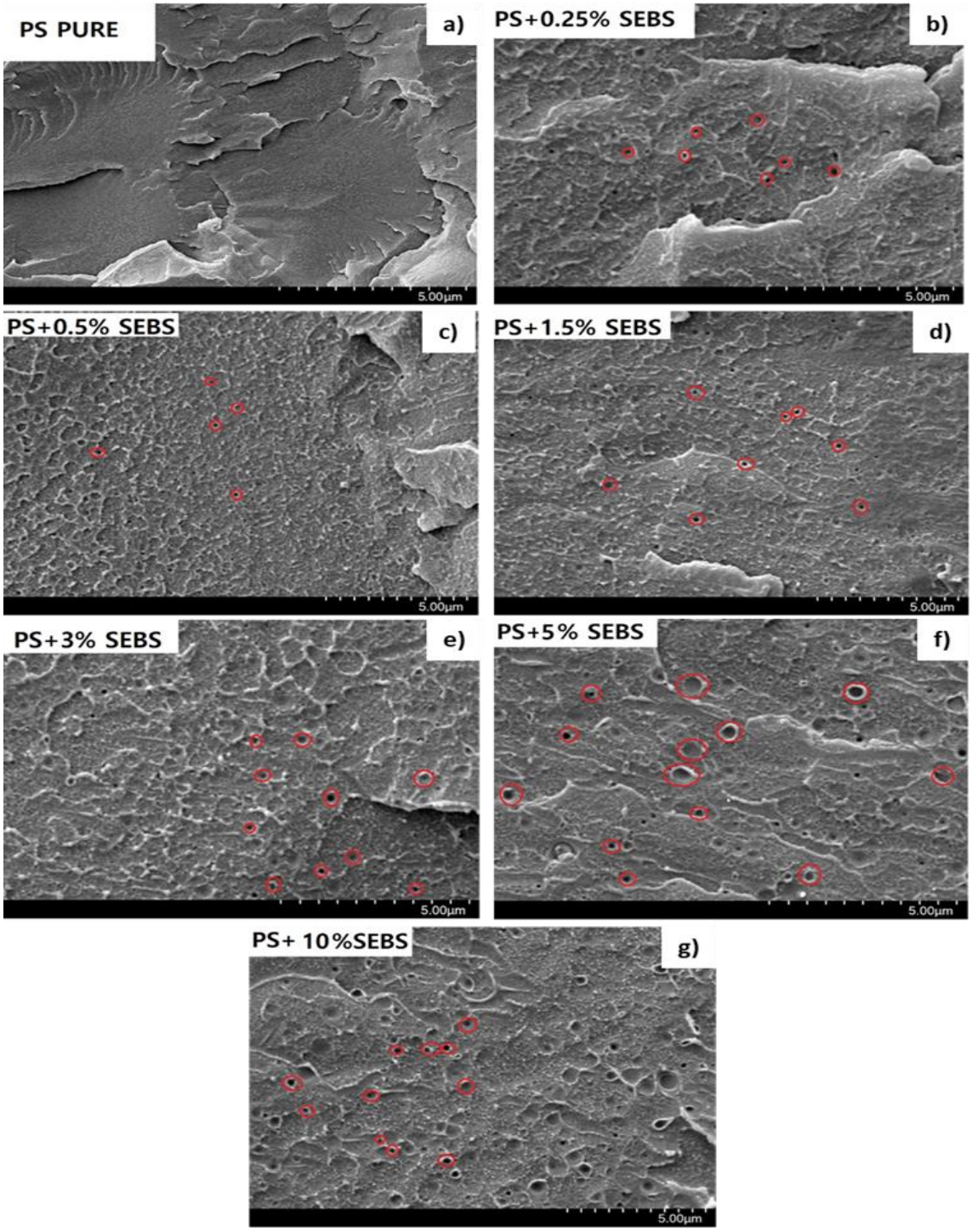


**Figure 1.** SEM micrographs of the solid formulations produced. (**a**) Pure PS; (**b**) PS +0.25% SEBS; (**c**) PS +0.5% SEBS; (**d**) PS +1.5% SEBS; (**e**) PS +3% SEBS; (**f**) PS +5% SEBS; (**g**) PS +10% SEBS. Red circles have been introduced to help with the visualization of the elastomeric phase.

**Figure 2** and **Table 1** show the results obtained after the DSC and the rheological characterization of the formulations containing SEBS. The results obtained by DSC indicate that the Tg remains constant for contents of SEBS lower than 1.5 wt.%. However, when the amount of particles is higher than 3 wt.% there is a

slight increment in the Tg. For instance, the Tg of the samples containing the maximum amount of SEBS (10 wt.%) is 5 °C higher than that of the pure PS. On the other hand, shear dynamic rheological results (Figure 2a) indicates that a decrease in the zero-shear viscosity is obtained when the amount of SEBS increases. This behavior is the expected one considering the significant differences between the melt flow indexes of the PS (10 g/10 min) and that of the SEBS copolymer (17.6 g/10 min), being the viscosity of the SEBS smaller than that of the PS. Results also indicate that when the content of SEBS is equal or higher than 5% the Newtonian regime is not detected and in this frequency range it is no longer possible to see a flat plateau, as it can be seen in Figure 2a. Banerjee et al. reported a reduced complex viscosity of the SEBS compared to the one of the PS, and an increase in the value of the complex viscosity, compared to the SEBS material, when different content of PS were introduced in the SEBS material [1]. An easy flowability is a usual characteristic of the TPE materials. When the content of SEBS is not remarkable (lower than 1.5. wt.%) the decrement observed in the viscosity due the higher flowability of the material is not notorious. However, when the formulations present higher SEBS contents, the values of the viscosity decrease remarkably.

**Table 1.** Glass transition temperature, shear and extensional rheology properties of the formulations produced.

| Name of the Sample | Tg (°C) | Zero Shear Viscosity (Pa·s) | Slope of G′ (Pa·s) | Slope of G″ (Pa·s) | Cross Over Points | Strain Hardening Coefficient |
|---|---|---|---|---|---|---|
| PURE PS | 94.96 | 3000 | 1.84 | 0.98 | 0 | 3.83 |
| PS + 0.25% SEBS | 93.31 | 2987 | 1.80 | 0.98 | 1 | 3.81 |
| PS + 0.5% SEBS | 93.31 | 2904 | 1.76 | 0.96 | 1 | 3.78 |
| PS + 1.5% SEBS | 94.61 | 2742 | 1.72 | 0.94 | 1 | 3.55 |
| PS + 3% SEBS | 97.40 | 2123 | 1.63 | 0.87 | 1 | 3.26 |
| PS + 5% SEBS | 98.04 | - | 1.56 | 0.81 | 1 | 2.03 |
| PS + 10% SEBS | 100.37 | - | 1.23 | 0.72 | 1 | 1.46 |

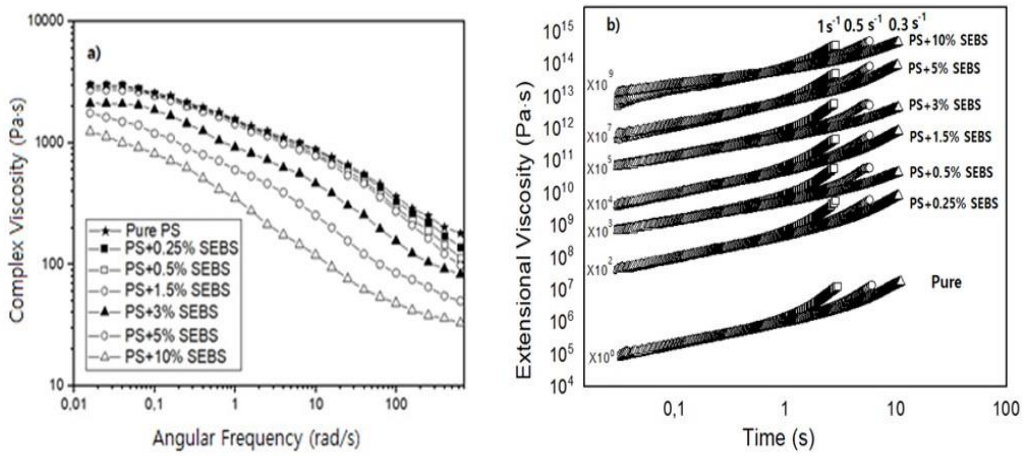


**Figure 2**. Results obtained after characterizing the rheological behavior of the different materials. (a) Shear dynamic rheology results. (b) Extensional rheology results.

Table 1 also shows that all the formulations present a single cross over point between the curves of the storage and loss modulus. In the work of Banerjee et al. is reported that when large domains of PS were created the flowability of the materials change due to the possibility of the SEBS to flow easily.[1] In the present work, we have not seen a notorious change in the behavior of the viscosity with the increment of the SEBS phase, which could indicate that large domains of SEBS have not been formed even when adding a content of SEBS of 10 wt.%. This fact agrees with the lack of change observed in the storage and loss modulus curves as well as in the cross over points between them.

The extensional rheological results (Table 1 and Figure 2b) show that the strain hardening coefficient of the materials is reduced as soon as the SEBS content increases. The extensional viscosity curves have been multiplied by a factor (included in the figure) to make possible the comparison of all the materials in a single figure. The reduction in the strain hardening is especially remarkable for the formulations that contains high quantities of SEBS (higher than 5%). A reduction of the strain hardening coefficient could lead to a worse foamability, resulting in materials that are not able to resist the extension during the foaming step leading to heterogeneous cellular structures with high cell sizes and high open cell contents.[7]

Figure 3 shows the SEM images of the foams produced with the different formulations. It is only necessary a very small amount of SEBS (0.25 wt.%), to reduce the cell size from 90 μm to 20 μm (see Table 2). When the SEBS content is lower than 2 wt.% it is possible to see that the cell size decreases as the cell content

increases, while the foam density remains almost constant (varying between 31–32 kg/m$^3$). This result indicates that the secondary phase (SEBS) is acting as a very efficient cell nucleation agent. When the content of SEBS varies between 2 wt.% and 5 wt.% the cell size still decreases as the content of SEBS increases. However, in these materials an increase in the foam density is detected as the SEBS content increases. Finally, for content of SEBS higher than 5 wt.% a significant increase is detected in both the foam density and the cell size. The cell size of the material containing 10 wt.% of SEBS (around 250 μm) is even higher than of the foam produced with the pure PS.

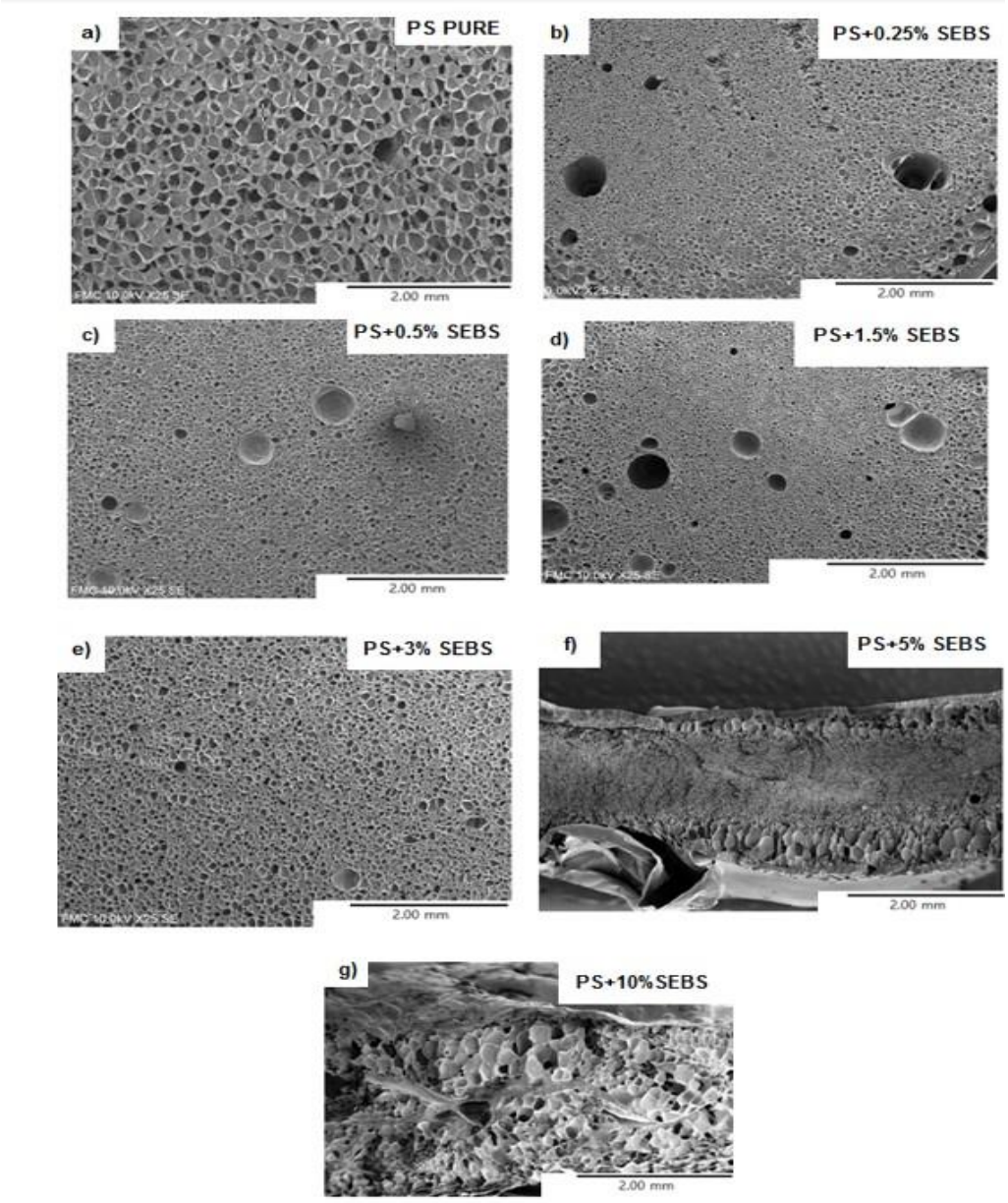


**Figure 3.** SEM micrographs of the cellular materials produced. (**a**) Pure PS; (**b**) PS + 0.25% SEBS; (**c**) PS + 0.5% SEBS; (**d**) PS + 1.5% SEBS; (**e**) PS + 3% SEBS; (**f**) PS + 5% SEBS; (**g**) PS + 10% SEBS.

Furthermore, the homogeneity of the cellular structure, that can be studied by the ratio between the standard deviation of the cell and the average cell size (SD/$\phi$) is lower in the foams containing 10 wt.% of SEBS, since higher values of the (SD/$\phi$) ratio are detected, than in the rest of cellular materials.

These results cannot be explained by the differences observed in the Tg, when adding high contents of SEBS. When maintaining the foaming temperature, like in this case that was 120 °C for all the materials, an increase in the Tg means that gap between the foaming temperature and the Tg is reduced. In other words, the polymer is less time in a rubbery state, which is an optimum approach to reduce the degeneration mechanisms. The obtained results can be explained considering the reduction of the strain hardening coefficient values observed in Table 1. If the strain hardening is very low the polymer is not able to resist the elongational forces occurring during the foaming process and it breaks. As a result, degeneration mechanisms like coalescence are favored leading to an increase of the foam density and also to a deterioration of the cellular structure.

Apart from the already mentioned behavior in the density, cell size and homogeneity of the cellular structure, the open cell content (see **Table 2**) slightly increases when the SEBS particles are introduced in the formulation up to values of 3 wt.%. For higher contents of SEBS a significant increase of this parameter is detected, which can be again explained by the reduction of the strain hardening coefficient.

Comparing the result obtained by using SEBS as nucleating agent with those obtained with other nucleating agents, like talc or some nanoparticles like sepiolites, it can be concluded that SEBS is the most efficient nucleating agent. A very small amount of SEBS (0.25 wt.%) lead to significant reduction of the cell size with respect with the pure PS (c.a. 78%). These reductions can be only achieved by incorporating high amounts of sepiolites (higher than 3 wt.%). Moreover, this significative reduction cannot be obtained with other nucleating agents like talc.[19]

**Table 2.** Density, cell size, cell nucleation density, homogeneity and open cell of the foams produced.

| Name of the Sample | Density (kg/m3) | Cell Size (μm) | Cell Nucleation Density (Nuclei/cm3) | SD/Φ | Open Cell Content |
|---|---|---|---|---|---|
| PS PURE | 31.07 ± 0.67 | 90.02 ± 25.14 | (4.76 ± 0.12) × 106 | 0.27 | 12 ± 1.03 |
| PS 0.25% SEBS | 31.15 ± 1.21 | 19.54 ± 3.14 | (3.50 ± 0.25) × 108 | 0.16 | 15 ± 0.63 |
| PS + 0.5% SEBS | 31.40 ± 0.78 | 16.40 ± 2.79 | (3.76 ± 0.44) × 108 | 0.17 | 13 ± 0.52 |

| | | | | | |
|---|---|---|---|---|---|
| PS + 1.5% SEBS | 32.16 ± 0.66 | 15.28 ± 2.18 | (3.98 ± 0.63) × 108 | 0.14 | 14 ± 0.47 |
| PS + 3% SEBS | 34.03 ± 1.03 | 8.14 ± 1.02 | (4.36 ± 0.87) × 108 | 0.12 | 17 ± 2.02 |
| PS + 5% SEBS | 41.62 ± 2.39 | 7.87 ± 2.33 | (3.53 ± 0.51) × 109 | 0.13 | 29 ± 3.74 |
| PS + 10% SEBS | 60.71 ± 4.56 | 256.3 ± 108 | (9.63 ± 0.76) × 105 | 0.42 | 14.18 |

## 5. CONCLUSIONS

In this paper an elastomeric phase based on a SEBS copolymer has been added to a PS matrix to evaluate its effect as cell nucleating agents. The morphology of the blends consists of a properly dispersed elastomeric phase comprising spherical particles with sizes between 0.2 and 0.5 μm. The size of the dispersed domains increases when the amount of SEBS increases, and the rheological behavior of the formulations are significative affected by the increase in the SEBS content. It has been found that the strain hardening is clearly reduced for SEBS contents above 5%. The SEBS phase has showed a remarkable nucleation effect. By incorporating only, a 0.25 wt.% of the elastomeric phase it is possible to reduce the cell size 5 times, keeping the density and open cell content. An increase of the SEBS content up to 2 wt.% allows reducing the cell size by 10 times with a small increase of density and open cell content. However, higher quantities of SEBS (between 5% and 10%) strongly increase the foam density and the open cell content. The present article constitutes, as far as the authors known, the first proof that SEBS is a very effective nucleating agent for PS foams. Furthermore, this elastomer is more efficient than other nucleating agents commonly used to improve the foamability of PS like talc or sepiolites.

## FUNDING

This research was funded from the Ministerio de Ciencia, Innovación y Universidades (RTI2018-098749-B-I00), from the Junta de Castilla y León (VA202P20) and the „Ente Público Regional de la Energía de Castilla y León" (EREN) are gratefully acknowledged.

## REFERENCES

[1] R. Banerjee, S.S. Ray, A.K. Ghosh. *Polymer*. **2018**, 10, 400.

[2] M.R. Qazviniha, M. Abdouss, M. Musavi, M. Mazinani, M. Kalaee. *Mater. Sci. Eng. Technol.* **2016**, 47, 47–52.

[3] X. Sang, L. Zhang, R. Wang, X. Chen, M. An, Y. Shen. *Adv. Mater. Res.* **2012**, 396–398, 1422–1425.

[4] C.R. Lindsey, D.R. Paul, J.W. Barlow. *J. Appl. Polym. Sci.* **1981,** 26, 1–8.

[5] V.Kalimaknov. *Nucleation Theory*. **2013,** Springer,Berlin, Germany.

[6] W. Qingfeng, C.B. Park, Z. Nanqiao, Z. Wenli. *J. Cell. Plast*. **2009**, 45, 303–319.

[7] E. Laguna-Gutierrez, A. Lopez-Gil, C. Saiz-Arroyo, R. Van Hooghten, P. Moldenaers, M.A. Rodriguez-Perez. *J. Polym. Res.* **2016**, 23, 251.

[8] V. Bernardo, J. Martin-De Leon, E. Laguna-Gutierrez, T. Catelani, J. Pinto, A. Athanassiou, M.A. Rodriguez-Perez. *Polymer* **2018**, 153, 262–270.

[9] V. Bernardo, J. Martin-de Leon, I. Sanchez-Calderon, E. Laguna-Gutierrez, M.A. Rodriguez-Perez. *Macromol. Mater. Eng*. **2020,** 305, 1900428.

[10] M. Haurat, M. Dumon. *Molecules* **2020**, 25, 5320.

[11] W. Qiang, D. Hu; T. Liu, L. Zhao. *J. Supercritial Fluids*. **2019**, 147, 329–337.

[12] R. Banerjee, R.; S.S. Ray, A.K. Ghosh. *J. Cell. Plast.* **2016,** 53, 389–406.

[13] R.W.B. Sharudin, M. Ohshima. *J. Appl. Polym. Sci.* **2012,** 128, 2245–2254.

[14] M. Santiago-Calvo, J. Tirado-Mediavilla, J.C. Rauhe. L.R. Jensen, J.L. Ruiz-Herrero, F. Villafañez, M.A. Rodriguez-Perez, *Eur. Polym. J*. **2018**, 108, 98–106.

[15] Greenspec. Insulation Materials and Their Thermal Properties, **2018**. Available online: http://www.greenspec.co.uk/building-desing/insulation-materials-thermal-properties/ (accessed on 5 March 2021).

[16] H.Münstedt, F.R.Schwarz. *Deformation and Flow of Polymeric Materials*. **2014** Springer: Verlag/Berlin, Germany.

[17] A. Ballesteros, E. Laguna-Gutierrez, P. Cimavilla-Roman, M.L. Puertas, A. Esteban-Cubillo, J. Santaren, M.A. Rodriguez-Perez. *J. Appl. Polym. Sci*. **2021,** 10, 51373.

[18] J.Pinto, E.Solorzano, M.A. Rodriguez-Perez, M.A.; J.A.De Saja. *J. Cell. Plast*. **2013**, 49,6.

[19] B.Notario, D.Velasco, A. Alvarez, A. Esteban-Cubillo, J. Santaren, M.A. Rodriguez-Perez. *In Proceedings of the International Conference on Foams and Foams Technology,* Barcelona, Spain,12–13 September **2012**.

# Chapter 8

## Conclusions and future work

*"Las cosas podrían haber sucedido de cualquier otra manera y, sin embargo, ocurrieron así."*

*El camino, Miguel Delibes.*

# INDEX

## 8.1 Conclusions

The articles published along this thesis have reported several important conclusions in the field of the cellular materials based on PS. The main conclusions obtained are collected in the following paragraphs.

### *8.1.1 Influence of the molecular weight in the PS foams.*

***About the influence of the molecular weight in the structural characteristics of PS:***

- The **molecular weight** of three different polystyrenes was **estimated by shear dynamic rheology** and **measured** experimentally **by GPC** technique (Chapter 4, section 4.2).
- The structural properties of pure PS are closely linked to their molecular weight (or their melt index). For instance, the polymer with the **highest molecular weight** presents the **highest glass transition temperature (Tg)**. The longer chains present in a polymer with a higher value of the molecular weight need a higher temperature to start the mobility rather than the ones of the polymer with a lower value of the molecular weight. The experimental values of the Tg were measured by the DSC technique and later compared to some theoretical models (Flory-Fox and Uberreiter and Kanning) that predict those temperatures based on the values of the molecular weight. There were found strong differences among those two values that could be attributed to other factors like flexibility or mobility of the chain, bulkiness, polarity and ionicity and free volume available (Chapter 4, section 4.2).
- Furthermore, the **polymer with the higher molecular weight** present the **bigger value of the zero-shear viscosity** in the terminal region and the **highest value of the strain hardening coefficient.** The higher molecular weight PS has a 76% more strain hardening coefficient than the lower molecular weight PS. This fact was important at the time of foaming the different grades of PS. Presenting the polymer with the lowest molecular weight (lowest strain hardening coefficient) a more remarkable appearance of degeneration phenomena that the other grades (Chapter 4, section 4.2).

***About the influence of the molecular weight in the sorption and diffusivity parameters:***

- **PS** with a **lower molecular weight** could **absorb around a 2% more of $CO_2$** in the supercritical state (at the same conditions of pressure, time, and

temperature) than other PS grades. Likewise, **the saturation of the polymer with a lower molecular weight occurred before** than those of the PS with a higher molecular weight. Moreover, the sorption diffusion coefficient of the lowest molecular weight PS was 94% higher than the one of the highest molecular weight. The above effects were explained through the greater free volume that the polymer with lower molecular weight presents (Chapter 4, section 4.2).

- PS with a **lower molecular weight** had a **slightly higher gas diffusivity** than its peers with a higher molecular weight. There was a difference of 22 % percent between the diffusion coefficient of the PS with low molecular weight compared to the one with highest molecular weight (Chapter 4, section 4.2).
- The **plasticizing effect was similar for the three grades of PS** studied regardless of the molecular weight value. The plasticization effect was analyzed using the Chow and Cha-Yoon models. It should be noted that, in the case of the **polymer with a lower molecular weight value**, due to its low starting Tg, the **effective Tg values** were **slightly higher than those of the saturation temperature**. Therefore, when the material was removed from the autoclave, it exhibits an opacity typical of a semi-foamed material (Chapter 4, section 4.2).

***About the influence of the molecular weight in the cellular structures and properties of the foams:***

- Once the foams were produced using the same parameters in the saturation and foaming steps, it was possible to see how that the **material that present the lowest density** (which expands the most) was the one with the **lowest molecular weight**. However, the **percentage of open cell obtained for the material with lower molecular weight was more than double compared to the polymer with higher molecular weight**. This fact may be due to the lower capacity of the material to resist gas expansion, according to its lower strain hardening coefficient (Chapter 4, section 4.2).
- Likewise, **the material with the smallest cell size, with a higher cell density, and a more regular and homogeneous structure**, was the **PS with the highest molecular weight.** The higher molecular weight polymer has a cell size of 43 μm compared to 264 μm for the lower molecular weight polymer. Although the **PS with the highest molecular weight** was the one that absorbs the least gas, it was also the one that had the **greatest capacity to withstand the expansion of the gases.** This means that phenomena of degeneration of the

cell structure as coalescence, which affect cell size and homogeneity of cell structure, was reduced for the polymer with highest molecular weight (Chapter 4, section 4.2). This fact can be seen in **Figure 8.1**.

- Finally, an intermediate PS was selected for subsequent studies, which allows reaching high expansions (low densities) without compromising cell size or open cell content (Chapter 4, section 4.2).

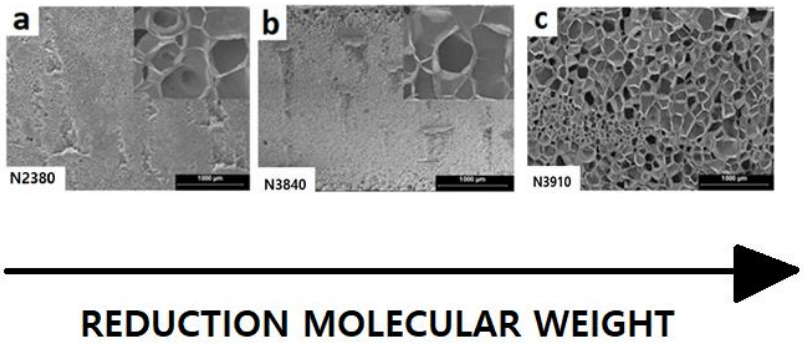


**Figure 8.1**. SEM micrographs of the cellular structure of the three PS foamed samples. a) Foam produced with the high molecular weight polystyrene N2380. b) Foam produced with the medium molecular weight polystyrene, Edistir N3840. c) Foam produced with the low molecular weight PS, Edistir N3910.

### *8.1.2 Blends of PS/ Sepiolites and cellular nanocomposites*

***About the dispersion and extensional rheological properties of the blends:***

- Different contents of sepiolites (from 2 wt.% until 10 wt.%) were introduced in the PS materials. Furthermore, three different kinds of sepiolites were investigated. One was a natural sepiolite without organomodification and the other two were treated on their surfaces with silane groups and quaternary ammonium salts. Moreover, the process conditions were also studied by processing the blends with one or two cycles in the extruder (Chapter 5, section 5.2, and section 5.3).
- The results **of shear rheology**, as well as **X-ray tomography**, shown that **sepiolites that were organo-modified with quaternary ammonium salts, were better able to be disperse in the PS matrix** than the other two kind of particles. Moreover, to achieve the percolation of the structure, 6 wt.% organomodified particles with quaternary ammonium salts was necessary, meanwhile 8 wt.% was needed. % of natural sepiolites (not superficially modified) and up to 10 wt.% for sepiolites treated with silane groups (Chapter 5, section 5.2). The better dispersibility of the sepiolites treated with quaternary ammonium salt can be seen in **Figure 8.2.**

- The **extensional rheological properties were reduced with the inclusion of sepiolites**. However, they were **better for formulations that contain unmodified sepiolites on their surface** (natural sepiolites) than for other composite materials. For example, at 2 wt.% of natural sepiolites the strain hardening coefficient was a 7% higher than for the formulation with quaternary ammonium salts and a 15% higher than for the formulations with silane group, possessing all the formulations the same amount of particles (Chapter 5, section 5.3). This conclusion can be seen better in Figure 8.3.
- Subject the formulations to **a greater number of extrusion cycles slightly reduced the shear viscosities of pure polymers and did not help to improve the dispersion of sepiolites in pure polymers.** The **extensional rheological properties were also reduced** by increasing the number of extrusion cycles. (Chapter 5, section 5.2, and section 5.3).

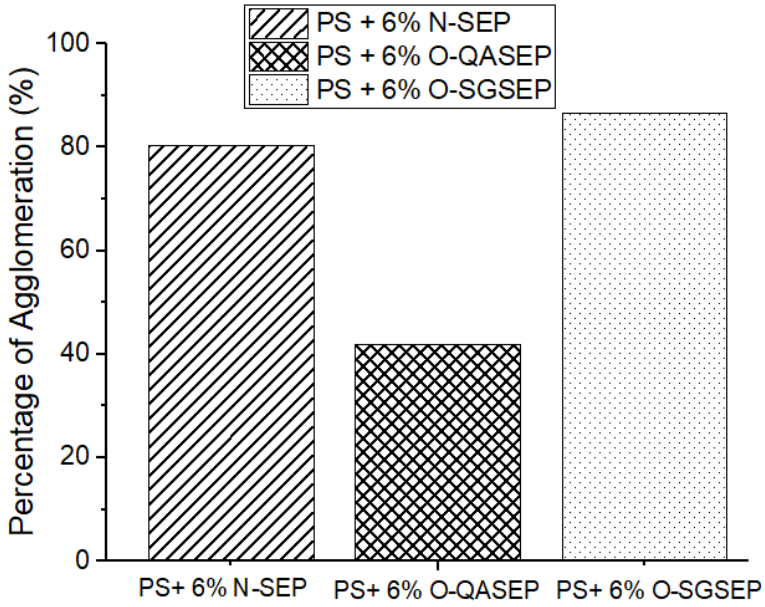


**Figure 8.2.** Percentage of agglomerates for the three formulations produced with the PS and 6 wt.% of particles, subjected to a single extrusion cycle.

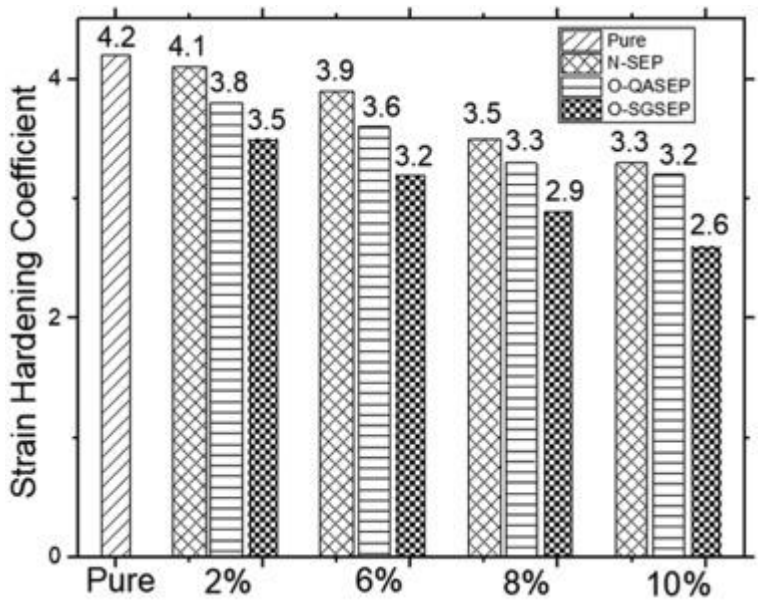


**Figure 8.3.** Strain hardening coefficient obtained for the pure PS and for the composites containing different contents of N-SEP, O-QASEP and O-SGSEP. This parameter has been determined for a time of 2.67 s and for a Hencky strain rate of 1 $s^{-1}$.

***About the gas concentration:***

- The use of **sepiolites achieves to slightly increase (c.a. 5%) the gas absorbed by the PS polymeric matrix,** until the percentage of sepiolites introduced is greater than 8 wt.%. According to the literature studied and referenced, sepiolites can function as gas absorbers thanks to their internal channels. (Chapter 5, section 5.3).

***About the cellular parameters of the nanocomposite foams produced:***

- **With high sepiolite contents (c.a. 10 wt.%), the relative density of the foams produced increases,** due to the higher density of the sepiolites compared to the density of pure PS. (Chapter 5, section 5.2, and section 5.3).
- The **open cell content increased with a higher percentage of sepiolites introduced**. This fact was not so remarkable for formulations containing natural sepiolites. However, the maximum open cell content obtained for the formulation with 10 wt.% of sepiolites modified with silane groups was 15% (which is a relatively low value) and should not cause excessive problems in the subsequent cellular structures. (Chapter 5, section 5.3).
- **Cell sizes were significantly reduced using sepiolites**. With just a 2 wt.% of sepiolites modified with quaternary ammonium salts, the cell size was reduced by 82% compared to the value of pure PS. Which **indicates a good behavior of this nanoparticle as a nucleating agent in PS**. The minimum cell

size achieved was 9 microns for an 8 wt.% of sepiolites modified with quaternary ammonium salts. (Chapter 5, section 5.2, and section 5.3).

- The **addition of sepiolites caused a bimodal cellular structure** with cells of different sizes. The number of larger cells represented around 10% to 20% of the sample volume. (Chapter 5, section 5.2, and section 5.3).
- To **achieve smaller cell sizes and more homogeneous cell structures, the dispersion of the particles must be optimized rather than the extensional rheological properties**. The formulations that presented a smaller cell size were those that have sepiolites modified with quaternary ammonium salts (the particles with the best degree of dispersion). (Chapter 5, section 5.3). This point can be seen in **Figure 8.4**

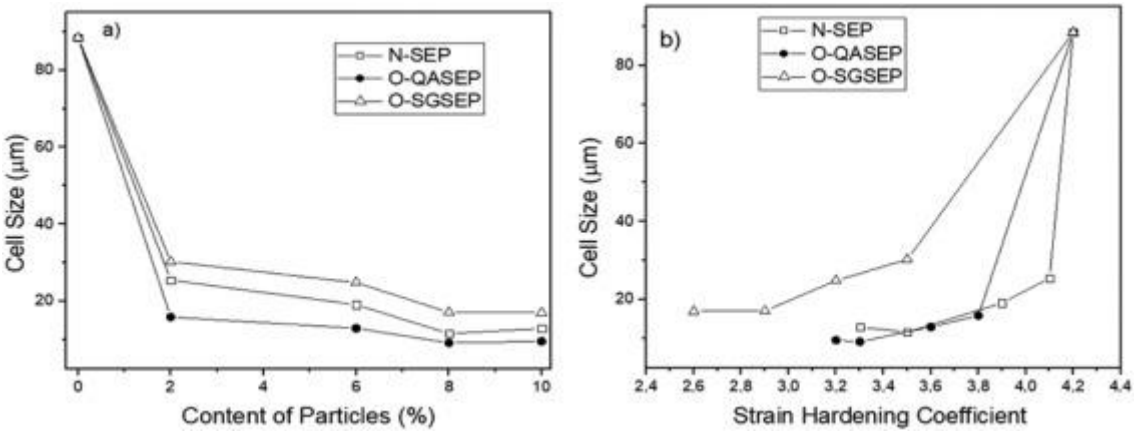


**Figure 8.4. (**a) Correlation between the cell size and the content of particles. (b) Cell size of the cellular materials as a function of the strain hardening coefficient.

- The **thermal conductivity of foams of PS/ sepiolites** with similar relative densities was studied. **Thermal conductivity was reduced as cell size was reduced too**. This phenomenon is true until reaching values **between 35-40 µm**. **For lower values of the cell size the thermal conductivity grows again**. This is due to the change in the dispersion method of infrared radiation. For very low values of cell size, the foam becomes a quasi "transparent" material to infrared radiation, thereby raising the overall thermal conductivity of the foam (Chapter 6, section 6.2). The phenomenon described before can be seen in **Figure 8.5.**
- The measured **extinction coefficient had a behavior very similar to thermal conductivity**. This phenomenon explains that it is the radiative term of thermal conductivity (infrared radiation) the one that was changing most remarkably due to the reduction in cell size.

- The experimental **thermal conductivity was compared with the thermal conductivity predicted using the Rosseland model. Both curves predict a similar behavior for the thermal conductivity curves.**

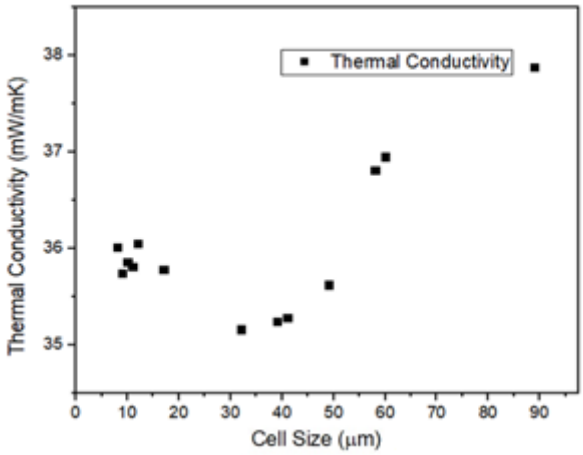


**Figure 8.5.** Thermal conductivity, experimentally determined, as a function of the cell size.

### *8.1.3 Blends of PS/ SEBS and foams produced*

***About the characteristics of the blends:***

- Different contents of SEBS (from 0.25 wt.% until 10 wt.%) were introduced in the PS materials.
- The shear rheology results shown that by *adding SEBS the shear viscosity is reduced*, On the other hand, there was no percolation of the PS / SEBS structure at high SEBS contents (5wt.% Or 10 wt.%). This is because SEBS is not an inorganic phase like sepiolites, but rather an organic polymeric phase (Chapter 7, section 7.2).
- **The addition of amounts of SEBS greater than 3 wt.%, causes that the glass transition temperature increased** compared to the Tg of pure PS (Chapter 7, section 7.2).
- **Adding SEBS reduced the strain hardening coefficient**. This phenomenon was very noticeable for SEBS values higher than 5 wt.%. For the formulation with a 10 wt. % SEBS the value of the strain hardening coefficient was a 61% lower than that of the pure PS polymer (Chapter 7, section 7.2).

***About the characteristics of the foams:***

- The **density of the foams was increased with the introduction of SEBS** in the polymeric matrix. This phenomenon was because SEBS limits the

expansion and growth of the foam. On the other hand, the open cell content remained constant for low SEBS contents. However, for a 10 wt. % SEBS open cell content raised to 45% (Chapter 7, section 7.2). This fact can be seen better thanks to the SEM micrographs that appear in **Figure 8.6.**

- It was important to highlight the **great nucleating capacity of SEBS** in PS. With only 0.25 wt. % of SEBS in the PS it was possible to reduce the cell size by 78%, compared to the pure polymer, or with 3 wt. % SEBS achieved a 90% cell size reduction. **These reductions were much more remarkable than those achieved with other inorganic particles such as sepiolites or more conventional nucleating agents such as talc**. On the other hand, the best results in the cell size achieved, as well as the homogeneity of the cell structure are achieved precisely with 3 wt. % SEBS in the polymer. For higher values of this organic phase, there was either a noticeable increase in cell size or a remarkable increase in density, or both. This phenomenon comes largely due to the reduction observed in extensional rheological properties for high SEBS contents (Chapter 7, section 7.2).

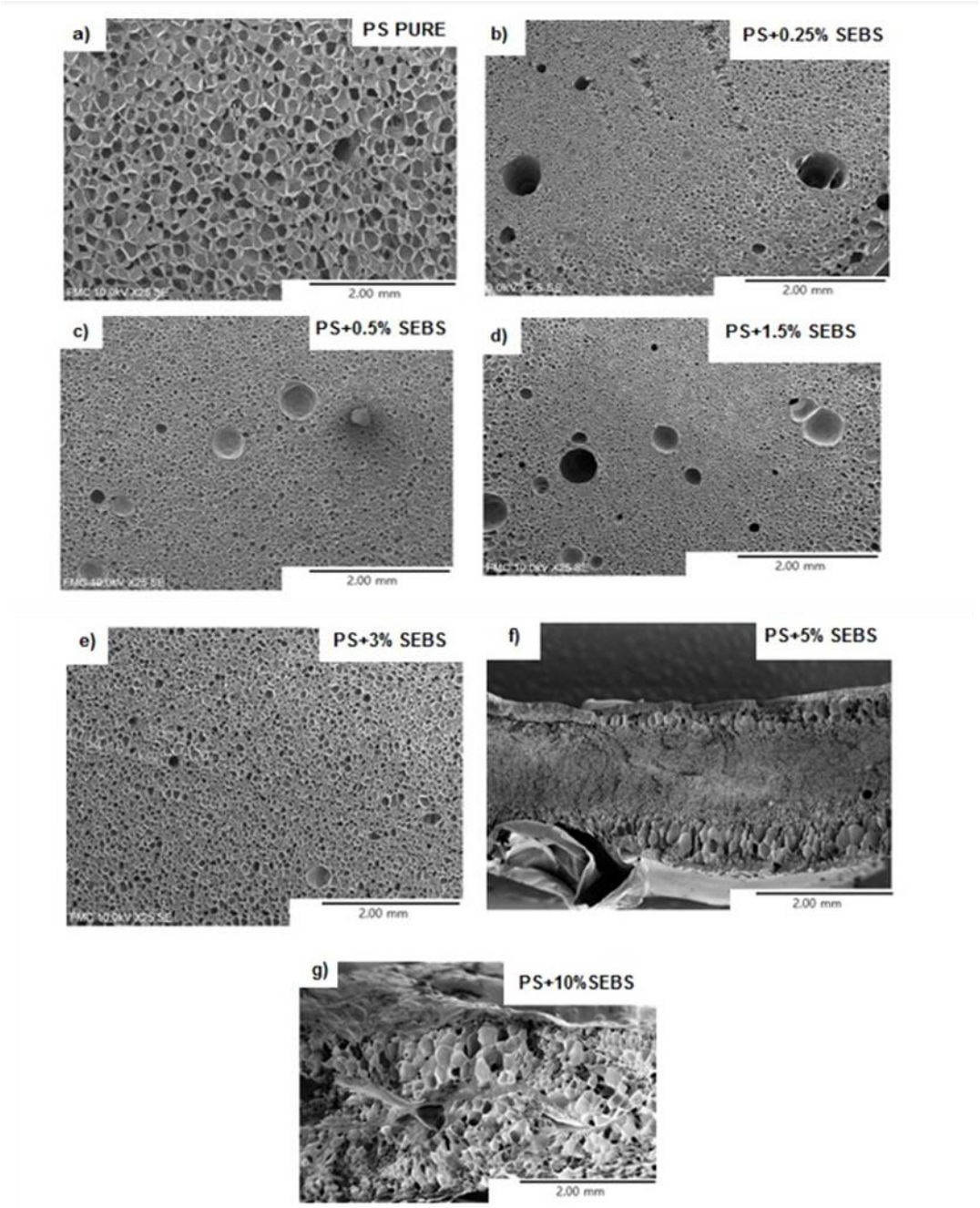


**Figure 8.6.** SEM micrographs of the cellular materials produced. (**a**) Pure PS; (**b**) PS + 0.25% SEBS; (**c**) PS + 0.5% SEBS; (**d**) PS + 1.5% SEBS; (**e**) PS + 3% SEBS; (**f**) PS + 5% SEBS; (**g**) PS + 10% SEBS.

### *8.1.4. An overview of the materials produced and state of the art after this thesis*

**Figure 8.7** is a graph that represent the percentage of reduction obtained in the cell size, compared to the pure polymer, as a function of the relative density for all the blend materials produced along the entire thesis. As can be seen in the figure, there is a broad range of cell sizes produced with similar values of the

relative density, thanks to introduction of the different fillers, employed along the thesis. The systems of PS/ O-QASEP and PS/SEBS allow the maximum reduction of the cell sizes. On the other hand, the relative density of the materials was slightly increased, compared to the pure polymer, due to the inclusion of the different nucleating agents. For the thesis, cellular materials with a cell nucleation density in a range from ($10^6$-$10^9$) nuclei/$cm^3$ have been produced. Concerning the nucleation efficiency, SEBS is the nucleating agent that allows reaching the highest nucleation at content of 5wt.%.

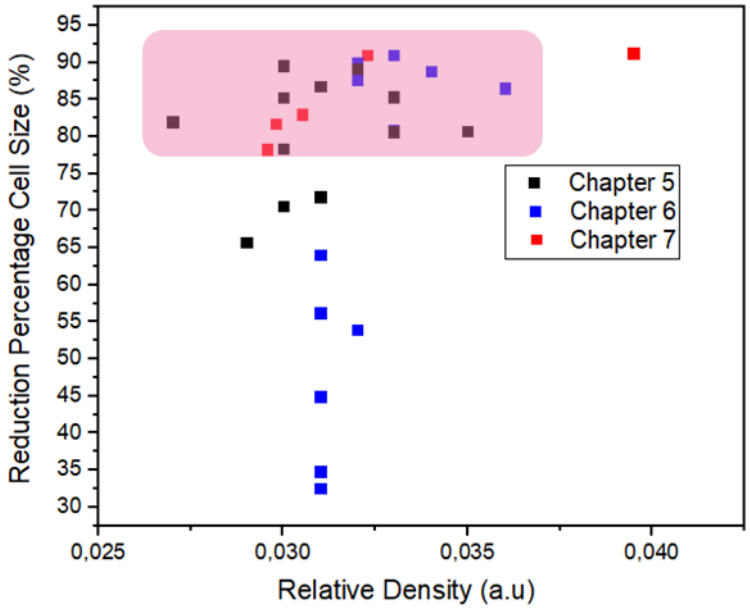


**Figure 8.7.** Reduction percentage in the cell size obtained along the thesis using the sepiolites and SEBS nucleating agents.

In **Figure 8.8** can be seen the graph of the percentage of reduction of the cell size as a function of the relative density for the samples produced in this thesis and compared to the previous state of the art in PS and nucleants nanocomposites.[1-7] As can be seen, now there are more points than before in the region of interest between lower relative densities and higher reductions in the cell size.

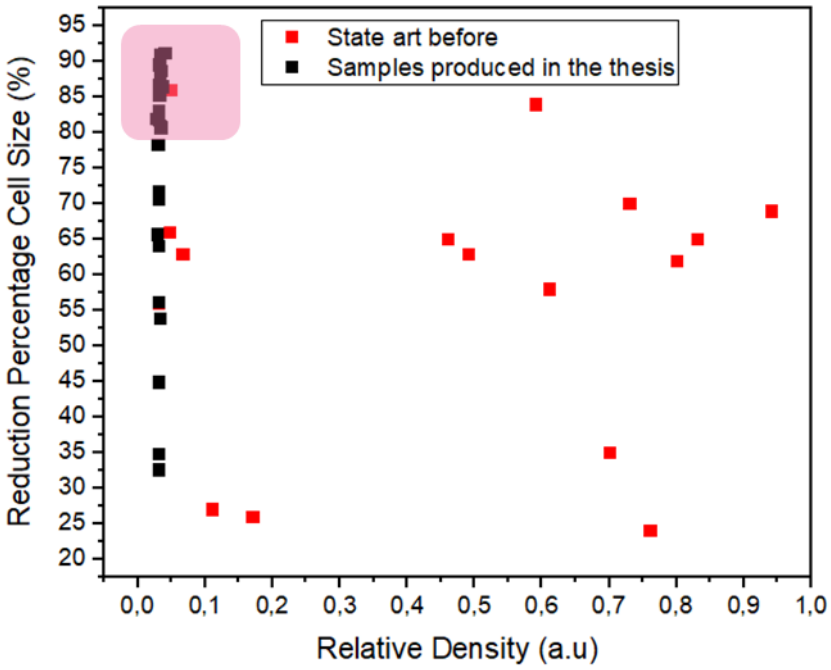


**Figure 8.8.** Comparison between the percentage of reduction of the cell density as function of the relative density for the samples before of this thesis and the samples produced now.

Furthermore, it was possible to check in chapter 6, section 6.2 a dependence between the final properties of the foams and the cellular structure. Achieving therefore, the objective proposed in this thesis of stablish a relationship between the composition-process-structure and properties of the foams.

## 8.2 Future Work

The actual work is the third thesis from the CellMat group, that aim to stablish a relationship between the composition-process-structure and properties of the foams.[8,9] As this methodology is one of the most followed in CellMat, it would be easy that new upcoming developments will be performed. In particular, some open topics of this work or some points not fully developed could be investigated.

In particular, the following list collect some of the open routes that could be followed this thesis:

- ***Analyze the mechanical properties of the PS foams produced:*** Even though during the actual work it was tried to reduce the thermal conductivity of the PS foams (because is the main drawback of PS foams compared to their main competitor, the PUR foams), it would be interesting to see if also the

mechanical properties of the foams had varied by the presence of the nucleating agent. A higher performance in the mechanical properties compared to the pure PS foams could lead also to a better future implementation in the insulation market.

- ***Complete the circle composition-process-structure properties for the PS/SEBS system:*** It was seen that SEBS was a marvelous nucleating agent for the PS foams. Furthermore, also the dispersion of this nucleating agent was analyzed thanks to shear and extensional rheology measurements. However, thermal, mechanical properties, etc. of the foams produced were not characterized during the thesis. For some properties, like thermal conductivity, we will need to adapt the saturation and foaming parameters, in order to obtain higher cell sizes that allows us to see if there is a reduction in the thermal conductivity by the presence of SEBS (without the increments observed in the chapter 6 in the thermal conductivity due to the low cell sizes values)
- ***Use another type of SEBS:*** Actually, there is only information of the nucleation capability in PS foams of just a type of SEBS. However, would be interesting to analyze if by changing some properties of the SEBS like molecular weight or the treatment of the nucleating agent (i.e. treated with maleic anhydride) the effect in the cellular structure is modified.
- ***Produce a model of the thermal conductivity:*** Based on the data found in chapter 6, it would be quite helpful to perform a theoretical model that could adapt the variation of the thermal conductivity according to the phenomena observed. For that purpose, other polymeric materials could be foamed trying to reach similar cell size range (10-100 μm) and same relative densities among them, in order to see if the behavior of increment of the thermal conductivity is again observed in the same range of cellular sizes ( for values lower than 40-30 μm ).
- ***Effect of the sepiolites in other polymeric matrices:*** During this work, has been possible to see the high nucleating effect of sepiolites in PS foams. However, it would be interesting to see if they can have similar effects in other polymers, like for example rigid polyurethane foams (PUR).
- ***New nucleating species:*** Other organic phases like styrene-butylene-styrene (SBS) or similar could also act as a potential nucleation agent. It would be interested to expand more the knowledge in the reduction of the cell size at

low relative densities, using organic phases, which are not really explored as could have been seen in previous chapters.

- ***Production of the PS based foams by other processes:*** Along the thesis, just a single method of introduced the gas in the foams (autoclave or batch foaming process) has been used. However, it will be provided a further knowledge, if some additional method, like extrusion foaming process will be used for producing the cellular materials. It would be possible that the preferable orientation of the sepiolites particles produced in the extrusion will have a meaningful effect in the mechanical properties in the mentioned direction. Furthermore, it would be also interesting to foam all the produced formulation in an expanded polystyrene autoclave or in extrusion foaming line that incorporate the underwater pelletizer system. One important step would be to see if the same formulations present a similar behavior in a scale up process.

## 8.3 Bibliography


[1] C. Li, G.Yang, H.Den, W.Ken, Q.Zhang, F.Chen, Q.Fu. *Polym.Int.* **2021**, 62(7),4394.

[2] J. Shen, X. Han, L. J. Lee. *J. Cell. Plast.* **2006**, 42 (2), 105–126.

[3] B. Notario, D. Velasco, M. A. Rodriguez-Perez, J. Santaren, A. Alvarez, and A. Esteban-Cubillo. *Improving the cellular structure and thermal conductivity of polysyrene foams by using sepiolites*. in *International Conference on Foams,Foams Technology, FOAMS* ***2012***, pp. 1–5.

[4] X. Han, C. Zeng, L. J. Lee, K. W. Koelling, D. L. Tomasko. *Polym. Eng. Sci.* **2004**, 43 (6), 1261–1275.

[5] Z. Guo, J. Yang, M. J. Wingert, D. L. Tomasko, L. J. Lee. **2008**, *Cell. Polym.* 28 (2), 162.

[6] W. Xiao, X. Liao, S. Li, J. Xiong, Q. Yang, G. Li. *Polym.Int.* **2018**, 67 (11) ,1488-1501.

[7] Y. Liu, L. Jian, T. Xiao,R. Liu, S. Yi, S. Zhang, L. Wang, R. Wang, Y. Ming .*Polymers (Basel).* **2019**, 11 (6), 985.

[8] C. Saiz-Arroyo. *Fabricación de Materiales Celulares Mejorados Basados en Poliolefinas. Procesado-Composicion-Estructura-Propiedades*. **2012**, PhD Thesis, University of Valladolid, Spain.

[9] E. Laguna-Gutierrez. *Understanding the Foamability of Complex Polymeric systems by Using Extensional Rheology*. **2016**, PhD Thesis, University of Valladolid, Spain.